


Spring 5-11-2018

Utilizing Ground-Penetrating Radar in the Delineation and Cultural Resource Management of Eroding Maine Coastal Shell Middens

Jacquelynn F. Miller

University of Maine, jacquelynn.miller@maine.edu

Follow this and additional works at: <https://digitalcommons.library.umaine.edu/etd>

 Part of the [Archaeological Anthropology Commons](#), [Geology Commons](#), [Geomorphology Commons](#), [Geophysics and Seismology Commons](#), [Social and Cultural Anthropology Commons](#), [Soil Science Commons](#), and the [Stratigraphy Commons](#)

Recommended Citation

Miller, Jacquelynn F., "Utilizing Ground-Penetrating Radar in the Delineation and Cultural Resource Management of Eroding Maine Coastal Shell Middens" (2018). *Electronic Theses and Dissertations*. 2863.
<https://digitalcommons.library.umaine.edu/etd/2863>

This Open-Access Thesis is brought to you for free and open access by DigitalCommons@UMaine. It has been accepted for inclusion in Electronic Theses and Dissertations by an authorized administrator of DigitalCommons@UMaine. For more information, please contact um.library.technical.services@maine.edu.

**UTILIZING GROUND-PENETRATING RADAR IN THE
DELINEATION AND CULTURAL RESOURCE
MANAGEMENT OF ERODING MAINE
COASTAL SHELL MIDDENS**

By

Jacquelynn F. Miller

B.S. in Geology, University of Kansas, 2015

A THESIS

Submitted in Partial Fulfillment of the
Requirements for the Degree of
Master of Science
(in Earth and Climate Sciences)

The Graduate School

The University of Maine

May 2018

Advisory Committee:

Alice R. Kelley, Instructor, School of Earth and Climate Sciences, and
Associate Research Professor, Climate Change Institute, Advisor

Joseph T. Kelley, Professor, School of Earth and Climate Sciences, and
Climate Change Institute

Daniel F. Belknap, Professor Emeritus, School of Earth and Climate Sciences,
and Climate Change Institute

Arthur E. Spiess, Senior Archaeologist, Maine Historic Preservation
Commission

Copyright 2018 Jacquelyn F. Miller

**UTILIZING GROUND-PENETRATING RADAR IN THE
DELINEATION AND CULTURAL RESOURCE
MANAGEMENT OF ERODING MAINE
COASTAL SHELL MIDDENS**

By Jacquelyn F. Miller

Thesis Advisor: Dr. Alice R. Kelley

An Abstract of the Thesis Presented
in Partial Fulfillment of the Requirements for the
Degree of Master of Science
(in Earth and Climate Sciences)

May 2018

Shell middens along the Maine coast archive up to 5000 years of cultural and climatic change, but the record is continually and rapidly lost to the sea through climate-driven coastal erosion and sea-level rise. These sites were constructed by the ancestors of Maine Tribes, and are composed of centimeters to meters of clam (*Mya arenaria*) and/or oyster (*Crassostrea virginica*) shells, other faunal remains, and cultural materials. Shell middens record human interaction with the environment and early coastal occupation and adaptation. The faunal remains reflect paleoenvironmental conditions and the distribution of extinct and extant forage-species along the western Gulf of Maine. This research utilized ground-penetrating radar as a rapid and cost-effective survey technique for cultural resource management (CRM) decisions. A subset of sites were surveyed to develop a rapid technique for making CRM decisions, but the methodology is applicable to shell middens worldwide.

Traditional methods of shell midden characterization involve expensive, destructive, and labor intensive archaeological excavation. Thus, a limited number of sites have been extensively described. Ground-penetrating radar (GPR) was used to obtain a high-resolution evaluation of vertical and lateral site extent and stratigraphy. Data are collected at a walking pace; thus, the process is rapid and noninvasive if additional ground-truth data are not required. GPR records below surface stratigraphy by noting differences in the electromagnetic properties of the material that reflect variations in layer composition, compaction, grain size, salinity, and/or water content. Of the fifteen sites selected for the study, six sites were surveyed as part of this research. A geographic information system (GIS) comparison of aerial photography time-series at three sites was carried out to determine the applicability of the method to the Maine coastline and attempt to quantify shoreline erosion through time. The historic aerial photo time-series did not provide conclusive results. Structure from Motion (SfM) photogrammetry was carried out on one site within the study, and it serves as a baseline for future high-resolution erosion monitoring through survey time-series comparison.

Also, a stakeholder meeting was held one year into the project. The meeting focused on the need for shell midden monitoring, and it allowed the development of the foundational ideas for a citizen-science monitoring network for shell midden sites along the coast of Maine.

This project demonstrated the applicability of: (1) GPR surveys to delineate and characterize midden extent and stratigraphy in a nondestructive to minimally invasive manner, (2) traditional shoreline change methods to quantify shoreline change at three research sites, and (3) a stakeholder meeting to cooperatively formulate a plan of site evaluation, monitoring, and rescue. Characterizing shell-rich layers and soil horizons and the nature of the underlying material across the site using GPR, using data from prior excavation units, informed a plan for prioritizing

areas for future archaeological study. As sea level continues to rise, and sites and the information they hold are currently disappearing, the need for the application of GPR and shoreline change studies of coastal shell midden sites in Maine is critical.

DEDICATION

This thesis is dedicated to my parents for supporting me in all I do. To my father, who is the reason I find joy in tinkering with and fixing things. To my mother, for setting an example of the strong, smart, woman with gusto, that I always wanted to be when I grew up.

ACKNOWLEDGEMENTS

A number of people and organizations made this master's journey possible and incredibly enjoyable. Namely, this research, my assistantship position, and my education would not have been possible without funding from Maine Sea Grant. I thank Rolfe Mandel, who offered geoarchaeological guidance during my days as an undergraduate at the University of Kansas. I would not of known about the opportunity to apply for graduate study at UMaine without him. Alice Kelley, as well as my committee, have offered incredible feedback and support, instruction, and guidance in all forms. I am forever grateful for the personal and professional growth that resulted from taking on this project.

When I encountered an issue involving Radan, Peter Leach always had time for a rewarding help session. Regular meetings of the geoarchaeology research group at UMaine resulted in a collaborative and supportive network of professors and students that provided multiple perspectives on research topics, and brought people together from the School of Earth and Climate Sciences (SECS), the Climate Change Institute (CCI), and the Anthropology Department. I thank this group for their feedback, the friendships it cultivated, and for everything that each person taught me. I am beyond appreciative of friends who graciously joined me for field work, specifically: Kate Pontbriand, Kendra Bird, Emily Blackwood, and Andrew Heller. Additionally, the Golden Fund provided Eric Ketzler, a SECS undergraduate student, the opportunity to assist in research efforts at the Tranquility Farm site. Field assistance from the aforementioned people, along with the field efforts and guidance offered by every person on my committee, made this research possible.

Additional external funds supported conference travel and professional development. I thank the Golden Family for their financial assistance through the

Golden Fund, and for the personal and professional growth that it allowed. Their support helped cover a portion of my travel to attend the 2017 meeting of the Society for American Archaeology (SAA), and allowed me the opportunity to volunteer with National Park Service geophysical specialists at Saint Croix International Historic Site in Calais, ME. I also received funding from the Graduate Student Government (GSG), which supported a portion of my travel expenses related to the 2017 SAA meeting, the 2017 Geological Society of America (GSA) meeting, and fully funded my travel to the 2018 SAA meeting. In addition, the Richard Hay Award from the Archaeological Geology Division of GSA also supported a portion of travel expenses for the 2017 GSA meeting.

I am grateful for the support of my family, friends, and mentors near and far. For their endless patience, hours of phone calls and Facetime chats, and constant encouragement, I thank my parents Charles and Lisa Miller; David and family; Carl and Mahlia and family; Kevin Fenyak; Kim Nguyen; and Sydney Runyan. I am thankful for my fellow graduate student friends that I could always count on for anything from academics to getting outside and experiencing Maine.

TABLE OF CONTENTS

DEDICATION	iii
ACKNOWLEDGEMENTS	iv
LIST OF TABLES	xii
LIST OF FIGURES	xv
LIST OF ABBREVIATIONS.....	xxvi

Chapter

1. INTRODUCTION	1
1.1 Organization	4
2. BACKGROUND	6
2.1 Surficial Geologic and Sea-Level History of Maine	6
2.1.1 Glaciation	6
2.1.2 Deglaciation/Isostasy and Sea-Level Change	6
2.1.2.1 Typical Stratigraphic Section	10
2.2 Regional Culture History Periods.....	10
2.2.1 Pre-Clovis and Paleoindian Period	10
2.2.2 Archaic Period	12
2.2.3 Ceramic Period	14
2.2.4 Contact Period.....	15

2.3	Maine Shell Middens	17
2.3.1	Site Preservation	18
2.3.2	Archaeological Practice at Regional Shell Middens Through Time	18
2.4	Site Reports	21
2.4.1	University of New England (UNE, Site 5.06)	23
2.4.2	Crescent Beach (CBE, Site 9.98)	24
2.4.3	Spear's Hill (SPH, Site 14.169)	25
2.4.4	Long Island North (LIN, Site 15.95)	25
2.4.5	Glidden and Whaleback (GLI/WHA, Sites 26.1 and 26.2)	26
2.4.6	Oyster Farm (DAM, Site 26.15)	27
2.4.7	Olson (OLS, Site 17.13)	28
2.4.8	Scott's Midden (SCO, Site 42.82)	29
2.4.9	Fernald Point (FRN, Site 43.24)	29
2.4.10	Tranquility Farm (TRQ, Site 44.12a)	30
2.4.11	Holmes Point East and West (HPE/HPW, Sites 62-6 and 62-8)	31
2.4.12	Reversing Falls (RVF, Site 80.15)	32
2.4.13	Sipp Bay (SIB, Site 80.25)	32
2.5	Summary	33

3. GROUND-PENETRATING RADAR AS A CULTURAL RESOURCE MANAGEMENT TOOL FOR ASSESSMENT OF ERODING SHELL MIDDENS.....	36
3.1 Abstract	36
3.2 Introduction	36
3.2.1 Maine Shell Middens	37
3.2.2 Factors Affecting Midden Erosion	38
3.2.3 GPR and Midden Archaeology	39
3.3 Protocol for Midden Assessment Using GPR	39
3.3.1 Site Evaluation.....	41
3.3.2 Determine GPR Survey Type (Site or Equipment)	42
3.3.3 GPR Survey.....	42
3.3.4 Data Processing.....	43
3.3.5 Comparison to Archaeological Profiles	43
3.3.6 GPR Data Representation	44
3.4 Application of the Methodology	44
3.4.1 Olson Case Study	45
3.4.2 Damariscotta Case Study	48
3.4.3 Error in Midden Thickness Calculations	52
3.5 Summary	53
3.6 Acknowledgements	55

4.	COMBINED METHODS, RESULTS, AND DISCUSSION OF SITES AND DETAILS EXCLUDED FROM CHAPTER 3: <i>GROUND-PENETRATING RADAR AS A CULTURAL RESOURCE MANAGEMENT TOOL FOR ASSESSMENT OF ERODING SHELL MIDDENS</i>	56
4.1	GPR Survey	56
4.2	Error in Shell Midden Depth Interpretation	57
4.3	Proposed Experimental Methods	58
4.4	University of New England (Site 5.06)	58
4.4.1	GPR and Archaeological Data Comparisons.....	60
4.5	Long Island North (Site 15.95).....	66
4.5.1	GPR and Archaeological Data Comparison.....	66
4.6	Damariscotta Oyster Farm (Site 26.15)	72
4.7	Olson (Site 17.13)	74
4.7.1	GPR and Archaeological Data Comparisons.....	75
4.7.2	Error in Shell Midden Depth Interpretation	82
4.8	Fernald Point (Site 43.24)	82
4.8.1	GPR and Archaeological Data Comparisons.....	84
4.9	Tranquility Farm (Site 44.12a).....	89
4.9.1	Error in Shell Midden Depth Interpretation	95
4.10	Summary	99

5.	STRUCTURE FROM MOTION AS A NEW METHOD OF ANALYZING SHORELINE CHANGE IN ARCHAEOLOGY: AN EXAMPLE FROM COASTAL MAINE	102
5.1	Abstract	102
5.2	Introduction	103
5.2.1	Bluff Erosion in Coastal Maine	106
5.3	Application of Methodologies at the Olson Site	106
5.3.1	Olson Air Photo Case Study	107
5.3.2	Olson SfM Case Study	111
5.3.3	SfM Model Construction	112
5.3.4	GPS as GCP	113
5.3.5	Photo Acquisition and Settings	115
5.3.6	Olson Survey Camera Settings.....	116
5.4	Conclusions	117
6.	COMBINED METHODS, RESULTS, AND DISCUSSION OF SITES AND DETAILS EXCLUDED FROM CHAPTER 5: <i>STRUCTURE FROM MOTION AS A NEW METHOD OF ANALYZING SHORELINE CHANGE IN ARCHAEOLOGY: AN EXAMPLE FROM COASTAL MAINE</i>	119
6.1	Shoreline Change Study	119
6.1.1	Damariscotta (Site 26.15)	120
6.1.2	Tranquility Farm (Site 44.12a).....	121
6.2	Summary	123

7. CONCLUSIONS	124
7.1 Future Work.....	127
REFERENCES	130
APPENDIX A – A BRIEF GUIDE TO RADAN.....	141
APPENDIX B – TOTAL STATION SURVEY	156
APPENDIX C – GPR PROFILE COLLECTION AND DATA PROCESSING INFORMATION.....	176
APPENDIX D – GPR PROFILE LOCATION MAPS	189
APPENDIX E – ARCHAEOLOGICAL WALL PROFILES	216
APPENDIX F – GROUND-TRUTH LOCATION INFORMATION.....	284
APPENDIX G – STRATIGRAPHIC INFORMATION FROM EXCAVATION FIELD NOTES.....	309
APPENDIX H – ADDITIONAL GPR AND ARCHAEOLOGICAL PROFILE COMPARISONS.....	317
APPENDIX I – ISOPACH MAPS	331
BIOGRAPHY OF THE AUTHOR	345

LIST OF TABLES

Table 2.1	Early cultural periods within the United States.....	12
Table 2.2	Ceramic Period Subdivisions after Sanger and Petersen (1991)	16
Table 4.1	Tranquility Farm (Site 44.12a) site midden thickness comparison: stratigraphic data and GPR interpretations	96
Table 5.1	Olson site SfM survey camera settings	117
Table B.1	Olson (Site 17.13) total station survey data	163
Table B.2	Tranquility Farm (Site 44.12a) total station survey data	167
Table C.1	Tranquility Farm (Site 44.12a) 500 MHz 5 meter GPR survey Radon profile names.....	186
Table C.2	Tranquility Farm (Site 44.12a) 500 MHz 5 meter GPR survey profile location data table 1.....	187
Table C.3	Tranquility Farm (Site 44.12a) 500 MHz 5 meter GPR survey profile location data table 2.....	187
Table C.4	Tranquility Farm (Site 44.12a) 500 MHz 5 meter GPR survey profile location data table 3.....	188
Table C.5	Tranquility Farm (Site 44.12a) 500 MHz 5 meter GPR survey profile location data table 4.....	188
Table E.1	Tranquility Farm (Site 44.12a) archaeological wall profiles	259

Table F.1	University of New England (Site 5.06) archaeological profile locations with respect to GPR profiles	284
Table F.2	Long Island North (Site 15.95) archaeological profile locations with respect to GPR profiles.....	287
Table F.3	Damariscotta Oyster Farm (Site 26.15) archaeological profile locations with respect to GPR profiles	290
Table F.4	Olson (Site 17.13) locations of stratigraphic note data with respect to GPR profiles	291
Table F.5	Olson (Site 17.13) archaeological profile locations with respect to GPR profiles	292
Table F.6	Olson (Site 17.13) archaeological profile photo locations with respect to GPR profiles	293
Table F.7	Fernald Point (Site 43.24) archaeological profile photo locations with respect to GPR profiles.....	295
Table F.8	Fernald Point (Site 43.24) archaeological profile locations with respect to GPR profiles	295
Table F.9	Tranquility Farm (Site 44.12a) archaeological profile locations with respect to GPR profiles.....	301
Table F.10	Tranquility Farm (Site 44.12a) archaeological wall profile photo locations with respect to GPR profiles.....	302
Table F.11	Tranquility Farm (Site 44.12a) location of metal placed during archaeological excavation with respect to GPR profiles.....	303
Table F.12	Tranquility Farm (Site 44.12a) stratigraphic information locations with respect to GPR profiles	304

Table H.1	Olson (Site 17.13) site midden thickness comparison:	
	stratigraphic data and GPR interpretations	326

LIST OF FIGURES

Figure 1.1	Study site locations along the Maine coast	3
Figure 2.1	Maine relative sea-level curve Kelley et al. (2010)	8
Figure 2.2	Maximum inland extent of late-glacial sea.....	9
Figure 2.3	Study site locations along the Maine coast with coastal compartments identified by Kelley (1987)	22
Figure 3.1	Site locations.....	40
Figure 3.2	Protocol flow chart	41
Figure 3.3	Olson site ground-truth and interpretation	46
Figure 3.4	Damariscotta site isopach map	47
Figure 3.5	Olson site GPR survey map and isopach map.	49
Figure 3.6	Damariscotta site ground-truth and interpretation	51
Figure 4.1	University of New England (Site 5.06) GPR and archaeological profile comparison of the 494E499N north wall	63
Figure 4.2	University of New England (Site 5.06) GPR and archaeological profile comparison of the 500E494N north wall	64
Figure 4.3	University of New England (Site 5.06) GPR and archaeological profile comparison of the 504E491N north wall	65
Figure 4.4	Long Island North (Site 15.95) isopach map with 500 MHz GPR survey transects	68

Figure 4.5	Long Island North (Site 15.95) isopach map.....	69
Figure 4.6	Long Island North (Site 15.95) redrafted archaeological profiles	70
Figure 4.7	Long Island North (Site 15.95) GPR profiles with archaeological profile positions overlain	71
Figure 4.8	Damariscotta (Site 26.15) 500 MHz GPR map overlain on Arthur Spiess' shell extent basemap.....	73
Figure 4.9	Damariscotta (Site 26.15) isopach map with 500 MHz GPR transects overlain	74
Figure 4.10	Olson (Site 17.13) east (1) GPR and archaeological profile comparison	78
Figure 4.11	Olson (Site 17.13) east (2) GPR and archaeological profile comparison	79
Figure 4.12	Olson (Site 17.13) east (3) GPR and archaeological profile comparison	80
Figure 4.13	Olson (Site 17.13) east (4) GPR and archaeological profile comparison	81
Figure 4.14	Fernald Point (Site 43.24) 10W to 8W south wall GPR and archaeological profile comparison	86
Figure 4.15	Fernald Point (Site 43.24) 45P to 45N west wall GPR and archaeological profile comparison	87
Figure 4.16	Fernald Point (Site 43.24) 64T to 64R west wall GPR and archaeological profile comparison	88
Figure 4.17	Tranquility Farm (Site 44.12a) disturbed area in GPR profile on western 500 MHz GPR survey grid	91

Figure 4.18	Tranquility Farm (Site 44.12a) underlying geology seen in photo and GPR profile	92
Figure 4.19	Tranquility Farm (Site 44.12a) isopach map with 500 MHz GPR survey transects overlain.....	93
Figure 4.20	Tranquility Farm (Site 44.12a) isopach map	94
Figure 5.1	Olson site location	104
Figure 5.2	Olson shorelines delineated from historic aerial photography	110
Figure 5.3	Olson site LiDAR versus SfM digital surface model	111
Figure 6.1	Shoreline change study locations with coastal compartments identified by Kelley (1987)	120
Figure 6.2	Digitized shorelines of the DAM site	121
Figure 6.3	Digitized shorelines of the TRQ site	123
Figure A.1	Prompt for batch filename	141
Figure A.2	Prompt for files	142
Figure A.3	Box for defining 3D batch grid extent.....	143
Figure A.4	File location and orientation (X-direction)	144
Figure A.5	File location and orientation (Y-direction)	144
Figure A.6	File details and "File Parameters" pop-up box.....	145
Figure A.7	Super 3D file creation main window.....	146
Figure A.8	"File Parameters" pop-up box.....	147
Figure A.9	Time zero correction window	149

Figure A.10	FIR filter window	150
Figure A.11	Range gain window	151
Figure A.12	Parameters for NOAA's <i>Data Access Viewer</i> coastal LiDAR datasets.....	153
Figure B.1	Olson (Site 17.13) total station survey map	160
Figure B.2	Fernald Point (Site 43.24) total station survey map	161
Figure B.3	Tranquility Farm (Site 44.12a) total station survey map	162
Figure D.1	University of New England (UNE Site 5.06) 1 meter 500 MHz GPR survey map	189
Figure D.2	Long Island North (Site 15.95) 1 meter 500 MHz GPR survey map	191
Figure D.3	Long Island North (Site 15.95) 1 meter 500 MHz GPR survey map overlain on Dick Doyle's archaeological excavation map	192
Figure D.4	Damariscotta (Site 26.15) 0.5 meter 500 MHz GPR detailed grid map.....	193
Figure D.5	Olson (Site 17.13) 500 MHz GPR survey overview map with grid corners	194
Figure D.6	Olson (Site 17.13) 1 and 0.5 meter 500 MHz GPR grid map 1.....	195
Figure D.7	Olson (Site 17.13) 1 meter 500 MHz GPR grid map 2.....	196
Figure D.8	Olson (Site 17.13) 1 meter 500 MHz GPR grid map 3.....	197
Figure D.9	Olson (Site 17.13) 1 meter 500 MHz GPR grid map 4.....	198
Figure D.10	Olson (Site 17.13) 1 meter 500 MHz GPR grid map 5.....	199

Figure D.11 Olson (Site 17.13) 1 meter 500 MHz GPR grid map 6.....	200
Figure D.12 Olson (Site 17.13) 1 meter 500 MHz GPR grid map 7.....	201
Figure D.13 Olson (Site 17.13) 1 meter 500 MHz GPR grid map 8.....	202
Figure D.14 Olson (Site 17.13) 5 and 10 meter 500 MHz GPR grid maps 9, 12, and 13	203
Figure D.15 Olson (Site 17.13) 1 meter 500 MHz GPR grid map 10	204
Figure D.16 Olson (Site 17.13) 1 meter 500 MHz GPR grid map 11	205
Figure D.17 Fernald Point (Site 43.24) 5 meter 500 MHz GPR grid map	206
Figure D.18 Fernald Point (Site 43.24) 5 meter 500 MHz GPR grid map overlain on D. Sanger's excavation map.....	207
Figure D.19 Fernald Point (Site 43.24) 1 meter 500 MHz GPR grid map	208
Figure D.20 Fernald Point (Site 43.24) 0.25 meter 500 MHz GPR grid map.....	209
Figure D.21 Tranquility Farm (Site 44.12a) 5 meter 500 MHz GPR grid map 1 with excavation units and 0.5 meter 500 MHz GPR grid location delineated	211
Figure D.22 Tranquility Farm (Site 44.12a) 5 meter 500 MHz GPR grid map 1	212
Figure D.23 Tranquility Farm (Site 44.12a) 0.5 meter 500 MHz GPR grid map	213
Figure D.24 Tranquility Farm (Site 44.12a) 5 meter 500 MHz GPR grid map 2	214
Figure D.25 Tranquility Farm (Site 44.12a) 500 MHz combined 5 meter GPR grid map	215

Figure E.1	Long Island North (Site 15.95) S23E8 and S22E8 east wall	217
Figure E.2	Long Island North (Site 15.95) S19E9 and S20E9 east wall	218
Figure E.3	Long Island North (Site 15.95) S17E8 east wall	219
Figure E.4	Redrafted Oyster Farm (Site 26.15) north wall profile	220
Figure E.5	Oyster Farm (Site 26.15) original north wall profile	221
Figure E.6	Redrafted Oyster Farm (Site 26.15) east wall profile	222
Figure E.7	Oyster Farm (Site 26.15) original east wall profile	223
Figure E.8	Redrafted Oyster Farm (Site 26.15) south wall profile	224
Figure E.9	Oyster Farm (Site 26.15) original south wall profile	225
Figure E.10	Redrafted Olson (Site 17.13) east (1) wall profile	227
Figure E.11	Olson (Site 17.13) original east (1) wall profile	228
Figure E.12	Redrafted Olson (Site 17.13) east (2) wall profile	229
Figure E.13	Olson (Site 17.13) original east (2) wall profile	230
Figure E.14	Redrafted Olson (Site 17.13) east (3) wall profile	231
Figure E.15	Olson (Site 17.13) original east (3) wall profile	232
Figure E.16	Redrafted Olson (Site 17.13) east (4) wall profile	233
Figure E.17	Olson (Site 17.13) original east (4) wall profile	234
Figure E.18	Redrafted Olson (Site 17.13) west (1) wall profile	235
Figure E.19	Olson (Site 17.13) original west (1) wall profile	236
Figure E.20	Olson (Site 17.13) west wall profile photo N0E0 to N2E0	237
Figure E.21	Olson (Site 17.13) west wall profile photo N2E0 to N4E0	238

Figure E.22	Redrafted Olson (Site 17.13) west (2) wall profile.....	239
Figure E.23	Olson (Site 17.13) original west (2) wall profile	240
Figure E.24	Olson (Site 17.13) west wall profile photo N4E0 to N6E0	241
Figure E.25	Olson (Site 17.13) west wall profile photo N6E0 to N8E0	242
Figure E.26	Redrafted Olson (Site 17.13) west (3) wall profile.....	243
Figure E.27	Olson (Site 17.13) original west (3) wall profile	244
Figure E.28	Olson (Site 17.13) west wall profile photo N8E0 to N10E0.....	245
Figure E.29	Olson (Site 17.13) west wall profile N10E0 to N12E0.....	246
Figure E.30	Redrafted Olson (Site 17.13) west (4) wall profile.....	247
Figure E.31	Olson (Site 17.13) original west (4) wall profile	248
Figure E.32	Olson (Site 17.13) west wall profile photo N12E0 to N14E0.....	249
Figure E.33	Olson (Site 17.13) west wall profile photo N14E0 to N16E0.....	250
Figure E.34	Olson (Site 17.13) west wall profile photo N14E0 to N16E0.....	251
Figure E.35	Redrafted Olson (Site 17.13) west (5) wall profile.....	252
Figure E.36	Olson (Site 17.13) original west (5) wall profile	253
Figure E.37	Olson (Site 17.13) west wall profile photo N16E0 to N18E0.....	254
Figure E.38	Fernald Point (Site 43.24) 1977 photo (1) of excavation area 50W-55W	256
Figure E.39	Fernald Point (Site 43.24) 1977 photo (2) of excavation area 50W-55W	257
Figure E.40	Fernald Point (Site 43.24) photo of surficial geologic materials underlying the shell midden	258

Figure E.41	Redrafted Tranquility Farm (Site 44.12a) N96W97 north wall profile	260
Figure E.42	Tranquility Farm (Site 44.12a) original N96W97 north wall profile	261
Figure E.43	Redrafted Tranquility Farm (Site 44.12a) N96W93 north wall profile	262
Figure E.44	Tranquility Farm (Site 44.12a) original N96W93 north wall profile	263
Figure E.45	Redrafted Tranquility Farm (Site 44.12a) N94W85 east wall profile	264
Figure E.46	Tranquility Farm (Site 44.12a) original N94W85 east wall profile	265
Figure E.47	Redrafted Tranquility Farm (Site 44.12a) N104W90 west wall profile	266
Figure E.48	Tranquility Farm (Site 44.12a) original N104W90 west wall profile	267
Figure E.49	Redrafted Tranquility Farm (Site 44.12a) N106W107 east wall profile	268
Figure E.50	Tranquility Farm (Site 44.12a) original N106W107 east wall profile	269
Figure E.51	Redrafted Tranquility Farm (Site 44.12a) N106W107 south wall profile	270
Figure E.52	Tranquility Farm (Site 44.12a) original N106W107 south wall profile	271

Figure E.53	Tranquility Farm (Site 44.12a) N105W104 south wall photo	272
Figure E.54	Tranquility Farm (Site 44.12a) N105W104 east wall photo.....	273
Figure E.55	Tranquility Farm (Site 44.12a) N105W104 photo view looking northeast	274
Figure E.56	Tranquility Farm (Site 44.12a) N105W104 west wall photo	275
Figure E.57	Tranquility Farm (Site 44.12a) N105W106 north wall photo	276
Figure E.58	Tranquility Farm (Site 44.12a) N105W106 west wall photo	277
Figure E.59	Tranquility Farm (Site 44.12a) N105W106 south wall photo	278
Figure E.60	Tranquility Farm (Site 44.12a) N105W106 east wall photo.....	279
Figure E.61	Tranquility Farm (Site 44.12a) N106W104 west wall photo	280
Figure E.62	Tranquility Farm (Site 44.12a) N106W107 north wall photo	281
Figure E.63	Tranquility Farm (Site 44.12a) N106W107 and N105W106 photo view southeast	282
Figure E.64	Tranquility Farm (Site 44.12a) N106W108 south wall photo	283
Figure F.1	Map of ground-truth locations and 500 MHz GPR survey at the University of New England site (Site 5.06)	285
Figure F.2	Long Island North (Site 15.95) ground-truth location map under 500 MHz GPR map (1)	288
Figure F.3	Long Island North (Site 15.95) ground-truth location map under 500 MHz GPR map (2)	289
Figure F.4	Map of ground-truth locations overlain on the 500 MHz GPR survey at the Olson site (Site 17.13)	294

Figure F.5	Fernald Point (Site 43.24) ground-truth location map	299
Figure F.6	Unlabeled Fernald Point (Site 43.24) ground-truth location map with the 500 MHz GPR survey transects overlain	300
Figure F.7	Labeled map of ground-truth locations at Tranquility Farm (Site 44.12a) with 500 MHz GPR survey transects overlain	307
Figure F.8	Unlabeled ground-truth locations at Tranquility Farm (Site 44.12a) with 500 MHz GPR survey transects overlain	308
Figure H.1	Olson (Site 17.13) west (1) GPR and archaeological profile comparison	319
Figure H.2	Olson (Site 17.13) west (2) GPR and archaeological profile comparison	320
Figure H.3	Olson (Site 17.13) west (3) GPR and archaeological profile comparison	321
Figure H.4	Olson (Site 17.13) west (4) GPR and archaeological profile comparison	322
Figure H.5	Olson (Site 17.13) west (5) GPR and archaeological profile comparison	323
Figure H.6	Olson (Site 17.13) N8E16 and N4E16 original base of midden pick on GPR profile	327
Figure H.7	Olson (Site 17.13) N0E24 original base of midden pick on GPR profile	328
Figure H.8	Olson (Site 17.13) N0W48 original base of midden pick on GPR profile	329

Figure H.9	Olson (Site 17.13) original base of midden pick on GPR profile for map points 7-9	330
Figure I.1	Damariscotta (Site 26.15) isopach map	335
Figure I.2	Olson (Site 17.13) isopach map	336
Figure I.3	Tranquility Farm (Site 44.12a) isopach map with grids and total station survey points overlain.....	337
Figure I.4	Tranquility Farm (Site 44.12a) isopach map with total station survey points overlain	338
Figure I.5	Tranquility Farm (Site 44.12a) isopach map (1) of the western portion of the 500 MHz GPR survey with transects overlain.....	339
Figure I.6	Tranquility Farm (Site 44.12a) isopach map (1) of the western portion of the 500 MHz GPR survey	340
Figure I.7	Tranquility Farm (Site 44.12a) isopach map (2) of the western portion of the 500 MHz GPR survey with transects overlain.....	341
Figure I.8	Tranquility Farm (Site 44.12a) isopach map (2) of the western portion of the 500 MHz GPR survey	342
Figure I.9	Tranquility Farm (Site 44.12a) isopach map of the eastern portion of the 500 MHz GPR survey with transects overlain.....	343
Figure I.10	Tranquility Farm (Site 44.12a) isopach map of the eastern portion of the 500 MHz GPR survey	344

LIST OF ABBREVIATIONS

3D - Three-Dimensional	GPR - Ground-Penetrating Radar
aDNA - ancient DNA	GPS - Global Positioning System
ASTER - Advanced Spaceborne Thermal Emission and Reflection Radiometer	LiDAR - Light Detection And Ranging
CCS - Coarse Crushed Shell	LIS - Laurentide Ice Sheet
cm - centimeter(s)	m - meter(s)
CRM - Cultural Resource Management	m.a.s.l. - Meters Above Sea Level
DEM - Digital Elevation Model	MCS - Medium Crushed Shell
eDNA - environmental DNA	RMS - Root Mean Square
FCR - Fire Cracked Rock	RMSE - Root Mean Square Error
FCS - Fine Crushed Shell	RTK - Real Time Kinematic
GCP - Ground Control Point	SfM - Structure from Motion
GIS - Geographical Information System	SLR - Sea Level Rise
	TLS - Terrestrial Laser Scanning

Chapter 1

INTRODUCTION

Coastal Maine shell middens are accumulations of centimeters to meters of consumed clam and/or oyster shell, animal bone remains, and artifacts all deposited by Native Americans. Virtually all are threatened by sea-level rise and climate change-related weather, as well as looting and development pressures. There are over 2000 shell middens along the coast of Maine (Spiess, 2017b), and they record up to 5000 years of human coastal occupation and forage-species distribution. Thus, they serve as an archive of cultural and climate information. The shell material within the middens serves as a buffer to Maine's acidic soil and provides excellent preservation of the organic remains. To understand the information contained within these coastal archaeological sites before their destruction, cultural resource management (CRM) decisions must be made relatively quickly with limited monetary resources.

This project outlines a rapid, cost-effective, and minimally invasive technique to survey the areal extent and thickness of shell middens using ground-penetrating radar (GPR). Often, midden investigation involves traditional archaeological methods, that necessitate destructive, expensive, labor- and time-intensive digging. GPR is a survey tool that produces a record of the complex stratigraphy of the site by pushing a cart-mounted antenna and receiver across the surface. A record of the strata below the ground surface is produced as the machine responds to differences in the electromagnetic properties of the materials below that reflect variations in layer composition, compaction, grain size, water content, and/or salinity. Fifteen coastal shell midden sites were examined, with six used to develop a protocol that utilizes GPR as a rapid CRM tool (Figure 1.1). Other studies have utilized GPR on middens (Pluckhahn et al., 2016; Berzins et al., 2014; Pluckhahn et al., 2010; Thompson et al., 2004), but the application of GPR for rapid site evaluation of

midden extent and thickness to inform CRM decisions has not been a focus of earlier studies. Kenady et al. (2018) compiled a table of geophysical studies at archaeological sites with a shell matrix, and concluded that only one study involved site quantification. This paper mapped shell mounds with terrestrial laser scanning (TLS), which can only differentiate topographic features and cannot distinguish shell midden from other materials in the ground (Kenady et al., 2018).

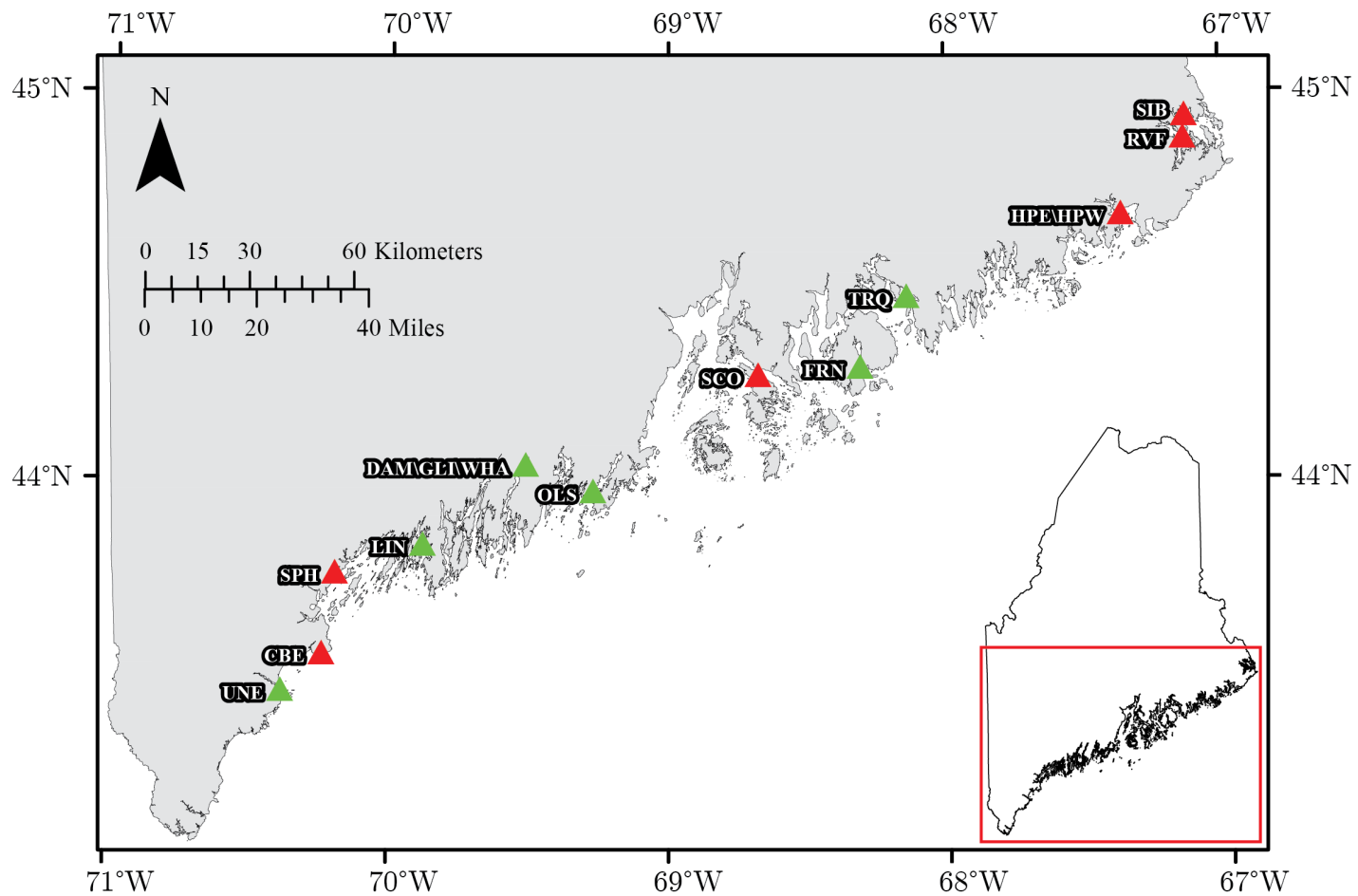


Figure 1.1: Study site locations along the Maine coast. Red triangles represent shell midden sites that were initially considered for GPR survey. These sites furthered method development, but time constraints, vegetation, midden thickness, and/or disturbance prevented GPR survey. Green triangles represent sites where GPR survey was carried out.

In addition to measuring the extent and thickness of a site using GPR, a regularly updated quantitative understanding of erosion at shell midden sites should inform CRM decisions. After identifying issues using time series aerial photography to measure shoreline change on the Maine coast, Structure from Motion (SfM) was explored as a way to identify erosion at a finer resolution and with less error than that produced using aerial photographs. SfM uses digital photography to capture the eroding midden face and processes the data using software to create a digital model, which can be compared to sequential models to identify change (Westoby et al., 2012; Clapuyt et al., 2016). This high-resolution photogrammetry requires a digital camera and open-source or inexpensive software options; thus, the method is accessible to a wide range of users.

This research outlines new applications of existing technology and highlights a successful collaboration between the University of Maine, Maine Sea Grant, and the State of Maine. Project results will inform a statewide plan to monitor, protect, and preserve Maine’s endangered coastal cultural heritage.

1.1 Organization

The following thesis is organized into chapters: 1) Introduction; 2) Background; 3) an invited paper: *Ground-Penetrating Radar as a Cultural Resource Management Tool for Assessment of Eroding Shell Middens*, submitted to the Journal of Conservation and Management of Archaeological Sites; 4) a combined methods/results/discussion section that includes study sites not included in the paper; 5) a paper submitted to Geoarchaeology: *Structure from Motion as a New Method of Analyzing Shoreline Change in Archaeology: An Example from Coastal Maine*; 6) a combined methods/results/discussion section that includes study sites not included in the paper; 7) Conclusions; and Appendices. The Appendices contain sections A through I respectively: A) A Brief Guide to Radar; B) Total Station

Survey; C) GPR Profile Collection and Data Processing Information; D) GPR Profile Location Maps; E) Archaeological Wall Profiles; F) Ground-truth Location Information; G) Stratigraphic Information from Excavation Field Notes; H) GPR Interpretations; and I) Isopach Maps.

Chapter 2

BACKGROUND

2.1 Surficial Geologic and Sea-Level History of Maine

Understanding Maine's unique archaeological record requires knowledge of the regional climatic, surficial geologic, and sea-level history. Maine's surficial geology reflects the interactions of glaciation/deglaciation, isostasy, and global sea level controlled by the advance and retreat of the Late Wisconsinan Laurentide Ice Sheet (LIS). The interactions among ice sheet, advance/recession, and isostasy created a complex sea-level history that shaped the coast. Geomorphic features record sea-level position, and permit the reconstruction of relative sea-level history, which is critical in understanding archaeological site presence or reasons for absence. The study of postglacial through Holocene sea level in the Gulf of Maine involves dating fossils within deglacial geomorphic features above present sea level, identifying and sampling offshore inter/subtidal formerly living things remaining in life position and possessing a known relationship to a tidal datum.

2.1.1 Glaciation

Glacial erosional and depositional features provide evidence for the glaciation and deglaciation of Maine. Glaciation in Maine began approximately 35 ka when the LIS expanded out of Quebec (Thompson and Borns, 2007). Advance of the late Wisconsinan LIS occurred from the northwest to the southeast, with the ice sheet extending over the continental shelf (Thompson, 2015).

2.1.2 Deglaciation/Isostasy and Sea-Level Change

Deglaciation of Maine and the following sea-level changes are reflected in the surficial record of the state. The LIS began a 45-150 m/yr northwest retreat across Maine about 15 ka due to a dramatically warming climate (Thompson, 2015; Borns

et al., 2004). Radiocarbon-dated shell material within marine sediments presently above sea level indicates the rapid deglaciation at 14 ka with emergence from the sea at around 15 ka (Retelle and Weddle, 2001; Borns et al., 2004). Deglaciation sequences composed of moraines and extensive glaciofluvial and glaciomarine features were deposited during this time. The timing of deglaciation is determined through surficial mapping of well exposed glacial features and dating of sediment cores from lakes and ponds (Borns et al., 2004) and offshore basins (Schnitker et al., 2001).

The study of shoreline terraces, unconformity surfaces, and lowstand deltas led to the determination of lower-than-present sea-level positions because their formation required constant oceanic wave action (Shipp et al., 1989, 1991; Belknap and Kelley, 2015; Thompson, 2015). Organic or fossiliferous material found in glaciomarine sediments interfingering with geomorphic features, such as end moraines, permits dating of the landform and a correlation with sea level (Borns et al., 2004). Recent work employed cosmogenic ^{10}Be dating (Gosse and Phillips, 2001) to measure the amount of time rocks have been exposed to sunlight (cosmic rays) (Koester et al., 2017; Hall et al., 2017).

Local isostasy related to deglaciation was the primary factor influencing Late Pleistocene to mid-Holocene sea-level history of Maine (Figure 2.1) The presence of the LIS over Maine caused approximately 240 m (787 ft) of crustal depression (Stuiver and Borns, 1975), allowing the sea to inundate Maine during glacial recession, even though global sea level was lower than present. This resulted in the creation of a local relative sea level highstand in areas 150 km inland from the present-day coast. Figure 2.2 depicts the maximum landward position of the late-glacial sea (Thompson, 2015). After recession of the LIS, and removal of the mass of ice, the land surface rebounded, outpacing eustatic sea-level rise. This

rebound continues to the present, albeit at a much lower rate, lower than the rate of modern sea-level rise, than in early post-glacial times.

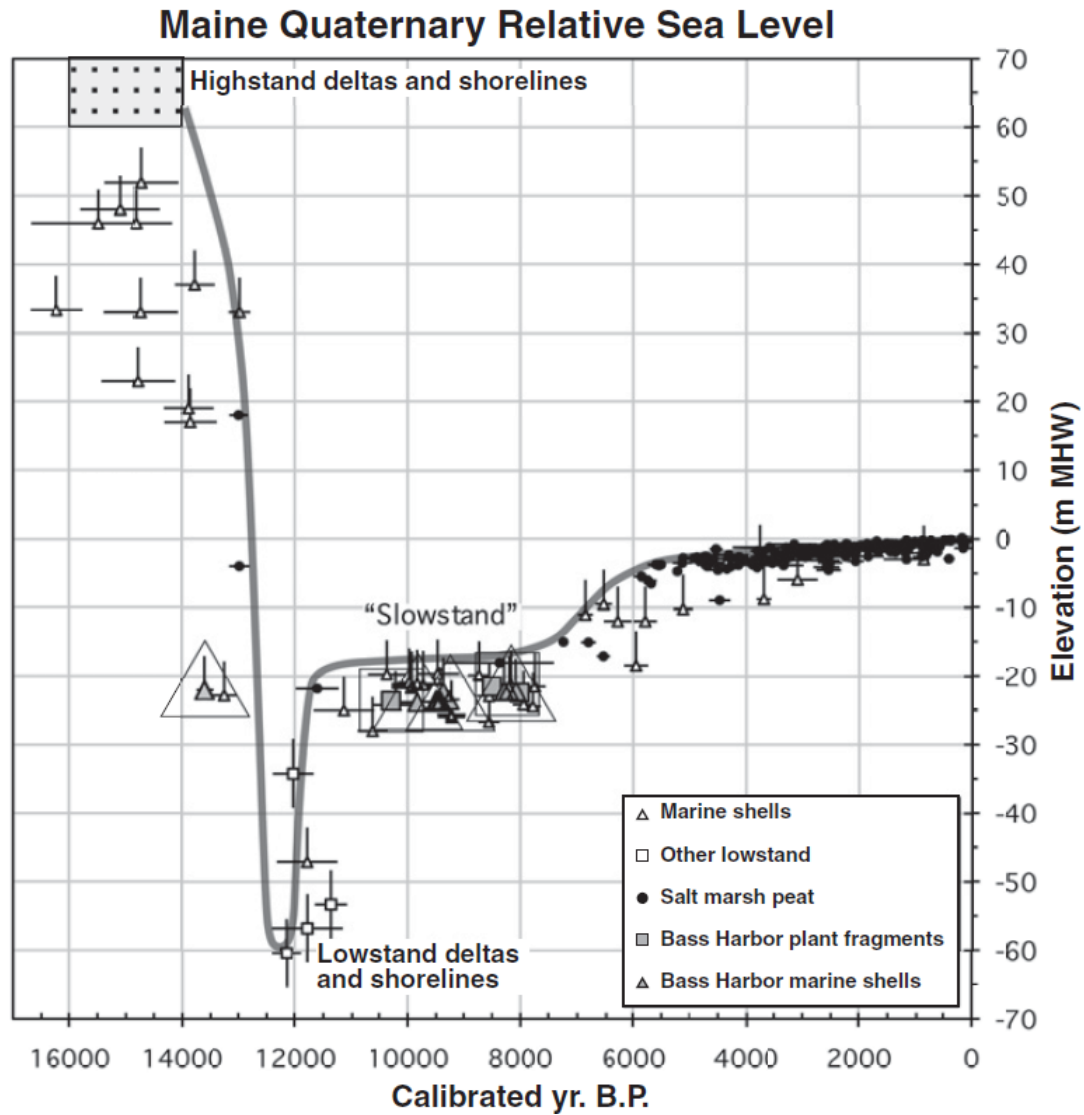


Figure 2.1: Maine relative sea-level curve Kelley et al. (2010).

This rapid isostatic rebound resulted in a relative sea-level fall offshore of central Maine to depths of approximately 60 m below present sea level around 12.5 ka (Belknap et al., 1987; Barnhardt et al., 1995; Kelley et al., 2013). Acceleration of local sea-level rise occurred after 12.5 ka, but leveled off at about -20 m by 11 ka (Barnhardt et al., 1995; Kelley et al., 1992). Radiocarbon dates extracted from vibracores out of the western Gulf of Maine defines a "slowstand" with sea-level rise

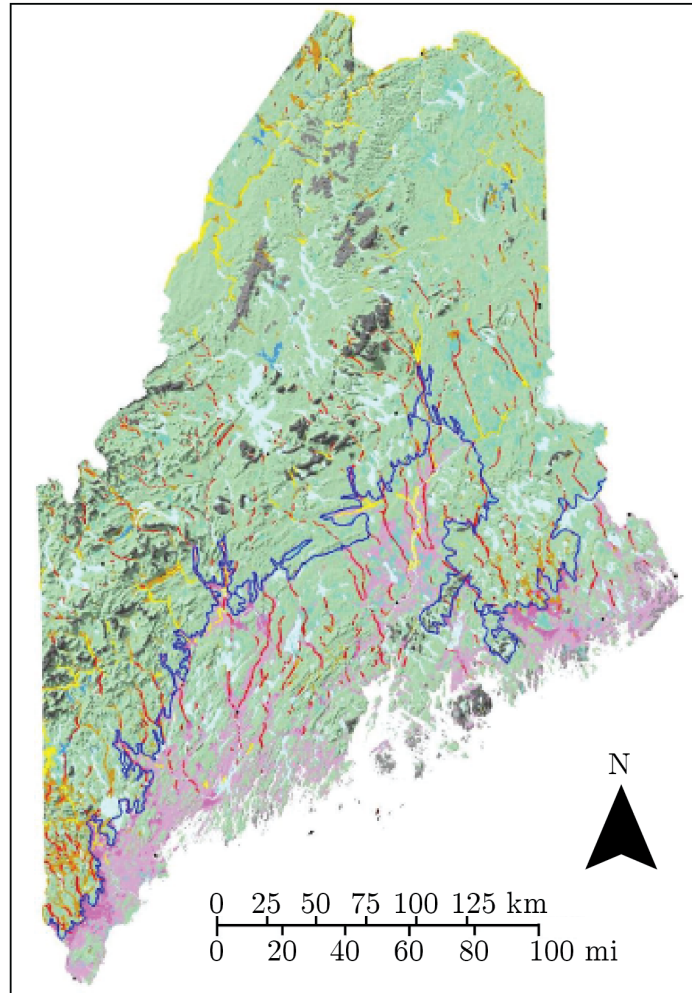


Figure 2.2: Maximum inland extent of late-glacial sea. The blue trace on the map represents the maximum inland extent of late-glacial sea. Modified from (Thompson, 2015).

less than 5 m occurred between 11,500 and 7,500 calendar years before present (Kelley et al., 2010).

The stability in sea level during this slow rise allowed erosion of glacial deposits and construction of spits and protected wetland environments (Kelley et al., 2010). Evidence of human occupation of this once terrestrial surface in the Bass Harbor area of Mount Desert Island, Maine, indicated habitation activity on what was once dry land, now 17-22 m below present sea level (Kelley et al., 2010, 2013). By the mid-Holocene, rising sea-level in nearshore Maine was dominated by increasing

ocean volume and temperature despite continuing uplift of the land (Kelley et al., 2013). Modern local relative sea-level rise along the Maine coast is approximately 2 mm/yr (NOAA).

2.1.2.1 Typical Stratigraphic Section

Polished bedrock was present at the base of most stratigraphic sections the GPR profiles, but it was often too deep for the 500 MHz antennae to resolve in most locations. Basal till often caps the bedrock, and this diamicton is almost ubiquitous in coastal Maine. Along the Maine coast, the late Wisconsinan glaciomarine Presumpscot Formation typically caps till. This was derived from meltwater from ice tunnels choked with silt and clay (Thompson, 2015). The glaciomarine deposit consists predominately of clay with mixed silt, sand, and gravel, and draped the lowlands of Maine approximately 16-12.5 cal. ka. (Belknap and Kelley, 2015). Emergence of the coastal lowlands caused erosion of sand and gravel from glacial features such as eskers and deltas, which resulted in coarse sediment overlying glaciomarine muds originally deposited in deeper water (Thompson, 2015).

2.2 Regional Culture History Periods

2.2.1 Pre-Clovis and Paleoindian Period

Glaciation and a fluctuating relative sea-level during pre-Clovis and Paleoindian periods heavily influenced the presence and/or preservation of the archaeological record in Maine. The earliest cultural periods within the United States are listed in Table 2.1. These periods span the Younger Dryas (12,900-11,600 cal yr BP), a period in which climate shifted to cooler and drier conditions, and ended with warm, dry conditions that persisted until 8000 cal yr BP in the New England-Maritimes (Quebec, the New England states, and New York) (Lothrop et al., 2016).

The presence or absence of a record left by the country's earliest inhabitants depends on a number of factors. Specifically, visibility and preservation of a Paleoindian site in the Northeast is dependent on: burial, submergence (sea or lake), and isostatic rebound with associated marine submergence (Lothrop et al., 2016). Additionally, the degree of sheltering in a marine environment determines site preservation potential (Belknap, 1995; Kelley et al., 2013). Within the Northeast, sites with the potential for a pre-Clovis component include Parson's Island, Miles Point, Cactus Hill, Cinmar, Barton, Mitchell Farm, Burning Tree Mastodon, and Meadowcroft (Lothrop et al., 2016).

Clovis peoples likely inhabited the Northeast beginning around 13,000 cal yr BP, entering from the west, southwest, or south (Lothrop et al., 2016). The Ohio Valley and mid-Atlantic was occupied first, and a northward migration followed (Lothrop et al., 2016). The position of relative sea level in Maine is critical to studying the spatial-temporal relationship of site locations. Price and Spiess (2013) estimated the arrival of Paleoindians to Maine to approximately 12,500 years ago, at the maximum offshore position of shoreline. The largest known Paleoindian gathering site in North America is likely the Bull Brook site in Ipswich, Massachusetts (Robinson et al., 2009).

Paleoindians were part of a highly mobile hunter-gatherer society and lived in small bands; thus, it is difficult to find the record they left behind. The accepted model of Paleoindian occupation in Maine involves the presence of sandy substrates, access to freshwater, and view across a commanding landscape (Spiess et al., 1998, 230). Diagnostic artifacts from the Paleoindian period include fluted points made of exotic, cryptocrystalline materials, obtained from trading or traveling long distances. Evidence for coastal adaptation by Paleoindians in Maine is difficult to prove because of the size of the record left behind and the low site preservation potential. Generally, faunal remains associated with Paleoindian sites in the northeast consist

of fragmented and calcined bones, impacted by site formation processes since the time of deposition (Spiess et al., 1985). An additional problem with preservation involves acidic soils that promote the rapid decomposition of faunal remains.

Table 2.1: Early cultural periods within the United States. Subdivisions after Lothrop et al. (2016).

Cultural Period	Timespan (cal. yr BP)
pre-Clovis	>13,400
Clovis	13,000-12,800 (or 12,615)
early Paleoindian	13,000-12,200
middle Paleoindian	12,200-11,6000
late Paleoindian	11,600-10,000

2.2.2 Archaic Period

The shift from the Paleoindian to Archaic Period occurred as the landscape changed from an open grassland supporting grazers to a wooded environment (Newby et al., 2005). In Maine, the Archaic Period spanned from 8600 to 3700 radiocarbon years BP, making it the longest cultural period in the region (Robinson, 2006). The Maine Archaic Period is divided into Early (10,000-8,000), Middle (8,000-6,000), and Late (6,000-3,000) subperiods (Leach and Belknap, 2007; Spiess, 2018). Coastal archaeological sites from the Early and Middle Archaic subperiods are submerged due to relative sea-level rise (Price and Spiess, 2013). Additionally, the Archaic Period unique to the region contains subdivisions like the Small Stemmed Point culture and Moorhead Phase (5,000-3,800 B.P) of coastal occupation, and the radically different Susquehanna tradition (3,800-2,800 B.P.) (Spiess, 2017b). Approximately 5,000 years ago, burials appear more structured

with respect to their position on the landscape, representing the transition to the Moorehead Burial Tradition (MBT) (Robinson, 2006). The MBT spanned from 5,200 to 3,700 radiocarbon years BP, and contains early, middle, and late phases (Robinson, 2006). These sites are found near seasonal encampments and distant from locations occupied for major portions of the year (Robinson, 2006). The Archaic Period in Maine contains several regionally unique phases, but relative sea-level rise resulted in submergence of coastal sites dating to the period.

Archaic age sites contain a unique cultural record. Overall, the Archaic Period is characterized by highly developed groundstone technology with a limited focus on chipped stone artifacts (Robinson, 2006). Archaic peoples developed tool forms made of local materials, and point styles become more regional. During this time, populations appear to grow, and sites are usually associated with freshwater bodies and streams. Swordfish rostra are also associated with Archaic material culture (Bourque, 2012).

Relatively few shell middens contain an Archaic Period component, resulting from a combination of preservation and visibility. The construction of shell middens during the Late Archaic Period (e.g., Turner Farm (Spiess and Lewis, 2001), Golden Cove (Bourque, 1971, cited in Spiess, 1985:112)) occurred, but most shell middens date to the Ceramic Period defined by Sanger and Petersen (1991) (Belcher and Sanger, 2017).

There is some indication of the preservation of Early Archaic Period occupations in submerged portions of the Maine nearshore. For example, areas attractive for habitation during the Early Archaic in the Bass Harbor area are currently 17-22 meters below current sea level (Kelley et al., 2010). Preservation factors for these Archaic Period coastal/submerged sites are related to Maine's complex sea-level history (Kelley et al., 2010). Price and Spiess (2013) worked with submerged archaeological finds in the Gulf of Maine and grouped them by 1) items dropped

from fishing events; 2) isolated discoveries in drowned terrestrial environments; and 3) archaeological sites. Methods utilized for identifying potential submerged sites from the Archaic Period include bathymetric mapping, seismic reflection, and vibracoring. Identifying and studying submerged coastal archaeological sites of the Archaic necessitates alternative approaches and an understanding of the region's sea-level history.

2.2.3 Ceramic Period

Often referred to as the Woodland or Maritime Woodland period elsewhere, the term "Ceramic Period" is unique to Maine and the Maritimes. In the far Northeast, ceramic artifacts offer a basis for chronology, as their characteristics evolved through the relatively long time-span (Sanger and Petersen, 1991)(Table 2.2). A chronology for stone tools of the Ceramic Period does not exist for Maine, though "Adena" or "Meadowood" point references occur, they are inconsistent within the literature (Newsom, 2017). Thus, in absence of pottery or reliable dates, an Early Ceramic Period site might not be recognized as such (Newsom, 2017). This period begins as early as ca. 3,050 B.P. in the far Northeast and spans to ca. 400 B.P. (Sanger and Petersen, 1991). Additionally, the period is subdivided into Early, Middle, and Late Ceramic periods (Spiess, 2017b) (Table 2.2).

Ceramic Period shell middens dominate the coast of Maine. Of the approximately 2,000 shell midden sites along the Maine coast, a majority of them span a 1,800-year period of time from 2,200 to 400 B.P., or the Middle to Late Ceramic Periods (Spiess, 2017b). At present, support for Ceramic period people occupying coastal sites all year-round is limited by too few vertebrate season-of-harvest studies at coastal shell midden sites along the coast of Maine (Spiess, 2017b). Sea-level rise and associated erosion in the time since shell midden construction have essentially destroyed earlier coastal sites.

The end of the Ceramic Period is marked by the disappearance of aboriginal ceramic manufacturing across the far Northeast due to contact with early European settlers (Sanger and Petersen, 1991).

2.2.4 Contact Period

Representing the start of European settlement and utilization of the region, the Contact Period spans from ca. 400 B.P. to 200 B.P. The archaeological signatures of the Early Contact Period are poorly understood in comparison to the Ceramic Period (Spiess, 1995). The termination at 200 B.P. coincides with the abandonment of traditional practices preserved in the material record (Sanger and Petersen, 1991), which contains European goods.

Because contact often occurred on the coast as opposed to the interior, shell middens of the Ceramic Period have the potential to record periods associated with European colonization (Newsom, 2017). Though written records exist, there are still issues related to understanding the Contact Period cultures within the Gulf of Maine. George Waymouth and Samuel de Champlain ushered in an era of sustained European contact within the Gulf of Maine, circa 1604-1605 (Spiess, 1995). European and French written records exist for multiple cultures along the Gulf of Maine, but the place locations and cultural groups are often difficult to identify (Spiess, 1995). Issues arise in the ethnonyms used, but Prins (1988) and Bourque (1989) have provided insight via rereading of original sources (Spiess, 1995).

Table 2.2: Ceramic Period Subdivisions after Sanger and Petersen (1991). Table after Newsom (2017).

Ceramic Period Designation (yr BP)	Sanger and Petersen (1991) Subdivision	Characteristics of Ceramic Material
Contact period (ca. 400-200 B.P.)	Ceramic Period 7	dominantly grit temper; thin vessel lot walls; collared rims; incision and fabric paddling applied to exterior
late Late Ceramic period (ca. 650-400 B.P.)	Ceramic Period 6	grit or shell/organic temper; undecorated bodies; globular bodies; decreased vessel lot wall thickness; fabric paddling appears; collared rims with geometric or chevron motifs; cord-wrapped stick and linear punctate exterior decoration
early Late Ceramic period (ca. 950-650 B.P.)	Ceramic Period 5	predominately shell/organic temper; decrease in diameter of punctate and cordage; excurve to straight simple rim; circular punctate and simple vertical cord-wrapped stick designs on exterior
late Middle Ceramic period (ca. 1350-950 B.P.)	Ceramic Period 4	shell/organic temper first appears; conoidal vessel lots; slightly excurve to simple rims; exterior upper portion of vessel only: typically has cord-wrapped stick and cylindrical punctate designs
middle Middle Ceramic period (ca. 1650-1350 B.P.)	Ceramic Period 3	grit temper; thicker vessel lot walls; thickened rims or low collars; pseudo-scallop disappears; circular and linear punctates; dentate exterior designs with dentate tooth size increasing
early Middle Ceramic period (ca. 2150-1650 B.P.)	Ceramic Period 2	grit temper; castellated rims appear; pseudo-scallop shell; linear designs; incision; non-standardized punctate; stamped and/or rocked design
Early Ceramic period (ca. 3050-2150 B.P.)	Ceramic Period 1	grit temper; conoidal base; simple rim; interior/exterior surfaces fabric-impressed

2.3 Maine Shell Middens

Shell middens typical of the region are composed of centimeters to meters of soft-shell clam (*Mya arenaria*) and/or oyster (*Crassostrea virginica*) shells, faunal remains of extant and extinct species, and cultural material. Quahog (*Mercenaria mercenaria*) are occasionally found in older layers. Shell middens and alluvial sites in Maine contain stratified deposits; thus, they are ideal for archaeological investigation (Spiess, 2018). Complex stratigraphy results from the spatially heterogeneous dumping of shell and other cultural material, preventing the development of continuous strata across a shell midden site (Sanger, 1981; Skinas, 1987; Belcher, 1988; Belcher and Sanger, 2017). A unique environment for the preservation of organic material is provided by the chemical buffering effect of the weathering shells in the midden. This neutral to alkaline pH is atypical of Maine's acidic soils, and acts to preserve a more complete paleoenvironmental and cultural record than that found in most interior sites within the state. Though it is rare, a coastal site with decent preservation of faunal material can exist in absence of the buffering effect provided by the shell midden, an example of which is the Nahanda site (Callum, 1994). The presence of shell enhances the preservation potential of organic remains at archaeological sites in Maine.

Shell middens in Maine are found in a variety of other geomorphic settings. The Glidden Midden in Newcastle, Maine, is situated along the tidally influenced Damariscotta River, and is one of the largest middens, by volume, on the New England coast. This and other middens along the upper estuary are unusual in that they are composed of oyster (*Crassostrea virginica*) shells and are not in a strictly marine setting. The majority of Maine's middens are composed of clamshells (*Mya arenaria*). These middens occur on bluffs of glacial sediment, beach, or bedrock outcrop.

Shell middens pre-dating the Ceramic Period are atypical along the Maine coast. The Golden Cove site (29-38) on Vinalhaven Island is an exception and contains uneroded evidence of coastal occupation where several areas at the midden base date to 7,500 years ago (Bourque, 1971, cited in Spiess, 1985:112). Additionally, the Turner Farm site located on North Haven Island in Penobscot Bay, Maine, contains cultural material dating to 5,300 BP (Spiess and Lewis, 2001).

2.3.1 Site Preservation

The detailed sea-level chronology for the coast of Maine serves as a guide for the highest probability locations for the preservation of coastal occupation sites, and also highlights potential time periods for preservation and erosion potential. The relative absence of middens with an Archaic component is likely directly related to erosion caused by sea-level rise.

Middens in Maine are threatened by natural and human disturbance, as well as climate-induced sea-level rise. Bioturbation, specifically rodent activity, tree falls, and root growth also impact site stratigraphy within shell middens (Mack, 1994). Modern human impacts to middens include looting and development pressures, but past mining for chicken feed, lime, and road fill have also destroyed middens (Sanger and Sanger Elson, 1986). As early as 1912, researchers noted coastal erosion impacts on sites (Spiess, 1985). A 1987 annual report Maine State Historic Preservation Commission (MHPC) recognized the potential impact of sea-level rise on archaeological sites (Shettleworth, 1987).

2.3.2 Archaeological Practice at Regional Shell Middens Through Time

Approaches to shell midden investigation in Maine have evolved through time. Early scientific interest in shell middens was initiated by state geologist C.T. Jackson in 1839 who was driven by an economic desire for the shell within the

Damariscotta oyster shell midden (Spiess, 1985). At the turn of the 19th century, Maine shell midden investigation frequently involved rapid site excavation, either focused on retrieving artifacts or working just ahead of mining, and a lack of published documentation (Spiess, 1985). An often criticized early influence on Maine archaeology, W.K. Moorehead, began surveying areas in Maine in May, 1912 (Spiess, 1985). Moorehead and his crew excavated sites rapidly, and focused on the contents as opposed to the context. For Moorehead's account of a portion of his time in Maine see Moorehead (1922).

Upon the hiring of Dean Snow by the University of Maine Orono (UMO) in 1966, institutions within the state saw a greater focus on the expansion of Maine archaeology (Spiess, 1985). Beginning in the 1970's through to the early 1990's, David Sanger and his University of Maine students focused on a uniform approach to shell midden archaeological practices (Belcher and Sanger, 2017). The analyses applied to middens by Sanger and his students included column sampling, whole-unit analysis, qualitative/quantitative descriptions, and facies analysis (Belcher and Sanger, 2017). Practices for gathering data on a shell middens continue to evolve, as evidenced by this project.

Landscape- and site-scale archaeology are both critical to understanding the site formation processes unique to shell middens. Kellogg's statistical analyses of coastal shell midden site locations (Kellogg, 1987, 1994, 1995) indicated that over 80% are found on even, well-drained ground, adjacent to a sand, gravel, or cobble beach, facing east through south or southwest (Spiess, 2017b). Often, protection against winter winds from the northwest determined site location (Kellogg, 1982). Also, southerly aspects offer the most sun through all seasons and relief from summer insects via breezes from the south (Kellogg, 1982). Narrowing in to the site-scale, shell midden stratigraphy is the direct product of human decision, and is therefore complex and discontinuous across a site (Sanger, 1981). Sanger's model of midden

occupation states that a generalized dumping area, up to a meter thick and containing mainly discarded artifacts and faunal remains, is found along the beachward portion of the site, and house floors and features are typically near the rear, or landward side (Sanger, 1981). Additionally, there are often greasy, black layers within or at the base of most shell middens in the northeast, which are attributed to decomposed organic matters (Sanger, 1981). Human choice influenced site formation, and is critical to understanding an individual shell midden.

Geoarchaeological study of shell middens and their landscape relationships began in the 1980's through collaborations and student research at the University of Maine. Sanger and Belknap (1987) reconstructed paleogeography and preservation potential of the Glidden Midden and Muscongus Bay sites. Belknap (1995) used coring and marine geophysics to delineate paleogeography and preservation potential at the Turner Farm site and surrounding areas of Penobscot Bay. Young (1990) and Young et al. (1992) used geophysics and coring to study Pemaquid Beach and Johns Bay in relationship to archaeological sites. Davies (1992) concentrated on the Glidden midden in a study of preservation potential in the upper Damariscotta estuary. Leach (2007) and Leach and Belknap (2007) used extensive geophysical and coring investigations to model archaeological site choices and preservation potential in the Damariscotta River, but were unable to identify intact submerged sites. Kelley et al. (2010, 2013) discovered potential sites submerged off Bass Harbor that relate to Middle Archaic artifacts recovered by scallop draggers. The reconstruction of submerged landscapes, let alone specific archaeological sites, is difficult, reflecting a low preservation potential, but modern geophysical and coring techniques are beginning to make inroads in such research.

Approaches to studying shell middens are varied, and developing. This project represents the first known application of GPR as a cultural resource management (CRM) tool for the delineation of shell midden extent and thickness. Future research

at shell middens in Maine could include analyses of ancient or environmental DNA (aDNA or eDNA). Ancient DNA are found in nonliving material like bone, tissue, paleofeces, plant remains, and seeds; whereas, environmental DNA are in soil and water samples (Hofman et al., 2015). Grealy et al. (2016) extracted aDNA from a 100-300 ya coastal midden in Madagascar, and found 23 families of fish. In soil, eDNA has been found to persist for decades to centuries following deposition (Andersen et al., 2012; Yoccoz et al., 2012, cited in Thomsen and Willerslev, 2015).

2.4 Site Reports

Initial site selection prior to field reconnaissance was accomplished in collaboration with Maine Historic Preservation Commission (MHPC) Senior Archaeologist, Arthur Spiess. Data on site integrity, composition, shell midden thickness and stratigraphy documented during excavation, and areal extent of the shell midden factored into the initial selection. Sites with data from previous archaeological investigation(s) were chosen because the existing ground-truth data precluded additional site disturbance. Out of the 15 sites selected for the study, GPR survey was carried out at 6 (Figure 2.3). A six-step protocol was developed for shell midden evaluation using GPR. Various factors contributed to the inability to apply the complete protocol to all of the sites, including but not limited to: site integrity, terrain and vegetation conducive for successful GPR survey, and time limitations. Each of the following sites, through their unique attributes, informed the development of the methodology.

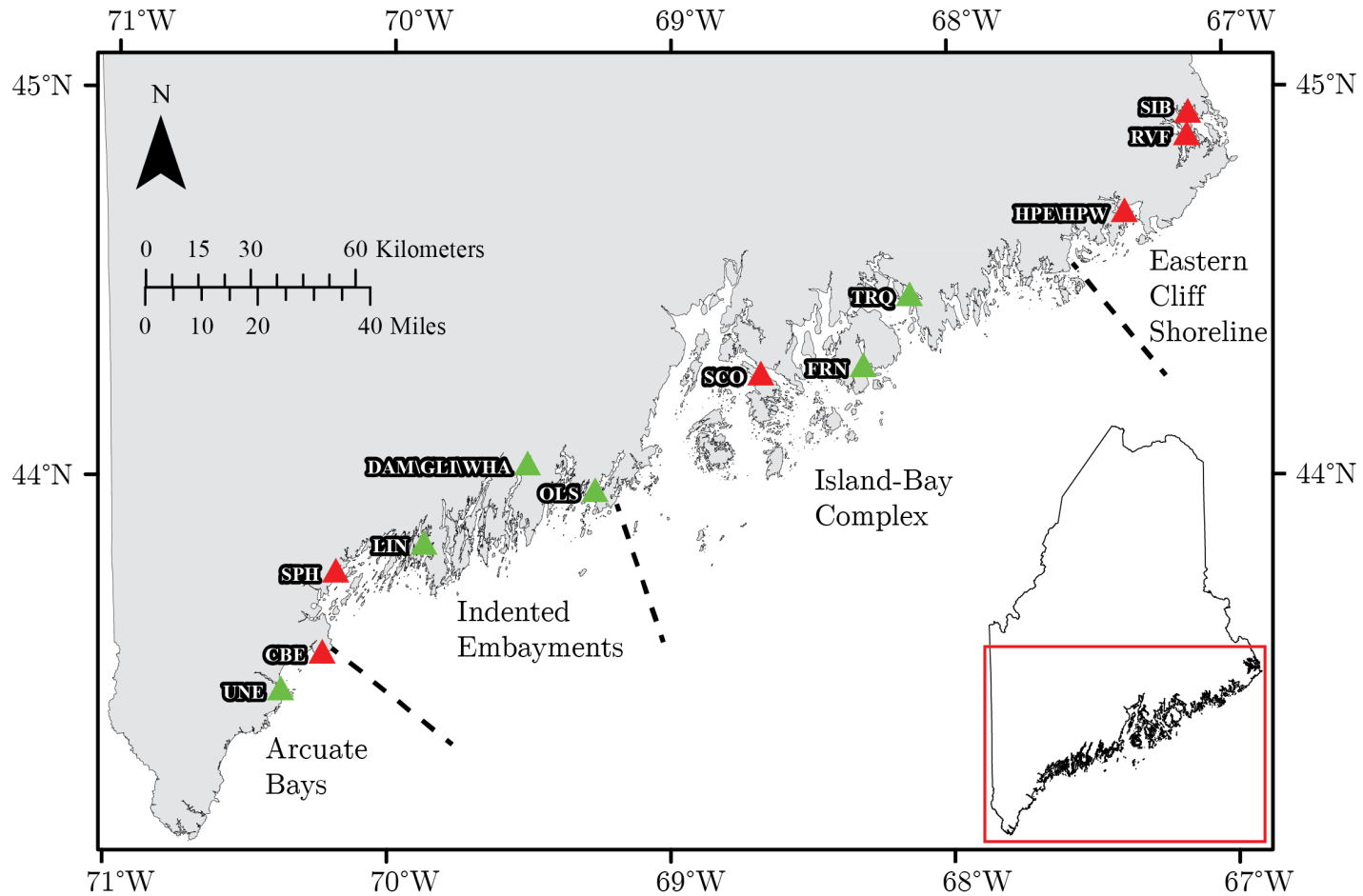


Figure 2.3: Study site locations along the Maine coast and the coastal compartments identified by Kelley (1987). Red triangles represent shell midden sites that were initially considered for GPR survey. These sites furthered method development, but time constraints, vegetation, midden thickness, and/or disturbance prevented GPR survey. Green triangles represent sites where GPR survey was carried out.

The 15 sites included in the study are arranged from south to north in the following site descriptions (Figure 2.3). The coastline of Maine is divided into coastal compartments, which each bear the heavy overprint of the last glaciation and are controlled by bedrock geology. The four coastal compartments are: arcuate bays, indented embayments, an island-bay complex, and the eastern cliff shoreline (Figure 2.3) (Kelley, 1987). In the initial stages of this study, it was thought that the attributes of each coastal compartment would influence erosional processes at the site-scale. However, it was determined that local factors such as coastal morphology, wave fetch, and storm duration and energy exhibited a greater control on site loss. The coastal compartment in which each site falls is mentioned in each site description, but the erosional effect was not observable at the site-scale.

2.4.1 University of New England (UNE, Site 5.06)

The University of New England site is located on the UNE campus in Biddeford, ME, and sits at the mouth of the Saco River. Bedrock at the site is the Berwick Formation gneiss and granofels (Osberg et al., 1985). Surficial geologic materials are marine regressive sand deposits with massive to stratified and cross-stratified well-sorted sand (Hildreth, 2007). The sand unit typically has a gradational basal contact with the Presumpscot Formation (Hildreth, 2007). Examination of the sections exposed at the site showed colluvial material over sand with distinct cultural layers.

Excavation at the UNE site was likely initiated in the 1960's or 1970's by Fred Warner of St. Francis College, but data and artifacts associated with the excavations are lost (Baker, personal communication to Arthur Anderson). Earlier excavations undertaken by someone connected with the Museum of Fine Arts in Boston may have taken place, but the only substantiating evidence is from brief mention in a newspaper (Baker, personal communication to Arthur Anderson).

Based on the limited surviving data, it remains uncertain if these excavations occurred at the site now designated as ME 5.06 or if they took place elsewhere on the UNE campus (Anderson, 2018).

In 1988, Emerson Baker began trial excavations while teaching an archaeology course at UNE. Richard Will of TRC, Inc. of Ellsworth, ME conducted an archaeological survey of the area prior to the construction of the Marine Science Center in 1999. Following the initial survey, several areas that would be destroyed during the Center's construction were excavated (Will and Mack, 1998; Mack and Will, 1999, 2000). Will returned to lead a field school with the Abbe Museum of Bar Harbor in 1999 and 2005, where the focus of excavation was near the modern day beach. With the exception of analysis on faunal remains from 1999 (Lore, 2004, 2006), results from the efforts are not formally published (Anderson, 2018).

2.4.2 Crescent Beach (CBE, Site 9.98)

The Crescent Beach State Park site (9.98) is in the Cape Elizabeth 7.5-minute quadrangle. Site 9.98 is in Cape Elizabeth, 800 m northeast of the Richmond Island breakwater, and adjacent to the Crescent Beach State Park boundary in Cumberland County, Maine. Underlying bedrock at the site is Middle-Late Ordovician Scarboro Formation of the Casco Bay Group, and is a very fine-grained, rusty and non-rusty weathering muscovite-biotite-chlorite-garnet-quartz phyllite (Hussey, 2012). Surficial materials underlying what was once midden were mapped as the fine-grained glaciomarine Presumpscot Fm. (Thompson and Borns, 1985), and thin drift (Clinch and Thompson, 1999). The site faces south on a high energy, gravel beach, overtopped by a grassy field.

The site was recorded as intermittent shell midden, with limited amounts of intermittent, thin shell midden no more than 2 m back from the eroding bank. Black/dark anthropogenic soil (without shell) 40 cm to 80 cm thick was noted with

an areal extent of 80 m by 15 m (Spiess, 2016a). Deposits here were generally Ceramic and Contact in age and included a bone artifact, a piece of trade copper, a non-stemmed biface, grit and shell tempered sherds, and scattered human bones (Spiess, 2016b). Severe erosion has occurred since the site was originally recorded in 1977 on a Maine archaeological survey form (Maine Historic Preservation Commission records), and the site is no longer present (Maine’s coastal storm of record occurred in the winter of 1978). The Crescent Beach site is an example of why this project is vital for assessing and documenting Maine coastal archaeology before natural and human processes erase the record.

2.4.3 Spear’s Hill (SPH, Site 14.169)

The Spear’s Hill site (14.169) is located in the Yarmouth 7.5-minute quadrangle in the town of Cumberland, Cumberland County, Maine. Site 14.169 faces east and sits several meters inland from a beach. Bedrock at the site is Ordovician-Precambrian Cushing Formation, and is made up of mafic to felsic volcanic rocks (Osberg et al., 1985). Surficial materials underlying the site are the Presumpscot Fm. (Retelle, 1999), but archaeological testing revealed cobbles, gravelly, sandy silt, representing wave modification of the fine-grained glaciomarine deposit (Spiess, 2018). The shoreward extent of the site is categorized as an unstable ledge bluff face (Bryant et al., 2002b). The site area is heavily forested, and thickness of shell (*Mya arenaria*) is likely only 20 cm with an aerial extent of 50 by 30 m (Spiess, 2016a). Impacts to the Spear’s Hill site include a bath house built prior to WW II, as well as a carriage road that extended over the site in the 1920’s (Spiess, 2018).

2.4.4 Long Island North (LIN, Site 15.95)

The Long Island North site (15.95) is located in the Orrs Island 7.5-minute quadrangle. Site 15.95 is located in the town of Harpswell, Cumberland County,

Maine, and faces east. The site is partially protected by an offshore ledge in the upper estuary in the Casco Bay area (Bryant et al., 2002a). Underlying bedrock is mapped as metamorphosed interbedded pelite and sandstone of the Ordovician-Precambrian Cape Elizabeth Formation (Osberg et al., 1985). Surficial geology underlying the shell midden is mapped as undifferentiated thin drift with many bedrock outcrops (Thompson and Borns, 1985). An open lawn tops the clam-shell (*Mya arenaria*) midden which is typically 50 cm to 65 cm and up to 1 m thick (Spiess, 2016a). Deposits at the Long Island North site date to Early-Middle Ceramic (Spiess, 2016a).

2.4.5 Glidden and Whaleback (GLI/WHA, Sites 26.1 and 26.2)

The Glidden Midden (26.1) and Whaleback (26.2) sites are in the Damariscotta 7.5-minute quadrangle in the towns of Newcastle and Damariscotta (respectively), Lincoln County, Maine. Almost entirely obliterated by a commercial mining operation in the 1880's, the Whaleback midden was once up to 5 m thick (Sanger and Sanger Elson, 1986). Glidden and Whaleback sit near the head of the Damariscotta River in a tidal estuary in a drowned river valley created by Holocene sea-level rise (Belknap and Shipp, 1986; Spiess, 1998). Whaleback midden sits on the eastern side of the Damariscotta River facing west and Glidden sits on the west side and faces east. Both sites are in the indented shoreline coastal compartment (Kelley, 1987).

Underlying bedrock is of the Silurian Bucksport Formation, a medium-bedded, light to medium gray, quartz-feldspar-biotite granofels with interbedded medium green to greenish-gray, diopside calc-silicate granofels (Grover and Newberg, 2016). Fine-grained glaciomarine Presumpscot Fm. overlies the irregular surface of glacial till at Whaleback. Additionally, Glidden is in an area mapped as an end moraine ridge composed of till potentially in combination with sand and gravel (Thompson,

2009), but field observation supports the presence of Presumpscot Fm. underlying the shell midden.

Whaleback and Glidden are both oyster middens. The application of geophysics to the geoarchaeology along and within the Damariscotta River was the focus of a master's thesis (Leach, 2007). Prior to Leach's work, Davies (1992) set out to understand the impact of local sea-level rise on the preservation potential of shell middens in the Damariscotta estuary. Refer to Leach (2007) and Leach (2008) for further details on the application of geophysics and vibracoring within the Damariscotta estuary. Radiocarbon dates of 1,800 BP (+/- 250) and 2,100 BP (+/- 250) came from Glidden Midden (Spiess, 2016b). Similarly, Whaleback deposits date from Middle to Late Ceramic with midden formation beginning 2,000 years ago (Spiess, 2016b). For a detailed account of the history of Glidden and Whaleback middens, refer to Sanger and Sanger (1986).

2.4.6 Oyster Farm (DAM, Site 26.15)

Site 26.15 is located in the Damariscotta 7.5-minute quadrangle in the town of Damariscotta, Lincoln County, Maine. Site location is approximately 370 m north of the Glidden and Whaleback midden sites. The site occupies a south facing point adjacent to the confluence of a small tidal stream and the Damariscotta River. Along with Glidden and Whaleback, the site is near the head of the Damariscotta River in a tidal estuary in a drowned river valley created by Holocene sea-level rise (Spiess, 1998). The bedrock and surficial material description for Glidden and Whaleback middens apply to this site as it is less than 400 m away. Material directly underlying the shell midden is Presumpscot Fm. Vegetation includes pasture land and dense milkweed (*Asclepias syriaca*) plants, making GPR survey difficult beyond a series of well-mowed paths.

Shell midden at this site measured approximately 1.1 m deep in a 1996 testpit and was predominantly composed of oyster shell. Site extent along the shore of the Damariscotta was documented during archaeological survey as approximately 150 m, and 75 m along the bank of the tidal creek with shell thickest at the southern point (Spiess, 1998). Of the 100 ceramic fragments found, all were middle Ceramic age CP-2 or CP-3 (Spiess, 1998).

Artifacts found also included charcoal, fire-cracked rock, a potential hearth, and bone tools (a beaver incisor graver, a fragment of a bone point, and worked bone) (Spiess, 1998). Faunal remains discovered at this site consisted of a cod otolith, bird and fish bone, and various large mammal bone fragments (Spiess, 1998). Lithics found include a rhyolite and a chert scraper, a stemmed fragment of a point, and a few flakes (Spiess, 1998). There is not a Contact Period component at this site (Spiess, 2016b).

The point is eroding rapidly with a vertical erosion scarp that exposes shell and silty soil (Spiess, 1998). Impacts to the site from the adjacent oyster farm operation appear minimal.

2.4.7 Olson (OLS, Site 17.13)

The Olson site (17.13) is located in the Friendship 7.5-minute quadrangle. Facing south to Maple Juice Cove, site 17.13 is in the town of Cushing, Knox County, Maine. Site 17.13 occupies a stable low coastal bluff (Sinson et al., 2002). An open grassy field covers the site, and it is adjacent to a low-energy beach (Timson, 1974). Underlying bedrock is Devonian granite (Osberg et al., 1985) with xenoliths and associated metasedimentary rocks. Surficial materials underlying the midden are till.

Excavation at the site occurred in 1982 and 1985 (Spiess, 2016a). Wigwam floors and associated post stains were found during the 1985 excavation (Spiess,

2016a). Shell midden ranges from 50 cm to 1 m thick, and areal extent is 150 m by 19 m (Spiess, 2016a). The majority of excavated material was approximately 2,400 years of age to Contact period (Spiess, 2016b). Surface evidence of looting was noted (Spiess, 2016b) along with active erosion as a slump block with midden was present on the beach during a 6/30/2016 visit.

2.4.8 Scott's Midden (SCO, Site 42.82)

Scott's Midden (42.82) is located within the Sargentville 7.5-minute quadrangle. Site 42.82 is north facing, and sits on the northernmost point of Deer Isle. Site 42.82 is adjacent to a gravel and shell beach on a 0.25 m stable coastal bluff (Kebblinsky et al., 2002), facing the north, with a wetland on the eastern side. Bedrock is mapped as Devonian Castine Formation (Osberg et al., 1985). Geologic material underlying the midden is fine-grained glaciomarine Presumpscot Fm. (Thompson and Borns, 1985). Alder, apple trees, goldenrod, and grasses cover the site.

The shell midden at the site appears as a thin layer just below the surface and ranges from 15 cm to 50 cm thick (Spiess, 2016b). Midden areal extent is reported as approximately 15 m by 22 m (Cox, 2009). Deposits at the site are Early Ceramic Period and potential Early Contact Period (Cox, 2009). Artifacts recovered include stone tools, early Ceramic Period pottery, and bone (Cox, 2009). Several pot-hunters holes are documented, and the walking path cuts straight through the site. Field schools excavated the area in 2007 and 2008 (Spiess, 2016b).

2.4.9 Fernald Point (FRN, Site 43.24)

The Fernald Point site (43.24) is located in the Southwest Harbor 7.5-minute quadrangle. Site 43.24 is south facing and sits on the western side of the narrows of Somes Sound, on Fernald Point (Sanger et al., 1980). The site is located in Southwest Harbor, Hancock County on Mount Desert Island, Maine. The beach adjacent to the site consists of shell and rocks ranging in size from boulder to sand,

and is classified as low energy (Timson, 1976b). The site is on a non-bluff shoreline (Dickson, 2005), and is covered by a grassy field, which had been plowed historically. Bedrock is Devonian granite with an intrusive breccia texture (Osberg et al., 1985). The site lies on a boundary of fine-grained glaciomarine deposits and thin till (Braun et al., 2016), and is located near a moraine ridge (Thompson and Borns, 1985).

The Fernald Point shell midden site is 65 cm thick and is 100 m by 40 m in areal extent (Spiess, 2016a). Site 43.24 potentially represents pre- and post-European contact period culture (Sanger et al., 1980). Excavation at the site prior to 1980 yielded a hearth, burials, and a possible house floor (Sanger et al., 1980). Fernald Point is impacted by erosion through wave action.

2.4.10 Tranquility Farm (TRQ, Site 44.12a)

The Tranquility Farm site (44.12a) is located in the Bar Harbor 7.5-minute quadrangle. The south-facing site is located on the east side of Flanders Bay in Gouldsboro, Hancock County, Maine. The site is a grassy field on top of a stable bluff varying between 1 and 3 meters high (Kebblinsky et al., 2006). The bedrock is Devonian-Silurian Bar Harbor Formation, a calcareous feldspathic sandstone (Osberg et al., 1985). The midden lies over till (Thompson and Borns, 1985; Borns, 1974).

This shell midden site was originally reported as 150 m by 30 m with shell up to 1-m thick (Spiess, 2016b). Previous excavation of the site by W.K. Moorehead occurred around 1935, and more recently the Abbe Museum field school in the 1990's and 2010-2015 (Spiess, 2018). The south facing bank is eroding at a moderate rate (Spiess, 2016b). Evidence of a potential storm event which caused heavy erosion at the base of the bluff was noted when the site was visited on 6/28/2016. Additional evidence for shoreline retreat included rosebushes from the bluff top sitting on the beach approximately 3 m below.

2.4.11 Holmes Point East and West (HPE/HPW, Sites 62-6 and 62-8)

Holmes Point East (62-6) and Holmes Point West (62-8) are approximately 300 m apart and sit within the Machias Bay 7.5-minute quadrangle. The sites have a southern aspect and are located on the east side of Machias Bay in Machiasport, Washington County, Maine. Holmes Point East is on an eroding bluff above and immediately adjacent to a mixed sand and gravel beach, near a coarse-grained intertidal flat (Timson, 1976a). Holmes Point West is adjacent to a beach with abundant gravel near mud flats (Timson, 1976a). Underlying bedrock at site 62-6 and 62-8 is the basalt member of the Silurian Leighton Formation (Osberg et al., 1985). The fine-grained glaciomarine Presumpscot Fm is present beneath both the Holmes Point East and West shell middens (Thompson and Borns, 1985).

The University of Maine field school excavated at both sites in 1973, and Hryn timer and Robinson (2012) focused on site 62-6 for their study of gravel floors. According to Hryn timer and Robinson (2012), the gravel at 62-8 severely inhibited gravel floor identification. Similarly, Bird (2017) mentioned that the Holmes Point West site is located on a wave-cut terrace, which contains wave-washed gravel, and directly overlies the glaciomarine Presumpscot Fm. At site 62-6, 15 cm gravel floors and 20 cm to 30 cm thick shell midden start approximately 160 cm below datum and end approximately 180 cm to 190 cm below datum (Hryn timer and Robinson, 2012). Holmes Point East deposits date to the Ceramic Period Hryn timer and Robinson (2012). Charcoal, fire-cracked rocks, and soft-shelled clam (*Mya arenaria*) chondrophores were found at Holmes Point East, and an engraved pebble was found at Holmes Point West Hryn timer and Robinson (2012). Thin shell midden at Holmes Point East is bioturbated, and both sites are disturbed due to looting/pot-hunting (Hryn timer and Robinson, 2012; Bird, 2017).

2.4.12 Reversing Falls (RVF, Site 80.15)

The Reversing Falls site (80.15) is located in the Pembroke 7.5-minute quadrangle. The site has a southern aspect and sits at the tip of Mahar Point in Reversing Falls Park in Pembroke, Washington County, Maine. The geomorphic setting is a salty bay mainland (Hryn timer and Webb, 2014) adjacent to a rocky beach on a 10 cm to 20 cm bank covered by a grassy field. Underlying bedrock is gabbro/diorite/ultramafic intrusive igneous rocks (Osberg et al., 1985). Materials underlying the midden are fine-grained glaciomarine deposits of the Presumpscot Fm. (Thompson and Borns, 1985).

Site 80.15 is a clam (*Mya arenaria*) and mussel shell midden with black soil (Spiess, 2016a). Areal extent was recorded as 100 m by 15 m with shell 50 cm to 60 cm deep (Spiess, 2016a). The site has Middle and Late Ceramic (Table 2.2), and Terminal Archaic components (3,800-3,000 BP) (Hryn timer and Webb, 2014). Artifacts found include lithic debitage, two Terminal Archaic bifaces, ceramic sherds, unmodified vertebrate animal bone, and *M. arenaria* shell (Hryn timer and Webb, 2014). Spiess et al. (1990) noted rapid erosion at this site.

2.4.13 Sipp Bay (SIB, Site 80.25)

The Sipp Bay archaeological site (80.25) is split between the Pembroke and Eastport 7.5-minute quadrangles. Site 80.25 is located within the Sipp Bay Maine Coast Heritage Trust Preserve in the town of Perry, Washington County, Maine. Underlying bedrock is the Lower Devonian Eastport Formation, composed of mafic to felsic volcanic rock (Osberg et al., 1985), which crops out commonly. Till and thin drift underlie the shell midden (Thompson and Borns, 1985).

The main shell midden site is at the apex of a crescent beach and continues into a forested bluff with a steep eroding face. Another area of potential interest once

served as a modern campsite and is significantly disturbed due to the placement and later removal of sewer lines and a shower house structure (Whitehead, 2016).

Although there is only one site number assigned, several shell middens were found. Areal extent of site 80.25 was recorded as 50 m by 20 m. Artifacts indicated the presence of a complete ceramic sequence (Spiess, 2016a). Another potential site is located northeast of the parking area. A caretaker of the preserve knows of a woman, who, in her childhood, came with her family to look for artifacts in the area. The property owner brought in several loads of soil some years later and buried the recreational digging location (Whitehead, 2016). Observed shell thickness at each site (i.e., excluding the recreational digging location) was approximately 20 cm to 30 cm, and each is dominantly composed of soft-shelled clam (*Mya arenaria*).

2.5 Summary

Glacial geomorphic processes in Maine resulted in a geologically young surficial landscape of erosional and depositional features modified by modern processes. The study of glaciation and sea-level history in coastal Maine is critical to understanding the landscape as well as the preservation of the cultural record.

Regional Archaeological periods include the pre-Clovis and Paleoindian Period, Archaic Period, Ceramic Period, and Contact Period. The presence and/or preservation of a pre-Clovis or Paleoindian record in Maine was heavily influenced by glaciation and a fluctuating relative sea-level. An additional challenge involved with locating Paleoindian sites is that the people were highly mobile and lived in small bands; thus, the record left behind is often discrete. The Archaic transition came at a time when the landscape shifted from supporting grazers to a wooded environment. Many coastal Archaic Period sites are submerged due to relative sea-level rise. Likely the result of both preservation and visibility, relatively few shell middens contain an Archaic Period component. The Ceramic Period is unique

to the region and is host to the majority of Maine's coastal shell middens. Following the Ceramic Period, the Contact Period represents the beginning of European settlement and utilization of the region. There are a number of challenges to understanding the native Contact Period cultures within the Gulf of Maine. The archaeological signatures of pre-Clovis through Contact Period peoples and the visibility of the coastal record they left behind are unique.

Approaches to studying coastal shell middens within the region have developed through time, but threats to site preservation are continually acting to destroy the record. The regional sea-level curve serves as a guide for the highest probability locations for coastal occupation sites, and identifies potential windows for preservation and erosion potential. Coastal shell middens in Maine are threatened by natural and human disturbance as well as imminent sea-level rise. Typical Maine middens occur in a number of unique geomorphic settings and contain centimeters to meters of soft-shell clam (*Mya arenaria*) and/or oyster (*Crassostrea virginica*) shells, faunal remains of extant and extinct species, and cultural material. Although Ceramic Period middens dominate the coast, older midden sites do exist.

Understanding site formation processes unique to shell middens involves awareness on both a landscape- and site-scale. This project represents one point in the evolution of regional shell midden investigation as practices for gathering data continue to evolve. Understanding impacts to the archaeological record involves a broad approach.

The interdisciplinary nature of this project fueled research from the initial stages. Selecting representative midden study sites distributed along the coast involved collaboration with MHPC Senior Archaeologist Arthur Spiess. Fifteen sites were included in the study, GPR was conducted at 6 sites, and a six-step protocol for shell midden evaluation using GPR was developed as a result. Additionally, it

was determined that the varying erosional influence of coastal compartments was not observed at the site scale.

Chapter 3

GROUND-PENETRATING RADAR AS A CULTURAL RESOURCE MANAGEMENT TOOL FOR ASSESSMENT OF ERODING SHELL MIDDENS

3.1 Abstract

With an increasing rate of sea-level rise inherently linked to climate change, numerous coastal archaeological resources are under threat. In Maine, virtually all 2000+ coastal aboriginal shell middens are eroding. Given limited time and resources, an efficient method for making informed cultural resource management decisions is critical. Herein, I describe a six-step protocol for a minimally invasive and cost-effective ground-penetrating radar (GPR) delineation of shell midden size and morphology. Benefits of the survey methodology outlined in this study include the efficiency of data collection, the nondestructive aspect of the technique, continuous records of site stratigraphy, and the lower cost as compared to large-scale excavation. Two case studies are presented to illustrate the advantages and challenges associated with this method.

3.2 Introduction

Increasing rates of climate-driven sea-level rise and associated coastal erosion are destroying irreplaceable cultural and paleoenvironmental information archived in shell middens. Thus, the rapid destruction of these sites calls for an efficient and cost-effective methodology for the evaluation of shell midden thickness and areal extent for data recovery and cultural resource management (CRM) decisions. This research focuses on using ground-penetrating radar (GPR) as a rapid, minimally invasive method for characterizing eroding shell middens in Maine, and serves as a model for application elsewhere.

Virtually all 2000+ midden sites in the state are eroding, with some previously documented sites already lost. GPR survey provides rapid and noninvasive characterization of shell-midden size and morphology. While GPR is a tool used in archaeological investigations for site prospection and stratigraphy, when combined with existing archaeological data or limited testing, it can provide stratigraphic correlation across broad areas more rapidly and at less cost than traditional excavations. By utilizing the characteristic electromagnetic signatures of shell layers in stratigraphic sequences, shell-rich strata are identified on GPR profiles and used to map the extent and thickness of the deposits.

3.2.1 Maine Shell Middens

Shell middens typical of the region range in size from a few square meters to over 2000 m², and are composed of centimeters to meters of soft-shell clam (*Mya arenaria*) and/or oyster (*Crassostrea virginica*) shells, faunal remains of extant and extinct species, and cultural material. The weathering of shells creates neutral to alkaline pH conditions in the midden. This situation is atypical of Maine's acidic soils, and acts to preserve a more complete paleoenvironmental and cultural record than that found in most archaeological sites within the state's interior.

Shell middens in Maine are found in a variety of geomorphic settings. Clamshell middens are adjacent to, either presently or in the past, a tidal flat (Kellogg, 1991). These middens may occur on a bluff of glacial sediment, beach, or bedrock outcrop. However, the upper Damariscotta River estuary hosts several oyster shell middens, including the Glidden Midden, the largest remaining midden by volume on the New England coast. These middens are unusual in that they are in a transitional estuarine setting, unlike the more widespread clam middens found in more marine settings.

Middens in Maine are threatened by human disturbance, as well as climate-induced sea-level rise. Modern impacts include looting and development pressures. Nineteenth century mining for chicken feed, lime, and road fill also destroyed middens, and almost entirely removed what was once Maine's largest midden, the Whaleback in Damariscotta (Sanger and Sanger Elson, 1986). As early as 1912, researchers noted coastal erosion impacts on sites (Spiess, 1985), and a 1987 annual report of the Maine Historic Preservation Commission identifies coastal erosion as a threat to archaeological sites (Shettleworth, 1987).

3.2.2 Factors Affecting Midden Erosion

Midden erosion is often indicated where beaches are covered by a distinctive apron of white shell fragments. Daily erosional processes are constantly impacting shell midden sites, but less frequent and more intense damage is caused by storm-driven waves. Sea-level rise increases the reach of wave-energy, exacerbating erosion as water levels increase (Himmelstoss et al., 2006). When combined with climate change's intensification of storm frequency, accelerated midden loss along the entire coast is anticipated. However, erosion is site-specific, as local factors, such as coastal morphology, wave fetch, and storm duration and energy, will influence the location and amount of loss associated with each storm.

Often, middens along the coast of Maine occur on bluffs composed of unconsolidated glacial material. These sites are also susceptible to other forms of erosion, including overland erosion, groundwater movement, and freeze/thaw action (Kelley and Dickson, 2000; Kelley, 2004). Bluff retreat is a dominant form of erosion along the Maine coast and affects bluff-top middens (Kelley and Dickson, 2000; Kelley, 2004). Retreat rates associated with bluffs are extremely variable over the terms of months or years, due to episodic slumping (Nordstrom and Jackson, 2012).

Middens located in sheltered environments, such as in coves or estuaries (Davies, 1992; Leach, 2007), are chiefly influenced by wind speed, direction and duration, and basin dimensions (Jackson et al., 2002). Also, boat wakes have a greater effect on these fetch-limited areas as vessels often pass near the shore (Nordstrom and Jackson, 2012).

3.2.3 GPR and Midden Archaeology

GPR is an electromagnetic technique for shallow subsurface investigations. Developed over the past 40 years (Davis and Annan, 1989), GPR uses the same fundamental principles as conventional radar, but the antennae are moved over a surface instead of rotating around a fixed point (Daniels, 2000). The depth of penetration and data resolution are controlled by frequency variations, with greater depth penetration associated with lower frequencies (<100 MHz). However, resolution of individual objects diminishes with lower frequencies (greater wavelengths).

GPR profiles record subsurface stratigraphy by noting differences in the electromagnetic properties of the material that reflect dissimilarities in layer composition, compaction, grain size, salinity, or water content. In shell middens, these characteristics are used to identify shell-rich layers, site disturbance, and cultural features.

3.3 Protocol for Midden Assessment Using GPR

This investigation focused on developing a protocol for GPR evaluation of shell midden size and morphology. The methodology is the result of initial investigation at 12 shell midden sites and detailed GPR survey at 6 sites in coastal Maine (Figure 3.1). Six distinct steps were recognized and are described below (Figure 3.2).

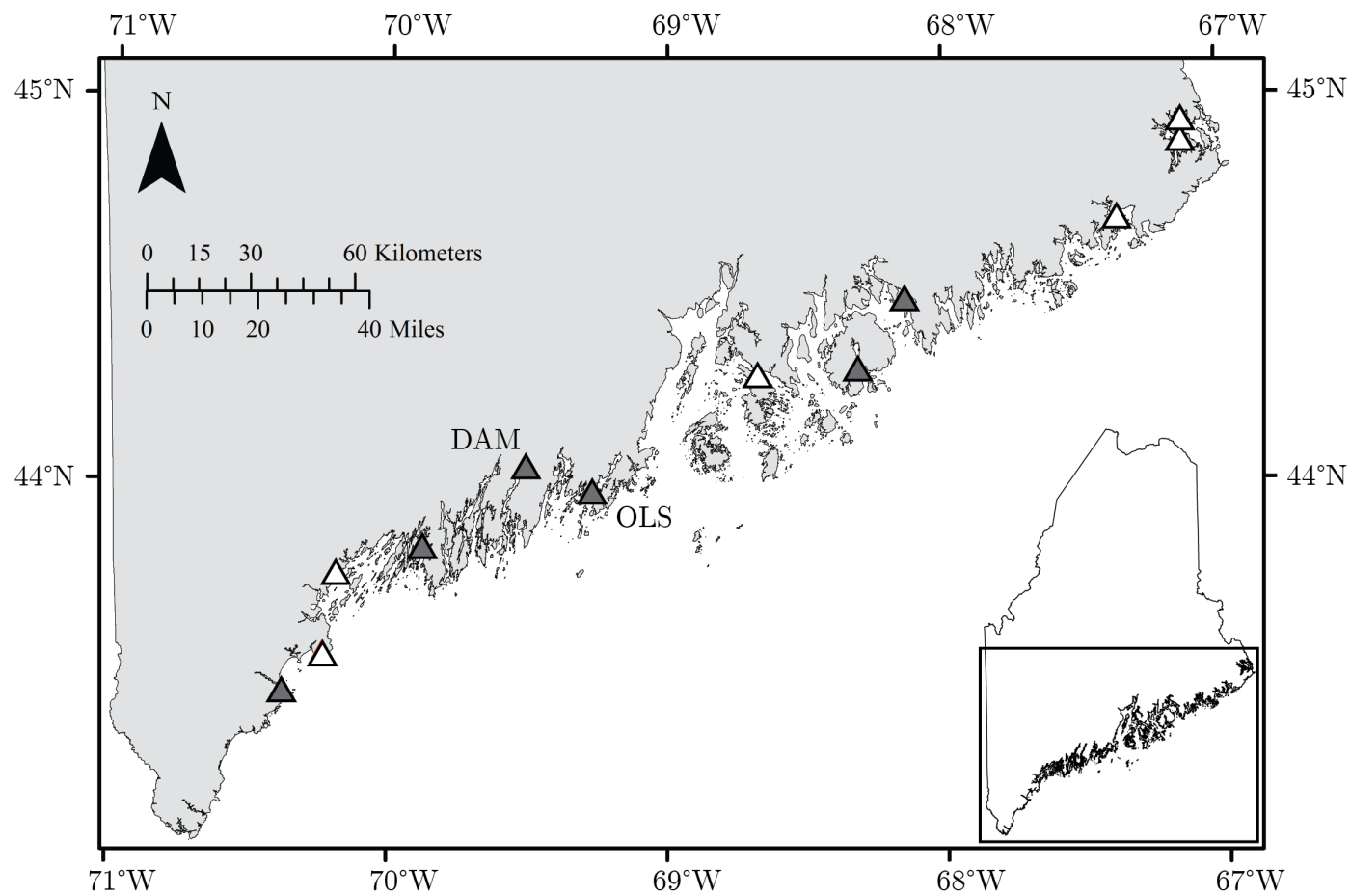


Figure 3.1: Site locations. Grey triangles represent shell middens where GPR data were collected. Source: Miller 2017.

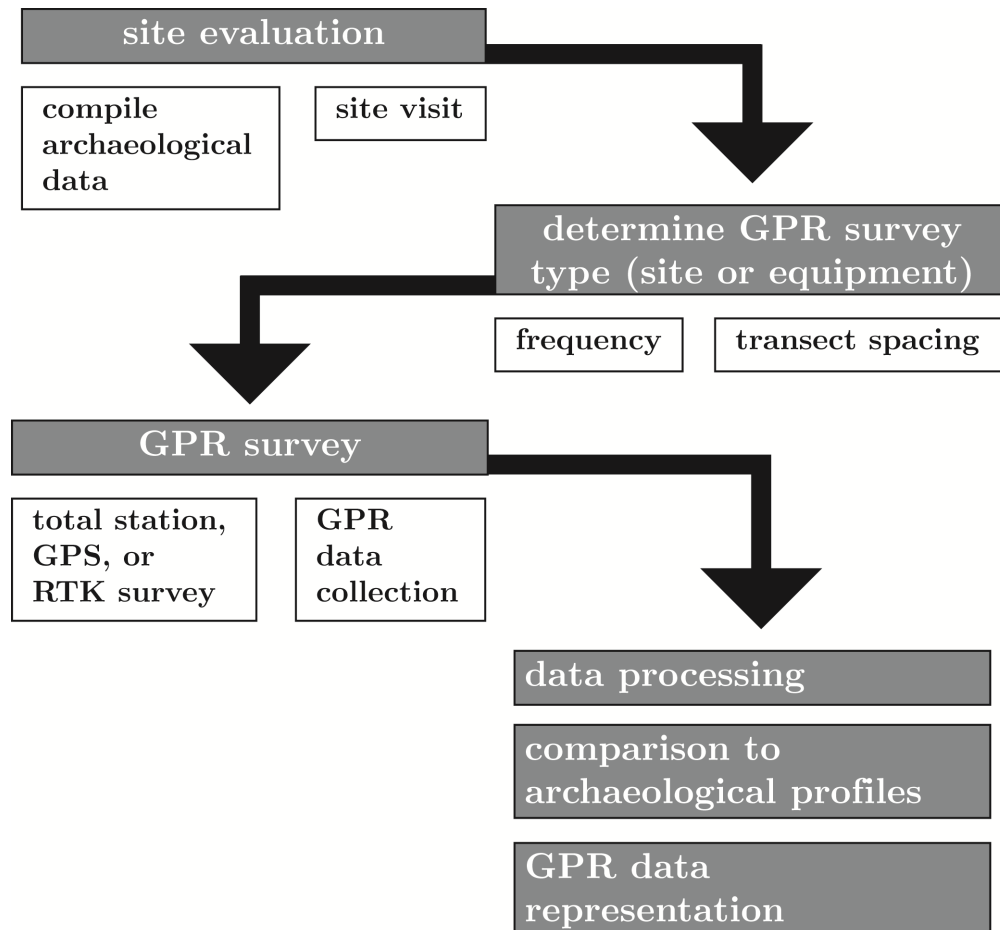


Figure 3.2: Protocol flow chart. A protocol for the application of GPR as an efficient, minimally invasive tool for shell midden evaluation. Source: Miller 2017.

3.3.1 Site Evaluation

The first step in the protocol is a general site evaluation. All existing data (field notes, photos, and existing stratigraphic profiles) from previous archaeological excavation(s) are compiled and evaluated before an initial site visit. A pre-survey site visit provides information regarding terrain and vegetation type and density. Sites with undulating terrain require topographic survey for accurate data interpretation. Thick vegetation precludes survey unless clearing of profile transects is possible. Characterization of erosion (if present), and the presence or absence of

exposed shell, provides insights to deposit thickness and geomorphic processes occurring at the site.

3.3.2 Determine GPR Survey Type (Site or Equipment)

Data from the initial site evaluation and existing archaeological investigations inform GPR equipment selection and survey layout. Shell midden thickness and the intended stratigraphic resolution control the suitable GPR antenna frequency for each site. Antenna frequency should be adequate to resolve the thickness of the midden layers, combined with enough depth penetration to investigate underlying geology. Antennae of 500 MHz are usually applicable to middens between 0.3 m to 2 m in thickness. Higher frequencies are required for thin (<30 cm layers), while thicker deposits (> 4 m) require lower frequencies, such as 200 MHz or less (Leach, 2008). Surficial geological investigations often use 100 MHz antennae.

The survey sampling strategy utilizes a balanced approach: obtaining detailed stratigraphic data for midden delineation, but limiting the temporal aspect to keep the method viable as a rapid technique. Survey transects are arranged orthogonally and parallel to any pre-existing site grids, with a 0.5 to 1 meter(s) spacing in areas of known stratigraphy to establish ground-truth for GPR profile interpretation. After capturing detailed data in a dense grid, the sampling may be coarsened to image the entirety of the midden.

3.3.3 GPR Survey

The survey grid is located in geographic space using standard total station or GPS techniques. Topographic control is important for reflector interpretation if the surface of the site is not relatively flat. GPR data are collected as if the surface is horizontal, and topographic variations are added during processing to provide an accurate representation of subsurface stratigraphy and morphology.

The collection of GPR data begins after grid establishment. It is useful to collect and examine a few test profiles prior to beginning the survey to verify data collection parameters, such as data stacking, the time window, and the dielectric constant used to approximate depth. Because shell midden stratigraphy is variable from site to site, GPR collection parameters are specific to each location. The length of individual profiles and the direction of profile collection are dictated by the processing software. Accurate field maps are critical to accurately assemble the GPR grid within the processing software.

3.3.4 Data Processing

Raw GPR profiles are processed to improve data presentation for interpretation, make accurate time/depth measurements, and to incorporate topography. GPR files are processed using uniform parameters in either a grid, or individually if the GPR survey configuration was irregular and prevented grid construction. Time-zero corrections are performed to bring the first reflection to the surface in each profile, removing the "air wave" and other surficial effects. A finite impulse response (FIR) filter and high and low-pass filters are applied to remove noise. Initial migration followed the standard procedure to collapse hyperbolae that cluttered the profiles. Data are then remigrated for depth correction by matching the thickness of the pure shell midden to ground-truth values. The profiles are exponentially range-gained to bring-out the upper portion of the profile.

3.3.5 Comparison to Archaeological Profiles

Pre-existing archaeological excavation provides stratigraphic sections for ground-truth in data processing and allows accurate identification of shell midden stratigraphy for correlation across the site. Layers composed almost entirely of shell are very distinctive in GPR profiles. Comparison of GPR data with ground-truth aids in interpretation of more complex sequences, such as those containing varying

amounts of soil. Unmigrated profiles were also used to allow matching of hyperbolae generated by rocks with rocks noted in stratigraphic sections. These features act as markers for local depth corrections.

3.3.6 GPR Data Representation

GPR data can be presented in a variety of ways to show midden thickness and extent. One approach is to create a "fence diagram" of individual, representative profiles across the site. However, for sites with closely spaced orthogonal grids or limited intersecting profiles, isopach maps are an excellent vehicle for the spatial display of shell midden thickness and extent. Checking the isopach maps against available midden thickness data provides a level of quality control and adjustment parameters.

3.4 Application of the Methodology

The protocol described above (Figure 3.2) was utilized, with adjustments for local site conditions or restrictions at six sites. Below are two case studies, one a clamshell midden and the other a predominately oyster shell midden. Both surveys were collected with a GSSI 500 MHz antenna. Data were processed using GSSI's Radan software (Beta7) with processing parameters described above. A three-dimensional grid was created for orthogonal surveys and all batch files were processed using the parameters described above. If profiles were not collected using a grid, files were individually processed with the same parameters.

Pre-existing archaeological information was available for each site in the form of hand-drawn stratigraphic profiles and photographs, as well as excavation records. These profiles were compared with unmigrated GPR profiles collected along the same grid lines, as unmigrated data are particularly useful in identifying rocks within GPR profiles noted in archaeological stratigraphic sections (Figure 3.3).

Following data interpretation, the base of the midden was traced on each profile using Radan software (Beta7). The resolution provided by the antennae frequency used in this study precluded fine-grained identification of layers or undulations in stratigraphy delineated in archaeological profiles. For this reason, thin layers are combined on the interpreted GPR profiles. Additionally, changes in elevation of strata surfaces and bases (<20 cm) were not captured by the GPR (Figure 3.3). Methods of identifying the base of the shell midden varied from site to site, but shell typically appeared as translucent/transparent horizons in the GPR profile as noted by Leach (2008), and a strong reflector often was present at the shell/subsoil interface. The ground surface was interpreted as the top of the midden for construction of the isopach maps. However, A or Ap horizons (approx. 20-30 cm) present in stratigraphic sections could sometimes be resolved on GPR profiles.

Migrated (depth-corrected) data formed the basis of isopach maps showing the lateral and vertical extent of the shell midden (Figures 3.3 through 3.4). A .csv file resulted from tracing the base of the midden reflector in Radan and was imported into ArcGIS. The isopach map was produced using the natural neighbor interpolation technique. If the GPR survey configuration prevented grid construction, a .csv file was created utilizing the UTM coordinates (x and y) and the depth of the midden base (z), and the isopach map was produced using ArcGIS. However, other programs, such as Surfer, could be used.

3.4.1 Olson Case Study

The Olson site (OLS) (Figure 3.1) is situated on a bluff approximately 4 m high above a low-energy beach in the town of Cushing, Knox County, Maine. As with many larger shell middens in Maine, an open grassy field covers the site. This correspondence between shell middens and agricultural activity suggests that early farmers recognized the less acidic conditions created by the underlying midden.

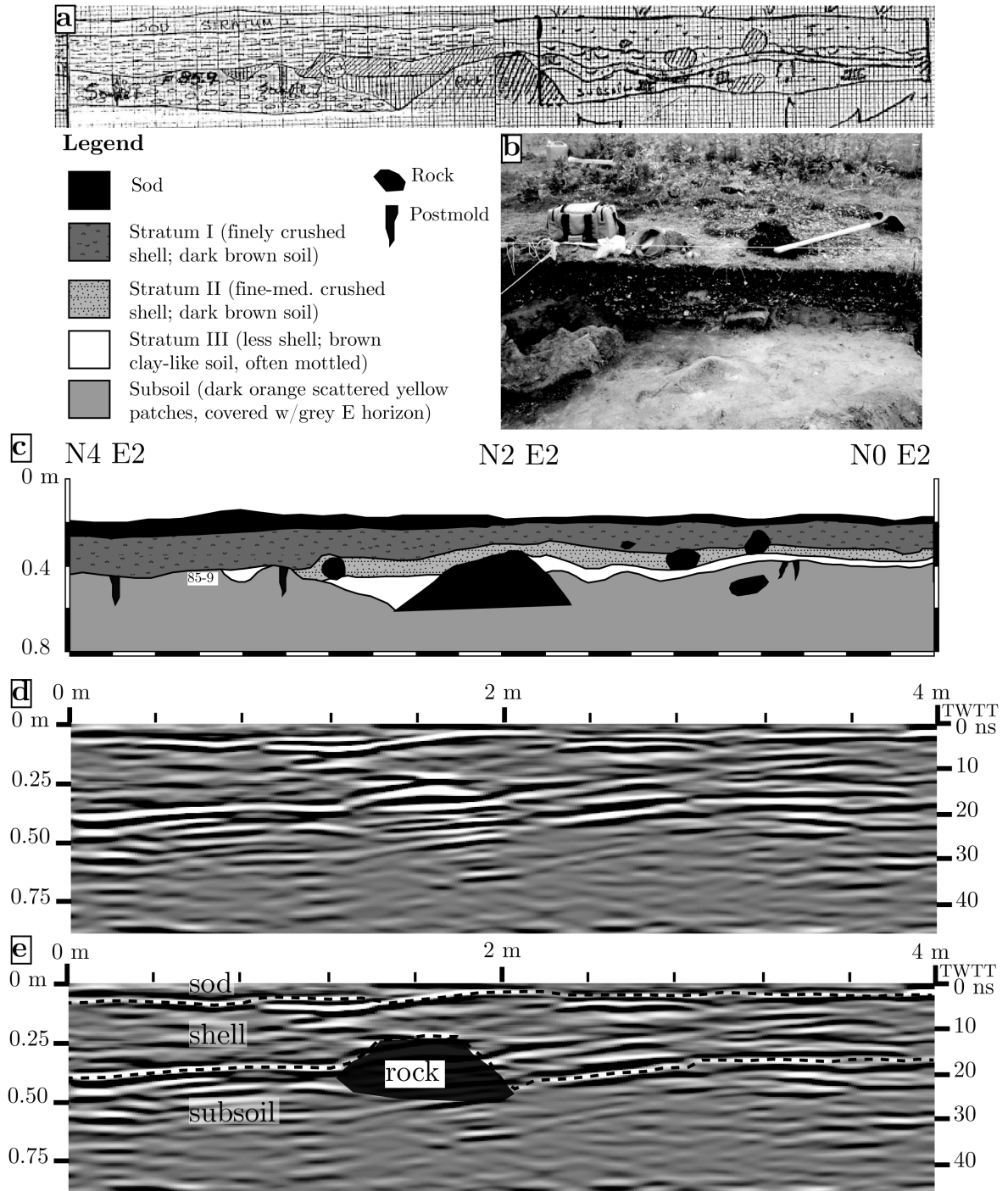


Figure 3.3: Olson site ground-truth and interpretation. Figure shows: a) the original archaeological profile, b) a photograph of a section of unit wall, c) a redrafted version of the archaeological profile, d) an unmigrated and uninterpreted GPR profile, and e) the same profile with interpretation overlain. Source: unpublished data, Maine Historic Preservation Commission (MHPC) (original profile, photo) 1985, reproduced with permission; Miller 2017.

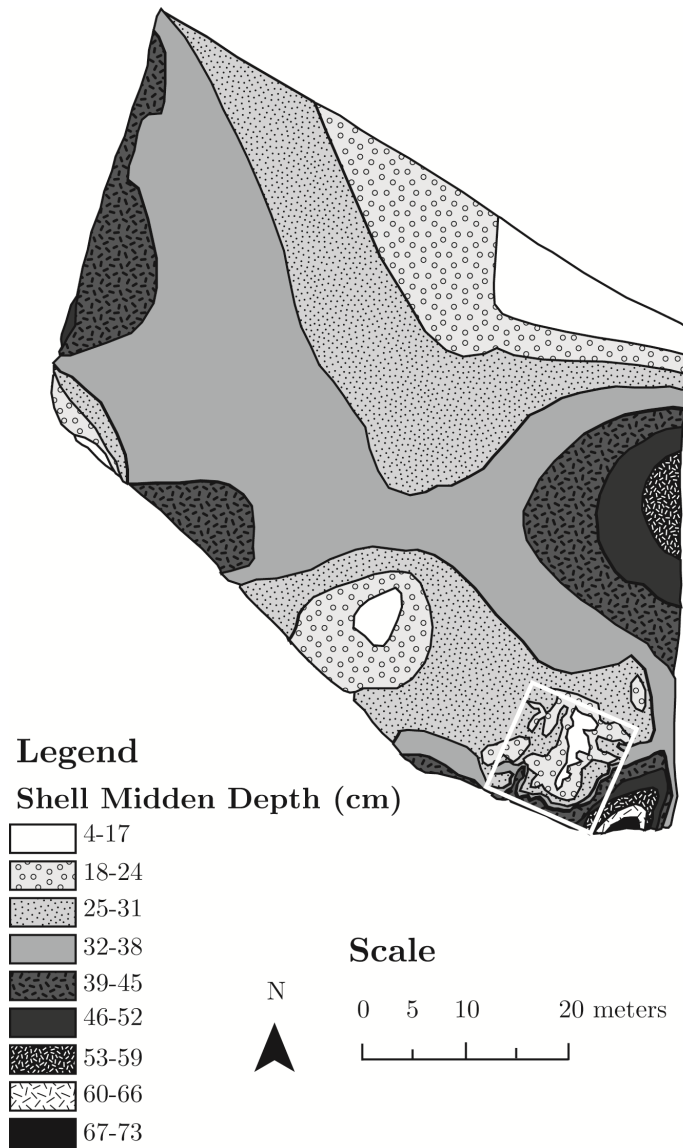


Figure 3.4: Damariscotta site isopach map. Area within the 10 m by 10 m white square represents a detailed 0.5 meter orthogonal GPR survey. The remainder of the isopach map is based on transects shown in Figure 5. Source: Miller 2017.

Surficial material is glacial till, and the bedrock is identified as Paleozoic metasediments and granite (Osberg et al., 1985). Archaeological excavation at the site in 1982 and 1985, identified aboriginal occupation from approximately 2400 years before present though European contact. Shell midden thickness ranged from 50 cm to 1 m, and areal extent was determined by shovel tests to be 150 m by 19 m (Spiess, 2016a). Surface evidence of looting was noted, along with active bluff

erosion. Ground-truth for GPR interpretation is based on a series of trench profiles (Figure 3.3), photos of excavation units (Figure 3.3), and notes from shovel tests. Additionally, some shell was exposed in the eroding bluff.

The GPR survey at the Olson site combined detailed orthogonal grids (1 m and 0.5 m) in locations with pre-existing data and coarse (5-10 m) transects in unexcavated areas. Comparison of archaeological profiles and photos with GPR profiles confirmed a boulder in the expected location in unmigrated GPR data (Figure 3.3). The boulder identification also further confirmed GPR survey grid agreement with archaeological site maps. Shell layers above and around the boulder are "translucent" (low reflectivity) with discontinuous radar reflectors (Figure 3.3). The boundary between sod and shell, as well as the interface between midden and the underlying compact till were interpreted as strong, continuous reflectors. Midden surface was assumed to be the ground surface.

An isopach map was created from the Radan grid file (Figure 3.5). The map and prior testing (1985) suggest the midden extends to the east, but a private residence prevented the extension of the GPR survey. Though shell was not present in the eroding bluff on the far western side, the isopach map indicates midden material in this location, which agrees with the original archaeological interpretation. The continuous profiles generated by the GPR survey allow a more complete understanding of the midden morphology than can be seen from widely spaced excavation units and shovel test pits.

3.4.2 Damariscotta Case Study

The Damariscotta site (DAM) (Figure 3.1) is a dominantly oyster shell (*Crassostrea virginica*) midden with a maximum thickness of one meter. The site is located in the town of Damariscotta, upriver from the Glidden and Whaleback middens. Local bedrock is identified as Silurian Bucksport Formation and is

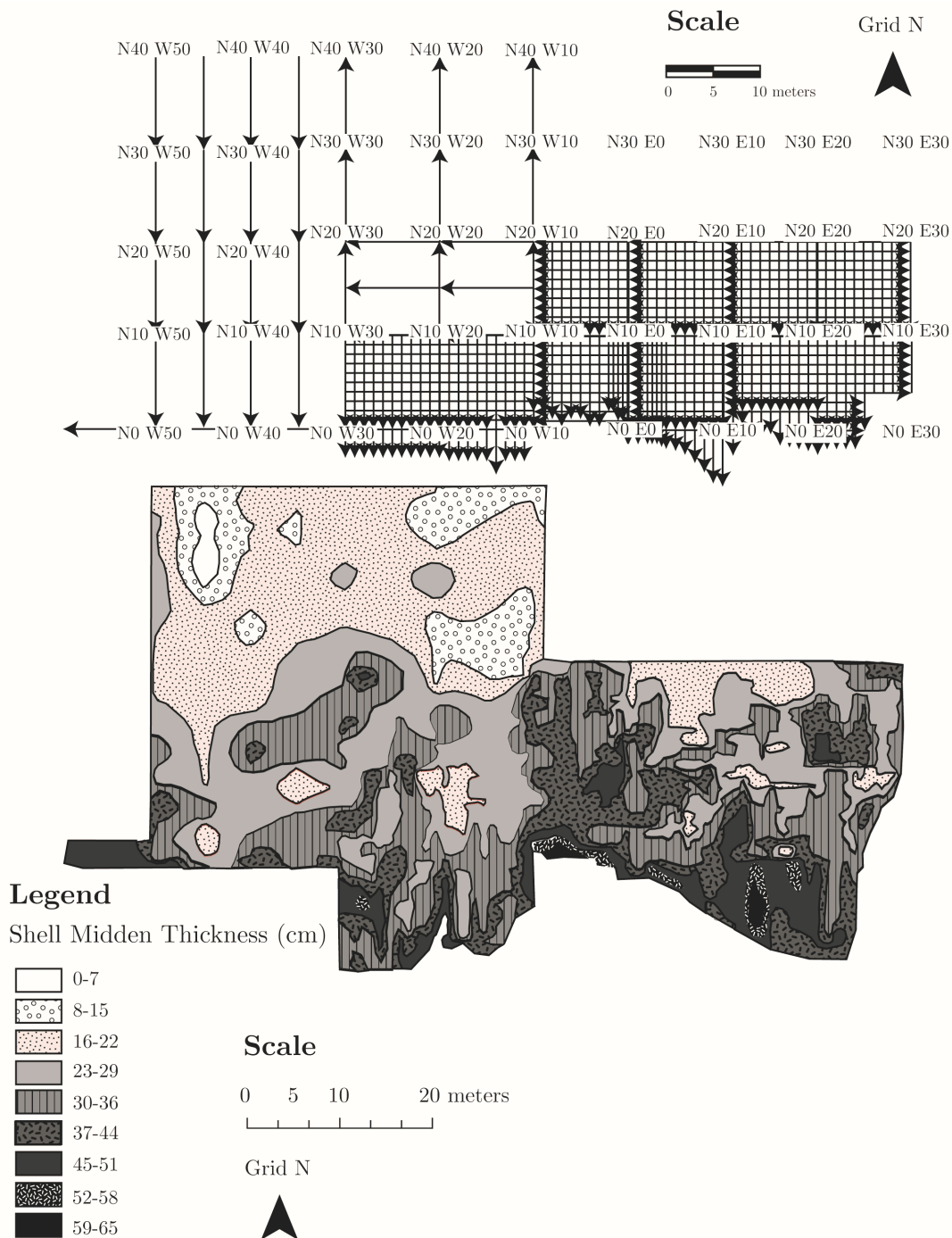


Figure 3.5: Olson site GPR survey map and isopach map. Source: Miller 2017.

overlain by fine-grained glaciomarine Presumpscot Fm. (Grover and Newberg, 2016; Thompson and Borns, 1985). Vegetation at the site included grass and milkweed (*Asclepias syriaca*).

Site extent was documented during archaeological survey as approximately 150 m by 75 m (Spiess, 1998), and the shell layer is thickest at the river's edge. The site is middle Ceramic Period in age (1650-1200 years before present). Artifacts encountered in excavations included charcoal, fire cracked rock, a potential hearth, and bone tools. Faunal remains included fish, bird and mammal bones.

As with each shell midden surveyed, the focus of investigations at this site was delineation of the midden areal extent and thickness. Stratigraphic sections from an earlier excavation (Spiess, 1998) provided ground truth (Figure 3.6). Additionally, the midden was exposed in an eroded bank along the river.

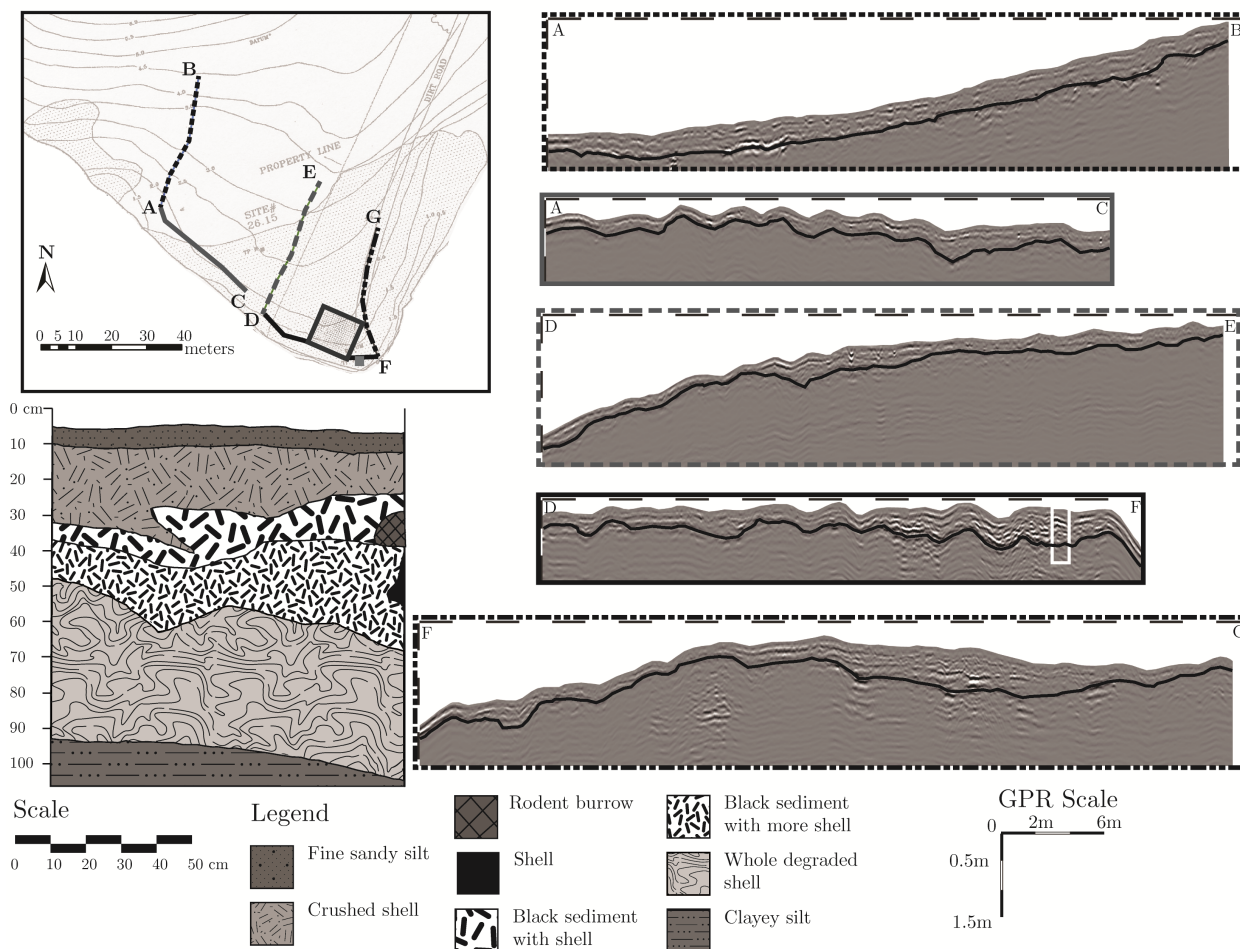


Figure 3.6: Damariscotta site ground-truth and interpretation. GPR profile locations at the DAM site correspond to letters on the survey map in the upper left corner (underlay map courtesy of A. Spiess). Associated GPR profiles are shown. The bottom of the midden is traced in black on each GPR profile. The white rectangle in profile D to F, is a test-pit represented by the solid grey square at the tip of the point on the map. Profile wall depicted in lower left. Sources: MHPC (unpublished basemap and profile) 1996, reproduced with permission; Miller 2017.

While much of the site was once pasture land, the growth of other vegetation, primarily the thick, woody stalks of milkweed (*Asclepias syriaca*) prevented the necessary contact between the ground surface and the GPR antenna. Because mowing of the entire site was not possible, only a 10 m by 10 m area around the known excavation was cleared by hand and surveyed on a 0.5 m orthogonal grid. The survey of the remaining portion of the midden was constrained to several 2 m wide mowed paths (Figure 3.6).

Shell layers on the GPR profiles were characteristically translucent/transparent, and the base of the midden was identified using the strong reflection between the porous shell layer and underlying impermeable, glaciomarine sediments. The ground surface was assumed to be the top of the midden, and may include a plow zone.

Two isopach maps were created for the Damariscotta site: a 5 meter resolution map for the entire area and a 0.5 meter resolution map for the 100 m² detailed survey block. These maps were combined to produce a composite isopach map for the site (Figure 3.4) using the protocol described above. The isopach map (Figure 3.4) and associated interpretation of the profiles (Figure 3.6) revealed that the thickest portion of the shell midden is at the southern tip of the site, as well as in an area of unexpected thick midden unidentified in the previous survey (eastern edge) (Profile F-G, Figure 3.6). Additionally, profiles in the western portion of the site (Profiles A to C and D to E, Figure 3.6) expanded the site boundaries and informed the limited knowledge of midden morphology. The thinnest portion of the midden corresponded to a topographic depression in the area of detailed survey, and is attributed to historic mining of shells for lime or chicken feed.

3.4.3 Error in Midden Thickness Calculations

In comparing interpreted profiles with available ground-truth, in some instances the thickness of the midden was either over- or under- estimated after processing.

This was particularly true in situations of complex stratigraphy. Areas with the greatest discrepancies at the Olson site correspond to disturbed areas, layers of differing amounts of shell and soil, and the variations in shell degradation or size. In the Damariscotta case study site, the depth of shell observed in archaeological excavation (95 cm) differs from the depth of shell interpreted on the GPR record (75 cm) (Figure 3.6), and are linked to the same conditions noted at the Olson site.

The calculated thickness of the midden is based on the use of a single coefficient for the two-way travel time of the radar energy through the midden that is calculated during migration of the data. In instances where the midden has a uniform composition, this value yields a midden thickness very close to those observed in excavations. However, in areas where varying amounts of soil are mixed with the shell or layers are devoid of shell, this single coefficient does not adequately capture the variations in electrical properties of the material. Processing programs that use a single two-way travel time (such as the program used for this study) for the entire section cannot express the true thickness of individual layers. This issue can be identified using pre-existing archaeological information or limited testing at the site (unit excavation or coring), and corrections applied during migration. Alternatively, a processing program that allows dielectric values for multiple, individual horizons could be used.

3.5 Summary

Detailed GPR surveys at six eroding shell middens on the Maine coast were used to develop a protocol for rapid and minimally invasive site delineation for CRM decisions. While GPR survey of shell midden sites will not replace excavation for artifact recovery and fine-grained stratigraphic analysis, this technique provides an efficient avenue for determining shell midden dimensions for the best use of limited data recovery resources.

Experience shows that stratigraphy at each shell midden is unique, and careful planning and understanding of survey conditions is important. Pre-existing information on site stratigraphy and archaeology from prior excavations or limited pre-survey testing (test unit or coring) informs equipment selection, survey planning, and post-survey processing. Antenna frequency is selected to resolve shell midden layer thickness and also investigate underlying geology. Survey grids are configured to parallel original excavation grids if present. GPR survey grid spacing is dependent upon time constraints, site estimated areal extent, and the desire to reproduce existing stratigraphic sections. The survey grid is located in geographic space using standard total station or GPS techniques. Topographic control is important given an undulating surface, and is provided by an on-site survey or existing LiDAR data. GPR data quality varies with site ground cover. Mowing or brush clearing may be required to produce good antenna-ground coupling. Data collection in a grid is desirable for efficient processing and presentation; however, non-orthogonal survey patterns are acceptable.

Because shell midden stratigraphy is unique to each site, data collection parameters, such as data stacking, the time window, and the dielectric constant used to approximate depth are determined for each site. This is most easily accomplished by completing two or more exploratory transects across the site, starting in an area of known stratigraphy (pre-existing excavation data or limited pre-survey testing). A field map of profile locations and data collection direction is created as the data are collected, and is essential for recreating survey grids for processing.

GPR files are processed using uniform parameters in either a grid or individually if the GPR survey configuration prevented grid construction. Processing improves data appearance for interpretation by removing noise and incorporating topography. Data are also migrated to correct depth scales to approximate shell midden thickness shown by ground truth profiles or photos. Unmigrated profiles are also

produced to allow identification of hyperbolae associated with rocks in the section. Processing parameters are kept constant for the entire site. Complex shell midden stratigraphy often results in under- or over-estimation of midden thickness using single velocity processing programs. The base of the midden is identified on individual processed profiles. Depth and position data of this information are used to create isopach maps illustrating midden extent and thickness. In some locations, the extent of the midden identified using this protocol exceeded previously determined site limits, and were independently verified through shovel testing.

In summary, this methodology describes a rapid and minimally invasive GPR technique for shell midden site delineation for CRM decisions regarding data recovery and site preservation. The application of this protocol results in continuous stratigraphic information across the site with minimum ground disturbance and in significantly less time and at lower cost than traditional excavation techniques. While developed in Maine, this protocol is applicable to shell middens in other portions of the world, as we seek to preserve the information contained in these important archives of human and environmental history.

3.6 Acknowledgements

This work is made possible by funding through Maine Sea Grant (NA14OAR4170072) and represents close collaboration between the University of Maine and Maine Historic Preservation Commission.

Chapter 4
COMBINED METHODS, RESULTS, AND DISCUSSION OF
SITES AND DETAILS EXCLUDED FROM CHAPTER 3:
GROUND-PENETRATING RADAR AS A CULTURAL
RESOURCE MANAGEMENT TOOL FOR
ASSESSMENT OF ERODING
SHELL MIDDENS

A 500 MHz GPR survey was carried out at six archaeological sites: University of New England, Long Island North, Damariscotta Oyster Farm, Olson, Fernald Point, and Tranquility Farm. Appendix B contains details of spatial data collection for Damariscotta Oyster Farm, Olson, Fernald Point, and Tranquility Farm. Specific location information tied to the surveys is on file with Maine Historic Preservation Commission (MHPC), and can be accessed with permission by contacting MHPC at: (207)-287-2132. GPR profile collection and processing data, as well as profile location maps for each site, can be found in Appendix C and D. Archaeological wall profiles and photos are located in Appendix E. Ground-truth location information with respect to the GPR data can be found in Appendix F. Notes taken during archaeological excavation at Olson and Tranquility Farm are in Appendix G, and additional GPR and archaeological profile comparisons are in Appendix H. Information on isopach map construction, as well as additional isopach maps, are located in Appendix I.

4.1 GPR Survey

Refer to Chapter 3 for a detailed explanation of the methodology used to evaluate each shell midden site included within this study. This section provides further explanation not included within the paper.

The archaeological grids re-established as part of this work were relocated with as much accuracy as possible, but some error exists, as permanent datums were not found at every site. Correlation with the GPR record and distinctive features in archaeological stratigraphic section such as rocks assisted in confirming good correlation between the original archaeological and GPR grids.

Spatial extent of the GPR surveys were influenced first by the approximate areal extent of the shell midden, determined from prior archaeological investigation, but increased during the survey as shell was identified on the GPR in the field beyond the expected area. GPR grid resolution became coarser (1-5 meters) as the anticipated survey area increased ($>3600 \text{ m}^2$), and as time in the field became limited.

4.2 Error in Shell Midden Depth Interpretation

Ground-truth data are important for interpreting shell midden stratigraphy and site thickness represented in the GPR record. Forcing the GPR depth scale to match closely with observed midden depth at ground-truth locations is critical to accurately and precisely map the thickness and extent of a shell midden site. Midden depth will likely be over- or underestimated in the absence of ground-truth data.

Data migration through traditional hyperbola matching did not provide an accurate correction for midden depth at any location. Two migrations were applied using the following methods: 1) traditional hyperbola matching, and 2) trial and error migration for depth agreement between ground-truth and midden depth interpreted in the GPR data.

The depth correction issue is caused by complex stratigraphy at each shell midden. Layers within the midden are composed of varying amounts of shell and soil, as well as differing degrees of crushed shell material. Thus, the electromagnetic

properties associated with each layer are unique. Applying individual dielectrics to each strata would result in an improved depth approximation.

4.3 Proposed Experimental Methods

Experimental shell midden research would result in an improved understanding of GPR data depth correction issues related to complex midden stratigraphy. The application of GPR to a series of experimental middens of varying stratigraphic complexities and compositions would provide ideal ground-truth and control to explore differences in the records produced. The methods utilized in this would be similar to those in Kenady et al. (2018), where the soil moisture conditions within the pits containing shell were monitored. Kenady et al. (2018) placed two 10 cm layers of oyster shell (1 m x 1.5 m) 42 cm apart within trenches filled with 1) coarse washed sand, and 2) a garden soil mix. The first layer of shell was at the base of each trench. A 500 MHz shielded antennae was used to survey the trenches. The GPR data from the organic-rich trench were inconclusive, and the basal shell layer in the sand-filled trench was not apparent in the GPR record (Kenady et al., 2018). Conducting this experiment using local materials that middens were constructed upon (i.e., till or Presumpscot Fm.) would improve the regional applicability. Additionally, the thickness of the experimental shell midden layers should match the GPR antenna available for the survey (i.e., 30-100 cm).

4.4 University of New England (Site 5.06)

Located on the mouth of the Saco River in Biddeford, ME, the University of New England site (UNE) contained little to no shell. An isopach map was not produced for this site, but GPR data informed future archaeological work. Details related to GPR data collection and processing are located in Appendix C.1.1. A GPR profile location map is in Appendix D.1.

Site 5.06 was surveyed with the 500 MHz GPR prior to archaeological excavation by Arthur Anderson's University of New England field school, held during the summer of 2017. Intact shell layers were not found during the 2017 excavations, but scattered shell was present in a backfilled unit. Three profiles and associated photos were used as ground-truth for the corresponding GPR profiles.

The stratigraphic sequence at the UNE site is represented by four to five well-defined layers, typically identified in archaeological unit wall profiles, numerically labeled in ascending order from the surface (Figures 4.1, 4.2, and 4.3). Photos, hand-drawn unit wall profiles, and stratigraphic descriptions provided by Anderson (2018) allowed insight as to the nature of the sediments. The layers were composed of uniform fine-grained sand, and contained sporadic, angular rocks.

At the surface, level 1 and 2 were composed of tan to olive colored loose sand (10YR 6/2 to 2.5Y 8/8). Level 1 and the interface with level 2 were disturbed by root mat, and had a loose texture. These levels contained no archaeological material and abundant modern material. Level 2 was identified as backfill from earlier field school excavations (1998, 1999, or 2005), but was difficult to confirm. Level 3 consists of more compact sand with a mottled surface due to invertebrate bioturbation, and is 10YR 3/4 in color. Archaeological materials were first encountered in level 3 and continued to be found in lower levels. Level 4 is dark (10YR 3/1), compact sand, and contains the greatest abundance of artifacts. Where present, level 5 was a lighter, olive, compact sand. These detailed descriptions are based on personal communication with Arthur Anderson, and from observations at units 504/5E491N and 494E491N.

The large, angular, sporadic rocks appeared in layers 2 through 5. The rocks are likely the result of human activity as they would not naturally occur with the fine-grained sediments. The area surrounding the site is relatively flat and is not

receiving slope wash to incorporate material; thus, this would not help to explain the presence of the rocks.

The color of each layer alternates between a dark brown and tan. The dark brown layers likely contain increased organic matter from anthropogenic activity, and the lighter, tan layers represent periods of abandonment, which are likely storm deposits. GPR data indicate layer five contains many strong, discontinuous reflectors consistent with rocks, uncharacteristic of the fine-grained sediments present at the site, suggesting human activity. The rocks should not naturally occur with sorted, fine-grained sand. At the base of strata interpreted as archaeological (level 4+ in the GPR records of Figures 4.1, 4.2, and 4.3) is a highly reflective glaciofluvial unit with discontinuous, dipping reflectors. The GPR data show that the identified layers are continuous across the area surveyed.

The surveyed area surveyed contained little to no shell, so an isopach map was not produced. Interpretation of the GPR profiles suggests that existing excavation units did not extend to the glaciofluvial unit at 1-1.2 m, and may not have tested the complete cultural sequence.

Testing this interpretation could be accomplished with one or multiple cores taken at the site. Additional information with minimal effort could also come from re-opening an excavation unit and continuing to 1 to 1.2 m, or taking a core in the unit at the base of one of the original excavations.

4.4.1 GPR and Archaeological Data Comparisons

Each of the following GPR profile comparisons contains an unmigrated GPR profile, and a duplicated migrated profile. One migrated profile contains interpretation. The scale of the unmigrated profile differs from the two migrated profiles as a result of the migration performed to match the midden thickness on the profile with archaeological ground-truth. Additionally, each comparison contains an

archaeological profile with the associated unit wall profile. When the archaeological information corresponded to a portion of the GPR profile, the position on the profile is delineated by a red box. Note that the archaeological profile and photo in each comparison were flipped about the vertical axis to agree with the direction of the GPR profile.

The archaeological profile for the north wall of 494E499N was excavated to a depth of 65 cm, and four strata were identified (Figure 4.1). A disturbed surface was noted on level 4, and two angular, 5-10+ cm (length) rocks were found within the level. The disturbed surface and presence of angular rocks are likely related to human activity. The GPR profile agrees with the interpretation of a minimum of four levels, with an unconfirmed fifth layer present (Figure 4.1). Intermittent, strong and discontinuous reflectors and occasional hyperboles suggest the presence of rocks in the fourth and fifth layer. The base of strata with the potential to contain archaeology is at 1.1 m, where strong, discontinuous, dipping reflectors are interpreted as a glaciofluvial unit.

The archaeological profile for the north wall of 500E494N delineates five strata, and extends to 90 cm (Figure 4.2). The profile is not located on a GPR transect, but begins 1 m before the start of the transect, terminating at the start of the surveyed transect. The GPR data support the surface disturbance of layer 4, as the reflector associated with the boundary appears intermittently (Figure 4.2). Layer 5 was not delineated in the interpreted GPR profile due to the absence of a continuous/obvious surface. Hyperbolae were found in layer 4 and 5, and are likely associated with rocks. The base of strata with the potential to contain archaeological materials is at 1.1 m in this location, at the contact with the glaciofluvial unit at the base of the profile.

Figure 4.3 shows the north wall of 504E491N and associated archaeological and GPR profiles. The unit was excavated to a depth of 90 cm, and identifies five layers.

The disturbed surface of layer 4 was present in the GPR data. Again, layer 5 was difficult to confidently identify in the GPR profile, and was not delineated.

Hyperbolae and intermittent, strong, discontinuous reflectors, indicative of rocks, are present within layer 4 and 5. The top of the glaciofluvial unit ranges from 1-1.2 m below the ground surface.

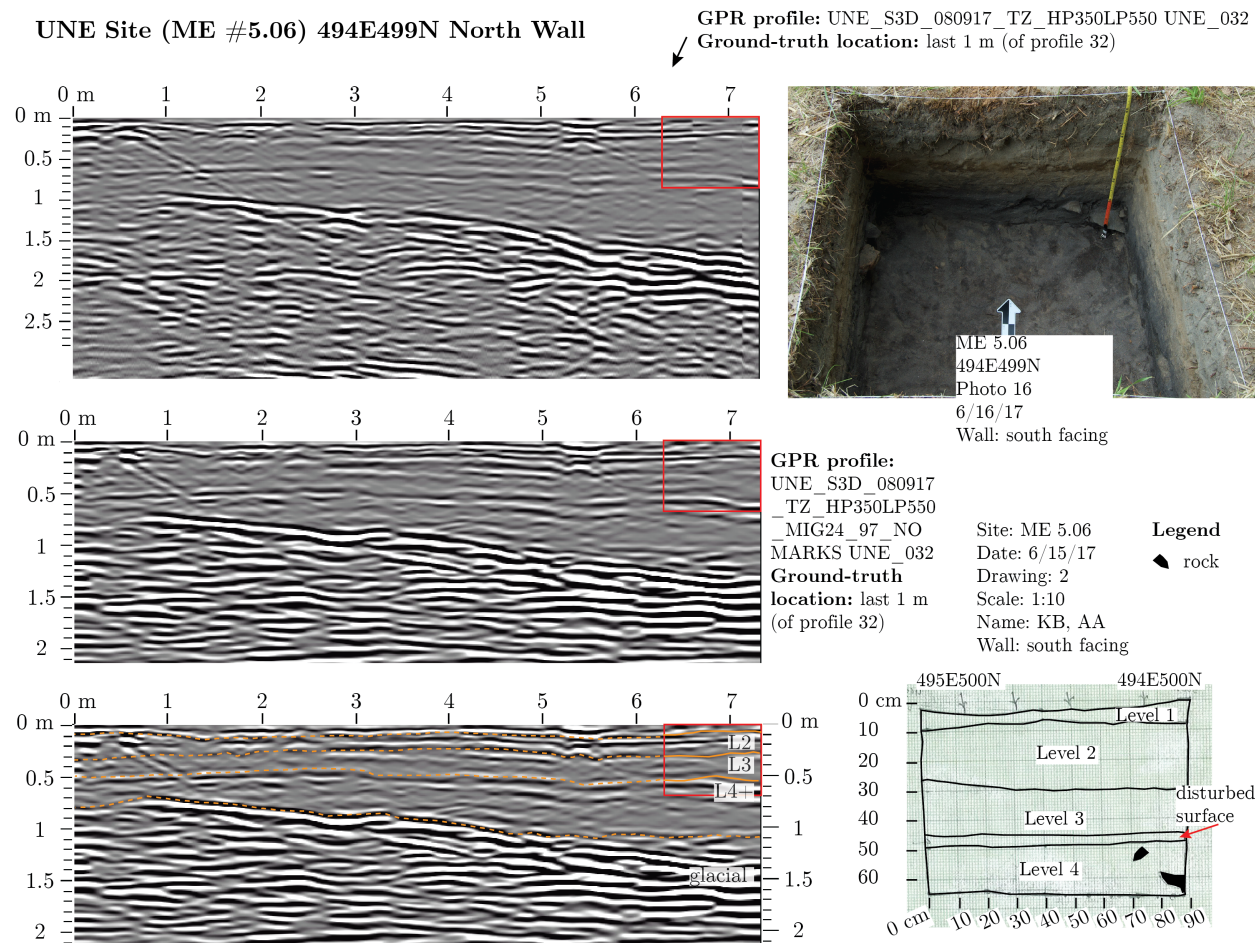
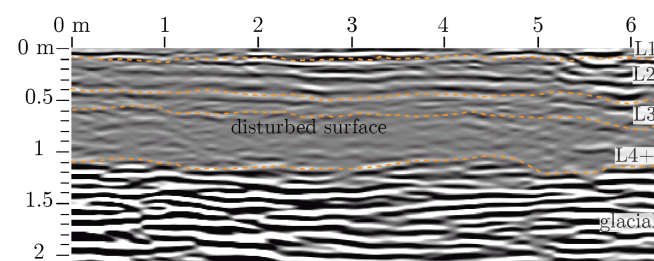
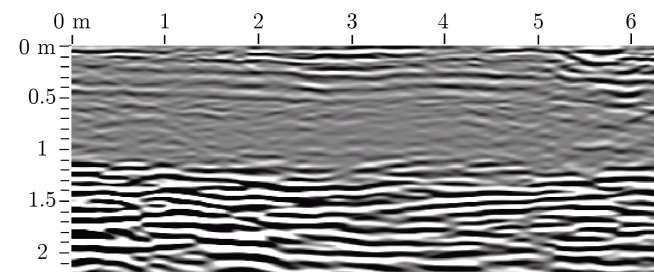
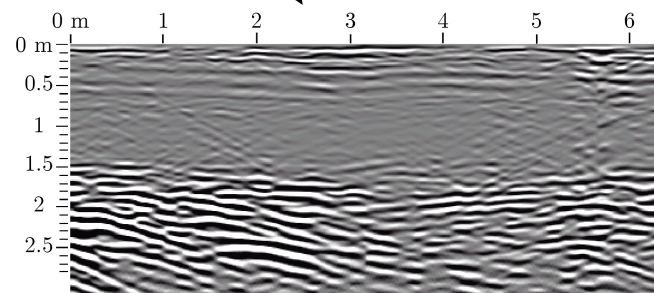


Figure 4.1: University of New England (Site 5.06) GPR and archaeological profile comparison of the 494E499N north wall. Original profile courtesy of Anderson (2018).

GPR profile: UNE_S3D_080917_TZ_HP350LP550 UNE_027
Ground-truth location: not intersected by GPR profile
 (-1 m to 0 m of profile 27) ↘



UNE Site (ME #5.06) 500E494N North Wall



Site: ME 5.06
 Date: 6/16/17
 Drawing: 6

GPR profile:
 UNE_S3D_080917_T
 Z_HP350LP550_MIG
 24_97_NOMARKS
 UNE_027

501E 500E
 495N 495N
 Name: KB, VB
 Wall: south facing

Ground-truth location: not
 intersected by GPR
 profile
 (-1 m to 0 m of
 profile 27)

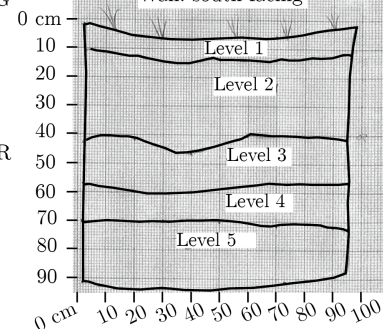


Figure 4.2: University of New England (Site 5.06) GPR and archaeological profile comparison of the 500E494N north wall. Original profile courtesy of Anderson (2018). The archaeological unit began 1 m prior to the start of the GPR transect; thus, there is no red box within the GPR profile.

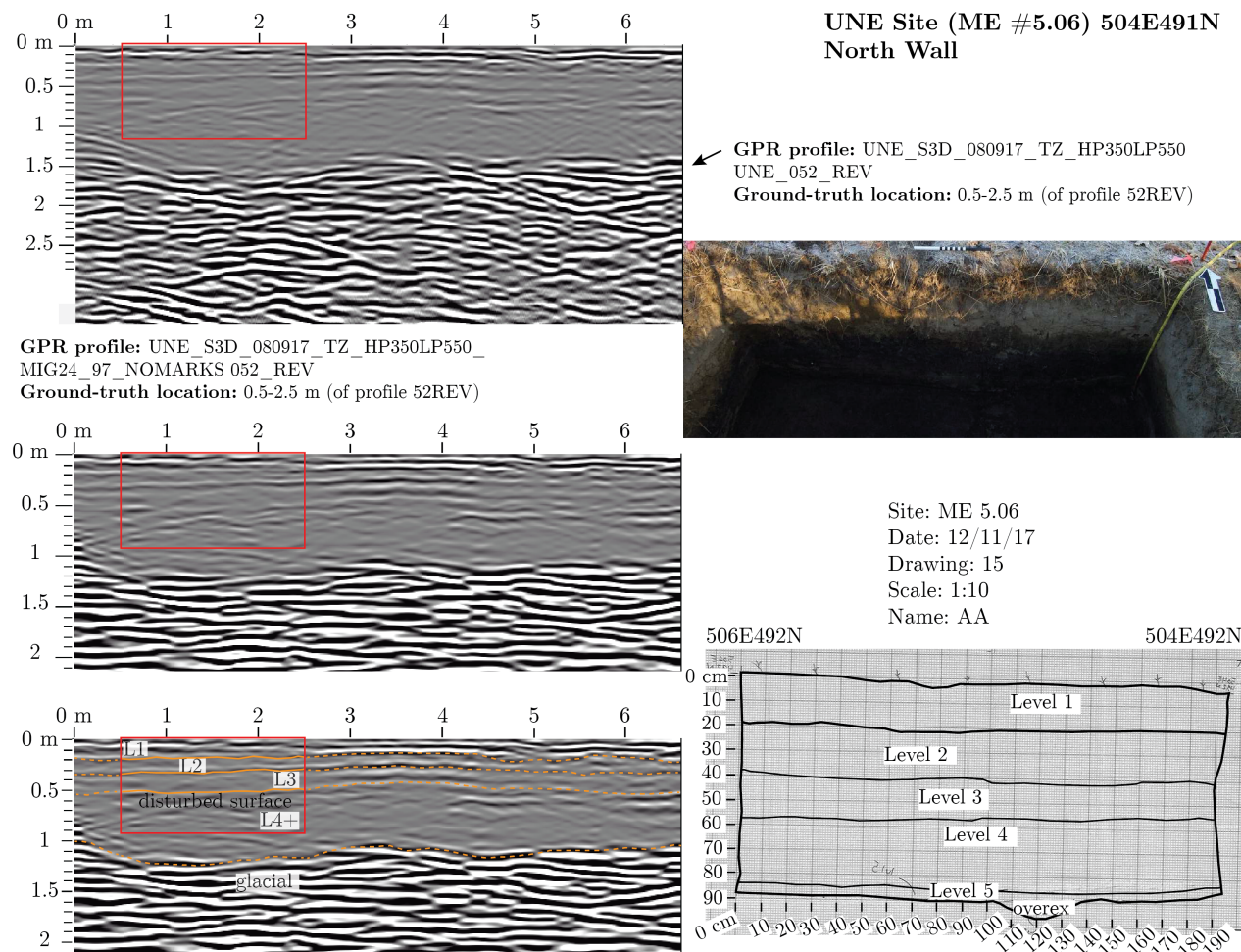


Figure 4.3: University of New England (Site 5.06) GPR and archaeological profile comparison of the 504E491N north wall. Original profile courtesy of Anderson (2018).

4.5 Long Island North (Site 15.95)

Situated in coastal Cumberland County, ME, the Long Island North site (LIN) faces east and contains dominantly clam-shell (*Mya arenaria*). Midden depth is often 50 cm to 1 m, and the deposits date to Early-Middle Ceramic (Spiess, 2016a). Metamorphosed interbedded pelite and sandstone of the Ordovician-Precambrian Cape Elizabeth Formation (Osberg et al., 1985) is close to the surface and also crops out in the northern area of GPR survey. Surficial material underlying the midden is undifferentiated thin drift (Thompson and Borns, 1985). The site is topped by a flat, grassy lawn.

Information on GPR profile collection and processing can be found in Appendix C.1.2, and profile location maps are found in Appendix D.2. Enlarged archaeological wall profiles are in Appendix E.1. Location data for ground-truth are in Appendix F.2. Isopach map construction and file details are located in Appendix I.3.1.

Archaeological profiles for the Long Island North site were very detailed, and the GPR survey was directly tied to the archaeological grid with confidence. In addition, the sod above the shell was typically 5 cm thick, often not exceeding 10 cm. Shell within the midden was often coarse and whole.

4.5.1 GPR and Archaeological Data Comparison

Distinguishing shell midden from underlying glacial material was not possible at the LIN site. In addition, delineating the bedrock proved challenging as the dielectric of the overlying material (midden or till) was too similar to that of the bedrock. A number of detailed archaeological profiles guided interpretation.

Ground-truth, hyperbolae, and rocks indicative of glacial till, were used to identify the position of the midden base. Fractures within the bedrock were observed within the GPR data. The presence of water within the fractures enhanced the GPR signal due to the difference between the dielectrics associated

with water and bedrock. The isopach map produced for this site represents the maximum potential depth of midden.

The isopach map (Figures 4.4, and 4.5) shows thick midden on the eastern side of the surveyed area, along the shoreline. There is a potential for relatively thick midden on the western side of the site, but it thins with distance (Doyle, 2018).

Profile B, in Figure 4.6, is 0.5 m east of the GPR transect. Profiles A and C are 0.5 m to the west of the GPR transect. The colored boxes associated with each profile in Figure 4.6 represent the position of the archaeological profiles, within the GPR profiles, in Figure 4.7. Figure 4.7 represents GPR profile LIN_2, and contains one unmigrated file with a duplicated migrated file. The scale of the unmigrated profile differs from the two migrated profiles as a result of the migration. The data show the subdued bedrock signal (Figures 4.6, and 4.7). Also, midden was present in each archaeological profile represented on the GPR profile, but a distinct signal was not apparent (Figures 4.6, and 4.7). Tree roots are present at the start of the GPR data.

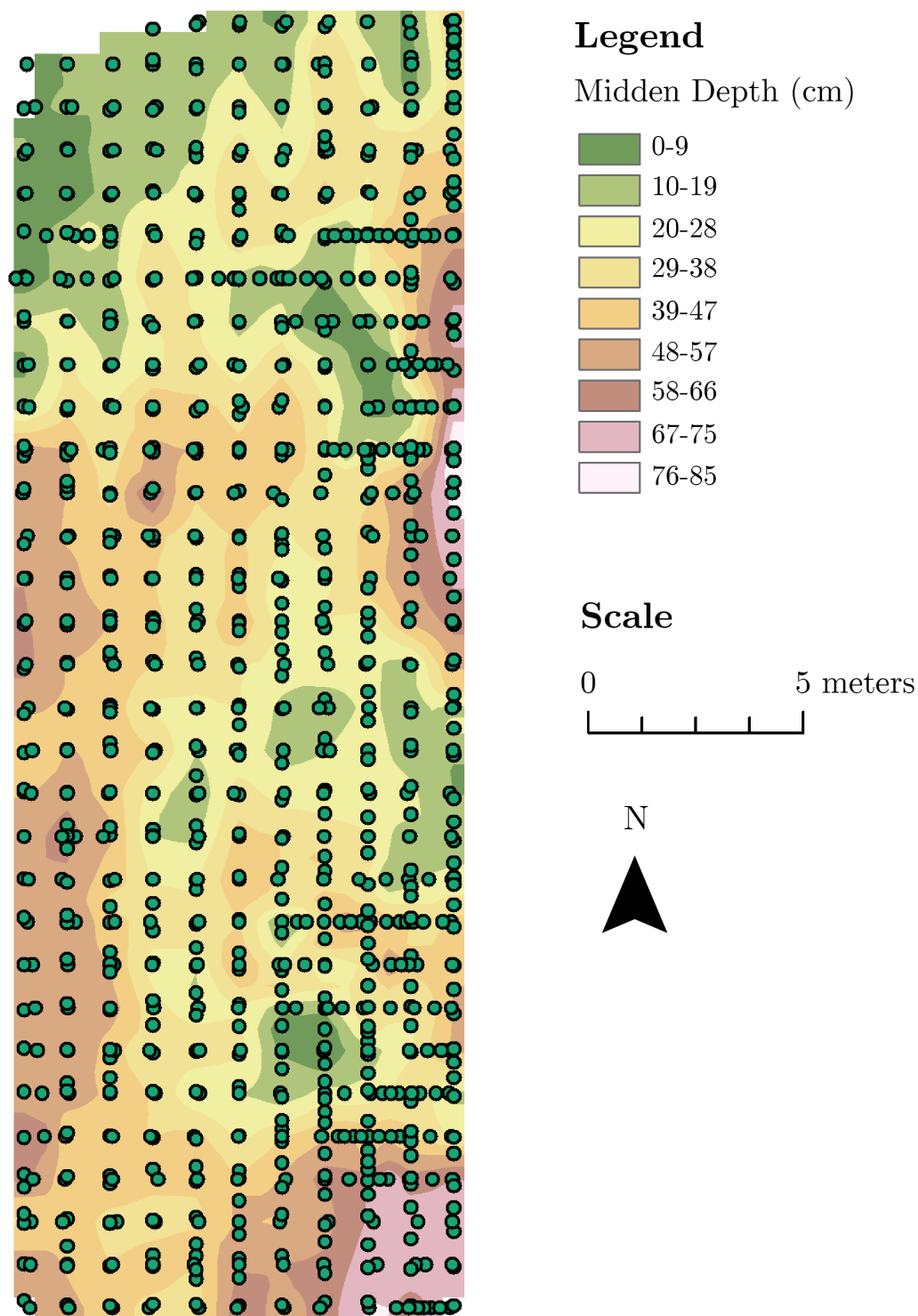


Figure 4.4: Long Island North (Site 15.95) isopach map 500 MHz GPR survey transects. Green dots represent 500 MHz GPR survey transects.

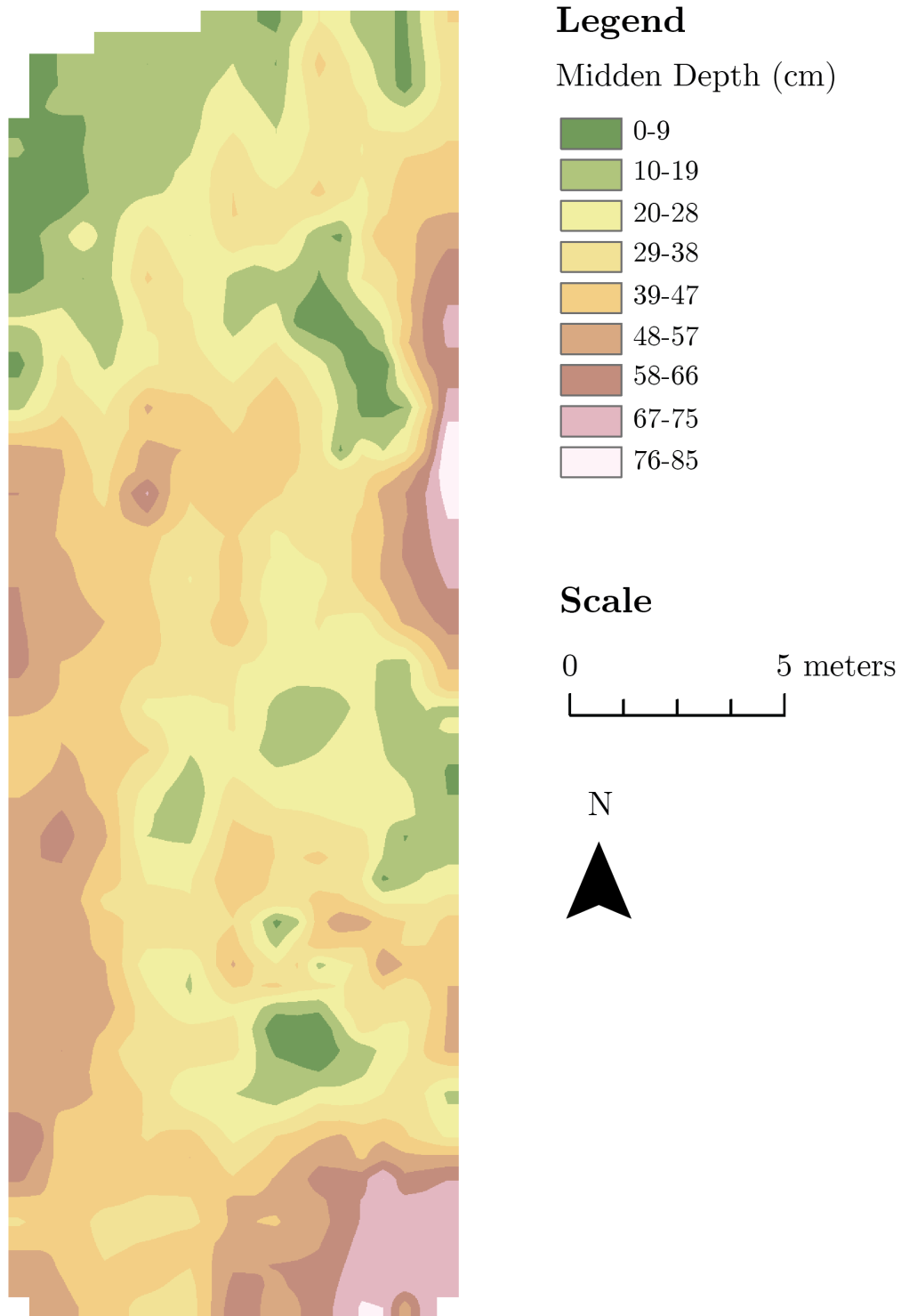


Figure 4.5: Long Island North (Site 15.95) isopach map.

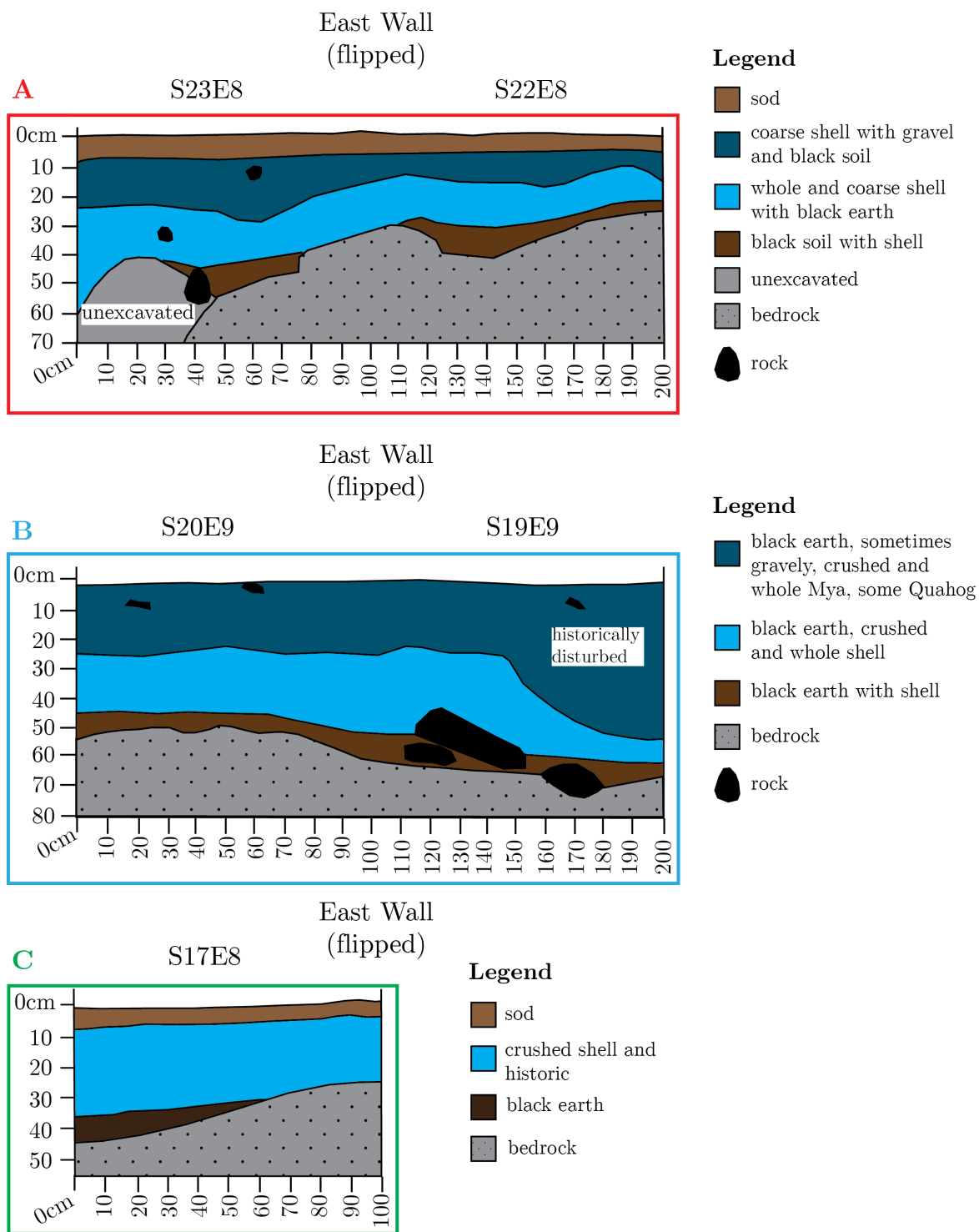


Figure 4.6: Long Island North (Site 15.95) redrafted archaeological profiles. Original profile courtesy of D. Doyle, personal communication. The colored boxes, labeled A through C, are represented on the GPR profiles in Figure 4.7.

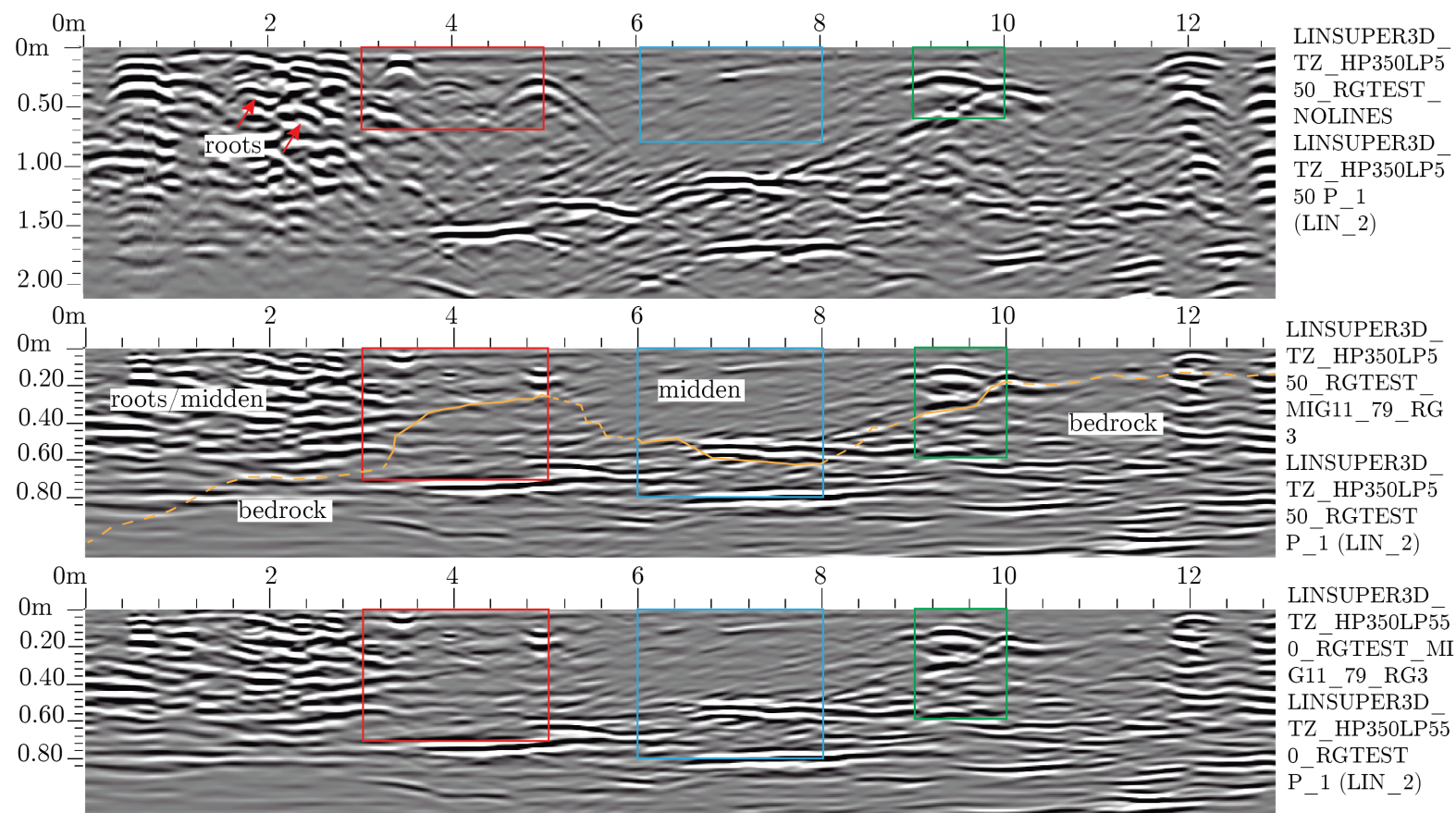


Figure 4.7: Long Island North (Site 15.95) GPR profiles with archaeological profile positions overlain. Colored boxes represent the position of the archaeological profile. The profiles associated with each box are depicted in Figure 4.6. Note that the migrated files have a filename associated with a migration of 11.79, but the scale is associated with an additional migration of 51.55.

4.6 Damariscotta Oyster Farm (Site 26.15)

The Oyster Farm site (DAM) is located approximately 370 m north of Glidden and Whaleback midden sites. Site 26.15 is situated on a south facing point of land, bounded on one side by a tidal stream, and the other by the Damariscotta River. Oyster shells (*Crassostrea virginica*) dominate midden deposits. Ceramic fragments date the midden to middle Ceramic age (CP-2 of CP-3) (Spiess, 1998). Additionally, the site does not contain a Contact Period component (Spiess, 2016b). The glaciomarine Presumpscot Fm. underlies the midden.

GPS data were collected at Site 26.15, and details are located in Appendix B.2.1. GPR profile collection and processing details, as well as profile location maps, can be found in Appendix C.1.3 and D.3. Enlarged archaeological wall profiles and photos are in Appendix E.2. Details of isopach map construction are found in Appendix I.3.2.

The depth to which the shell is present in the soil profile (Figure 3.6) does not directly correlate with the interpreted depth of shell in the GPR record. Midden bottom was typically the strongest reflector, representing the sharp contrast between porous and permeable shell midden mixed with soil, and the silty-clay Presumpscot Fm. The strongest reflector appeared at the contact of the two different materials and/or at a surface where water is ponding. The scale in the profiles drawn from 1996 archaeological work at the site holds the most weight.

Disagreement between the depth scale on the GPR record is the result of complex midden stratigraphy and differences in dielectrics for each layer. Also, the test unit was identified by a cut in the stratigraphy consistent with a dug area.

The Oyster Farm survey is an example of the utility of this technique to provide results with limited time and ground-truth data. Information from one test unit was used, and the interpretation was carried across the site. The vegetation forced the

survey configuration to follow widely spaced transects, but a 10 m by 10 m grid allowed detailed survey at the tip of the point (Figure 4.8).

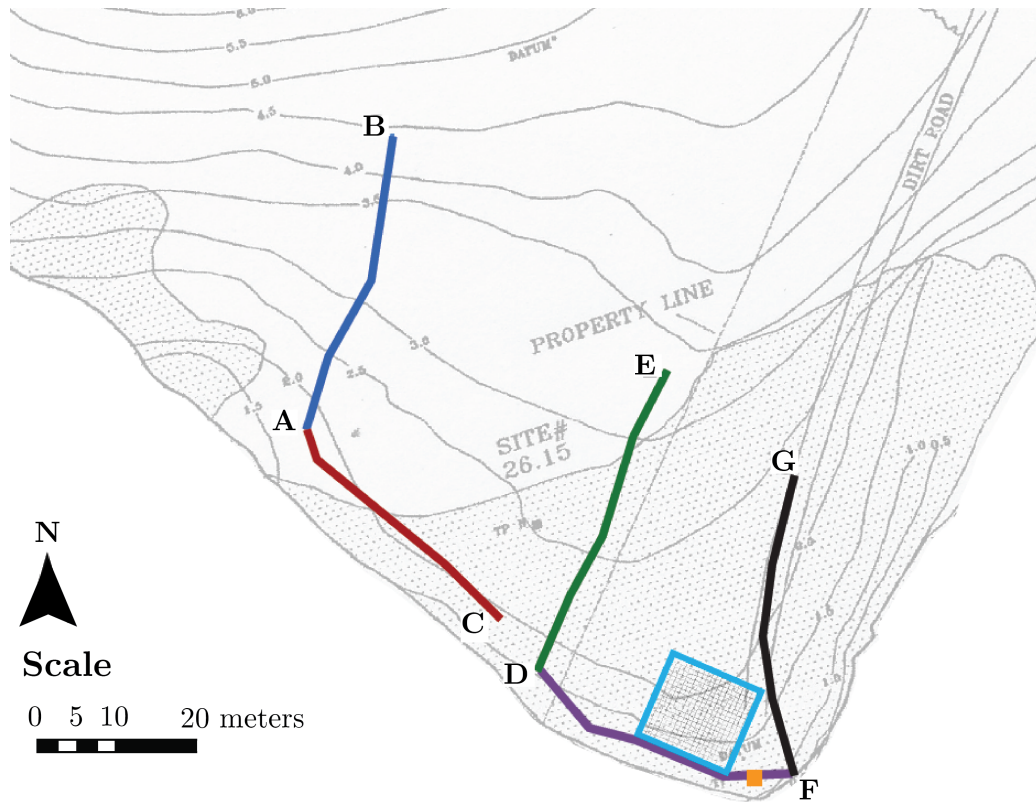


Figure 4.8: Damariscotta (Site 26.15) 500 MHz GPR map overlain on Arthur Spiess' shell extent basemap. The archaeological map shows shell midden extent (modified from Spiess, 1998). The detailed 0.5 meter grid is shown in the blue box, with a solid gold box representing a testpit location. GPR profiles collected on mowed paths are shown as colored lines with letters as beginning/end points.

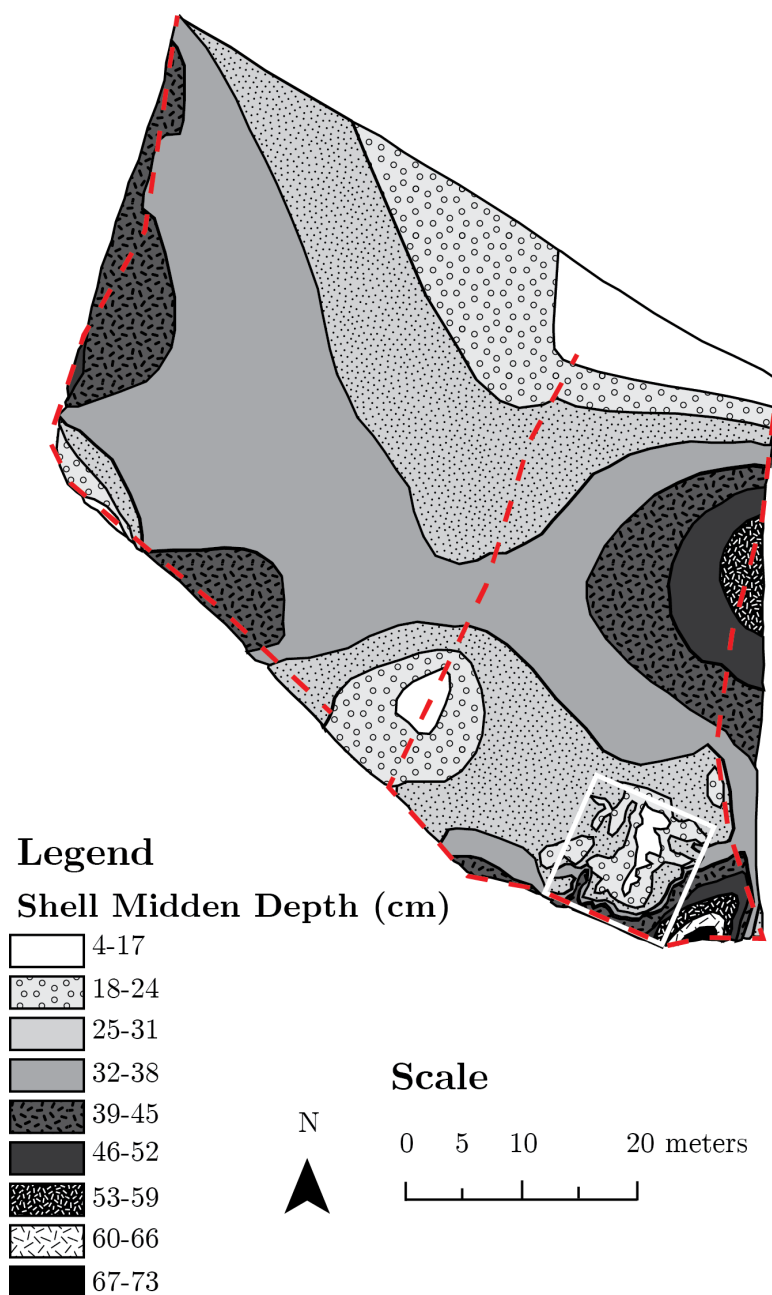


Figure 4.9: Damariscotta (Site 26.15) isopach map with 500 MHz GPR transects overlain. Dashed red lines represent 500 MHz GPR transects. A 10m by 10m white box outlines the area of detailed, 0.5 meter 500 MHz survey.

4.7 Olson (Site 17.13)

Located in the town of Cushing, Knox County, Maine, the Olson site faces south and contains dominantly clam-shell (*Mya arenaria*). An open grassy field covers the

site. The midden is up to 1-m thick and is underlain by glacial till. Excavated material ranged from approximately 2,400 years in age to Contact Period (Spiess, 2016b).

The Olson Site was discussed in the previous chapter, but the length of the paper prevented the inclusion of every aspect of the data. A total station survey of the grid was conducted during GPR data collection, with details presented in Appendix B.3.1. GPR profile collection and processing details as well as profile location maps can be found in Appendix C.1.4 and D.4. Enlarged archaeological wall profiles and photos are in Appendix E.3. Ground-truth location information data are in Appendix F.4. Stratigraphic notes from archaeological excavation are in Appendix G.1. Additional GPR and archaeological data comparisons are located in Appendix H.1. Information on isopach map construction is found in Appendix I.3.3.

Ground-truth information, along with the relocation of the archaeological grid, allowed confidence in interpretation of the GPR data. Shovel tests across the site and two trench profiles provided observations that refined the isopach map. Additionally, photos taken during excavation enhanced GPR interpretation.

4.7.1 GPR and Archaeological Data Comparisons

Sixteen meters of GPR interpretation for the east side of an archaeological trench dug in 1985 are displayed in Figures 4.10, 4.11, 4.12, and 4.13. Interpretation for the west side of the archaeological trench can be found in Appendix H.1. Each figure contains one unmigrated profile and a duplicated migrated profile. One migrated profile contains interpretation. The scale of the unmigrated profile differs from the two migrated profiles as a result of the migration.

A possible house floor was noted in the archaeological profile in Figure 4.10, and the surface associated with the postmolds appears as the strong reflector. The rock in the ground-truth profile provided confidence in GPR profile location and grid

orientation as it appears in the predicted location in the GPR data. Predicted shell thickness ranged from 25-35 cm in the GPR profile and 15-40 cm in the archaeological data. The base of the midden was picked at 35 cm on the N0E2 side of GPR profile (10m), but it is approximately 20 cm depth on the archaeological profile. The red arrows at 1 m and 3 m are pointing to a surface associated with postmolds in the next profile N8E2 to N4E2.

The archaeological profile in Figure 4.11 shows postmolds from N8E2 to N6E2. The red arrows point to a surface that appears as a strong reflector in the GPR data. Such a reflector could appear at the contact of two dissimilar materials, where water ponds, and in compacted areas. The strata on either side of the strong reflector appear cut and discontinuous, which would indicate digging associated with the formation of the compacted area. The area correlates with postmolds in the archaeological profile, and likely represents a housefloor. The compacted surface is approximately 2.2 m in length. Shell thickness ranged from 35-40 cm on the GPR interpretation and 15-24 cm on the archaeological profile.

Figure 4.12 represents N12E2 to N8E2, and it contains a feature identified in both the archaeological and GPR record. The 60 cm wide, pink basin-shaped feature, that appears to be dug into the midden, is circled in yellow on the interpreted GPR profile. The feature appears to occur on a rise delineated in both profiles. The GPR record supports the observation that the feature was dug into the midden and glacial material. The interpreted thickness of the shell ranged from 30 cm to 50 cm in the GPR profile and 25 cm to 38 cm in the archaeological profile.

No features of note were identified in the archaeological or GPR profile for the area from N16E2 to N12E2 in Figure 4.13. The thickness of the shell interpreted in the GPR record ranged from 45-50 cm, but the shell layer thicknesses ranged from 24-30 cm in the archaeological data. The reflector selected for the midden base in

Figure 4.13 appears washed-out in the area of ground-truth, and the true midden base would result in thicknesses between 25-40 cm.

A fire-reddened rock that appears to be standing upright in a pit feature in the first two meters of the western trench wall is of note (Figure H.1). Kendra Bird (2017) discussed a similar feature in her master's research on Holmes Point West (Site 62-8). The Holmes Point West feature was identified as "the standing stone" in Brian Robinson's field journal and was a large, oblong rock with an unmodified, flat base, and stood upright in a pit feature (Bird, 2017). Brian Robinson found that Ojibwa peoples used rounded boulders in medicine lodges, referred to as "grandfather stones" (Bird, 2017). Ethnographic accounts associated with the lodges made reference to bears, symbolized by the stones, that move through subsurface layers following hibernation (Bird, 2017).

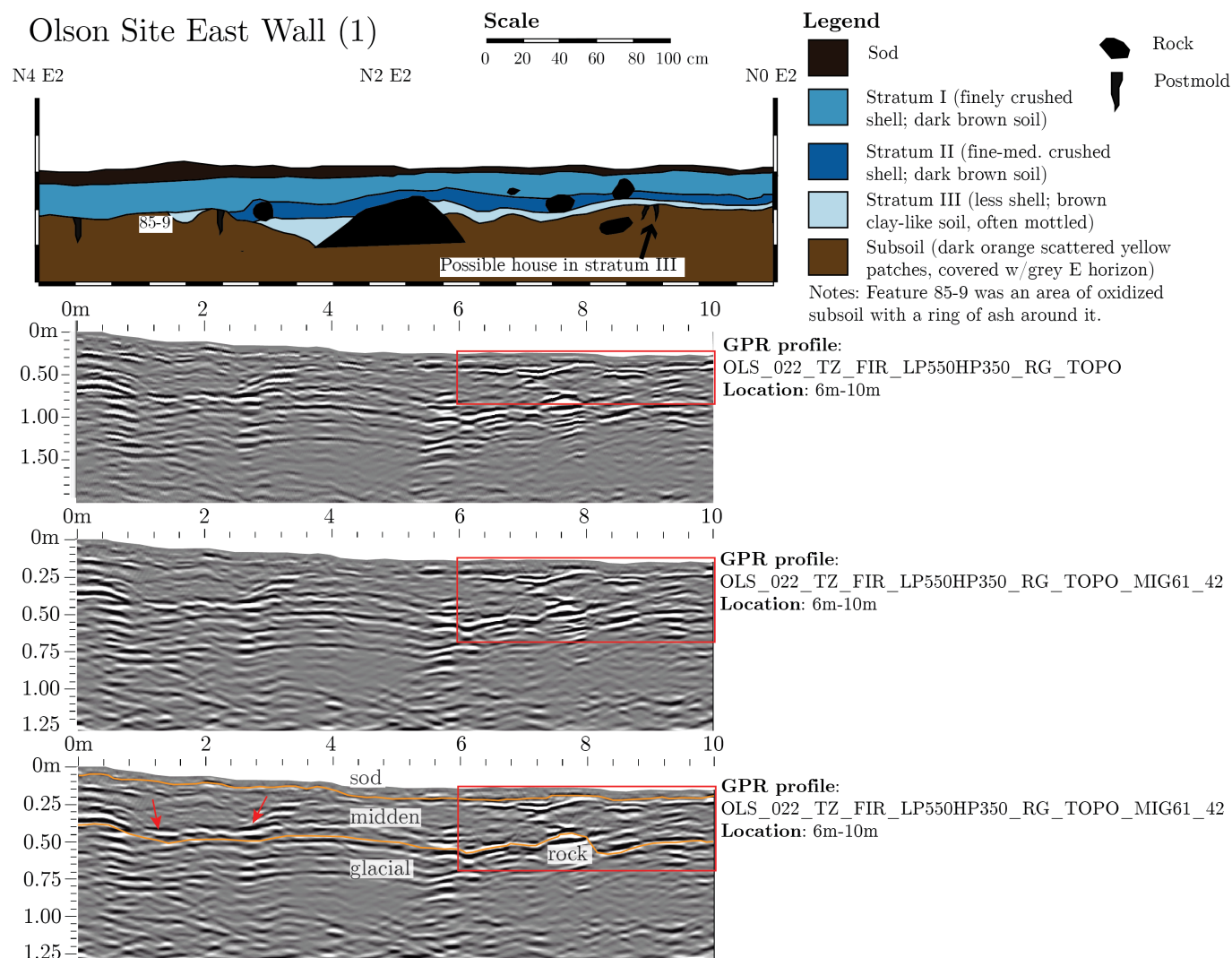


Figure 4.10: Olson (Site 17.13) east (1) GPR and archaeological profile comparison.

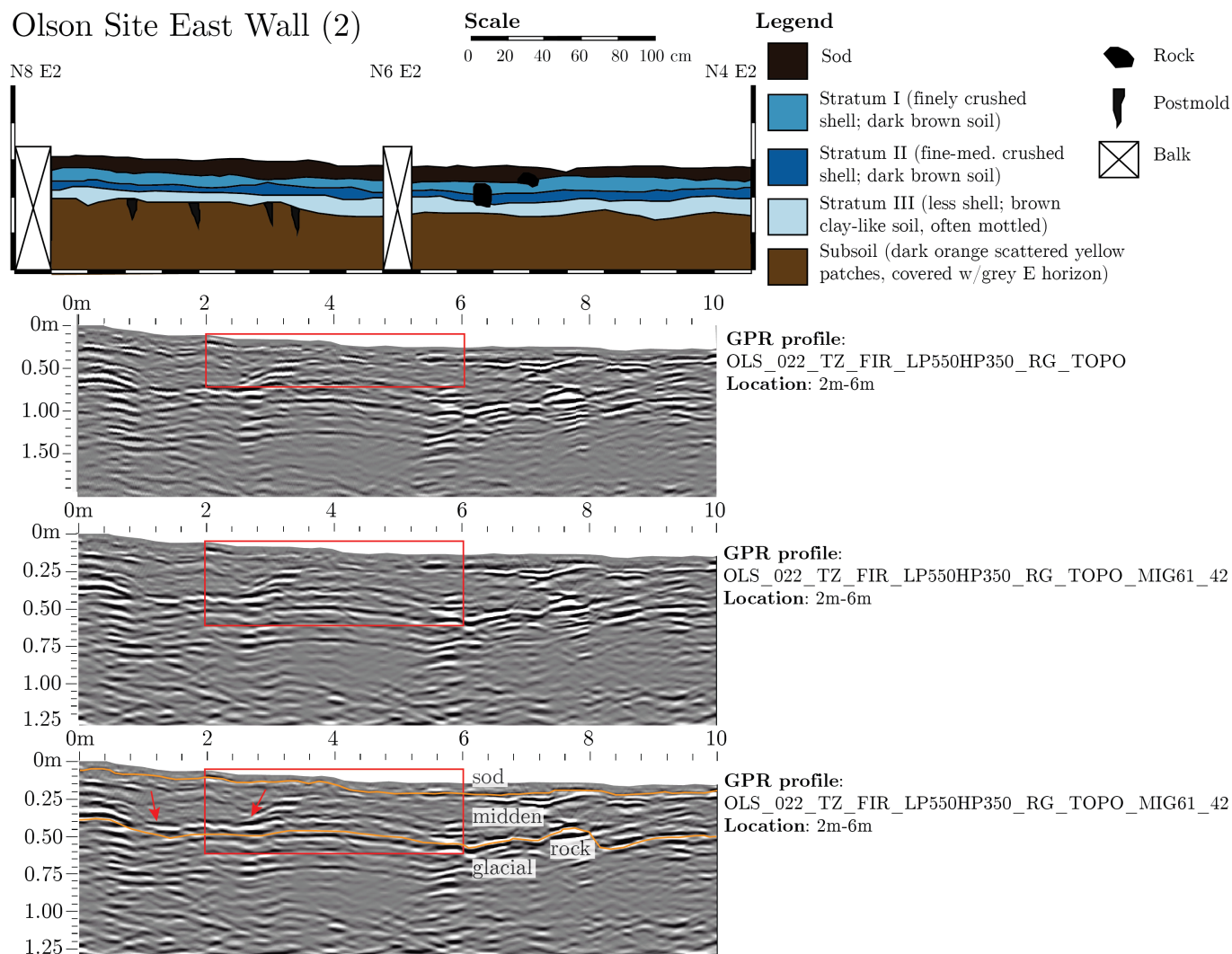


Figure 4.11: Olson (Site 17.13) east (2) GPR and archaeological profile comparison.

Olson Site East Wall (3)

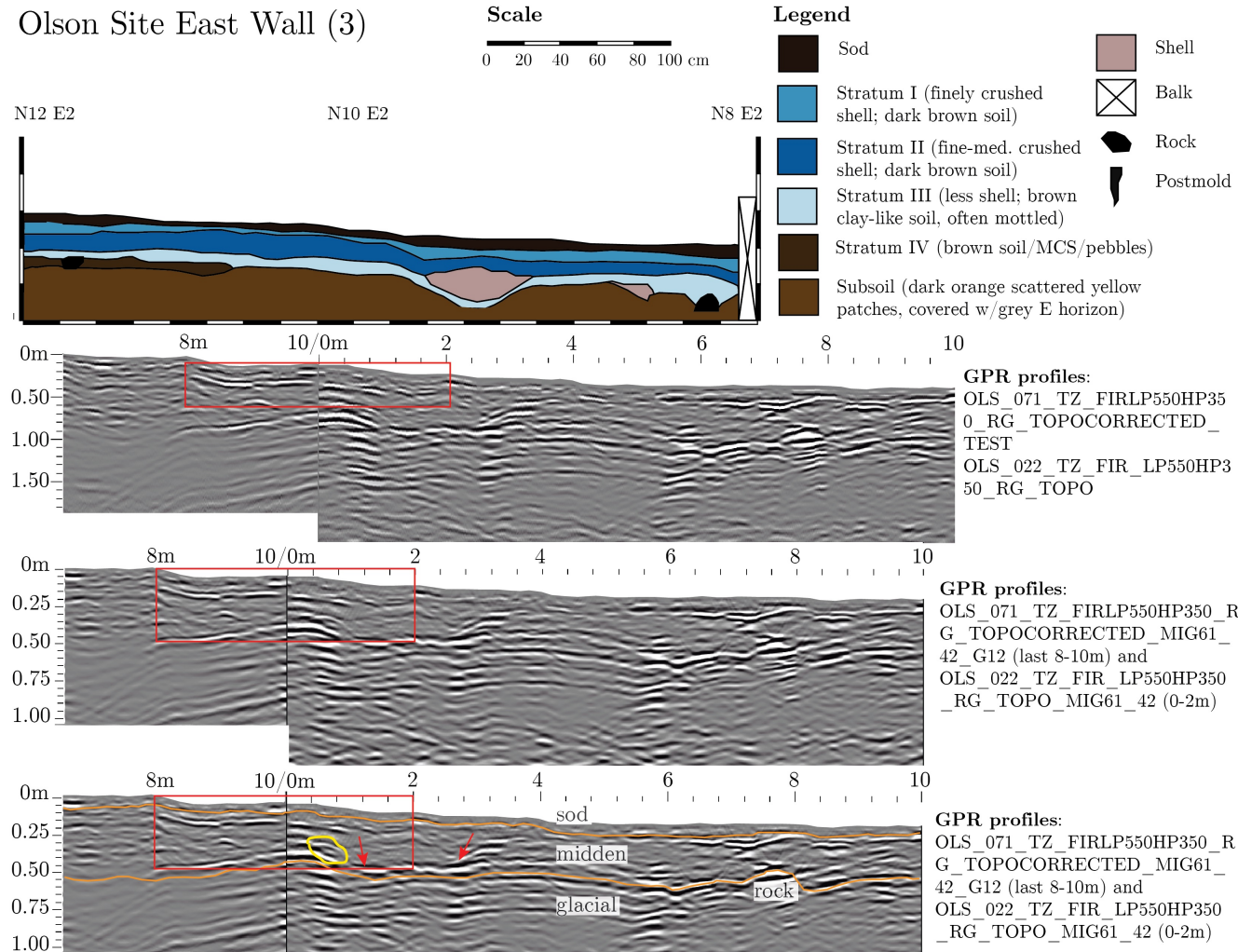


Figure 4.12: Olson (Site 17.13) east (3) GPR and archaeological profile comparison.

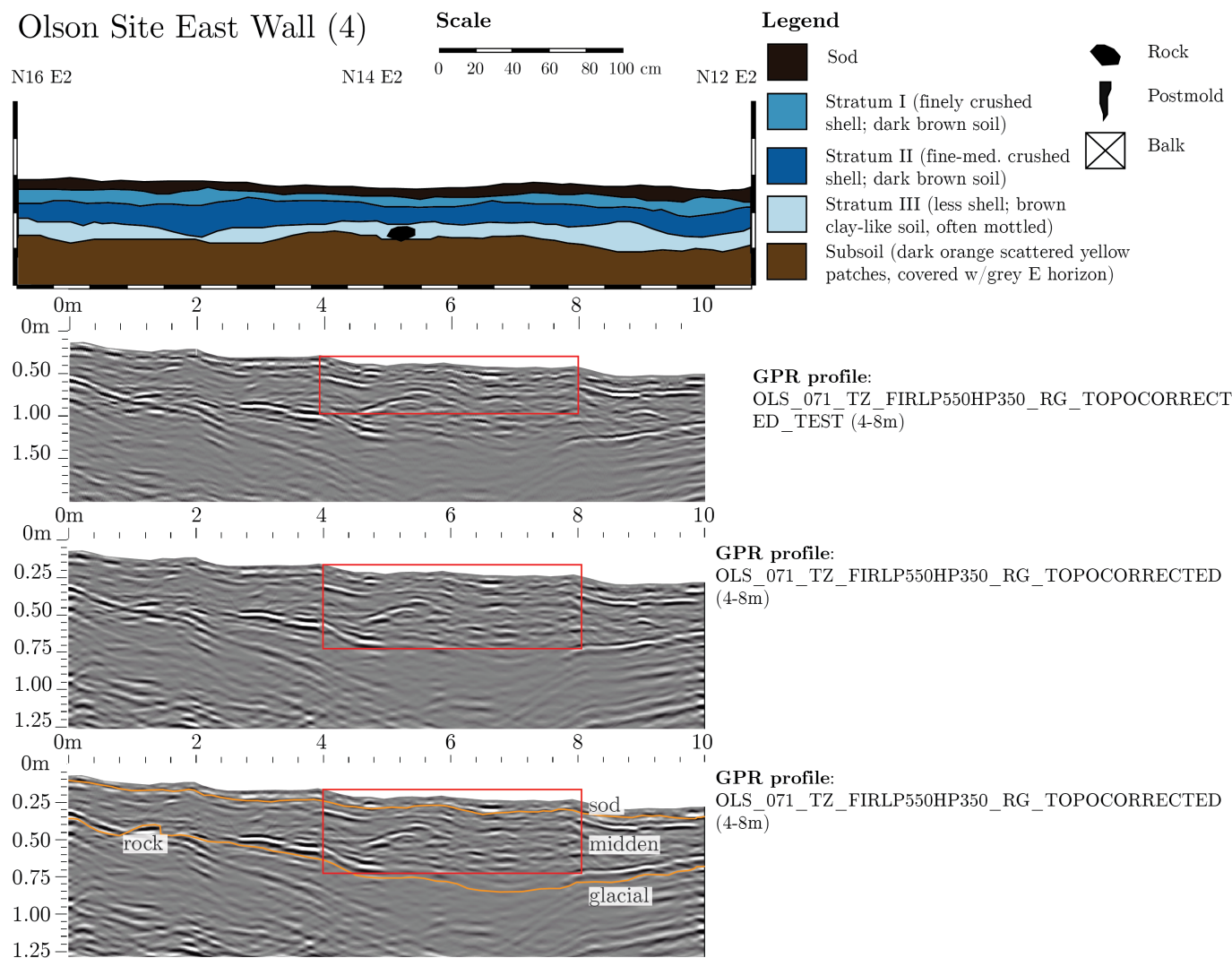


Figure 4.13: Olson (Site 17.13) east (4) GPR and archaeological profile comparison.

4.7.2 Error in Shell Midden Depth Interpretation

For the isopach map, the base of the midden was picked prior to the availability of ground-truth data. Table H.1 shows a comparison of the depth of shell midden noted during archaeological testing and the interpreted depth of midden from GPR profiles. Checking the original GPR picks against the ground-truth data revealed areas where the interpretation could more closely agree with the archaeological information. Detailed information is located in Appendix H.1.2.

4.8 Fernald Point (Site 43.24)

The Fernald Point site is situated in Southwest Harbor, Hancock County on Mount Desert Island, Maine. Site 43.24 is predominantly comprised of clam-shell (*Mya arenaria*), and is located near a moraine ridge. The shell midden overlies the mapped boundary between fine-grained glaciomarine deposits and thin till (Braun et al., 2016). The site was previously recorded as up to 65 cm thick, and 100 m by 40 m in areal extent (Spiess, 2016a). Fernald Point has the potential to represent pre- and post-European Contact Period culture (Sanger et al., 1980).

A RTK GPS survey of the GPR grid was conducted by Karen Anderson, National Park Service, Acadia National Park, and details are located in Appendix B.2.4. The GPS survey and pin-flagging every 10 m on a 60 m x 60 m grid prior to GPR survey dramatically decreased time in the field for grid set-up. Additionally, the equipment that allowed the rapid RTK survey was not available at the University of Maine during the time of data collection. Location information tied to the survey is on file with MHPC. GPR profile collection and processing information can be found in Appendix C.1.5, and associated profile maps are found in Appendix D.5. Enlarged archaeological wall profiles and photos are found in Appendix E.4. Location data for ground-truth are found in Appendix F.5.

The original datum of the archaeological grid was not relocated; thus, the spatial relationship with the GPR survey grid and the previous archaeological work is unknown. Visually matching the archaeological map with the location of the dock as well as the area with standing water and trees provided some level of confidence in the correlation between the grid used for the 1970's archaeological excavations and the current GPR survey.

Through the National Park Service, Acadia National Park, 38 archaeological profiles and several photos provided ground-truth information for Fernald Point. Gravel was common in GPR profiles across the site and was identified in archaeological profiles. During the GPR survey, gravel was observed eroding from one of the uppermost shorelines that cross the walking path and on the modern shoreline. Profile descriptions contained limited details on shell and shell content, and focused on the gravel component. Some descriptions included subjective/vague information such as "heavy shell midden," which made ground-truth of shell layers in the GPR record challenging.

Shell was always in association with gravel, but gravel layers did not always have shell. This suggests that not all the gravel layers are associated with cultural activity, and that some are related to storm deposits. The uppermost layer at the site was described as sod with beach gravel, often 10 cm thick. Storm deposits are common on the lower portion of the site, and were also likely deposited when sea level was higher and waves were shaping the terraces. An isopach map was not created because the midden would be traced on the basis of the signal of the gravel, and the gravel was not always associated with cultural activity. Additionally, it was difficult to identify midden layers without descriptive ground-truth, compounded with the inability to confidently relocate the archaeological grid.

4.8.1 GPR and Archaeological Data Comparisons

Three comparison profiles were made for the Fernald Point site, and the location information refers to a map (Figure F.5). The photos in Figure 4.14 were taken roughly from the position of point A, looking at the south wall of the 2 m unit. In Figure 4.15, the photo shows a majority of the unit wall represented by point D, and profile 38. Photos in Figure 4.16 are of wall profile 33, and also marked with point B for a general location. The red box in the GPR profiles identifies the location of the archaeological wall profile, or photo, when a profile was unavailable. The midden layer in each profile grouped all strata between the base of the sod and the upper contact of the subsoil noted in the archaeological profiles (glacial material).

The high electrical conductivity of salt causes attenuation of the GPR waves, and signal depth penetration becomes limited. Because the first 4 m of the record were topographically low enough to experience wetting by saltwater, the presence of salt prevented adequate depth penetration to image the midden with GPR in the area of ground-truth (Figure 4.14). The base of the shell is at 90 cm in the leftmost photo, but this window of shell was not observed in the corresponding location on the GPR profile. The midden that was once in that location is likely to have eroded in the time between excavation and GPR survey as this site has been heavily impacted by storms, notably, those that occurred during the winter of 1978. After the salt-washed out area in the GPR data, the GPR signal resolved the potential base of the midden in the remaining 6 m of profile. However, interpretation is not certain due to the lack of ground-truth and lack of confidence in correlation between the original archaeological profile and the GPR record. The midden is deposited upon glacial material, which is identified on the basis of strong, discontinuous, dipping reflectors at the base of the profile (Figure 4.14).

Figure 4.15 contains a close-up photo of approximately 40 cm of the midden in the west wall of 45P to 45N. The location of the photo is represented by the area

delineated with the red box on the archaeological profile. Sod is consistently 10-20 cm thick across the GPR profile, and confirmed by the archaeological data. GPR data suggest the underlying midden layer ranges from 28-38 cm, and it is 20-28 cm thick in the archaeological profile. Red arrows point to either side of the actual 2 m excavation unit.

The west wall of 64T to 64R is depicted in Figure 4.16. The thickness of the midden layer ranged from 26-32 cm in the GPR data, and 22-32 cm in the archaeological profile. Photos in the upper right corner of Figure 4.16 show large rocks within the midden as well as the gravelly nature of the Fernald Point site.

Fernald south wall 8W to 10W

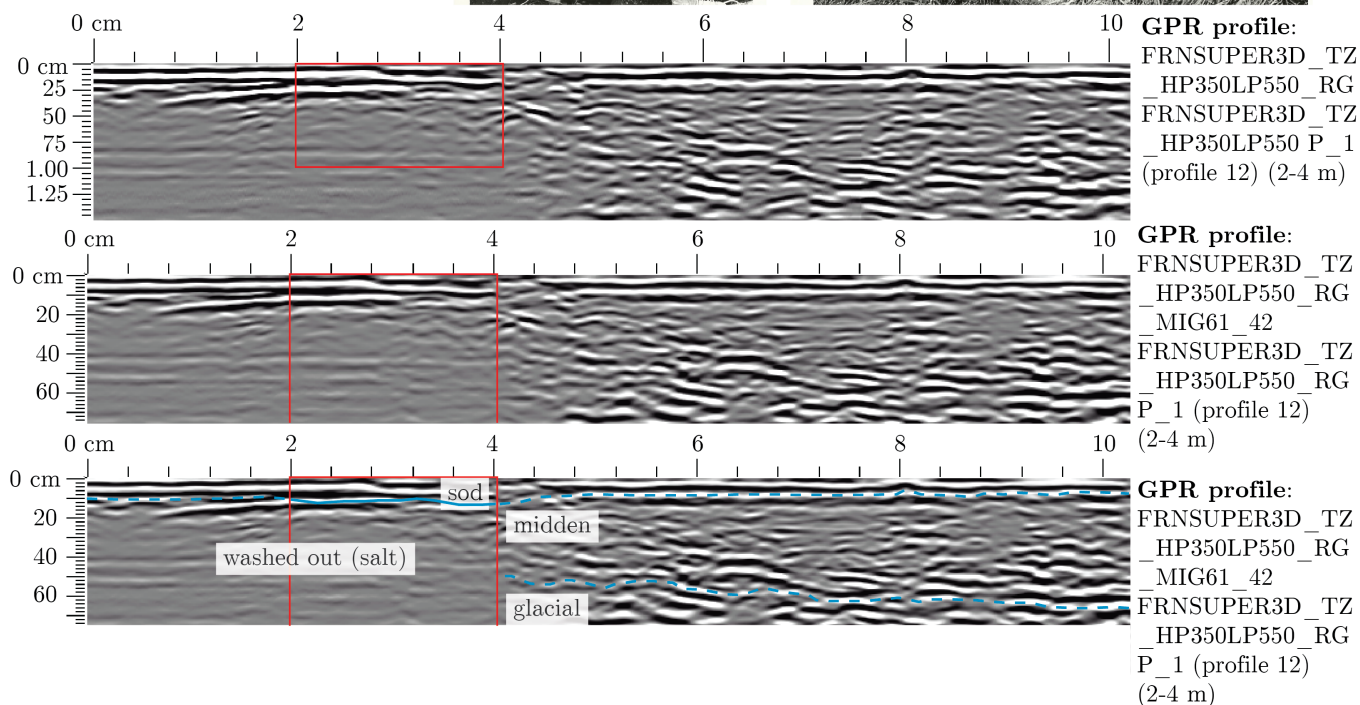


Figure 4.14: Fernald Point (Site 43.24) 10W to 8W south wall GPR and archaeological profile comparison. The red boxes on the GPR profiles represent the archaeological profile location. Photo and original profile courtesy of Acadia National Park.

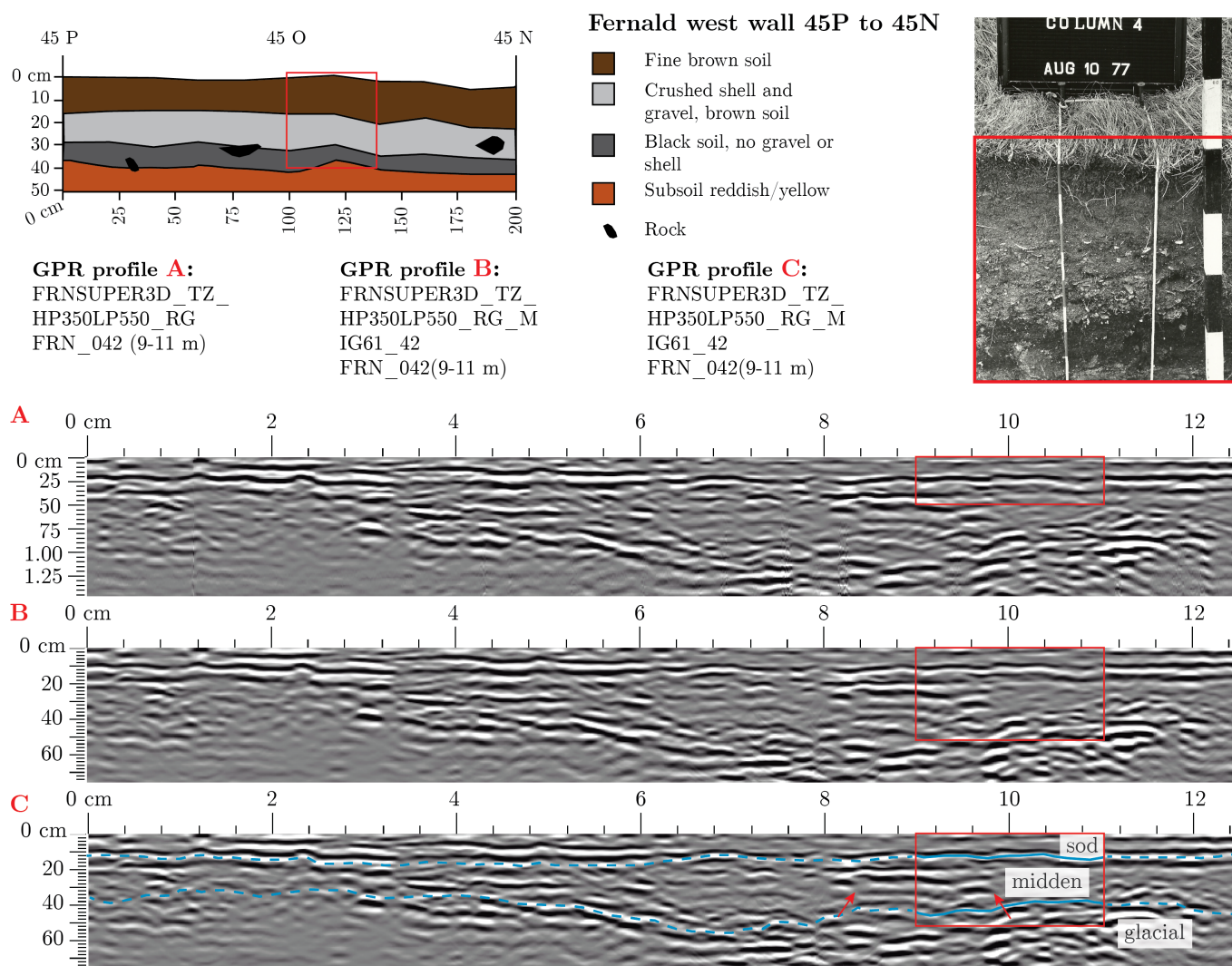


Figure 4.15: Fernald Point (Site 43.24) 45P to 45N west wall GPR and archaeological profile comparison. The red boxes on the GPR profiles represent the archaeological profile location. Red arrows point out the start and end of the potential 2 m unit location. Photo and original profile courtesy of Acadia National Park.

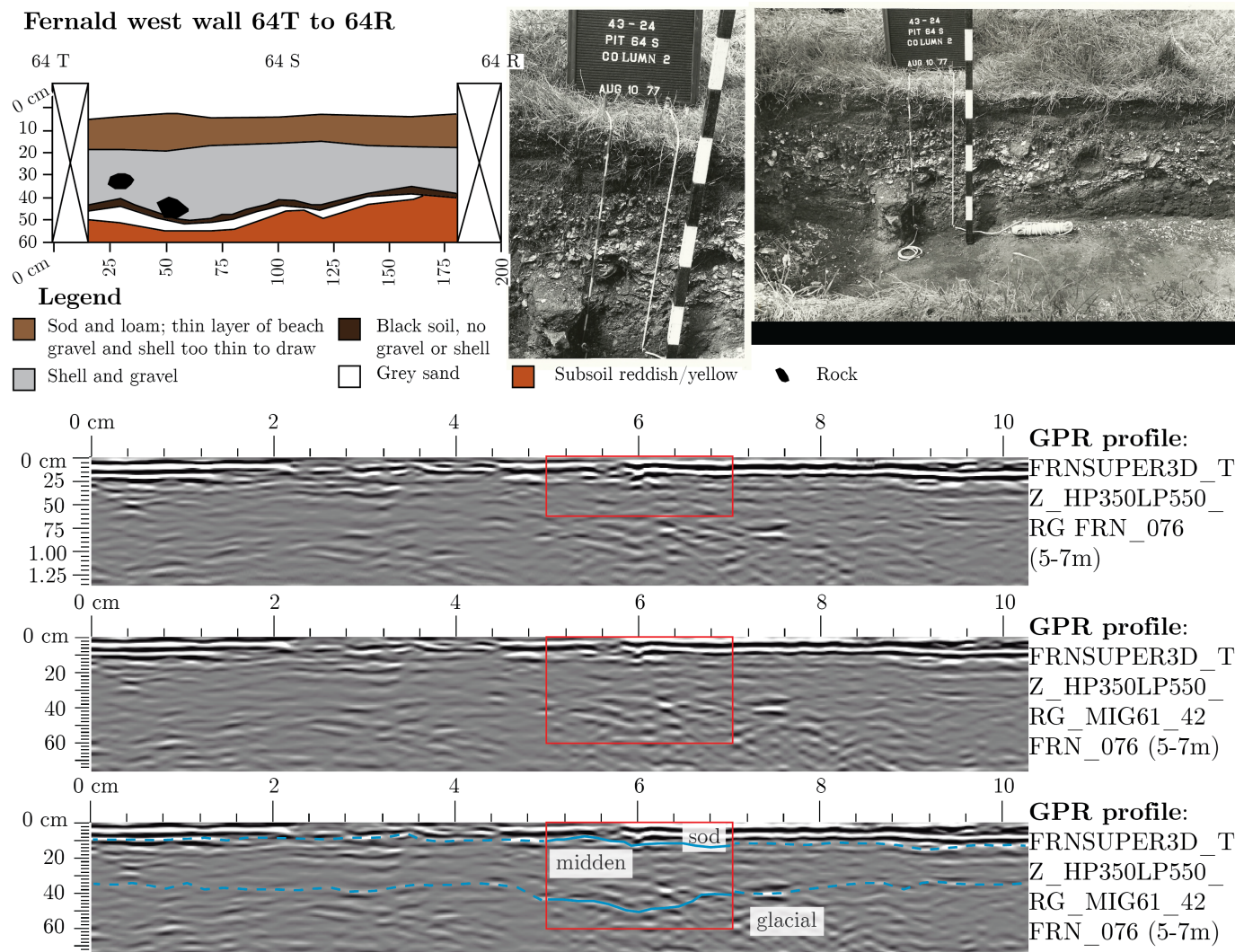


Figure 4.16: Fernald Point (Site 43.24) 64T to 64R west wall GPR and archaeological profile comparison. The red boxes on the GPR profiles represent the archaeological profile location. Photo and original profile courtesy of Acadia National Park.

4.9 Tranquility Farm (Site 44.12a)

Situated in Gouldsboro, Hancock County, Maine, the Tranquility Farm site faces south and contains predominately clam-shell (*Mya arenaria*). The midden overlies wave-washed glaciomarine material and is covered by a grassy field. Original midden dimensions were reported as 150 m by 30 m with shell depth up to 1-m.

A total station survey was conducted during GPR data collection, and details are located in Appendix B.3.2. Information on GPR profile collection and processing can be found in Appendix C.1.6 and C.2. Maps of profile locations are in Appendix D.6. Enlarged archaeological wall profiles and photos are in Appendix E.5. Ground-truth location information is found in F.6. Stratigraphic notes from archaeological profiles are located in Appendix G.2. Details related to the isopach file information and alternate versions of the isopach maps are located in I.3.4.

The base of the midden at Tranquility Farm was identified in GPR profiles by selecting the horizon between strata impacted by past cultural activity and GPR signal associated with regular and repetitive geology. Figure 4.17 represents a disturbance into the underlying geology, associated with midden strata. The feature begins at the surface of past cultural activity, and does not represent modern digging, as the overlying strata are intact. Underlying wave-washed glacial material, with dipping beds, was exposed in the eroding bluff. Figure 4.18 shows the strata in photographs and in a GPR profile.

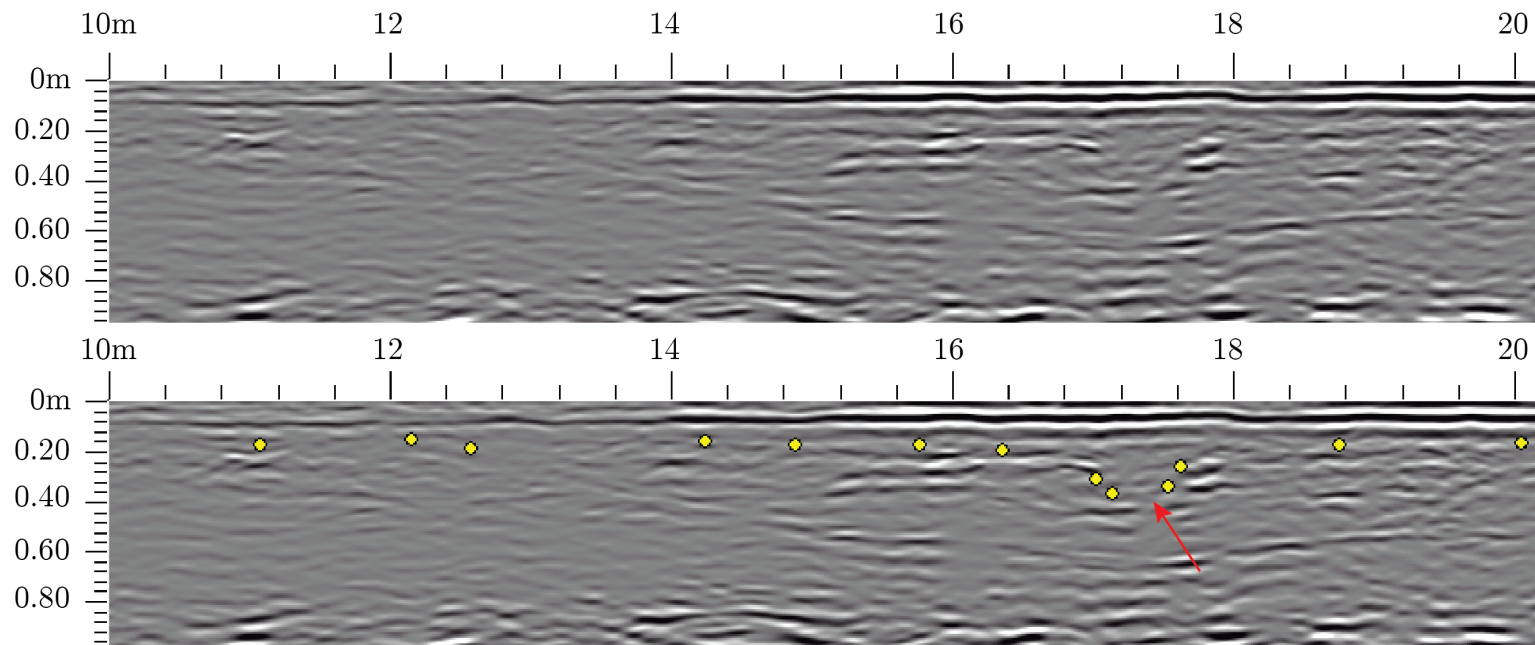
An isopach map was created after delineating the midden base in the GPR profiles. Figure 4.19 contains green dots that represent GPR transects, and Figure 4.20 is a duplicate that lacks transects. The southeastern section, between the two maps, is an area that was disturbed by W.K. Moorehead in the early 1900's. The blank portion in the middle of the two maps is the position of the cabin. Shell midden is thickest on the easternmost isopach map. The thickest portion of midden

is represented by pink and white, on the southwestern side of the easternmost isopach map. The midden in this area is bounded by the sea, and under threat.

Midden is present throughout the isopach maps, but the original size of the site was likely much more extensive. Following Sanger's (1981) model of midden occupation, the thickest portion of the site, commonly up to 1 m thick, should be at the beachward edge. The isopach (Figure 4.20) shows an eroding/eroded site front.

Areas of localized midden were found around the main site during GPR survey. These satellite middens are likely concomitant with the formation of the larger midden, but do not have dates associated with them. With the exception of one area, all other mini-middens were found in slump material along the beach. The last area was identified when support posts were dug, but no shell was observed in adjacent slump material along the bank. Locations taken with a hand-held GPS (Garmin GPSMAP 62St), as well as brief descriptions, are on-file with MHPC.

TRQ_G2TEST2_TZ_FIR_LP550HP350_RG_MIG64_41_PICKS_NOYELLOWDOTS TRQ_APP136-
TO139 P_1121



TRQ_G2TEST2_TZ_FIR_LP550HP350_RG_MIG64_41_PICKS TRQ_APP136TO139 P_1121

Figure 4.17: Tranquility Farm (Site 44.12a) disturbed area in GPR profile on western 500 MHz GPR survey grid.

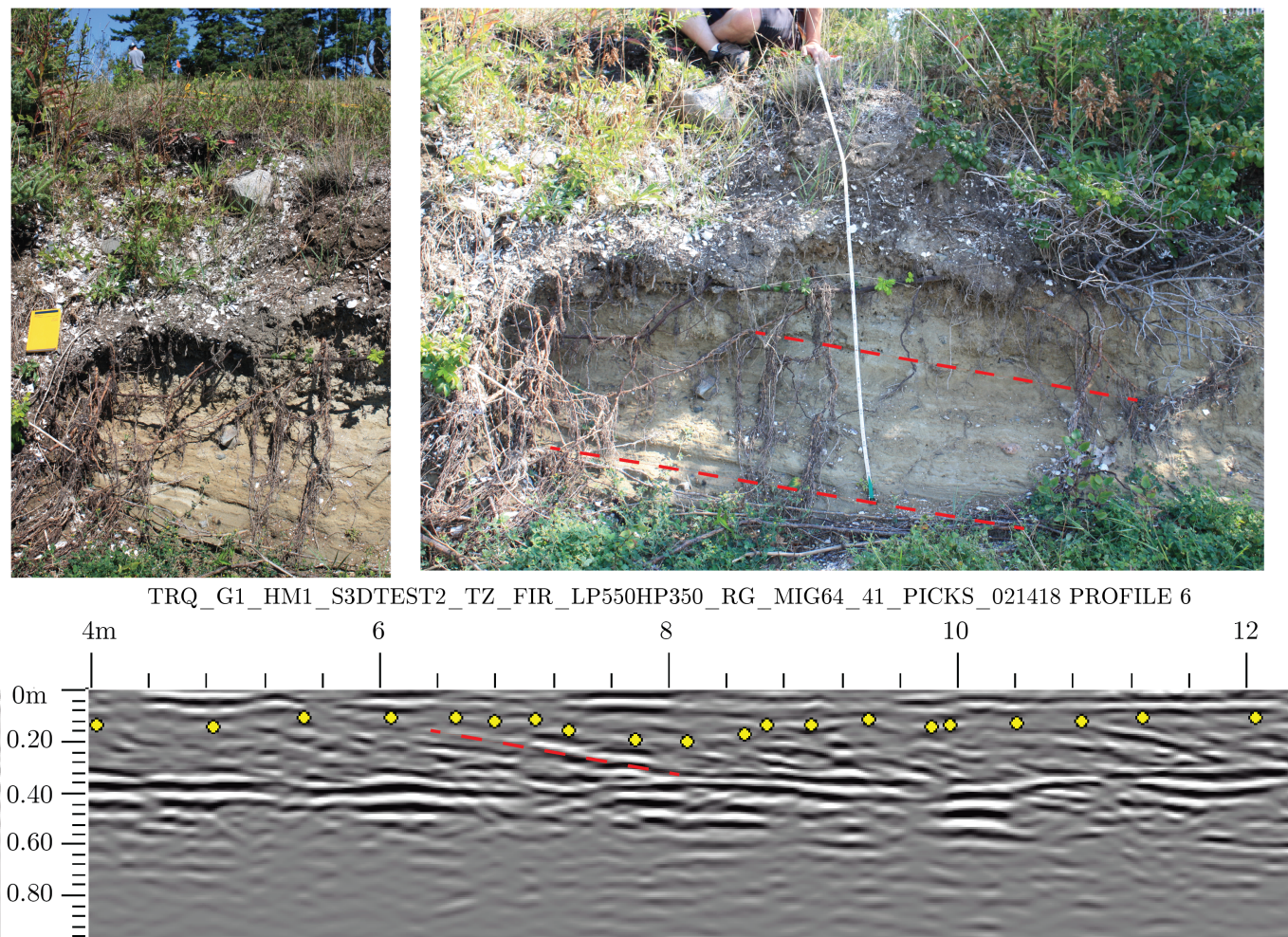


Figure 4.18: Tranquility Farm (Site 44.12a) underlying geology seen in photo and GPR profile. Red dashed lines highlight the dipping strata. The yellow dots denote the base of the midden, which is also the top of the dipping strata.

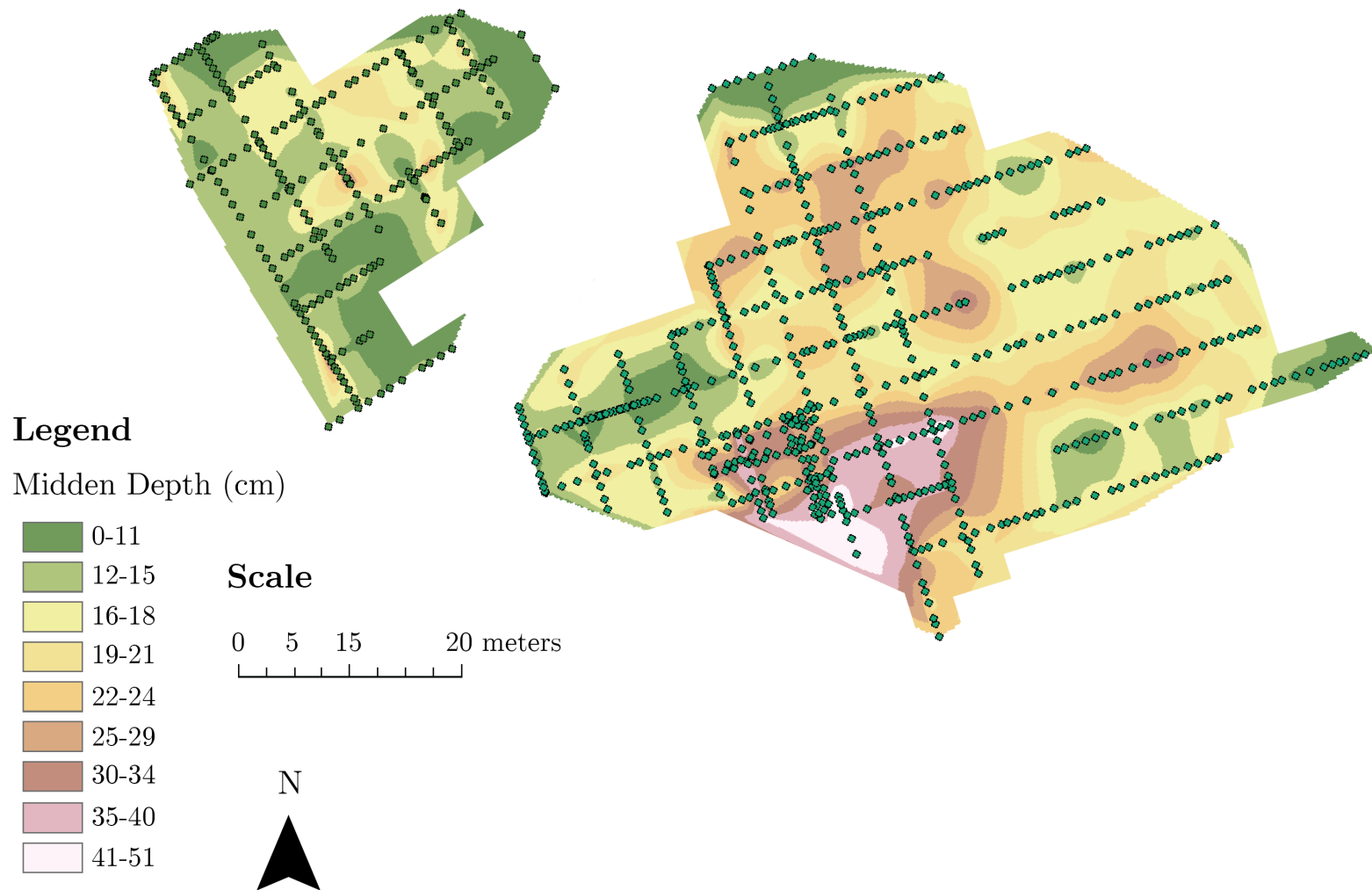


Figure 4.19: Tranquility Farm (Site 44.12a) isopach map with 500 MHz GPR survey transects overlain. GPR survey transects are represented by the green dots.

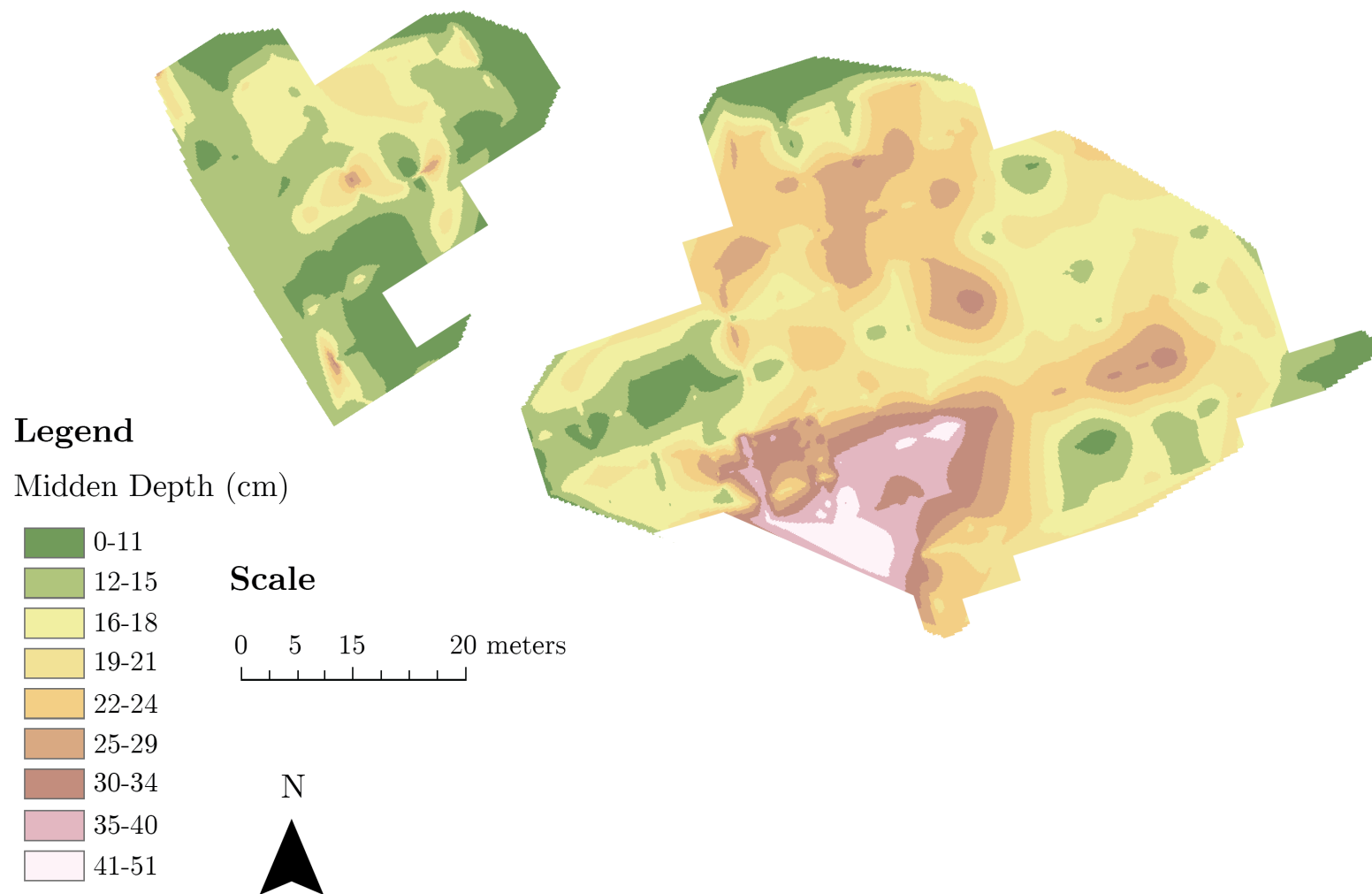


Figure 4.20: Tranquility Farm (Site 44.12a) isopach map.

4.9.1 Error in Shell Midden Depth Interpretation

Stratigraphic information from shovel tests across the eastern area of 500 MHz GPR survey proved most useful for ground-truth during data interpretation. Each location shown in Table 4.1 is marked with the associated letter on the map in Appendix F.7. Detailed stratigraphic notes are located in Appendix G.2. Ground-truth data do not exist for the western area of 500 MHz GPR survey.

Archaeological profiles and photos exist for the site (Appendix E.5), but they are in large areas of disturbance resulting from archaeological excavation. The profiles near to the disturbed sections are also disturbed as they are in the same excavation zone. Profiles in less disturbed areas are several meters from the GPR profile ideal for comparison. Given the variability of shell middens, a direct comparison is most ideal.

Areas of stratigraphic information from shovel tests are compared to interpreted shell midden depths from GPR profiles in Table 4.1. Depths show good agreement. An exception to this agreement is in an area marked as no site, but the difference lies in the interpretation of "site". The GPR data show a layer above the glacial sediments that appears to be impacted by human activity, though no shell was identified in the shovel test.

Table 4.1: Tranquility Farm (Site 44.12a) site midden thickness comparison: stratigraphic data and GPR interpretations.

Map ID	GPR Profile ID	Distance from GPR Transect	Location on GPR Transect	Map Location	GPR Pick Depth (cm)	Actual Depth to Subsoil (cm)
a	Profile12	1 m south	10 m	N94W85	24	base of shell: 24 cm
b	43	on profile	7 m	N106W107	37	dense gravel: 25 cm (isopach)
c	Profile9	on profile	8 m	N105W92	40	base of shell: 45 cm (0-30 cm FCS)
d	Profile12	2 m south	8 m	N93W87	22 cm	subsoil: 30 cm
e	45/22	on profile	4m/5m	N105W104	25 (isopach)	3-4 postmolds 8 cm diameter; interpreted as housefloor
f	Profile12	1 m south	8 m	N94W87	22	base of shell: 34 cm
g	45/24	on profile	5 m	N105W105	30 (isopach)	40 cm MCS
h	47/26	on profile	6 m	N104W106	24/30	subsoil: 30 cm

Table 4.1: Continued

Map ID	GPR Profile ID	Distance from GPR Transect	Location on GPR Transect	Map Location	GPR Pick Depth (cm)	Actual Depth to Subsoil (cm)
i	41/28	on profile	7m/3m	N107W107	33/43	subsoil: 45 cm
j	Profile8	on profile	23 m	N110W102	25	>30 cm MCS, beach gravel, black soil
k	Profile6	on profile	27 m	N115W98	25	>30 cm MCS, black soil
l	Profile5	on profile	15 m	N120W95	24	>30 cm MCS, beach gravel, dark brown soil; potential house floor
m	Profile4	on profile	10 m	N125W95	23	>25 cm MCS, gravel; S edge of field road
n	Profile3	on profile	5 m	N130W95	26	>25 cm black sandy soil
o	Profile2	1 m south	5 m	N134W95	21	no site
p	Profile8	on profile	45 m	N110W80	21	>30 cm MCS and beach gravel in black soil

Table 4.1: Continued

Map	GPR	Distance	Location	Map	GPR	Actual Depth to
ID	Profile	from	on GPR	Location	Pick	Subsoil (cm)
	ID	GPR	Transect		Depth	
		Transect			(cm)	
q	Profile8	on profile	55 m	N110W70	22	20 cm FCS

4.10 Summary

The first step in the midden delineation using GPR protocol involved gathering ground-truth data from previous archaeological excavations at each site. Anderson (2018) provided ground-truth information on the University of New England site. Archaeological profiles and maps related to the Long Island North site were provided by Doyle (2017). Maine Historic Preservation Commission provided archaeological profiles, photos, stratigraphic information and archaeological maps for the Oyster Farm, Olson, and Tranquility Farm sites. The National Park Service, Acadia National Park provided access to ground-truth data for the Fernald Point site.

Shell middens were selected for GPR survey following a site visit to determine the suitability for GPR survey in terms of site condition and vegetation. The survey began after the original archaeological grid was reestablished to utilize existing stratigraphic data. Confidently tying the location of the GPR profiles to past archaeological grids is critical to the minimally invasive nature of this approach. It is possible to carry an interpretation across a large area, but accurately locating and linking the GPR survey to the grid from which the ground-truth data are associated with is a necessity. Effort was made to closely follow the known archaeological grid, but slight deviations exist if the original archaeological datum was unknown.

GPR data collection began after the survey grid was spatially referenced with a total station, handheld gps, or RTK survey. Transect spacing was determined by the estimated areal extent of the site, the area conducive to GPR survey, and time constraints. Data were then processed in the lab for interpretation.

Stratigraphic profiles were redrawn to standardize the interpretation of the stratigraphic data and facilitate comparison to the GPR record. Additionally, information from the stratigraphic notes was disseminated and input into a table or list form.

Ground-truth data were compared to the GPR records, and the interpreted midden depth was forced to closely match the observed midden depth at ground-truth locations. Traditional hyperbola matching during data migration did not result in thicknesses that agreed with the observed shell midden depths. The differences between midden depth in the archaeological and GPR profiles are attributed to a number of factors. GPR data could not entirely resolve the level of detail within the archaeological profile due to the resolution associated with the 500 MHz antenna, material properties, and error in depth resolution. A higher frequency antenna (900 MHz) would provide greater resolution, but the shallow depth penetration would not allow investigation of the underlying geology. The properties of midden layers with dissimilar amounts of crushed and whole shell, with varying amounts of soil, result in dielectric constants unique to each layer. Radan (Beta 7) forced a single dielectric for the entire GPR profile, which prevented a depth correction tailored to each unique strata.

Each shell midden site had dissimilar material properties, and showed variability in composition across the individual site. Utilizing archaeological data from areas outside of major ground disturbance is ideal for interpretation. Alternatively, GPR transects may be placed closer together near the outer regions of the disturbed areas.

The shell midden extent and thickness were delineated following the GPR record depth correction and ground-truth data comparison. Interpreting the base of the midden at each site required a unique approach. The University of New England site was an exception as no shell was observed in-situ, but strata were identified in comparison profiles (Figures 4.1, 4.2, and 4.3). These strata were continuous across the surveyed area at UNE. Interpreting the Long Island North GPR data proved challenging as the dielectrics of the bedrock and overlying midden and till were similar. The Damariscotta and Olson middens were delineated on the basis of a strong reflector at the contact of porous and permeable midden material

and impermeable glacial material. Site delineation with the Tranquility Farm data involved differentiating between geological and human-altered strata, as the strong reflector was not always associated with the midden base.

Finally, the X, Y, and Z data from the interpretation/delineation process was input into ArcGIS to create an isopach map for Long Island North, Damariscotta, Olson, and Tranquility Farm. The isopach map produced for the LIN site represents the maximum potential depth of midden as shell midden was difficult to distinguish from till. A combination of factors prevented isopach map construction with the Fernald Point data, including the presence of gravel occurring throughout the profiles in natural and cultural contexts, intensive site erosion, limited shell information within the profile descriptions, and the inability to relocate the archaeological grid.

This project highlights the importance of thorough note taking during archaeological excavation, and record management in the time following. Data from excavations are critical as sites continue to erode and resources dedicated to cultural resource management are limited. Correlating existing archaeological information with GPR profiles is dependent upon the relocation of the original archaeological grid. For example, the Fernald Point site had ample ground-truth information, but the original archaeological grid could not be relocated. The available data only permitted a rough alignment between the Fernald Point excavation and GPR survey maps.

Utilizing a standardized, or quantitative set of descriptors for shell middens could ensure the collection of critical details. Additionally, high-resolution photography is ideal for informing stratigraphic interpretation.

Chapter 5
STRUCTURE FROM MOTION AS A NEW METHOD
OF ANALYZING SHORELINE CHANGE IN
ARCHAEOLOGY: AN EXAMPLE
FROM COASTAL MAINE

5.1 Abstract

Approximately 2000 aboriginal shell middens along the coast of Maine archive a unique record of cultural and climatic change, but these archaeological sites are continually lost to the sea through climate-driven sea-level rise and coastal erosion. A shell midden refers to a cultural accumulation of centimeters to meters of clam and/or oyster shell in association with artifacts and faunal remains. Documenting the impacts of shoreline change provides insight as to which sites to prioritize for rescue or preservation, which is critical with limited resources. One archaeological site was chosen for this study, and two methodologies were applied to analyze shoreline change: traditional historic aerial imagery time-series, and *Structure from Motion* (SfM). Historic imagery was georeferenced in ArcMap geographic information system (GIS) platform (ArcCIS 10.4; Esri software). Additionally, the United States Geological Survey Earth Explorer (USGS EE) site was used to download georeferenced orthoimagery as GeoTIFFs and non-georeferenced or orthorectified vertical cartographic imagery. The aerial imagery allowed the construction of a long-term (decadal) comparison of shoreline change; however, the poor resolution prevented definitive conclusions concerning shoreline change. *Structure from Motion* is presented as a practical alternative because it provides a finer-grained record of site loss and coastal erosion at less cost and with greater ease for repeat survey than LiDAR and aerial photography.

5.2 Introduction

Quantitatively documenting erosion at coastal archaeological sites plays a critical role in the prioritization of limited time and monetary resources to the rescue and preservation of cultural heritage. Understanding the impacts of episodic erosion at each site is vital as factors influencing the severity are unique for each shell midden. A shoreline change study was carried out on the basis of historic aerial photography, but the resolution for the rate of change observed and the lack of periodicity in erosional events contribute to the method's inability to capture the necessary level of detail in Maine. Issues with shoreline change investigations along the coast of Maine were also encountered by Kelley and Kelley (2006), who noted episodic, storm-driven erosion from decades of coastal observation. In addition, Kellogg (1982) was unable to detect erosion when he compared both US Coastal survey charts with USGS quadrangle maps and historic aerial photography of a section of the Maine coast, for a 100-year and a 40-year span respectively.

ArcGIS provided a platform from which to analyze shoreline change at the Olson (OLS) archaeological shell midden site, located along the coast of Maine (Figure 5.1). Aerial photos were georeferenced to create a series of images from which to trace shorelines through time. Pre-georeferenced and orthorectified imagery provided the source for georeferencing.

Terrestrial laser scanning (TLS) is another method for shoreline change analyses. Neitzel (2014) utilized TLS to obtain sub-centimeter resolution bluff erosion data at seasonal transition points. TLS would provide the scale required for monitoring bluff retreat along the coast of Maine, but a major reason for the lack in widespread usage is the price of the hardware. In contrast, SfM utilizes digital photography to capture the area of interest and software to model it in a 3D environment at a similar resolution as TLS survey data. This dramatically decreases entry costs and increases accessibility. SfM survey was identified as the superior

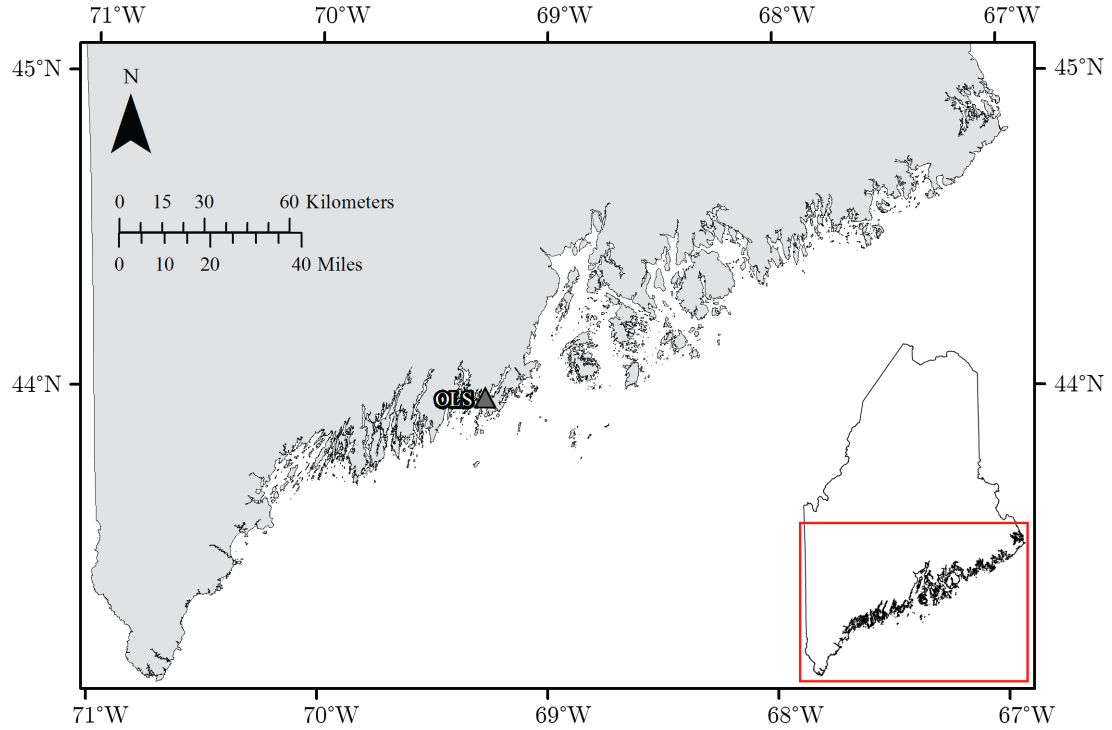


Figure 5.1: Olson site location.

methodology due to the accessibility and robustness as the least subjective method to record midden erosion over time. We show that the application of SfM survey techniques will offer the ability to maintain a more regular and finely detailed record of erosion and site loss.

High-resolution digital cameras, available to the general public, capture a rich level of detail and when mounted to a consumer grade unmanned aerial vehicle (UAV). These devices enable the capture of a range of perspectives through aerial photography, especially close-up oblique views of the bluff face, with only a few hours of flight. Computers, empowered by modern graphics processing units and expanded memories are more capable than ever of rendering digital surface models. Applications of SfM rival products of terrestrial LiDAR and boast a reduction in data-collection time by nearly 80% (James and Robson, 2012). Acquisition of high-quality site-specific geomatics data is no longer barred by high operational and logistical costs (Westoby et al., 2012; Clapuyt et al., 2016). Unmanned aerial

vehicles UAVs make photograph acquisition from varied perspectives simple, merely limited by battery life, fair weather, and clear space to fly.

Unlike TLS or LiDAR, where the precise location of a measurement system must be established to properly range a signal between the scanner and the subject to construct a model, Structure from Motion exploits the principles of parallax to reconstruct a scene in three dimensions. Given a sufficient variety of perspectives and overlap within photographs, information about the precise position of the camera is unnecessary and is back-calculated during the SfM process. Our application of SfM is streamlined by the use of Agisoft's Photoscan (version 1.3.4 build 5067; under an Educational License), a succinct program that marries foundational computer-vision techniques such as Multiview Stereopsis (Furukawa and Ponce, 2010) and Scale-Invariant Feature Transform (Lowe, 1999, 2004).

The SfM survey of the Olson Site demonstrates the applicability of SfM to document shell midden site loss with greater frequency of observation due to little need for expert training, expensive equipment, or time-intensive surveys (James and Robson, 2012). The record created with SfM results in finer-scale data than permitted by traditional aerial photography, which is typically reported to a precision ratio of 1:1000 (James and Robson, 2012). The SfM model of the Olson site digitally preserved the state of the eroding midden edge at the time of survey, and serves as a baseline for repeat, future measurements. Approximately 350 photographs were taken during 1 hour of a UAV flight . Processing in Photoscan resulted in the selection 213,779 photogrammetric tie points and generated a point cloud model comprised of 62,685,358 dense cloud points and was constrained by a set of Topcon global-positioning system units (GB-1000, with a PG-A1 + GroundPlane antenna) placed around the site. The resulting digital surface model boasts an approximate resolution of 2 cm/pixel.

5.2.1 Bluff Erosion in Coastal Maine

White shell covering the beach serves as an indicator of shell midden loss. Sites are constantly impacted by chronic erosional processes, but less frequent storm-driven waves cause more intense damage episodically. Wave-energy reach increases with a rising sea level; thus, erosion is exacerbated (Himmelstoss et al., 2006). Increased freeze-thaw action due to climate-change will likely lead to accelerated shell midden site loss along the entire coast. Factors such as wave fetch, coastal morphology, and storm energy and duration are unique at each site and control erosion on a local scale.

In general, Maine middens typically occur on coastal bluffs comprised of unconsolidated glacial sediments, which are susceptible to subaerial and the marine erosion. Bluff retreat via erosion is common along the coast of Maine, thus, bluff-top middens are often impacted (Kelley and Dickson, 2000; Kelley, 2004). Rates of bluff retreat vary considerably as a result of episodic slumping (Nordstrom and Jackson, 2012). Subaerial erosional processes include groundwater movement, overland erosion, and freeze/thaw action (Kelley and Dickson, 2000; Kelley, 2004).

These middens also occur on bluffs in sheltered environments, such as estuaries or coves (Davies, 1992; Leach, 2007). Wind duration, direction and speed, as well as basin dimensions, are major factors influencing wave heights in fetch-limited environments (Jackson et al., 2002). Also, wakes resulting from watercraft passing near the shore have a greater impact on sites in fetch-limited areas (Nordstrom and Jackson, 2012).

5.3 Application of Methodologies at the Olson Site

Covered by an open grassy field, the Olson site is located near Cushing, Knox County, Maine, USA (OLS) (Figure 5.1). The bluff on which the midden sits is approximately 1-4 m in height and is surrounded by a low-energy beach (Timson,

1974). Glacial till makes up the surficial material, and bedrock is Paleozoic metasediments and granite (Osberg et al., 1985).

Historic aerial photographs and orthophotos were chosen because they provided the longest record. Where data exist, air photos are the most common source in the determination of past shoreline position (Boak and Turner, 2005), and are often used to examine change along 10 to 100 km of shoreline (Smith et al., 1990). Other studies have utilized satellite imagery which can have a spatial resolution of 30x30 meters (m) or 60x60 m, but the shift in shoreline was observed on a delta with a high rate of change (8.6 to 42.6 m/year) compared to that expected in this study (Louati et al., 2015). Pixel resolution is a limiting factor due to the scale and rate at which bluff erosion occurs in coastal Maine.

SfM is highlighted in this paper as an ideal alternative because it requires no specialized equipment, minimal training, and freedom to survey at will. Thus, the barrier to entry is low. Capturing a significant variety of perspectives; getting a feel for the appropriate distances between camera and scene, providing sufficient overlap between photographs; and conducting survey under the best atmospheric conditions requires practice. Also, the processing power of the computer equipment governs the maximum number of photographs included in the model and the resulting resolution of the SfM product. Major limitations to SfM are battery life and poor weather. Another benefit of capturing the 3D environment with SfM is the associated digital preservation of the scene.

5.3.1 Olson Air Photo Case Study

Shoreline change analysis using aerial photography involved the georeferencing of aerial photos and shoreline digitization in ArcGIS. Aerial imagery from the late 1960's was obtained from the Maine Geologic Survey (MGS) and scanned at 2400 dpi. These photographs, along with additional non-georeferenced, vertical

cartographic imagery from USGS Earth Explorer (EE) (1953) were georeferenced in ArcGIS using a nearest neighbor algorithm. National Agriculture Imagery Program (NAIP) GeoTIFF aerial photographs dated 2009, 2011, and 2015 were downloaded from USGS EE and imported into ArcGIS. All images were projected in NAD 1983 UTM Zone 19 N.

Distortion and error result from the translation of a three-dimensional earth surface into a two-dimensional picture. Correcting imagery for internal distortions due to sensor error and topographic effects through orthorectification improves the accuracy of the data. The process of orthorectification produces an ortho-image where scale is constant and accurate distance measurements can be made from the image (Jaud et al., 2014). Metadata on NAIP GeoTIFF imagery states that the photographs are orthorectified, but the USGS EE data were not. Also, aerial photos obtained from MGS and converted into digital form could not be orthorectified as the metadata was unavailable.

NAIP 2013 imagery downloaded from the Maine GIS (MEGIS) website was used as the base map for georeferencing scanned aerial photographs and imagery downloaded from USGS EE. The georeferencing tool within ArcGIS was used to tie ground control points (GCPs) in the imagery without a spatial reference frame to the MEGIS GeoTIFFs. Selected GCPs included building roofs, road intersections, and features on the landscape. Effort was made to distribute GCPs in a nonlinear fashion while georeferencing to avoid distortion or warping. Proper GCP distribution was often difficult as coastal aerial photographs are dominated by ocean, which limited the potential area for GCPs. After selecting these points (N=30), the root-mean-square error (RMSE) value was lowered by identifying a statistically favorable combination that reduced the number of GCPs (N=6 to 9). ArcGIS then stretched the image based on the selected locations. The RMSE associated with the georeferenced image represents the calculated offset between data values and

model-predicted values; additionally, a lower value indicates a better relationship. Within ArcGIS, RMS values for the 1953 and 1966 imagery were 2.6 and 4.9. The RMSE value associated with the georeferenced images provides a quantitative error value, but the error associated with the GeoTIFFs (NAIP imagery) is unknown.

Shorelines at the Olson site were digitized within ArcGIS after georeferencing the imagery without a spatial reference frame. The lack of metadata on the aerial photos and the limited resolution required shoreline digitization follow the vegetation line. Typically, the vegetation line coincided with the bluff top termination, but was often difficult to accurately digitize with the presence of trees.

Discrepancies between aerial photographs produced inconsistent shoreline traces at the Olson site (Figure 5.2). The presence of shrubs and trees, in combination with the poor resolution, prevented accuracy and precision during the shoreline delineation. Additionally, the subjectivity involved with selecting the position of the shoreline can result in a spatial error that exceeds the change predicted (Boak and Turner, 2005). The 1953 and 1966 traces do not correlate with each other or with the NAIP imagery (2009, 2011, and 2015). This lack of correlation may be the result of differences in collection methods and/or the camera angle. NAIP imagery clustered together, and differences in position likely relate to erosion and/or error involved with following the vegetation line. Trends observed along the shoreline were not always consistent. Additionally, the resolution of the imagery is not likely to record the change expected during the six years where the traces appeared internally consistent. Dominant sources of error in the aerial photo shoreline change analysis resulted from georeferencing non-orthorectified aerial photography, imagery resolution, and the sporadic/limited time-series available. Difficulty in accurately digitizing the vegetation line stemmed from image quality and the presence of trees or shrubbery obscuring the coastline.

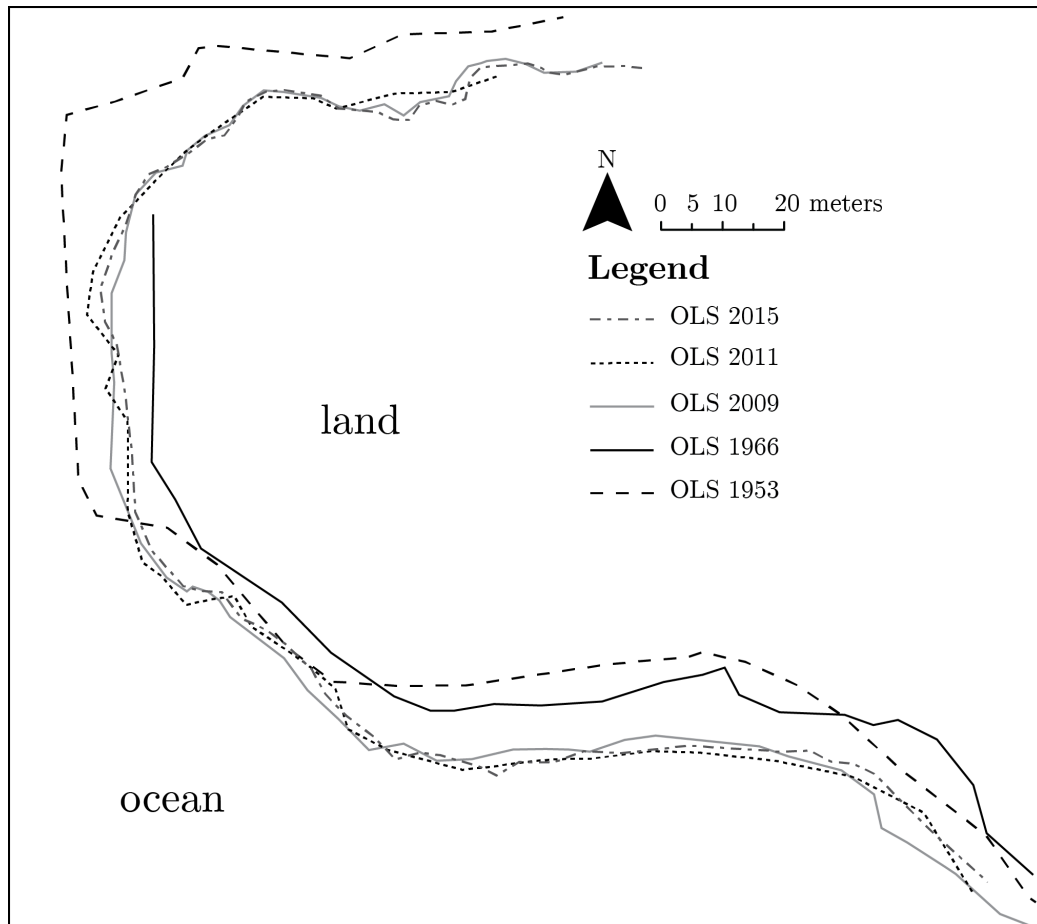


Figure 5.2: Olson shorelines delineated from historic aerial photography.

The change observed within the timescale available proved too fine for shoreline change analysis relying solely on aerial photography. In addition, the position of the tide at the time of image capture heavily influences the ability to determine coastal erosion (Kellogg, 1982). Other studies have used air photos with success (Fletcher et al., 2003; Robinson et al., 2010), but data available for the coast of Maine do not exhibit the resolution, frequency of record, or contain the necessary metadata to base confident conclusions about shoreline change. Thus, SfM is a desirable technique for its cost-effectiveness and ease of deployment.

5.3.2 Olson SfM Case Study

The SfM digital surface model (DSM) resolution is approximately 2 cm/pixel, and the detail produced using this method is striking in comparison to the 2 m LiDAR data (Figure 5.3). Due to the high cost associated with each airborne LiDAR flight, the data are not time-series and comparisons at a single site cannot be made. Two arrows in Figure 5.3 (image B) point out a circular feature approximately 35 m in diameter, and a linear depression approximately 18 m in length and 2 m wide. The circular feature is the result of shorter vegetation in an area where a grazing horse was tethered. The linear depression corresponds to an archaeological trench that was excavated in the 1980's.

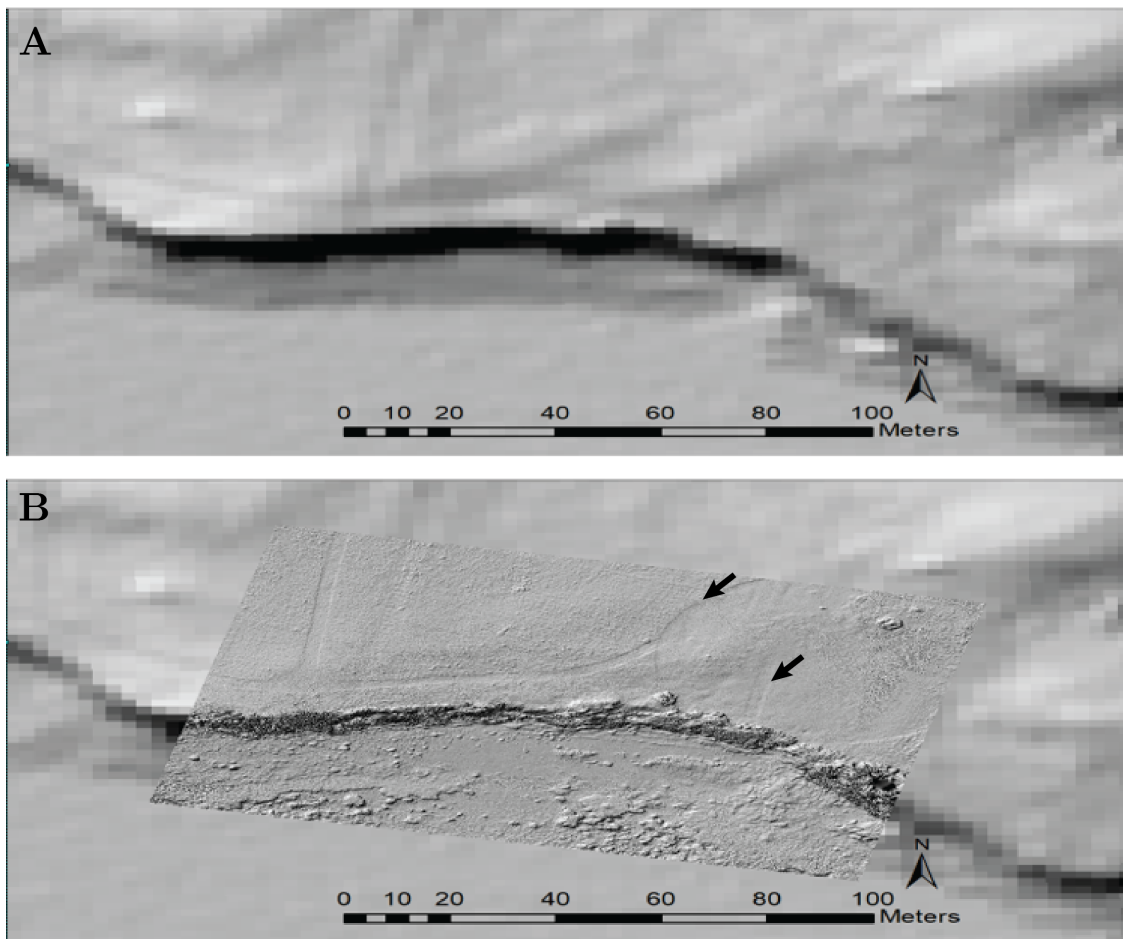


Figure 5.3: Olson site LiDAR versus SfM digital surface model.

5.3.3 SfM Model Construction

After loading photos into Photoscan, images are rated with a tool that produces an estimate of confidence for the potential error associated with each photograph. The rating is particularly responsive to motion-blur and image sharpness. Photographs are selected or removed by the user, with a balance between removing lesser-quality images and eliminating gaps in coverage of the overall scene. Through trial and error, we generally excluded any image with a rating of less than 80%. This both reduces error and the over-all number of photographs analyzed, improving processing times and relieving memory constraints. All images are analyzed for patterns in visual textures along with the edge-detection of arbitrary subjects, or features. Each image contains thousands of virtual tie-points chosen by the software, which are associated with distinct features within each image. These points must have stable spatial relationships; specifically, that they are invariant to image scaling, translation, and rotation and at least partially invariant to lighting changes or 3D projection (Lowe, 1999).

Following the calculation of tie-points, each image is iteratively compared to its companions and the consequent recognition of the previously detected features. This then supports the mapping and interpretation of the parallax differences from each frame of view. As the parallax is understood between two-, and three-, and then n-photographs, the potential arrangements of all features are accepted or rejected by the software. In conjunction with the metadata associated with the supplied photoset, Photoscan utilizes a database of common camera models and their lens geometries to identify the relative location where each photograph was recorded with respect to the scene. This produces a three-dimensional point cloud containing tens to hundreds of thousands of points, fully refined again with each introduction of every subsequent image.

With a full point cloud constructed, Photoscan returns to the original photo-set and "fills in the gaps" between every surficial point with visual information from the photographs. The final product is a high-resolution digital surface model in true color as a dataset of (x, y, z, R, G, B) type coordinates, on the order of tens of millions of points, consistent in both scale and orientation. Photoscan also grants the added luxury of simplifying the transformation of this dataset, referred to as the Dense Point Cloud, to a wealth of export products such as orthomosaics; digital surface rasters in common coordinate systems; and triangulated mesh or wireframe models for use in other systems.

With the inclusion of a scale bar, or measurable ground control points within the surveyed area, the user can impart a sense of scale and geospatial-reference within a subset of images. During the processing stage, the scales included in the survey define the scale for the entire point cloud construction in three dimensions.

5.3.4 GPS as GCP

Robust ground control is a significant concern for utilizing SfM in an environment as dynamic as a beach/bluff system and as sensitive as an archaeological site. In anticipation of further erosion, and in an effort to avoid site disturbance, placing landmarks as ground control points (GCPs) is not an option. Instead, stationary precision GPS equipment was placed and utilized within the study area during the flight. The equipment was captured in situ, within the photographs collected, so they would be present within the SfM product.

It is not critical to reuse the original GPS ground control points from survey to survey. Placing the GPS within the survey defines reliable scale and orientation information independent of the change to the environment, reducing dependency on static or seemingly static objects. The success of repeat surveys is not reliant on familiarity with previous datums.

The UAV onboard GPS is insufficient as the sole source for ground control due to wide error, and conflicts of position/parallax for the precision required for erosion monitoring at this scale. Error range associated with a budget-grade GPS could be upwards of meters; as a result, the UAV will label photographs captured within the error range with overlapping coordinates. The difference in apparent parallax between the photos with incorrect GPS information results in warping and skewing errors, arising from the conflict of information in the metadata. This does not mean that the onboard GPS measurements should be abandoned altogether. In fact, the information lessens processing time, as the data provide clues to the general range of perspectives relative to the scene. Thus, Photoscan to treat images in optimized clusters rather than having to evaluate the spatial relationship of each image in regards to the photoset. Onboard coordinates provided by the UAV should not be the sole source of georeference as they can be error-prone, especially in the vertical direction. Therefore, the inclusion of ground control points within a SfM construct is necessary for proper georeferencing and applications involving the measurement of change over time.

The GPS antennas serve as known high-precision ground control points and impart a sense of scale within the model. GPS data is downloaded from the receivers and checked for accuracy. A table of GCPs is built and the distances between all combinations of GPS devices are calculated. By default, SfM accepts coordinates in decimal degree notation and distances in units of meters. The model is scaled in reference to antenna position, then the calculable distance between each GPS GCP is used as a virtual scale bar, across the model. This virtual scale bar can "pass through" obstacles while still defining precise distances within the scene. Visually present scaling objects are not necessary.

Most GPS systems take an antenna height above the ground as an input in order to report on the ground position beneath the antenna. SfM sees the antenna

itself as part of the scan; therefore, it often obscures the ground beneath it. It is important then to zero the antenna height within the receiver, so that it reports on its own position in space. Otherwise, errors result as SfM tries to reconcile the reported position of the GCP and the parallax effect between the antenna mount and the ground. As the model product is spatially invariant throughout, the positions of the point beneath the antenna can be measured from within the model, and the antenna itself is appropriately oriented in space.

5.3.5 Photo Acquisition and Settings

Select cameras and camera settings result in a better SfM product. It is important to use a camera with lossless compression capabilities as well as one that does not alter the image upon recording. For example, a smartphone algorithmically doctors lighting and saturation, and these changes introduce errors in SfM feature detection during tie-point alignment. Clapuyt et al. (2016) concluded that a broader focal length (comparing 28mm to 50mm) often results in less error. This seems counterintuitive as a greater focal length (50mm) should result in higher-resolution photographs. However, a greater focal length also narrows the field of vision, further exaggerating the distortion between each image. Control of the shutter-speed is less important, as long as care is taken to acquire images with consistent lighting quality and with minimal motion blur, especially during a UAV flight. Altering the lens geometry of a camera between photographs will alter the perspective between those images. Changes to the focal length, aperture, and ISO sensitivity cause errors by changing relative distances captured in each image, and results in processing time penalties as the software works to reconcile the disparities. With a UAV, these parameters can and should be locked before each flight.

Capturing the SfM scene in two flights, or specifically at two elevations, provides the model with context and detail. The first flight, named here as a context flight,

takes to a higher altitude and follows a regular, planimetric pattern covering the entire survey area. The greater distance from the ground surface results in reduced resolution but, the broader coverage ensures the inclusion of all GCPs, enhances georeferencing, and enables the nesting of higher-resolution SfM product.

Immediately following the context flight, the UAV is flown to capture greater detail for erosion measurements and comparison to other repeat surveys. It is important that both flights occur subsequently with little to no time passing in between, as the two are meant to capture the same environment. The second flight, referred to here as a complementary flight, is conducted closer to the scene and does not need to follow a regular pattern. A complementary flight provides additional and higher-resolution photographs of the subject serving to enrich the end product digital surface model. The photographs collected during each flight are treated as components of the same survey and are input into the same Photoscan project.

5.3.6 Olson Survey Camera Settings

A two-flight approach was used during the Olson site SfM survey, and details on the flight are located in Table 5.1. The aperture on the camera attached to the UAV was locked at f/8 in order to prevent depth-of-field changes by the camera geometry. It is critical to model generation, and fundamental to SfM, that depth of field is altered by the relocation of the camera with respect to the scene. Shutter speed was allowed to vary as the digital camera auto adjusted. It is not uncommon for digital cameras to feature a shooting mode that locks an aperture setting and actively balances suitable shutter speeds for consistent results. The UAV camera was set to record photographs at a 5 second interval.

UAVs are often used for the bird's eye view that they offer. However, it is worth noting that their powerful stabilization technology and ease of control allow for them to better support the development of a SfM product with consistent

Table 5.1: Olson site SfM survey camera settings.

Parameter Options	Specific Parameter Details
Camera Model	FC6310 (DJI)
Resolution	5464 x 3070
Focal Length	8.8 mm
Total Number of Images	350
Maximum Flying Altitude	29.6 meters above sea level
Ground Resolution	6.85 mm/pixel
Coverage Area	1,160 m ²

low-altitude oblique imagery. For example, during the complementary flight, care was taken to pass the UAV across the face of the midden/bluff maintaining altitude a meter above the water. This is particularly important for beach and slope profiling as there can be greater error associated with just a top-down approach that risks less perspectives represented in the photoset.

5.4 Conclusions

Quantifying erosion at coastal shell midden sites in Maine is critical as sea-level rise threatens the valuable cultural and climatic record they contain. Change is visible from repeated site visits in the form of broken shells on the beach, erosion scarps, and slump blocks. However, quantifying the erosion is challenging with traditional methods. The Olson site was analyzed using a time-series of relatively high-resolution aerial imagery in ArcGIS, but the methodology did not provide conclusive results. A UAV survey of this site resulted in a high-resolution DSM after processing the photos using SfM. The DSM will provide a baseline for repeat surveys, and will allow site loss measurements from the comparisons. Additionally,

the model created may allow the relocation of archaeological test units. There is error and offset involved with studying shoreline change from aerial imagery, but SfM serves as a practical alternative methodology to document erosion at coastal shell midden sites.

Chapter 6
COMBINED METHODS, RESULTS, AND DISCUSSION OF SITES
AND DETAILS EXCLUDED FROM CHAPTER 5: *STRUCTURE
FROM MOTION AS A NEW METHOD OF ANALYZING
SHORELINE CHANGE IN ARCHAEOLOGY: AN
EXAMPLE FROM COASTAL MAINE*

6.1 Shoreline Change Study

The following chapter is an expanded version of sites that were not flown with the UAV methodology discussed in Chapter 5. Future work documenting erosion at the Damariscotta Oyster Farm (DAM), and Tranquility Farm (TRQ) is suggested as rates of shoreline change can be used as a basis for prioritization of sites for rescue or preservation.

A traditional method to accomplish measurement of shoreline change is the use of sequential aerial photographs. This method was applied to three shell midden sites included in this broader study: Damariscotta Oyster Farm (DAM), Olson (OLS), and Tranquility Farm (TRQ). DAM and TRQ are discussed here. The portion of the aerial photogrammetry the shoreline change study at OLS is discussed in the previous chapter. Approximately 8 aerial photos were georeferenced, between the three sites (DAM:N=2, OLS:N=2, TRQ:N=4), in ArcMap geographic information system (GIS) platform (ArcCIS 10.4; Esri software). Additionally, United States Geological Survey Earth Explorer (USGS EE) was used to download georeferenced orthoimagery as GeoTIFFs and non-georeferenced or orthorectified vertical cartographic imagery. The aerial imagery allowed the construction of a long-term (decadal) comparison of shoreline change, but the poor resolution prevented definitive conclusions concerning shoreline change.

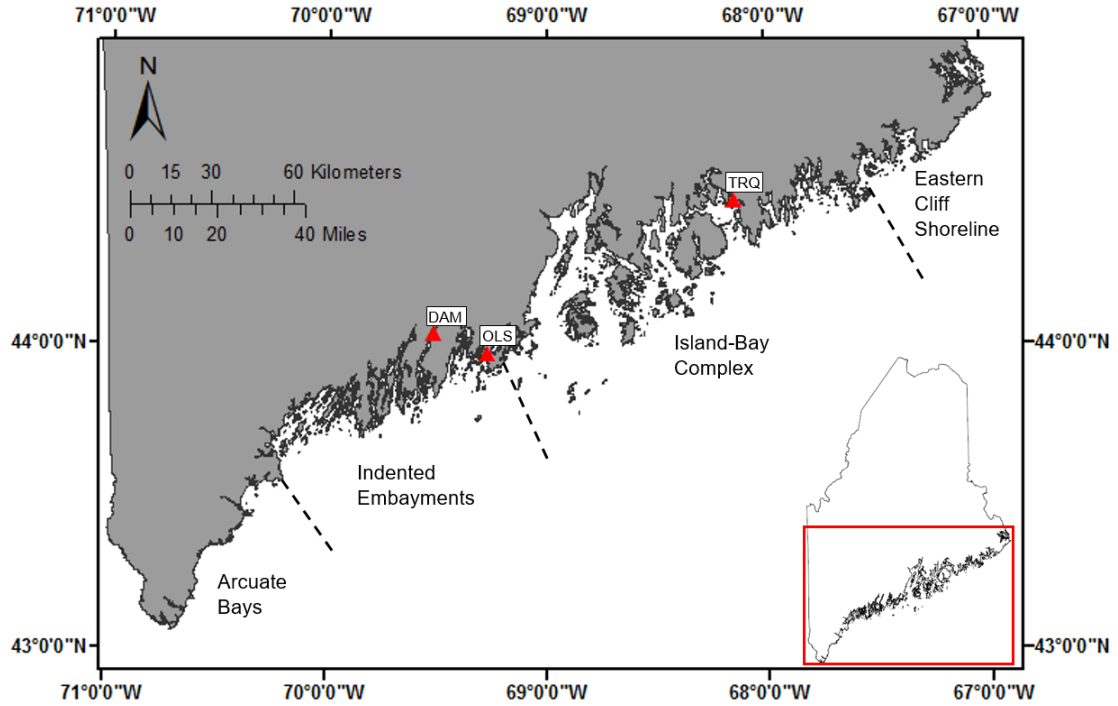


Figure 6.1: Shoreline change study locations with coastal compartments identified by Kelley (1987)

6.1.1 Damariscotta (Site 26.15)

Shorelines digitized for the DAM site are based on (NAIP) imagery dated 2009, 2011, 2013, and 2015; imagery downloaded from USGS EE (1967); and an aerial photograph obtained from MGS (1980). The RMSE associated with the 1967 and 1980 imagery are 4.9 and 2.6. Figure 6.2 displays the aforementioned shoreline traces.

NAIP orthophotographs (2009, 2011, 2013, and 2015) and USGS EE imagery (1967) best represented the change along the coast of the DAM site (Figure 2). Digitized shorelines indicate a loss along the northwest side of the study area, but the northeast side appears to have changed less. The 1980 shoreline appears to be offset, but traces from NAIP imagery (2009, 2011, 2013, and 2015) cluster with the 1967 trace. The Damariscotta river runs along the southwestern portion of the site, and a tidal stream is adjacent to the southeastern extent of the midden. If the data

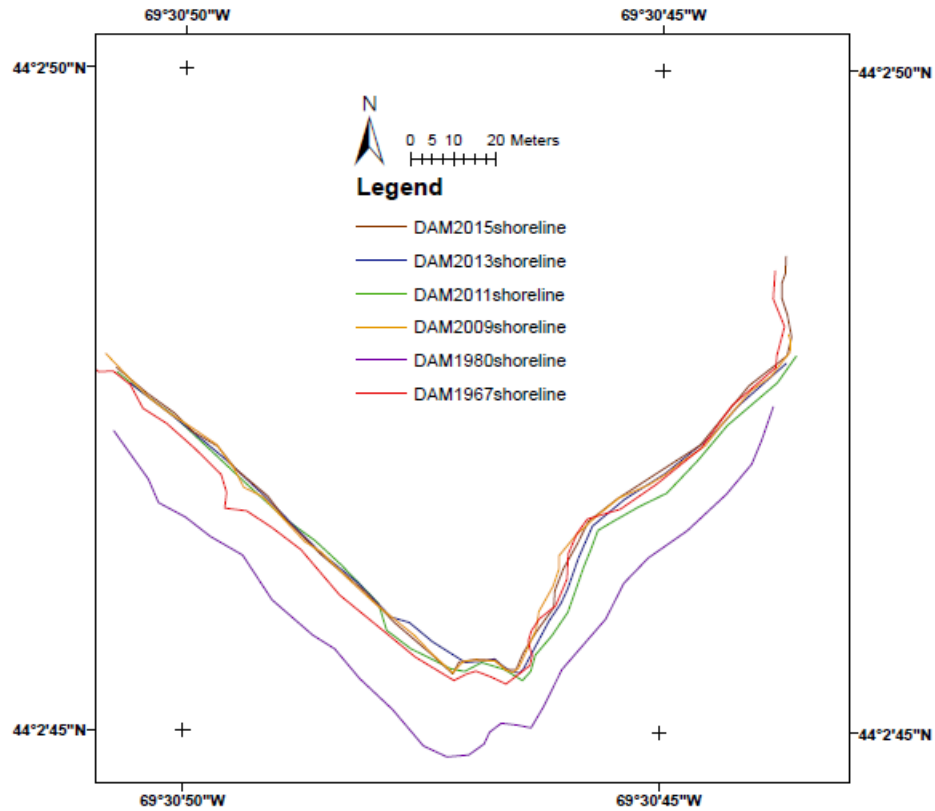


Figure 6.2: Digitized shorelines of the DAM site.

from 1967 are considered, most of the erosion has occurred on the side bordering the river and at the confluence of the river and the tidal stream. The shoreline trace from 1967 indicates approximately 5 meters of erosion, but the root mean square error (RMSE) in the image is 4.9. Interestingly, the RMSE in the 1980 shoreline is lower at 2.6. Shoreline trends at the DAM site indicate erosion in select areas, but there is little consistency.

6.1.2 Tranquility Farm (Site 44.12a)

Shoreline change at the TRQ site is shown by shorelines digitized from NAIP imagery (2015) and georeferenced aerial photography from USGS EE (1997, 1956, and 1940) and MGS (1981). RMS values for the 1997, 1981, 1956, and 1940 vertical

cartographic images are 0.79, 2.2, 0.86, and 2.1 respectively. Figure 6.3 displays the digitized shorelines for the entire TRQ site.

Select shorelines at the Tranquility Farm site appear erroneous when compared to the overall shoreline trend. Trees along most the TRQ coast made shoreline digitization/delineation difficult. The 1940 and 1956 data appear to correlate well with each other, and provide evidence for erosion in the northwestern 180 meters of shoreline (Figure 6.3). Error related to using vegetation line change for shoreline change likely produced the appearance of accretion in this dataset. The 2015 shoreline appears to be an outlier along the northwestern most 80 meters. Erosional change at this site is difficult to measure from the shoreline data as trends only appear in select areas, and there is little consistency.

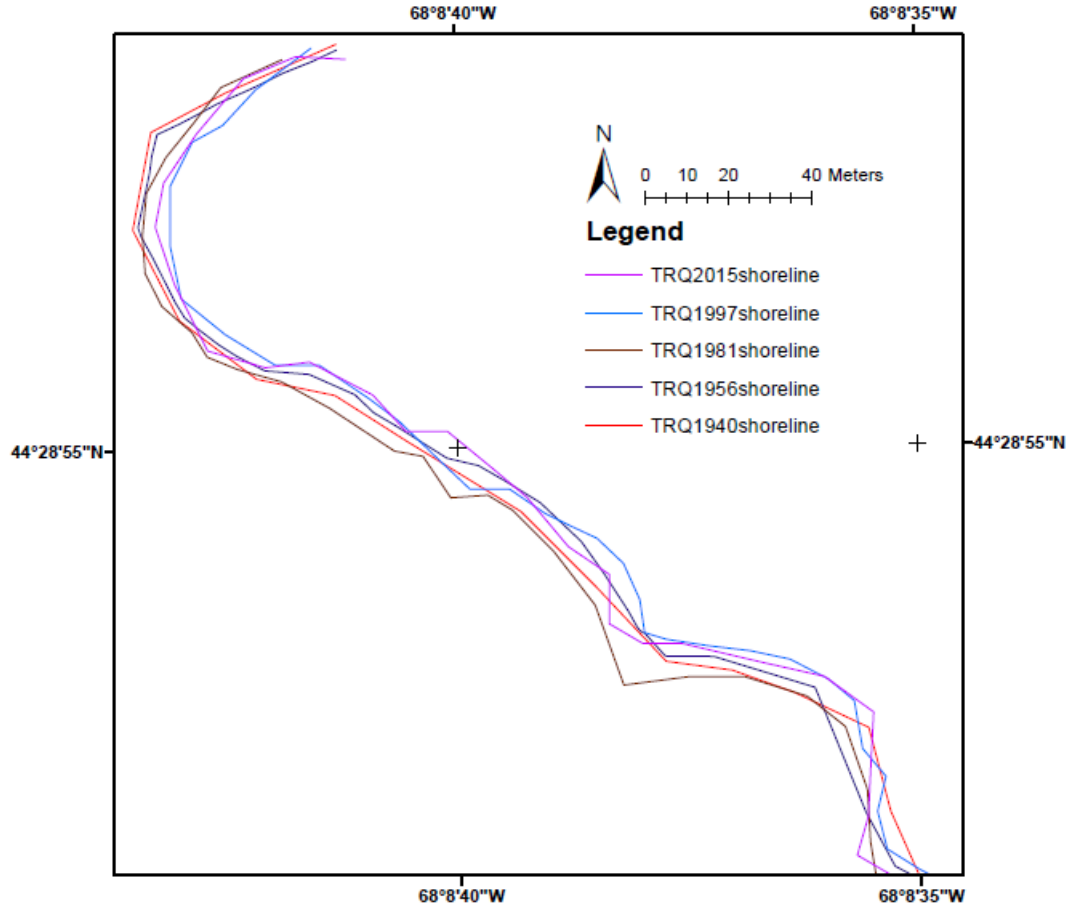


Figure 6.3: Digitized shorelines of the TRQ site.

6.2 Summary

Change detection utilizing the historic aerial photography proved too coarse and inconsistent over the timescale available. Middens are typically situated on bluffs that erode episodically, with a frequency that is dependent upon winter storms. Available aerial imagery do not exhibit the resolution and frequency of record necessary for shell midden erosion analyses. A method that can provide greater resolution of the eroding bluff, with the potential for frequent data capture, is an ideal alternative to traditional aerial photo time-series comparison. Confident conclusions about shoreline change are necessary for the prioritization of archaeological sites for protection or rescue.

Chapter 7

CONCLUSIONS

Middens are the key to understanding the first residents of the Maine coast, but erosion caused by climate-change induced sea-level rise, intensification of storm frequency, and an increase in freeze-thaw cycles threatens the information they hold. Midden erosion is visible, but the impact reaches beyond the lost materials, as these are the last records of a culture. These archaeological sites archive an unwritten history and provide insight to the lives of those who created them, their movement on the landscape, and the environment in which they lived. Clues to the relationship of Ceramic Period people with the interior and coastal regions lies within shell middens. The archaeological sites serve as an archive for paleoclimate and a lifeway that no longer exists in its original context. The decedents of these peoples are in Maine and practice resource procurement today, but European influx dramatically changed who owned the land and the way that it was owned. Thus, land utilization by the descendants of those who created middens was impacted and influenced. Though it is a biased sample, faunal material and potential DNA archived in the middens, could provide much needed paleoenvironmental data for the Gulf of Maine.

Through this work, a methodology was created that is applicable to shell midden areal extent and thickness in a variety of settings. This technique allows noninvasive to minimally invasive stratigraphic information with the use of existing archaeological information for GPR data ground-truth. Data quality depend on material properties unique to each site, and this research demonstrates the variability of results within the same region. Specifically, the differences in the electromagnetic properties of the dissimilar midden matrices, and the contrast, or lack thereof, between the archaeological site and the geological material below it, control the record produced by the GPR.

From the sample of middens included in this study, there is no one consistent or preferred material upon which middens were constructed. The Long Island North midden sits on both thin till and bedrock. Presumpscot Fm. underlies the Oyster Farm site. The Olson site was deposited on glacial till. Located near a moraine ridge, the Fernald Point midden is sitting atop the boundary between glaciomarine material and till. Lastly, Tranquility Farm is underlain by wave-washed glaciomarine deposits.

Each shell midden site differed in a number of ways, and the dissimilarities are reflected in the GPR profiles collected. Stratigraphic complexity was present across sites, and resulted in error in the interpreted midden thicknesses. Often, disturbed strata, the presence of rocks within well-sorted material or their general presence, and the absence of geologic strata, allowed interpretation of shell midden extent. A strong reflector represented the base of the midden at sites where the midden sat on an extremely impermeable surface of glacial material. In all cases, the GPR data added to the knowledge of the site, and enhanced the understanding of the areas lost and under threat. For example, a thick portion of shell midden was found on the northeastern portion of the site (transect F to G in Figure 3.6), behind the known area on the point. The minimally invasive nature of GPR, in combination with ground-truth, is a viable methodology for shell midden delineation.

The methodology allows rapid, nondestructive to minimally invasive, and cost-effective site evaluation, but ground-truth data aid in confident interpretations. The use of existing stratigraphic data is ideal, but is dependent on the relocation of the archaeological grid and the level of detail within drawn profiles, notes, and photos.

GPR survey is ideal for informing a site prioritization metric for CRM decisions when temporal and monetary resources are limited. The data allow the evaluation of vertical and areal site extent at more sites than traditional excavation methods

allow. The full protocol developed as a result of this work was applied to 6 sites, and completed in a two year period. However, method development was the major focus of research. With the protocol in place, the survey of more shell middens is possible.

The original size of each shell midden is unknown, and there is not yet an approach for estimating it. The complex stratigraphy characteristic of shell midden sites, in combination with a dynamic local relative sea level and lack of erosion rates, preclude a quantitative understanding of the original site dimensions.

These sites were much more extensive, given they are currently eroding on a scale apparent from storm to storm, and between freezing and thawing cycles. The GPR data show that the thickest portion of the sites, are found at the eroding edge at Long Island North, Damariscotta Oyster Farm, Olson, and Tranquility Farm. The thickest portion of the midden has the potential to contain the most information. Thus, if the deepest portion of the shell midden is under threat at each site where an isopach map was created, the same might be true for the remaining middens.

Quantifying erosion at coastal shell midden sites in Maine is critical as sea-level rise threatens the valuable cultural and scientific record they contain. An understanding of the rate and amount of erosion at each threatened archaeological site is important in informing cultural resource management decisions. Three sites along the coast of Maine were analyzed using a time-series of relatively high-resolution aerial imagery in ArcGIS, but with disappointing results. Although change is visible from repeated site visits (i.e., eroded shells on the beach and slump blocks), detecting the shoreline retreat using the traditional aerial photo time-series methodology did not provide conclusive results. Shorelines delineated from the imagery were not consistent in showing erosion, and showed accretion in some areas. However, the bluff top was traced at each site and accretion is not occurring. Historic aerial photo time-series comparisons did not provide a reliable or consistent estimation of midden erosion, and this research brought further awareness to the

issues involved with the application of this technique to archaeological sites on the coast of Maine.

Comparing a time-series of Structure from Motion (SfM) digital surface models (DSMs) is a realistic and practical alternative to shoreline change analyses using historic aerial imagery. Although the record must be created for each site, change is detected is on the order of centimeters as opposed to meters with historic imagery. The frequency and flexibility allowed with SfM survey is such that community monitoring groups could regularly and easily collect photos of a shell midden site with little training or background, but the implementation of the monitoring program would require a person dedicated to processing the data from the surveys and data archival. Additionally, the DSMs created with drone imagery permit detailed topographic information if site vegetation is low or packed down after snow melt. The DSM data may allow the relocation of archaeological excavations as demonstrated at the Olson site.

7.1 Future Work

Additional survey with high-frequency GPR equipment along the established transects at Long Island North, Damariscotta Oyster Farm, Olson, Fernald Point, and Tranquility Farm, could provide a more detailed record for comparison with the data collected during this study. Ideally, the collection of the higher frequency records would have occurred during the 500 MHz survey for similar site conditions (e.g., soil moisture) but such an antenna was not available during data collection.

Following precipitation, carrying out a higher frequency GPR survey along the same grid as the 500 MHz survey at Long Island North might produce a record where midden material differed enough from the bedrock to identify a distinct boundary between them. The electromagnetic properties of the bedrock and overlying glacial and midden material were too similar, thus, they were often

indistinguishable in the 500 MHz survey data. The fractures within the bedrock were apparent in the GPR record, likely because there was water within them. Additionally, the record would likely allow the opportunity to resolve stratigraphy within shallow areas of the midden. Limited high-frequency survey, along the archaeological trench at the Olson site and along transects in the thin areas of the Damariscotta Oyster Farm site would allow enhanced detail of midden layers. Distinguishing shell midden at Fernald Point was challenging, but the greater resolution associated with the higher frequency could resolve areas of thin strata within the midden. At Tranquility Farm, survey with high-frequency GPR over carefully selected, undisturbed areas, with nearby ground-truth, would provide a detailed geophysical record for comparison with the 500 MHz data.

Radan was utilized for data processing, but a software program better suited to archaeological application would likely address data processing issues. Utilizing software that allows topographic correction of batch data files would be ideal for the proper stratigraphic representation of the grids of 500 MHz GPR data. Additionally, the ability to apply unique dielectrics for individual layers would result in a more realistic depth correction. Acquiring the ideal software remains an issue of high cost and proprietary data formats.

During the stakeholder meeting that was held in August of 2017 (Sea Grant project website link), there was a focus on developing a network of entities and individuals who could monitor shell middens. The monitoring program would involve collaboration with Maine Tribes, community groups, and conservation agencies. Land trusts were identified as one target group as they have an existing web of members with the common interests in conserving resources.

Raising awareness to cultural resources within land trust groups is key as they move from procuring land to maintaining and protecting their acquired spaces. In the absence of an individual familiar with cultural resources, individuals might not

be aware of archaeological sites, such as shell middens, on their property. Thus, the protection and monitoring middens would not be a priority. Additional widespread outreach to community-based groups, on the importance, protection, and preservation of archaeological resources would improve the current level of public understanding and awareness of cultural resources.

Creating SfM DSM records for shell midden sites in Maine is the next step to document and begin to understand erosion occurring at individual sites. Camera surveys carried out by citizen-scientist groups along the coast, following the methods described in Chapter 5, have the potential to provide the data collection frequency required to quantitatively measure site loss. However, these surveys must be combined with a network to process and archive the data.

This study resulted in a widely applicable technique for rapid, minimally invasive, and cost effective shell midden delineation using GPR. However, ground-truth data are important for the interpretation of the GPR profiles. Detailed archaeological profiles are optimal if the location of the original grid is known in relation to the GPR survey grid. If ground-truth data do not exist, a minimally invasive technique is suggested (e.g., coring or a small test-pit). Complex midden stratigraphy, varying matrix compositions, and unique geological substrates necessitate individualized interpretations for each site. Additionally, analyses of historic aerial photo time-series brought further attention to the need for an alternative methodology for assessing site erosion. Structure from Motion (SfM) photogrammetry can provide cm-scale resolution at less cost and with greater frequency than traditional aerial or terrestrial options.

REFERENCES

- Andersen, K., Bird, K., Rasmussen, M., Haile, J., Breuning-Madsen, H., Kjaer, K., and Orlando, L., G.M.W.E., 2012, Meta-barcoding of "dirt" DNA from soil reflects vertebrate biodiversity: *Molecular Ecology*, v. 21, p. 1966–1979.
- Anderson, A., 2018, University of New England, personal communication.
- Baker, E., University of New England, personal communication to Arthur Anderson.
- Barnhardt, W., Gehrels, W., Belknap, D.F., and Kelley, J.T., 1995, Late Quaternary relative sea-level change in the western Gulf of Maine: Evidence for a migrating glacial forebulge: *Geology*, v. 23, no. 4, p. 317–320, doi:10.1130/0091-7613(1995)023<0317:LQRSCL>2.3.CO;2.
- Belcher, W.R., 1988, Archaeological Investigations at the Knox Site (30-21), East Penobscot Bay, Maine [M.S. thesis]: University of Maine, Orono, 267 p.
- Belcher, W.R., and Sanger, D., 2017, The Roque Island Archaeological Project, Maine, USA: Methodologies and Results: *North American East Coast Shell Midden Research: Journal of the North Atlantic*, v. 10, p. 126–142.
- Belknap, D.F., 1995, Geoarchaeology in central coastal Maine, Appendix 5, *in* Bourque, b.j., diversity and complexity in prehistoric maritime societies: A gulf of maine perspective: New York, Plenum Press, p. 275–296.
- Belknap, D.F., Andersen, B., Anderson, R.S., Anderson, W., Borns, H.W.J., Jacobson, G.L., Kelley, J.T., Shipp, C.R., Smith, D., Stuckenrath, R.J., Thompson, W.B., and Tyler, D., 1987, Late Quaternary sea-level changes in Maine: The Society of Economic Paleontologists and Mineralogists Special Publication, v. 41, p. 71–85.
- Belknap, D.F., and Kelley, J.T., 2015, Geology of the Nearshore and Coastal Presumpscot Formation from High Resolution Seismic Profiling and Vibracores: Symposium on the Presumpscot Formation, p. 1–14.
- Belknap, D.F., and Shipp, R., 1986, Quaternary geology of the Damariscotta estuary, *in* Newberg, D., ed., Guidebook for field trips in southern maine; neigc 78th ann. mtg.: Lewiston, ME, Bates College, p. 254–274.
- Berzins, V., Brinker, U., Klein, C., Lübke, H., Meadows, J., Rudzite, M., Schmölcke, U., Stümpel, H., and Zagorska, I., 2014, New research at Rinnukalns, a Neolithic freshwater shell midden in northern Latvia: *Antiquity*, v. 88, no. 341, p. 715–732, doi:10.1017/S0003598X0005064X.

- Bird, K.D., 2017, Spatial Organization and Erosion at the Holmes Point West Archaeological Site, Machiasport, Maine [M.S. thesis]: University of Maine, 302 p.
- Boak, E.H., and Turner, I.L., 2005, Shoreline Definition and Detection: A Review: *Journal of Coastal Research*, v. 214, p. 688–703, doi:10.2112/03-0071.1.
- Borns, H.W., Doner, L.A., Dorion, C.C., Jacobson, G.L., Kaplan, M.R., Kreutz, K.J., Lowell, T.V., Thompson, W.B., and Weddle, T.K., 2004, The deglaciation of Maine, U.S.A.: *Developments in Quaternary Science*, v. 2, no. 2, p. 89–109, doi:10.1016/S1571-0866(04)80190-8.
- Borns, H.W.J., 1974, Reconnaissance surficial geology of the Bar Harbor [15-minute] quadrangle, Maine: Maine Geological Survey, Open-File Map 74-1, map, scale 1:62,500.
- Bourque, B.J., 1971, Prehistory of the Central Maine Coast [Ph.D. dissertation]: Harvard.
- Bourque, B.J., 1989, Ethnicity on the Maritime Peninsula, 1600-1759: *Ethnohistory*, v. 36, no. 3, p. 257–284.
- Bourque, B.J., 2012, *The Swordfish Hunters: The History and Ecology of an Ancient American Sea People*: Bunker Hill Publishing Inc.
- Braun, D.D., Lowell, T.V., and Foley, M.E., 2016, Surficial geology of the Southwest Harbor quadrangle, Maine: Maine Geological Survey, Augusta, ME, Open-File Map 16-21, scale 1:24,000.
- Bryant, M., Barnhardt, W., Dickson, S., and Kelley, J., 2002a, Coastal bluffs in the Orrs Island quadrangle, Maine: Maine Geological Survey, Open-File Map 02-201, scale 1:24,000.
- Bryant, M., Barnhardt, W., Dickson, S., and Kelley, J., 2002b, Coastal bluffs in the Yarmouth quadrangle, Maine: Maine Geological Survey, Open-File Map 02-223, scale 1:24,000.
- Callum, K., 1994, The Geoarchaeology of the Nahanda Site (16-90) Pemaquid Beach, Bristol, Maine [M.S. thesis]: University of Maine, Orono, 262 p.
- Clapuyt, F., Vanacker, V., and Van Oost, K., 2016, Reproducibility of UAV-based Earth Topography Reconstructions Based on Structure-from-Motion Algorithms: *Geomorphology*, v. 260, p. 4–15.
- Clinch, J.M., and Thompson, W.B., 1999, Surficial geology of the Cape Elizabeth quadrangle, Maine: Maine Geological Survey, Open-File Map 99-80, map, scale 1:24,000.

- Cox, S., 2009, Archaeological Investigations at the Scott's Midden Site, Deer Isle: The Maine Archaeological Society Bulletin, v. 49, no. 2, p. 5–15.
- Daniels, J., 2000, Ground Penetrating Radar Fundamentals: Prepared as an appendix to a report to the U.S. EPA, Region V,
- Davies, C., 1992, Estuarine preservation potential model for archaeological sites in coastal Maine [M.S. thesis]: University of Maine, Orono, 195 p.
- Davis, J., and Annan, A., 1989, Ground-penetrating radar for high-resolution mapping of soil and rock stratigraphy: Geophysical Prospecting, v. 37, p. 531–551.
- Dickson, S., 2005, Coastal landslide hazards in the Southwest Harbor quadrangle, Maine: Maine Geological Survey, Open-File Map 05-35, scale 1:24,000.
- Doyle, D., 2017, personal communication.
- Doyle, D., 2018, personal communication.
- Fletcher, C., Rooney, J., Barbee, M., Lim, S.C., and Richmond, B., 2003, Mapping Shoreline Change Using Digital Orthophotogrammetry on Maui, Hawaii: Journal of Coastal Research, , no. 38, p. 106–124.
- Furukawa, Y., and Ponce, J., 2010, Accurate, dense, and robust multiview stereopsis: IEEE Transactions on Pattern Analysis and Machine Intelligence, v. 32, no. 8, p. 1362–1376, doi:10.1109/TPAMI.2009.161.
- Gosse, J.C., and Phillips, F.M., 2001, Terrestrial in situ cosmogenic nuclides: theory and application: Quaternary Science Reviews, v. 20, p. 1475–1560, doi:10.1016/S0277-3791(00)00171-2.
- Grealy, A., Douglass, K., Haile, J., Bruwer, C., Gough, C., and Bunce, M., 2016, Tropical ancient DNA from bulk archaeological fish bone reveals the subsistence practices of a historic coastal community in southwest Madagascar: Journal of Archaeological Science, v. 75, p. 82–88, doi:10.1016/j.jas.2016.10.001.
- Grover, T., and Newberg, D., 2016, Reconnaissance bedrock geology of the Damariscotta quadrangle, Maine: Maine Geological Survey, Open-File Map 16-22, scale 1:24,000.
- Hall, B.L., Borns, H.W., Bromley, G.R., and Lowell, T.V., 2017, Age of the Pineo Ridge System: Implications for behavior of the Laurentide Ice Sheet in eastern Maine, U.S.A., during the last deglaciation: Quaternary Science Reviews, v. 169, p. 344–356, doi:10.1016/j.quascirev.2017.06.011.
- Hildreth, C.T., 2007, Surficial geology of the Biddeford quadrangle, Maine: Maine Geological Survey, Open-File Map 07-81, scale 1:24,000.

- Himmelstoss, E., FitzGerald, D., Rosen, P., and Allen, J., 2006, Bluff Evolution along Coastal Drumlins: Boston Harbor Islands, Massachusetts: *Journal of Coastal Research*, v. 22, no. 5, p. 1231–1240.
- Hofman, C.A., Rick, T.C., Fleischer, R.C., and Maldonado, J.E., 2015, Conservation archaeogenomics: Ancient DNA and biodiversity in the Anthropocene: *Trends in Ecology and Evolution*, v. 30, no. 9, p. 540–549, doi:10.1016/j.tree.2015.06.008.
- Hrynicky, G.M., and Robinson, B.S., 2012, Quantifying Gravel from a Ceramic Period Living Surface in Downeast Maine: *The Maine Archaeological Society Bulletin*, v. 52, no. 2, p. 27–43.
- Hrynicky, G.M., and Webb, J., 2014, 2013 Archaeological Testing at the Reversing Falls Site (80.15 ME) and the Devil’s Head Site (97.10 ME), Washington County, Maine: Report submitted to the Maine Historic Preservation Commission, Augusta, Maine.
- Hussey, A.I., 2012, Bedrock geology of the Cape Elizabeth quadrangle, Maine: Maine Geological Survey, Open-File Map 12-32, 6 p. report, 9 figures, 1 plate, photographs, color map, cross section, scale 1:24,000.
- Jackson, N., Nordstrom, K., Eliot, I., and Gerhard, M., 2002, “Low energy” sandy beaches in marine and estuarine environments: a review: *Geomorphology*, v. 48, no. 1-3, p. 147–162.
- James, M., and Robson, S., 2012, Straightforward Reconstruction of 3D Surfaces and Topography with a Camera: Accuracy and Geoscience Application: *Journal of Geophysical Research*, v. 117.
- Jaud, M., Rouveure, R., Faure, P., Moiroux-Arvis, L., and Monod, M., 2014, Method for orthorectification of terrestrial radar maps: *ISPRS: Journal of Photogrammetry and Remote Sensing*, v. 97, p. 185–194.
- Kebblinsky, C., Gardiner, N., Ferland, K., Hall, J., Raineault, N., Miller, C., Dickson, S., and Kelley, J.T., 2006, Coastal bluffs in the Bar Harbor quadrangle, Maine: Maine Geological Survey, Open-File Map 06-70, scale 1:24,000.
- Kebblinsky, C., Gardner, N., Ferland, K., Barnhardt, W., Dickson, S., and Kelley, J.T., 2002, Coastal bluffs in the Sargentville quadrangle, Maine: Maine Geological Survey, Open-File Map 02-211, scale 1:24,000.
- Kelley, J.T., 1987, An Inventory of Coastal Environments and Classification of Maine’s Glaciated Shoreline, *in* Rosen, P., and FitzGerald, D., eds., *A treatise on glaciated coastlines*: San Diego, Academic Press Inc., p. 151–176.

- Kelley, J.T., 2004, Coastal Bluffs of New England. in M.A. Hampton and G.B. Griggs, Coastal Cliff Erosion: Status and Trends: US Geological Survey Professional Paper 1693.
- Kelley, J.T., Belknap, D.F., and Claesson, S., 2010, Drowned coastal deposits with associated archaeological remains from a sea-level "slowstand": Northwestern Gulf of Maine, USA: *Geology*, v. 38, no. 8, p. 695–698, doi:10.1130/G31002.1.
- Kelley, J.T., Belknap, D.F., Kelley, A.R., and Claesson, S.H., 2013, A model for drowned terrestrial habitats with associated archeological remains in the northwestern Gulf of Maine, USA: *Marine Geology*, v. 338, p. 16, doi:10.1016/j.margeo.2012.10.016.
- Kelley, J.T., and Dickson, S., 2000, Low-Cost Bluff Stability Mapping in Coastal Maine: Providing Geological Hazard Mapping Without Alarming the Public: *Environmental Geoscience*, v. 7, p. 46–56.
- Kelley, J.T., Dickson, S., Belknap, D.F., and Stuckenrath, R.J., 1992, Sea-Level Change and Late Quaternary Sediment Accumulation on the Southern Maine Inner Continental Shelf: *Quaternary Coasts of the United States: Marine and Lacustrine Systems*, SEPM Special Publication, , no. 48, p. 23–34.
- Kelley, J.T., and Kelley, A.R., 2006, Acadia National Park Bluff Management Plan: 2005-2006: Report submitted to Acadia National Park, ME.
- Kellogg, D.C., 1982, Environmental Factors in Archaeological Site Location for the Boothbay, Maine Region with An Assessment of the Impact of Coastal Erosion on the Archaeological Record [M.S. thesis]: University of Maine, Orono, 283 p.
- Kellogg, D.C., 1987, Statistical Relevance and Site Locational Data: *American Antiquity*, v. 52, no. 1, p. 143–150.
- Kellogg, D.C., 1991, Prehistoric landscapes, paleoenvironments, and archaeology of western Muscongus Bay, Maine [Ph.D. dissertation]: University of Maine, Orono, 317 p. [Ph.D. thesis]: .
- Kellogg, D.C., 1994, Why did they choose to live here? Ceramic period settlement in the Boothbay, Maine Region: *Northeast Anthropology*, v. 48, p. 25–60.
- Kellogg, D.C., 1995, How has coastal erosion affected the prehistoric settlement pattern of the Boothbay region of Maine?: *Geoarchaeology*, v. 10, p. 65–83.
- Kenady, S.L., Lowe, K.M., Ridd, P.V., and Ulm, S., 2018, Creating volume estimates for buried shell deposits: A comparative experimental case study using ground-penetrating radar (GPR) and electrical resistivity under varying soil conditions: *Archaeological Prospection*, p. 1–16, doi:10.1002/arp.1594.

- Koester, A.J., Shakun, J.D., Bierman, P.R., Davis, P.T., Corbett, L.B., Braun, D., and Zimmerman, S.R., 2017, Rapid thinning of the Laurentide Ice Sheet in coastal Maine, USA, during late Heinrich Stadial 1: *Quaternary Science Reviews*, v. 163, p. 180–192, doi:10.1016/j.quascirev.2017.03.005.
- Leach, P., 2007, Marine geoarchaeological investigation of Damariscotta River, Maine, USA [M.S. thesis]: University of Maine, Orono, 164 p.
- Leach, P., 2008, Ground-penetrating radar investigation of the Glidden Point Midden, Newcastle, Maine: Preliminary Results: Society for American Archaeology Meeting, March 12-16, Vancouver, B.C.
- Leach, P., and Belknap, D.F., 2007, Marine geophysics and vibracoring applied to the search for submerged prehistory in Damariscotta River, Maine, USA, *in* Wilson, L., Dickinson, P., and Jeandron, J., eds., *Reconstructing human-landscape interactions*: chap. 8, Newcastle, UK, Cambridge Scholars Publishing, p. 141–158.
- Lore, R., 2004, Ceramic Period Adaptations in the Gulf of Maine: Maritime, Terrestrial, and Horticultural Inputs Faunal Analysis of an Armouchiquois Indian Village [M.S. thesis]: University of Maine, Orono, 271 p.
- Lore, R., 2006, Adaptations in the Edge Environment: Faunal Analysis of an Armouchiquois Indian Village: *Maine Archaeological Society Bulletin*, v. 46, no. 1, p. 1–22.
- Lothrop, J.C., Lowery, D.L., Spiess, A.E., and Ellis, C.J., 2016, Early Human Settlement of Northeastern North America: *PaleoAmerica*, v. 2, no. 3, p. 192–251, doi:10.1080/20555563.2016.1212178.
- Louati, M., Saïlidi, H., and Zargouni, F., 2015, Shoreline change assessment using remote sensing and GIS techniques: a case study of the Medjerda delta coast, Tunisia: *Arabian Journal of Geoscience*, v. 8, p. 4239–4255.
- Lowe, D.G., 2004, Distinctive Image Features from Scale-Invariant Keypoints: *International Journal of Computer Vision*, v. 60, no. 2, p. 91–110, doi:http://dx.doi.org/10.1023/B:VISI.0000029664.99615.94.
- Lowe, D., 1999, Object recognition from local scale-invariant features: *Proceedings of the Seventh IEEE International Conference on Computer Vision*, v. 2, p. 1150–1157, doi:10.1109/ICCV.1999.790410.
- Mack, K., 1994, Archaeological Investigations at the Todd Site (17-11), Muscongus Bay, Maine [M.S. thesis]: University of Maine, Orono, 271 p.

- Mack, K., and Will, R., 1999, Additional Phase I Archaeological Survey of the Proposed University of New England Marine Center, Biddeford, York County, Maine. Report on File at the Maine Historic Preservation Commission.
- Mack, K., and Will, R., 2000, Results of Phase III Archaeological Testing of the Proposed University of New England's Marine Studies Center, Biddeford, York County, Maine. Report on File at the Maine Historic Preservation Commission.
- Miller, J.F., 2017, No Title.
- Moorehead, W.K., 1922, *Archaeology of Maine: Andover, Mass., The Andover Press.*
- Neitzel, G.D., 2014, Monitoring event-scale stream bluff erosion with repeat terrestrial laser scanning: Amity creek, Duluth, MN [Ph.D. thesis]: University of Minnesota, 1–118 p.
- Newby, P., Bradley, J., Spiess, A.E., Shuman, B., and Leduc, P., 2005, A Paleoindian response to Younger Dryas climate change: *Quaternary Science Reviews*, v. 24, p. 141–154.
- Newsom, B.D., 2017, *Potters on the Penobscot: an Archaeological Case Study Exploring Human Agency, Identity, and Technological Choice* [Ph.D. dissertation]: University of Massachusetts Amherst, 276 p.
- NOAA, 2018, National Oceanic and Atmospheric Administration: <https://tidesandcurrents.noaa.gov/sltrends/>.
- Nordstrom, K., and Jackson, N., 2012, Physical processes and landforms on beaches in short fetch environments in estuaries, small lakes and reservoirs: A review: *Earth-Science Reviews*, v. 111, p. 232–247.
- Osberg, P., Hussey, A., and Boone, G., 1985, *Bedrock Geologic Map of Maine*. Augusta, ME: Department of Conservation, Maine Geological Survey, Print Map, scale 1:500,000.
- Pluckhahn, T.J., Thompson, V.D., and Rink, W.J., 2016, Evidence for Stepped Pyramids of Shell in the Woodland Period of Eastern North America: *American Antiquity*, v. 81, no. 2, p. 345–363, doi:10.7183/0002-7316.81.2.345.
- Pluckhahn, T.J., Thompson, V.D., and Weisman, B.R., 2010, Toward a New View of History and Process at Crystal River (8Cl1): *Southeastern Archaeology*, v. 29, no. 1, p. 164–181, doi:10.1179/sea.2010.29.1.011.
- Price, F.H., and Spiess, A.E., 2013, Three Prehistoric Lithic Tools Recovered by Fishermen off the Maine Coast: *The Maine Archaeological Society Bulletin*, v. 53, no. 2, p. 9–29.

- Prins, H., 1988, Tribulations of a Border Tribe: A Discourse on the Political Ecology of the Aroostook Band of Micmacs (16th-20th Centuries) [Ph.D. dissertation]: University of Michigan.
- Retelle, M.J., 1999, Surficial geology of the Yarmouth quadrangle, Maine: Maine Geological Survey, Open-File Map 99-105, map, scale 1:24,000.
- Retelle, M.J., and Weddle, T.K., 2001, Deglaciation and relative sea-level chronology, Casco Bay Lowland and lower Androscoggin River valley, Maine, *in* Special paper 351: Deglacial history and relative sea-level changes, northern new england and adjacent canada: Geological Society of America, p. 191–214, doi:10.1130/0-8137-2351-5.191.
- Robinson, B.S., 2006, Burial Ritual, Technology, and Cultural Landscape in the Far Northeast: 8600-3700 B.P., *in* Sanger, D., and Renouf, M., eds., The archaic of the far northeast: Orono, ME, University of Maine Orono Press, p. 341–381.
- Robinson, B.S., Ort, J.C., Eldridge, W.A., Burke, A.L., and Pelletier, B.G., 2009, Paleoindian Aggregation and Social Context at Bull Brook: American Antiquity, v. 74, no. 3, p. 423–447.
- Robinson, M., Alexander, C., Jackson, C., McCabe, C., and Crass, D., 2010, Threatened archaeological, historic, and cultural resources of the Georgia Coast: Identification, prioritization and management using GIS technology: Geoarchaeology, v. 25, no. 3, p. 312–326.
- Sanger, D., 2008, personal communication to Kelley, J.T.
- Sanger, D., 1981, Unscrambling Messages in the Midden: Archaeology of Eastern North America, v. 9, no. Fall, p. 37–42.
- Sanger, D., and Belknap, D.F., 1987, Human responses to changing marine environments in the Gulf of Maine: Man and the Mid-Holocene Climatic Optimum, Proc. 17th Ann. Chacmool Conference, p. 245–261.
- Sanger, D., Johnson, B., McCormick, J., and Sorg, M.H., 1980, Archaeological Salvage and Test Excavations Fernald Point, Acadia National Park, Maine: Report, p. 1–97.
- Sanger, D., and Petersen, J.B., 1991, An Aboriginal Ceramic Sequence for Maine and the Maritime Provinces, *in* Deal, M., and Blair, S., eds., Prehistoric archaeology in the maritime provinces: Past and present research: Frederickton, NB, Council of Maritime Premiers, p. 121–178.
- Sanger, D., and Sanger Elson, M.J., 1986, Boom and Bust on the River: The Story of the Damariscotta Oyster Shell Heaps: Archaeology of Eastern North America, v. 14, no. Fall, p. 65–78.

- Schnitker, D., Belknap, D.F., Bacchus, T.S., Friez, J.K., Lusardi, B.A., and Popek, D.M., 2001, Deglaciation of the Gulf of Maine, *in* Special paper 351: Deglacial history and relative sea-level changes, northern new england and adjacent canada: Geological Society of America, p. 9–34, doi:10.1130/0-8137-2351-5.9.
- Shettleworth, E.J., 1987, FY87 End-of-Year Report, Maine Historic Preservation Commission, unpublished report.
- Shipp, R., Belknap, D.F., and Kelley, J.T., 1991, Seismic-stratigraphic and geomorphic evidence for a post-glacial sea-level lowstand in the northern Gulf of Maine: *Journal of Coastal Research*, v. 7, p. 341–364.
- Shipp, R., Belknap, D., and Kelley, J., 1989, A submerged shoreline on the inner shelf off the Maine coast, Northwestern Gulf of Maine, *in* Tucker, R., and Marvinney, R., eds., *Studies in maine geology: chap. Studies in*, Augusta, ME, Maine Geological Survey, p. 11–28.
- Sinson, D., Henze, T., Daly, J., Dickson, S., and Kelley, J., 2002, Coastal bluffs in the Friendship quadrangle, Maine: Maine Geological Survey, Open-File Map 02-189, scale 1:24,000.
- Skinas, D., 1987, The Todd Site: A Case Study of Shell Midden Formation [M.S. thesis]: University of Maine, Orono, 254 p.
- Smith, G.L., Zarillo, G.A., and Zarillo, G.A., 1990, Calculating Long-Term Shoreline Recession Rates Using Aerial Photographic and Beach Profiling Techniques: *Journal of Coastal Research*, v. 6, no. 6, p. 111–120.
- Spiess, A.E., 1985, Wild Maine and the Rusticating Scientist: A History of Anthropological Archaeology in Maine: *Man in the Northeast*, v. 30, p. 101–129.
- Spiess, A.E., 1995, Early Contact Period Context: The Maine Archaeological Society Bulletin, v. 34, no. 2, p. 1–20.
- Spiess, A.E., 1998, Damariscotta Shell Midden Historic District, Nomination to the National Register of Historic Places: Maine Historic Preservation Commission, Augusta, Maine.
- Spiess, A.E., 2016a, Lost to the Sea: Maine's Ancient Coastal Heritage (Maine Sea Grant) 2015-7, Possible Archaeological Sites for GPR and Field Work Screening, unpublished working document, personal communication to Alice Kelley.
- Spiess, A.E., 2016b, Maine Historic Preservation Commission, personal communication.
- Spiess, A.E., 2017a, Maine Historic Preservation Commission, personal communication.

- Spiess, A.E., 2017b, People of the Clam: Shellfish and Diet in Coastal Maine Late Archaic and Ceramic Period Sites: *Journal of the North Atlantic*, v. 10, p. 105–112.
- Spiess, A.E., 2018, Maine Historic Preservation Commission, personal communication.
- Spiess, A.E., Bradley, J.W., and Wilson, D., 1998, Paleoindian Occupation of the New England-Maritimes Region: Beyond Cultural Ecology: *Archaeology of Eastern North America*, p. 26–264.
- Spiess, A.E., Curran, M.L., and Grimes, J.R., 1985, Caribou (*Rangifer Tarandus* L.) Bones from New England Paleoindian Sites: *North American Archaeologist*, v. 6, no. 2, p. 145–159.
- Spiess, A.E., and Lewis, R., 2001, The Turner Farm Fauna: 5000 years of Hunting and Fishing in Penobscot Bay, Maine: *Occasional Publications in Maine Archaeology*, , no. 11, p. 178.
- Spiess, A.E., Trautman, E., and Kupferschmid, T., 1990, Prehistoric Occupation at Reversing Falls, report on file, Maine Historic Preservation Commission #2566.
- Stuiver, M., and Borns, H.W.J., 1975, Late Quaternary Marine Invasion in Maine: Its chronology and Associated Crustal Movement: *Geological Society of America Bulletin*, v. 86, p. 99–104.
- Thompson, V., Reynolds, M.D., Brian, H., Jefferies, R., Johnson, J.K., and Humphries, L., 2004, The Sapelo shell ring complex: shallow geophysics on a Georgia sea island: *Southeastern Archaeology*, v. 23, no. 2, p. 191–201.
- Thompson, W., and Borns, H.W.J., 1985, Surficial Geologic Map of Maine: Department of Conservation, Maine Geological Survey, Print Map, scale 1:500,000.
- Thompson, W.B., 2009, Surficial geology of the Damariscotta quadrangle, Maine: Maine Geological Survey, Open-File Map 09-6, map, scale 1:24,000.
- Thompson, W.B., 2015, Surficial Geology Handbook for Southern Maine: Maine Geological Survey Bulletin, v. 44.
- Thompson, W.B., and Borns, H.W.J., 2007, Maine's Ice Age Trail: Geologic Site of the Month.
- Thomsen, P.F., and Willerslev, E., 2015, Environmental DNA - An emerging tool in conservation for monitoring past and present biodiversity: *Biological Conservation*, v. 183, p. 4–18, doi:10.1016/j.biocon.2014.11.019.

- Timson, B.S., 1974, Coastal marine geologic environments of the Friendship quadrangle, Maine: Maine Geological Survey, Open-File Map 74-22, scale 1:24,000.
- Timson, B.S., 1976a, Coastal marine geologic environments of the Machias Bay quadrangle, Maine: Maine Geological Survey, Open-File Map 76-106, scale 1:24,000.
- Timson, B.S., 1976b, Coastal marine geologic environments of the Mt. Desert SE [Southwest Harbor 7.5'] quadrangle, Maine: Maine Geological Survey, Open-File Map 76-110, scale 1:24,000.
- Westoby, M., Brasington, J., Glasser, N., Hambrey, M., and Reynolds, J., 2012, 'Structure-from-Motion' photogrammetry: A Low-cost, Effective Tool for Geoscience Applications: *Geomorphology*, v. 179, p. 300–314.
- Whitehead, D., 2016, Maine Coast Heritage Trust, personal communication.
- Will, R., and Mack, K., 1998, Phase I Archaeological Survey of the Proposed University of New England's Marine Studies Center, Biddeford, York County, Maine. Report on File at the Maine Historic Preservation Commission.
- Yoccoz, N.G., Bråthen, K.A., Gielly, L., Haile, J., Edwards, M.E., Goslar, T., Von Stedingk, H., Brysting, A.K., Coissac, E., Pompanon, F., Sonstebo, J.H., Miquel, C., Valentini, A., De Bello, F., Chave, J., Thuiller, W., Wincker, P., Cruaud, C., Gavory, F., Rasmussen, M., Gilbert, M.T., Orlando, L., Brochmann, C., Willerslev, E., and Taberlet, P., 2012, DNA from soil mirrors plant taxonomic and growth form diversity: *Molecular Ecology*, doi:10.1111/j.1365-294X.2012.05545.x.
- Young, R., 1990, Late Quaternary Evolution and Geoarchaeology of Johns Bay and Pemaquid Beach, Maine: [M.S. thesis]: University of Maine, Orono, 95 p.
- Young, R., Belknap, D.F., and Sanger, D., 1992, Geoarchaeology of Johns Bay, Maine: *Geoarchaeology*, v. 7, p. 209–249.

Appendix A

A BRIEF GUIDE TO RADAN

A.1 Creating a 3D Batch of Files

Creating a 3D batch of files is ideal for constructing the GPR grids that are the building blocks of a super 3D grid. If you have multiple grids, it necessary to assemble the profiles in a 3D batch of files because this is the format that goes into the super 3D grid. Alternatively, a 3D batch of files is sufficient if it can contain all the GPR profiles required by the project.

A.1.1 Step 1

To create a 3D batch of files, a new Radan window is necessary. Check the global settings window to ensure the desired source and output directory set to the desired location. Navigate to the blue G in the upper left corner of the Radan window. Click on it. Hover over "assemble data file" and select "3D batch of files." The window that pops up will ask for a batch filename (Figure A.1). Click next.

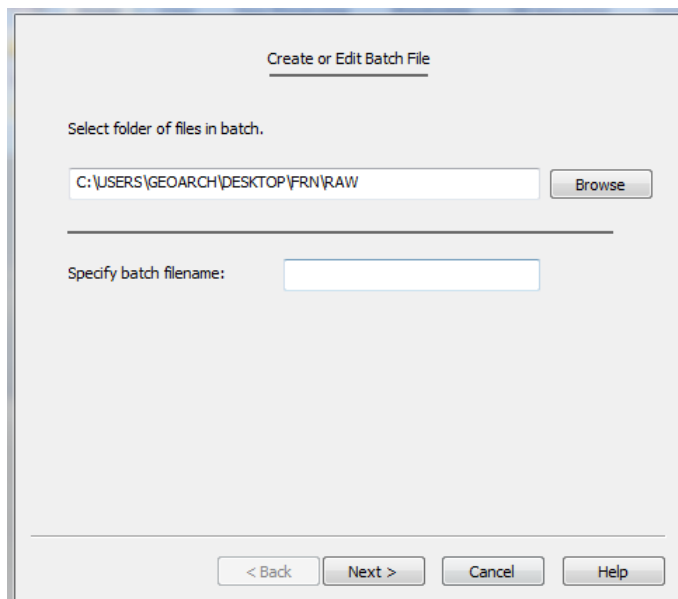


Figure A.1: Prompt for batch filename.

A.1.2 Step 2

The next pop-up (Figure A.2) prompts the user to select the GPR profile files from the source directory. Select all of the files that the grid requires in the left box, and click add. Click next.

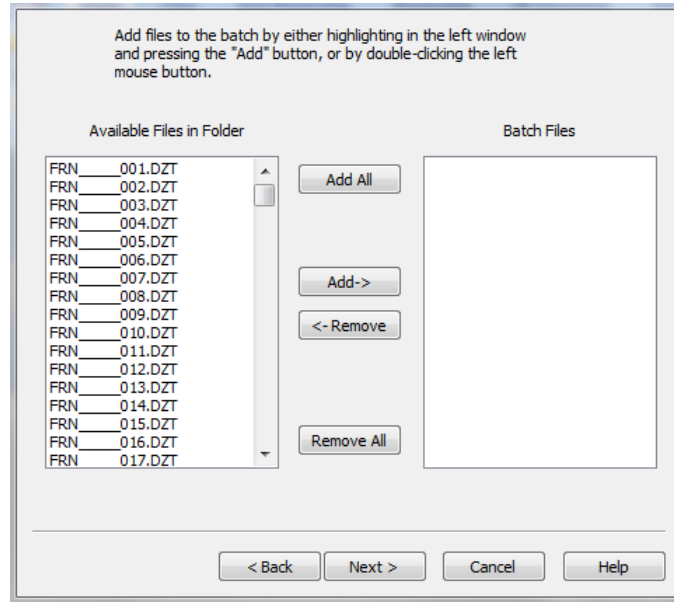


Figure A.2: Prompt for files.

A.1.3 Step 3

The following window (Figure A.3) allows the user to define the areal extent of the grid as well as the directions of the file groups (i.e., x and/or y). Type in grid dimensions. If your grid contains profiles that run in both the x and y directions, check both boxes. Click next.

A.1.4 Step 4

This step will allow the user to select files in the X-direction. The window will look almost identical to Figure A.2. Only select the files that run in the X-direction. The Y-direction file selection is separate and appears after completing the process for the X-direction. Select next.

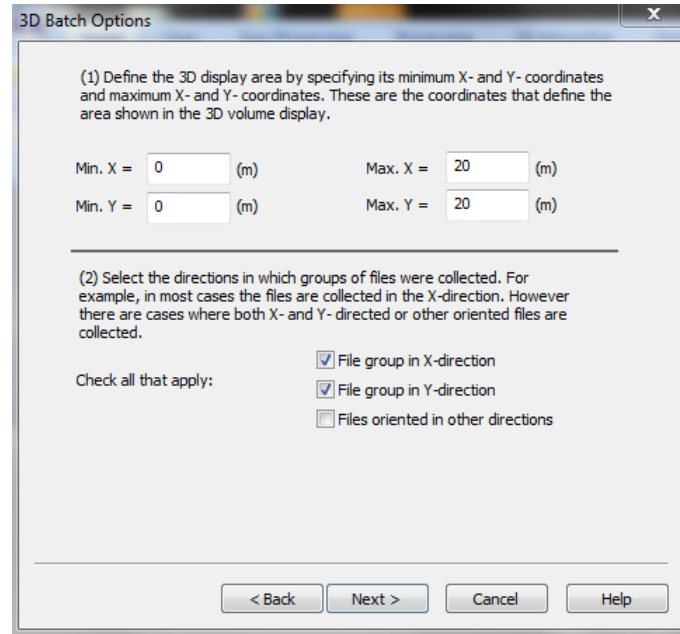


Figure A.3: Box for defining 3D batch grid extent.

A.1.5 Step 5

The window will now be labeled "File Group 3D Area" (Figure A.4). Typically, the selection of "Use entire 3D display area selected earlier" is the best option for a simple grid. However, this changes when profiles start at some point within the grid instead of at a common baseline. If this is the case, select "Use different 3D area" and type in the x and y dimensions. Next, specify the direction and order the files were collected in. The arrows on the yellow background in Figure A.4 represent profiles collected from the bottom left corner of the grid, moving north on the zero baseline. The window looks similar for files in the Y-direction (Figure A.5). The arrows on the yellow background in Figure A.5 represent profiles collected from the bottom left corner of the grid, moving right along the zero baseline. Select next.

A.1.6 Step 6

The next window allows the user to double-check that profiles were placed in the correct order by Radan. If the 3D area occupied by the selected profiles is different than originally specified, the X and Y start and end locations will be

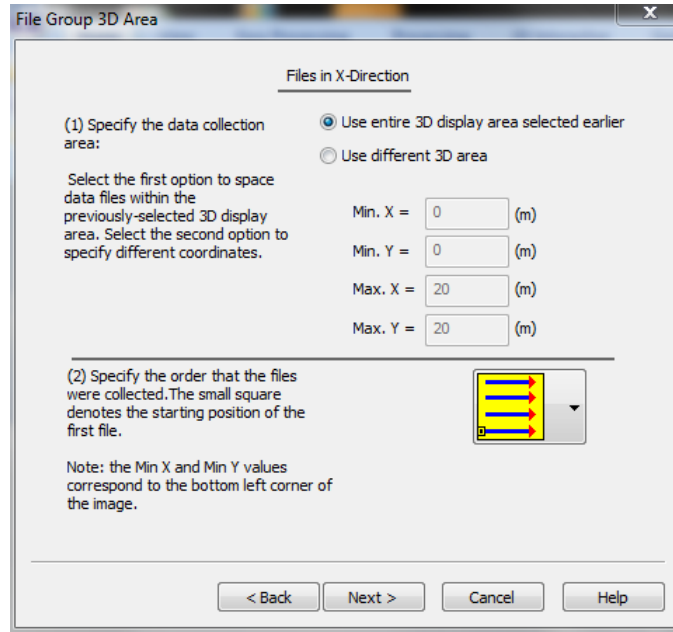


Figure A.4: File location and orientation (X-direction).

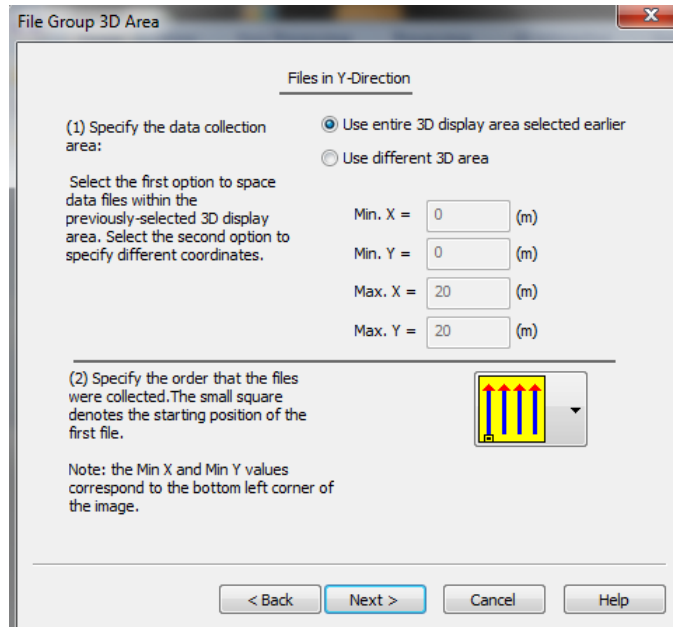


Figure A.5: File location and orientation (Y-direction).

incorrect. Fixing this will require the user to select "back", select "Use different 3D area", and enter the correct dimensions. Note, this will not change the dimensions of the grid itself. Alternatively, a manual correction is possible in the "File Group Details" window by clicking on the filename of interest. A "File Parameters" box

will pop-up which will allow the user to edit the start and end locations of the profiles (Figure A.6). Once the profiles are correctly referenced, click next.

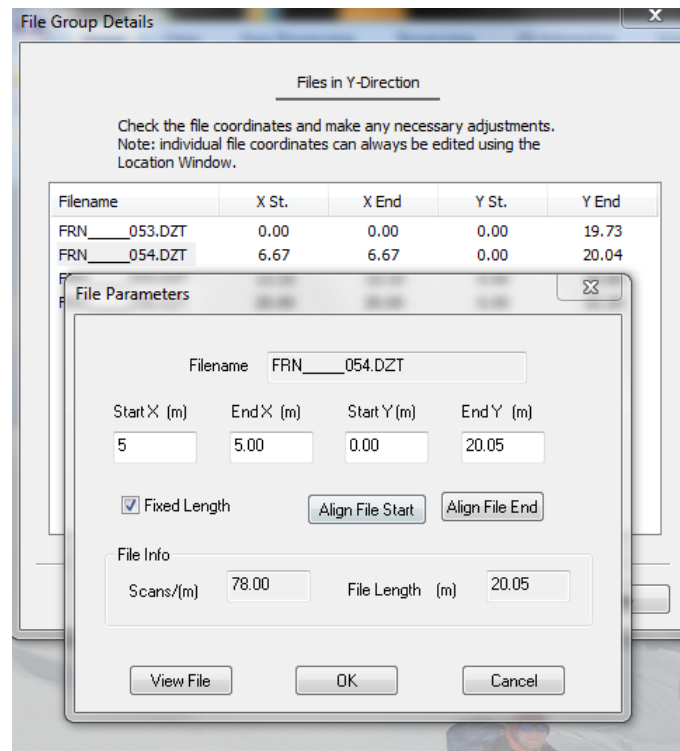


Figure A.6: File details and "File Parameters" pop-up box. Edit profile start and end locations here.

A.1.7 Step 7

The following window will prompt the user for GPS locations. This step allows the user to view the grid corners in Google Earth. Click finish to skip this step.

A.2 Super 3D File Creation

Three-dimensional batch files make-up a super 3D file. Constructing a super 3D grid allows the user to process all GPR profiles at the same time while applying the same parameters to each profile.

A.2.1 Step 1

Open a new Radan window. Navigate to the blue "G" in the upper left corner and click on it. Hover the mouse over "Assemble Data File," move to the menu that pops-up to the right and click "Super 3D." A window prompting for the source file will pop-up just as in the construction of the batch 3D file. The default source directory is the source directory set under "global settings." Name the super 3D file in the text box. Click next.

A.2.2 Step 2

The following window will look similar to Figure A.7, although it will not have the red and blue boxes which represent already uploaded 3D batch files. Select "Add File" to begin construction of the super 3D grid.

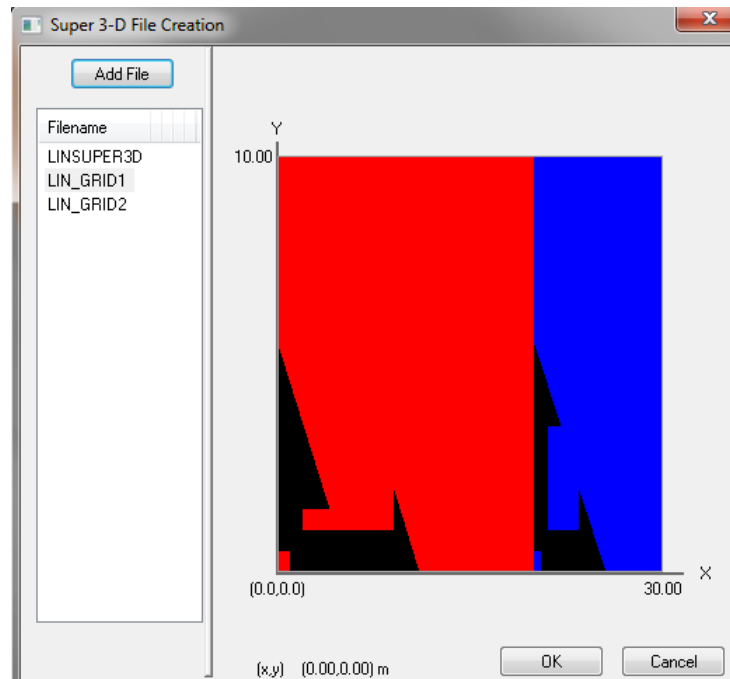


Figure A.7: Super 3D file creation main window.

A.2.3 Step 3

The "File Parameters" box will open (Figure A.8). Select a 3D batch file by clicking "Filename". Note, the starting coordinates are always those of the lowermost left corner of the batch 3D file. Enter the respective origin coordinates for the batch 3D file, and Radan will input the ending coordinates. Click "OK." The footprint of the batch 3D file appears in the previous "Super 3D File Creation" window. Also note, the direction which individual profiles run within the batch 3D file will not change as a result of this super 3D file construction.

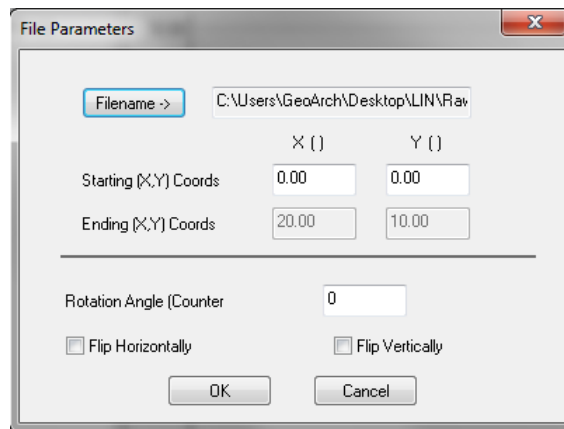


Figure A.8: "File Parameters" pop-up box. This is where the user assigns starting coordinates to batch 3D files.

A.2.4 Step 4

Clicking "OK" will produce the super 3D file. Click "Location" to view a layout of the grids within the super 3D file. Click through each line by advancing with the arrows in the lower left of the window and drag the mouse across each profile to see a point on the location map advancing on the particular profile. This will allow the user to check that the profiles are in the proper location and run in the correct direction.

A.3 GPR Profile Processing

This particular guide to processing GPR profiles within Radan highlights the general steps carried out on most of the data within the project. Radan also provides a guide to processing steps.

A.3.1 Step 1

The first step in processing is to perform a time zero correction on the GPR data. Click "Time Zero" in the "Easy Processing" or "Processing" tab. A window will appear in the left portion of the Radan window (Figure A.9). Click the trace and drag it up so that the 0.0 mark is in the center of the first positive peak, as shown in Figure A.9. Select "Apply" for a preview. Select "Ok" to complete the step.

A.3.2 Step 2

Next, the frequency-filtering step is carried out using the FIR filter. Navigate to the "Filters" box within the Processing tab. Select "FIR" and a box will appear in the left portion of the Radan window (Figure A.10). Under the bold "Horizontal", click the box to the right of "Length (scans)" and type "77777". Radan will change this value to the maximum number of scans, typically 20001. Low and high frequency filters applied in this step are 550 MHz and 350 MHz respectively. Type the corresponding frequencies into the boxes adjacent to "Low Pass" and "High Pass", under "Vertical (MHz)" (Figure A.10). Select "Apply" for a preview of the step. Select "Ok" to complete the FIR filter step.

A.3.3 Step 3

Following frequency filtering, select "Migration" under the "Processing" tab. Note, dielectrics calculated as a result of the migration step were unique to each dataset. A window will pop-up in the left portion of the Radan window. Along with

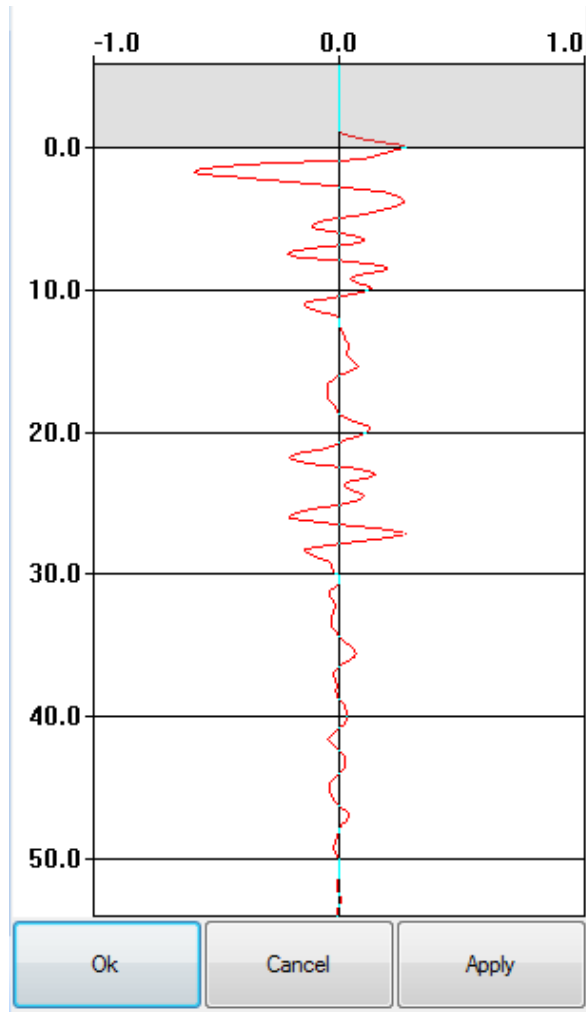


Figure A.9: Time zero correction window. Notice that the trace is centered within the first positive peak.

the window, a hyperbola will appear within the GPR profile window. The hyperbola that appears on the GPR record is often difficult to distinguish in the default black and white profile view. This issue is resolved by changing the color of the GPR record by selecting "Color Tables" under the "Home" tab. Adjust the hyperbola by dragging the boxes located on the tails and top, and match it to representative hyperbola within the profile. Click "Apply" to preview the step. Click "Ok" to complete GPR data migration.

<div> <div></div> FIR Filters </div>	
# of Channels	1
Design	BOXCAR
<div> <div></div> Horizontal </div>	
Type	BKGR REMOVAL
Length (scans)	20001
<div> <div></div> Channel Parameters </div>	
<div> <div></div> Vertical (MHz) </div>	
Low Pass	550
High Pass	350
<div> <div></div> Samples </div>	
Start	0
End	511

Low Pass

Removes High Frequency Noise

Figure A.10: FIR filter window.

A.3.4 Step 4

The settings applied during the range gain step were unique to each dataset. Under the "Processing" tab, select "Range Gain" which is listed within the "Gain" box. After selecting this processing step, a window will appear in the left portion of the Radan window. To obtain a window similar to Figure A.11, select "Exponential" in the drop-down box adjacent to "Gain Type". Type "12" in the window adjacent to "# Of Points". Gain parameters can be entered in text boxes adjacent to the "Gain #" boxes. Alternatively, the points on the wavelet are adjustable by dragging. Select "Ok" to apply the range gain settings.

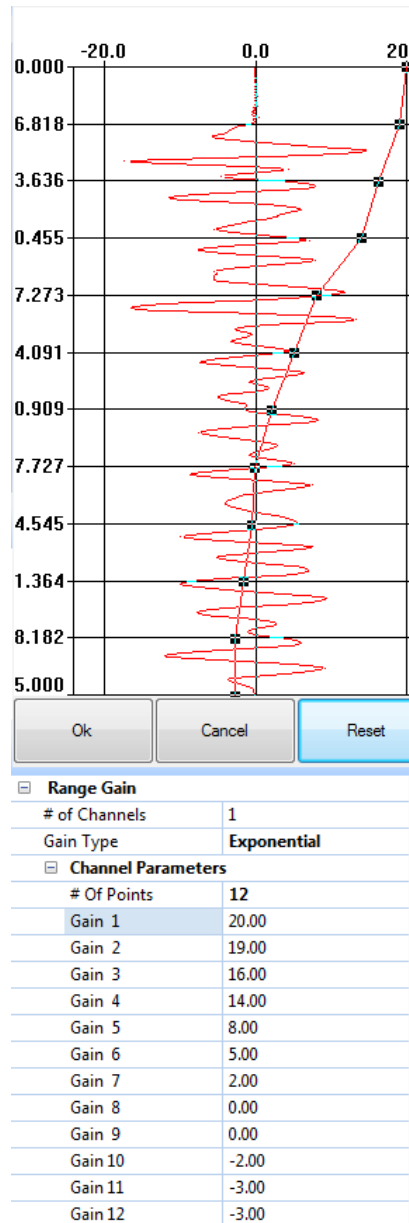


Figure A.11: Range gain window.

A.4 Topographic Correction

Correcting GPR profiles for topography was completed in Radan for profile processing, but an ArcGIS environment for the collection of topographic data. The source of topographic information for correcting GPR profiles could come from another source if the sampling strategy suited the desired resolution of the topographic correction.

A.4.1 Obtaining Topographic Information

To obtain elevation information by way of LiDAR datasets, navigate to NOAA's Data Access Viewer at <https://coast.noaa.gov/dataviewer/#/>. Click the "Elevation" button. The next window will show a map of the available datasets. To view a particular location, type the address in the search window in the upper left corner. The area of interest is shaded red within a yellow box. Available datasets appear on the right side of the page.

Click on the shopping cart located on the right side of the page, below the data of interest. The user shopping cart is in the upper right corner of the page. Click it. Click next at the bottom of the page that appears. The following page requires the user to select parameters for the dataset format (Figure A.12 displays parameters used in this project). Click next. The following page requires an email address for data retrieval. Click next. It will likely take up to 48 hours for the data delivery.

A.4.2 Extracting Topographic Information in ArcMap

Open a new project in ArcGIS. Import the dataset downloaded from NOAA's digital coast. The product will likely be a DEM and will not require conversion. Ideally, well-constrained GPS GPR grid corner locations exist for the project area. The user should also import this file into the current ArcGIS project.

Draw a line which represents the desired profile location. Complete this task by using the draw tool and selecting "Line" from the drop-down menu. Double-click at the line terminus to complete the line. Assure that the line graphic is selected. Click "Drawing" on the Draw toolbar and select "Convert Graphics to Features." In the window that appears, check the box "delete graphic after conversion." Select "OK." When the process is almost finished, ArcMap will ask to add the feature to the map as a layer. Select yes. The line will appear on the screen.

Lidar

Projection & Datum Options:

Projection: <div>UTM ▼</div>	Zone: <div>Zone 19 Range 072W-066W ▼</div>
Horizontal Datum: <div>NAD83 ▼</div>	Horizontal Units: <div>Meters ▼</div>
Vertical Datum: <div>NAVD88 ▼</div>	Vertical Units: <div>Meters ▼</div>

Output Options:

Output Product: <div>Raster ▼</div>	Output Format: <div>Grid - GeoTiff 32-bit ▼</div>
Grid Method: <div>Average ▼</div>	Grid Units: <div>Meters ▼</div>
<input checked="" type="checkbox"/> Fill Small Gaps	Grid Size: <div>1</div>

Data Options:

☐ Use Advanced Options

Data Classes:

Ground

All

☐ Add Intensity Images

Figure A.12: Parameters for NOAA's *Data Access Viewer* coastal LiDAR datasets.

The next step results in point features on the line at user-defined intervals. To complete this step, type "generate points along line" in the ArcGIS search window. Select this process. The window prompts the user for a line layer file, and the point spacing. Enter the desired topographic correction sampling resolution, keeping in mind that the DEM resolution is 1 meter. Select "OK." The point file is now added to the project.

An additional step is necessary to assign elevations to the points. Find and click on the ArcGIS search window. Type "extract values to points" and select the operation. The window requires the user to enter "input point features" and an

"input raster." The input raster is the DEM downloaded from NOAA Digital Coast. Click "OK." When the process is complete, right-click on the output file in the "Layers" display window and select "Open Attribute Table." Numbers listed under "rastervalu" are elevations in meters. To see proper point labels on the map, right-click on the output file and click "Properties." Click "Labels" on the following menu and select "objectid" in the label field drop-down box. Click "OK." Labels will not display until right-clicking the output file and selecting "Label Features."

Finally, the elevations and their associated locations are apparent. Transcribe them to an excel sheet that contains the line location in meters, objectid, the associated GPR scan. The scans per meter was typically set at 78, but checking the Radan file header is recommended.

A.4.3 Assigning Topographic Information within Radan

Radan requires a manual topographic correction. The Excel sheet created in the previous step will allow the user to transcribe the information in the most efficient manner. This step involves entering topographic information at desired intervals along the GPR profile.

Open the select GPR profile within Radan. Under the "Home" tab, open the "Tables" pane. Within the "Tables" pane select the "Way Points" tab. Dragging the top of the window will expand it vertically. Critical columns within this pane are Scan, Dist(m), and Elev(m). The Dist(m) column is auto-populated by the system based on the "Units/mark" setting. Enter the elevations and associated distances. Save the Radan file.

Navigate to the "Processing" tab. Select "Surface Normalization." The window that will pop-up on the left side contains "Normal Level," "Vertical Scale," and "Auto Level." The "Normal Level" represents the line from which the GPR record will hang. To customize the normal level, select "no" under "Auto Level." Choosing

a normal level value slightly above the highest elevation value is recommended. Profiles with little change in topography are best represented with a 1:1 or 1:2 vertical scale. Extreme differences in topography are best represented by the 1:4 vertical exaggeration. Selecting "Apply" will not result in a preview as it does with other processing steps. Select "OK" and save the Radan file.

Drag the tables pane up or down to make the vertical scale match the horizontal scale. For an image of the profile, select the blue G and hover over "Export." Select the desired image format.

A.5 Tracing a Layer

A layer file is required in order to create an isopach map within any external software. Radan does not have the capability to produce isopach or contour maps. Also, all profiles must be processed within a batch 3D file or super 3D file prior to picking/tracing a continuous layer within each profile.

With the processed batch 3D file or super 3D file open within the Radan window, navigate to the "2D Interactive" tab. Check that the "Target" is set to "Layer" and not "Pipe" or "Rebar". Digitize the reflector in all of the lines. Save the file and disable 2D interactive. Navigate to the blue G in the upper left corner of the Radan screen and scroll to the bottom of the menu. Select "Export Picks," and a .csv file will result. Open the .csv file and sort all picks according to amplitude, then delete picks without an amplitude value. Sorting and deleting is especially important if "EZ Tracker" was used as this excludes picks that the user did not make. The .csv file can then be imported into ArcMap or Surfer.

Appendix B

TOTAL STATION SURVEY

B.1 Data Collection

Spatial location information was collected at four sites (Damariscotta Oyster Farm, Olson, Fernald Point, and Tranquility Farm). A handheld GPS unit (Garmin GPSMAP 62St) provided location information for the corners of a detailed grid as well as the start and end points of each exploratory transect at the Damariscotta Oyster Farm. A total station (Sokkia SET4B) was used to survey the GPR grid at the Olson and Tranquility Farm sites. An RTK survey of the 60 m by 60 m GPR survey grid at Fernald Point, with data every 10 m, was carried out by Karen Anderson of the National Park Service, Acadia National Park.

B.2 Data Processing

The amount of spatial data processing varied between sites and with each collection technique. Spatial positions of data from the total station survey were calculated using Pythagorean Theorem and an Excel spreadsheet. A Topcon positioning system (GB-1000) was used to gain precise and accurate location and elevation information for each base station at Tranquility Farm and the Olson Site. The Topcon units were stationary on a point that was directly below the tripod and collected data for a minimum of two hours. The handheld GPS data required conversion to UTM format. Karen Anderson, National Park Service, Acadia National Park, provided a shapefile with location and elevation information from the RTK survey, and it required no processing.

B.2.1 Damariscotta Oyster Farm (Site 26.15)

A total station survey was not conducted for site 26.15, but a hand-held GPS (Garmin GPSMAP 62St) was used to collect location data on grid corners as well as the start and end position of exploratory profiles. The original GPS information was in decimal degree format, but Earth Point was used to allow a batch conversion to UTM format. The Earth Point website requires signing up for an account which is free to those in academia. Selecting "Batch Convert" from the "Worldwide Utilities" menu results in a user-friendly page full of instructions. The file containing the location information for site 26.15 is titled DAM_UTMforGIS.csv.

B.2.2 Olson (Site 17.13)

Select points within the Olson Site total station survey required manual correction within ArcGIS. Problematic points were not internally consistent, nor did they appear consistently offset from correct point locations. Using the edit mode in ArcGIS, individual offset points were selected and moved to their approximate measured location. A critical component ensuring the accuracy and justification for this methodology was the grid location labels associated with each known and confirmed surveyed point.

After the select points were manually moved to their proper location, using distances measured from known correct grid points, the "add XY coordinates" tool was used in ArcGIS to extract their UTM values. The attribute table containing this information was exported and saved as a pdf titled OLS_totalstation_Table_Printout. The file named OLS_TotalStationSurvey_final contains the original survey information (under tab OrigData) as well as a tab that contains the corrected values labeled "Corrected Data". This file includes the new UTM locations of points from row 90 to row 113 in the OrigData tab. These UTM points with elevations make up OLS_SurveyPoints_final (a .csv file) which can be

downloaded to an ArcGIS project for a visual representation of the survey information. Data from the total station survey at the Olson site is listed in Table B.1, and a final version of the total station survey is depicted in Figure B.1.

B.2.3 Tranquility Farm (Site 44.12a)

The western portion of the Tranquility Farm survey data required additional correction. Incorrectly positioned grid points were internally consistent, but they were rotationally offset from the majority of the grid points. Upon importing the xyz dataset of UTM coordinates and elevations into ArcGIS, the offset points were rotated, as a group, by 27 degrees. This step was accomplished in editor mode within ArcGIS, using the rotate tool to shift the points to a proper orientation via visual estimation. Entering "A" post-rotation provided the measurement for the angle of rotation.

Next, a right triangle was drawn from one of the shifted points taken along the shoreline to measure movement in the X- and Y-direction of the group of points. A right triangle was chosen to allow an additional check for accuracy of measurement and to allow a 2D characterization of movement. A georeferenced air photo allowed estimation of a corrected position. Approximate shift in the X-direction was -7.22 meters and -11.35 meters in the Y-direction; where, negative numbers represent movement left (west) and down (south).

After the necessary corrections were made to the survey data, UTM coordinates were extracted from the new point locations. This step was completed within ArcGIS. ArcToolbox contains "Data Management Tools" where a "Features Toolbox" is found, and an option exists to generate xy data. The completion of this step will yield new columns in the attribute table labeled "point-x" and "point-y".

In order to compile UTM data for the Tranquility Farm Site in one file, the attribute table in ArcGIS was exported as a pdf file titled

editTRQhalf_tryCfinal_Table_Printout. The UTM locations representing the corrected survey points were added to the TRQ_SurveyPoints_final Excel document. Additionally, a .csv file labeled TRQ_SurveyPoints_final contains correct UTM and elevation information in simple xyz form for import to ArcGIS. Data from the total station survey at site 44.12a is listed in Table Table B.2, and a final version of the total station survey is shown in Figure B.3.

B.2.4 Fernald Point (Site 43.24)

An RTK survey was carried out by Karen Anderson, surveyor for Acadia National Park. A 60 x 60 meter grid for GPR survey was established with grid corners recorded every 10 meters. Data was provided via a GIS shapefile where coordinates are in UTM, Zone 19N, meters using datum NAD83 (2011 realization). Additionally, elevation data is listed in meters. Figure B.2 shows the area of GPR survey at the Fernald Point site.

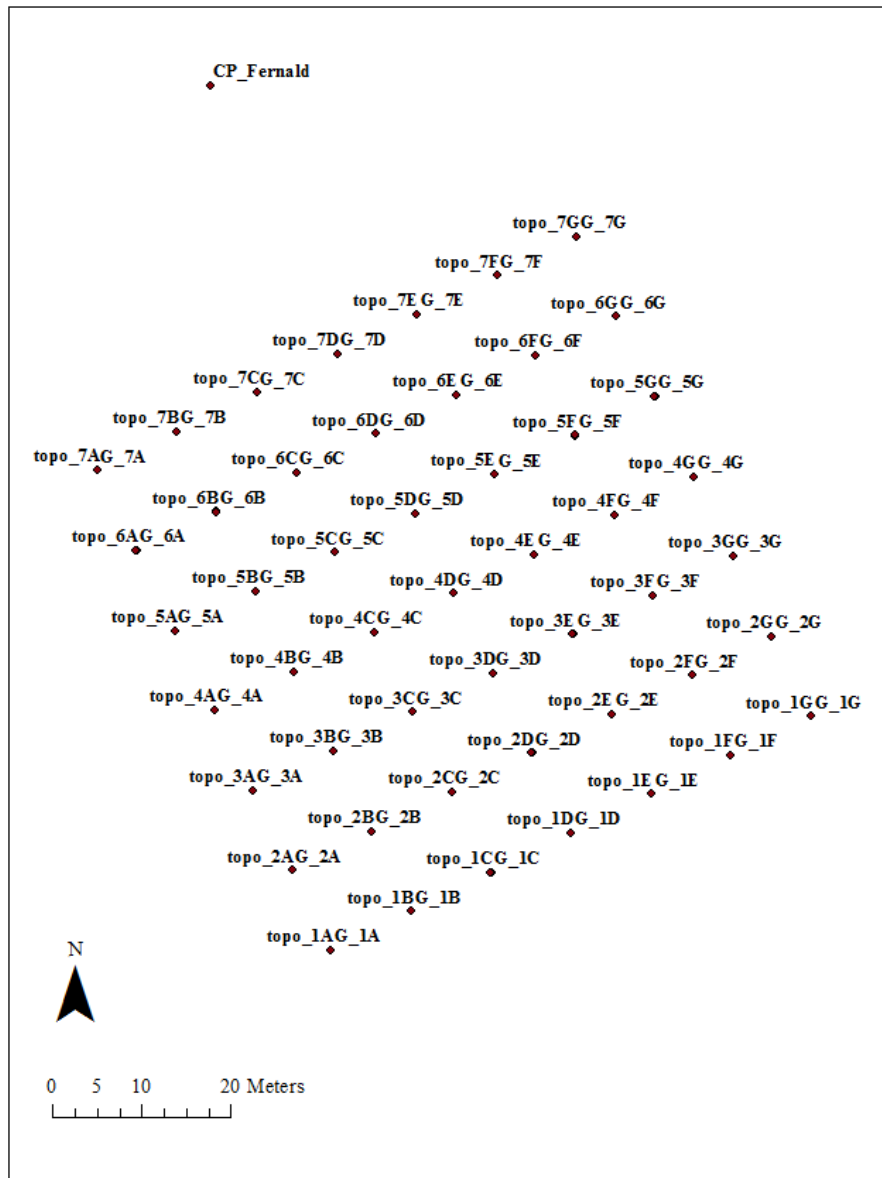
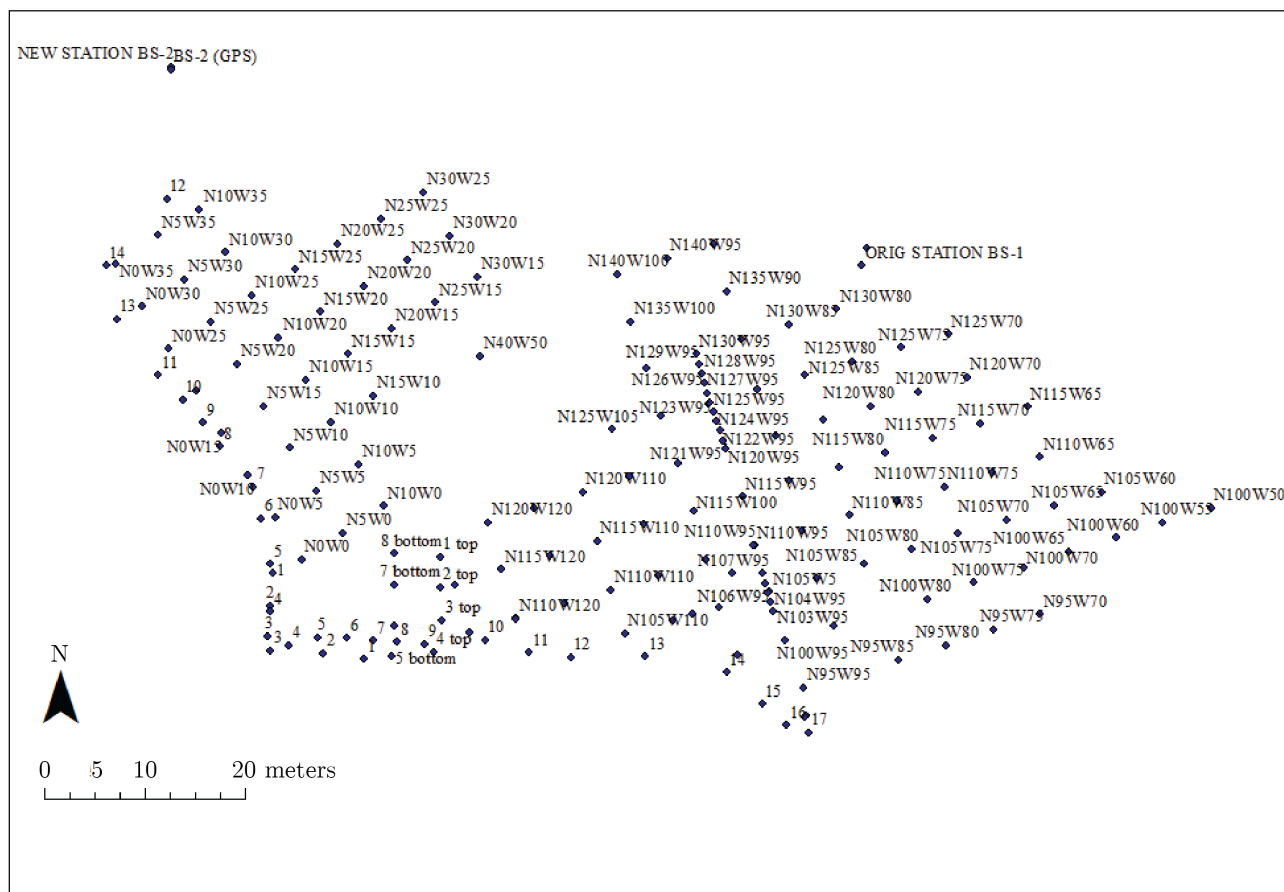


Figure B.2: Fernald Point (Site 43.24) total station survey map. Data courtesy of the National Park Service, Acadia National Park.



B.3 Total Station Data

B.3.1 Olson (Site 17.13)

Table B.1: Olson (Site 17.13) total station survey data.

Point ID	Distance ft.	Elev. Diff ft.	Relative Decimal Azim.
BS-1	—	—	—
10N10E	62.44	-3.16	151.57
15N10E	46.16	-2.67	152.52
20N10E	29.75	-2.37	154.89
20N05E	35.50	-1.97	182.27
20N00E	46.89	-1.13	199.29
15N00E	58.77	-2.04	186.62
10N00E	72.20	-2.97	178.61
10N05E	65.44	-2.98	166.21
15N05E	49.96	-2.53	171.69
10N05W	81.97	-2.95	188.48
15N05W	69.92	-1.33	197.38
20N05W	60.56	-0.78	209.57
20N10W	75.68	-1.48	215.18
15N10W	83.41	-1.45	204.80
10N10W	93.73	-2.66	196.19
16N07W	73.65	-0.71	203.15
20N15E	32.68	-2.34	124.75
15N15E	47.96	-2.71	132.80
10N15E	64.00	-3.40	136.80
10N20E	68.99	-3.34	123.13

Table B.1: Continued

Point ID	Distance ft.	Elev. Diff ft.	Relative Decimal Azim.
15N20E	54.65	-2.68	115.62
20N20E	42.08	-2.18	103.55
N00E25	96.06	-4.41	140.18
N05E25	79.79	-3.65	138.89
N05E30	83.68	-3.82	127.37
N00E30	99.24	-4.22	130.75
Bluff Edge 10E	116.80	-5.33	149.62
Bluff Edge	129.32	-5.71	142.78
15E Bluff Edge	132.02	-5.22	134.90
20E			
20N25E	55.51	-2.13	90.98
15N25E	65.66	-3.00	102.96
10N25E	77.43	-3.56	111.82
05N25E	90.62	-4.07	118.27
00N25E	104.53	-4.51	123.71
00N30E	88.52	-3.29	103.26
05N30E	78.04	-2.86	94.66
10N30E	69.70	-2.14	83.51
RECON	49.92	-2.07	94.84
N20E23			
RECON	41.48	-0.48	53.10
N30E23			

Table B.1: Continued

Point ID	Distance ft.	Elev. Diff ft.	Relative Decimal Azim.
RECON	55.13	1.38	17.41
N40E23			
N20W15	90.89	-2.40	218.65
N15W15	97.15	-2.11	209.49
N10W15	106.45	-2.43	201.57
N20W20	106.78	-2.40	221.33
N15W20	112.58	-2.13	213.33
N10W20	119.91	-2.41	206.23
N10W25	134.33	-2.69	209.88
N15W25	127.18	-1.67	216.22
N20W25	122.74	-2.04	223.43
N20W30	136.34	-1.46	225.17
N15W30	142.91	-1.79	218.67
N10W30	146.95	-2.53	212.81
N30W10	69.67	-1.66	240.17
N40W10	78.18	-1.77	265.03
N30W20	102.49	-1.52	239.18
N40W20	107.88	-1.93	256.94
N30W30	134.19	-2.07	241.38
N40W30	137.98	-2.15	252.56
N05W10	105.40	-3.70	189.06
N05W15	117.80	-3.50	195.31
N05W20	128.81	-3.27	199.73
N05W25	143.28	-2.75	203.75

Table B.1: Continued

Point ID	Distance ft.	Elev. Diff ft.	Relative Decimal Azim.
N05W30	156.68	-2.65	207.14
N02W115 to N02W30	123.09	-3.45	191.58
N02W17	127.54	-3.41	193.86
N02W19	131.99	-2.77	195.98
N02W20	134.51	-2.65	196.84
N02W22	139.83	-2.80	198.45
N02W24	145.22	-3.00	199.88
N02W26	150.87	-3.03	201.27
N02W28	156.17	-2.64	202.71
N02W30	161.40	-2.56	204.36
N0E0	101.98	-4.22	346.68
N5E0	86.98	-3.66	350.70
N10E0	72.40	-3.04	355.94
N15E0	58.77	-2.07	4.17
N20E0	47.08	-1.19	16.93
N0E5	97.23	-4.00	337.51
N0E10	95.44	-4.44	327.71
N5E10	78.72	-3.85	328.21
N10E10	62.42	-3.25	320.22
N10W5	81.91	-3.03	5.91
N5W5	95.27	-3.96	359.55
W5bank edge	114.06	-4.09	355.30
W10N20	75.67	-1.60	32.74

Table B.1: Continued

Point ID	Distance ft.	Elev. Diff ft.	Relative Decimal Azim.
W10N15	83.38	-1.52	22.31
W10N10	93.65	-2.76	13.70
W10N5	105.29	-3.74	7.11
W10 bank	118.35	-3.89	2.99
edge			
Datum C of	74.14	-0.64	19.04
Art 1980			
fence 1	142.28	-5.77	308.29
fence 2	118.41	-4.83	299.29
fence 3	95.35	-3.41	283.06
fence 4	87.08	-1.95	265.69

B.3.2 Tranquility Farm (Site 44.12a)

Table B.2: Tranquility Farm (Site 44.12a) total station survey data.

Point ID	Distance ft.	Elev. Diff ft.	Relative Decimal Azim.
BS-1	—	—	—
N140W100	80.52	-3.02	18.04
N140W90	49.47	-0.70	28.34
N135W90	45.32	-2.04	9.31
N130W90	46.57	-3.80	348.83
N125W90	53.38	-4.69	330.57
N120W90	62.84	-4.95	317.12

Table B.2: Continued

Point ID	Distance ft.	Elev. Diff ft.	Relative Decimal Azim.
N115W90	74.57	-6.28	308.72
N110W90	89.29	-7.20	302.83
N105W90	103.95	-7.91	298.24
N100W90	118.64	-8.96	294.60
N95W85	130.32	-10.02	284.65
N105W85	97.95	-7.50	289.74
N115W85	66.80	-5.00	296.71
N120W85	52.26	-4.62	304.31
N125W85	40.60	-4.20	317.67
N130W85	30.78	-2.75	341.35
N130W80	16.57	-1.82	320.13
N125W80	31.72	-3.67	295.52
N120W80	46.31	-4.40	286.47
N115W80	62.00	-4.44	282.79
N110W80	78.54	-5.25	281.52
N105W80	94.60	-6.71	280.17
N100W80	111.83	-7.69	278.84
N95W80	127.74	-9.27	277.53
N95W75	127.28	-7.56	270.21
N100W75	110.57	-6.11	270.51
N105W75	93.71	-5.13	270.28
N110W75	77.50	-4.21	269.53
N115W75	61.36	-4.06	267.54
N120W75	45.52	-3.70	265.89

Table B.2: Continued

Point ID	Distance ft.	Elev. Diff ft.	Relative Decimal Azim.
N125W75	29.69	-2.60	264.84
N125W70	36.34	-2.07	238.57
N120W70	50.17	-2.76	246.83
N115W70	64.89	-3.21	253.05
N105W70	96.19	-4.18	260.38
N100W70	112.49	-4.92	261.90
N95W70	128.68	-5.64	262.94
N100W65	115.93	-3.52	254.06
N105W65	101.03	-3.20	251.21
N110W65	86.02	-2.82	247.09
N115W65	71.68	-2.20	240.40
N105W60	108.39	-2.12	243.41
N100W60	122.35	-2.43	246.95
N100W55	130.09	-0.90	240.47
N100W50	139.70	-0.72	234.82
N125W95	67.81	-5.09	338.13
N115W95	85.54	-7.00	317.42
N100W95	125.76	-10.41	301.60
N95W95	140.01	-11.80	297.97
N92W95	149.24	-12.58	297.14
N135W100	78.23	-4.48	6.40
N130W100	78.81	-5.37	354.57
N125W100	82.63	-6.68	343.20
N120W100	88.56	-7.27	332.98

Table B.2: Continued

Point ID	Distance ft.	Elev. Diff ft.	Relative Decimal Azim.
N115W100	97.88	-7.71	324.56
N110W100	109.47	-8.95	317.96
N105W100	121.77	-10.48	312.65
N100W100	134.25	-11.26	307.83
N105W103	127.61	-10.90	316.01
N105W105	132.03	-11.13	318.07
N115W105	111.36	-8.93	330.14
N120W105	103.53	-8.20	337.89
N125W105	98.33	-8.12	346.75
N120W110	118.29	-9.77	340.96
N115W110	125.65	-10.81	333.93
N105W110	143.97	-12.39	322.82
N115W115	140.11	-11.99	337.16
N120W115	134.01	-11.63	343.53
N120W120	149.08	-12.28	345.53
N115W120	155.01	-12.87	339.88
N110W120	162.40	-13.59	334.48
N110W125	176.89	-14.86	336.97
N115W125	170.42	-13.85	341.91
to BS-2	236.29	-1.28	36.06
JDatum	149.4	-12.48	297.27
N92W95			
N105W5	111.65	-8.5	306.01
N110W95	98.6	-7.5	311.15

Table B.2: Continued

Point ID	Distance ft.	Elev. Diff ft.	Relative Decimal Azim.
N120W95	75.4	-6.1	326.75
N130W95	61.8	-4.3	351.86
N140W95	64.2	-1.9	22.07
1	218.7	-18.3	352.44
2	224.5	-18.7	350.15
3	230.4	-19.9	348.09
4	226.1	-19.3	346.52
5	216.9	-17.9	345.67
6	209	-17.8	344.12
7	202.6	-17.7	342.48
8	196.9	-17.8	341.04
9	190.2	-16.7	339.14
10	174.7	-14.7	335.21
11	167.9	-14.5	330.71
12	160.5	-13.8	326.60
13	146.9	-12.1	319.01
14	141	-11.6	308.41
15	147.9	-12.2	302.80
16	153.2	-12.9	299.34
17	154.5	-12.7	296.56
N110W70	80.2	-3.87	257.83
N110W75	77.7	-4.2	269.54
N110W80	78.2	-5.2	281.55
N110W85	82.1	-6.44	292.87

Table B.2: Continued

Point ID	Distance ft.	Elev. Diff ft.	Relative Decimal Azim.
N110W90	89.2	-7.19	302.91
N110W95	98.7	-7.55	311.14
N110W100	109.6	-8.91	312.85
N110W105	121.9	-10.35	323.35
N110W110	134.8	-11.52	327.79
N110W115	148.2	-12.31	331.44
N110W120	162.5	-13.52	334.45
N110W125	176.8	-14.67	336.92
N103W95	117.3	-9.6	304.39
N104W95	114.7	-9.55	305.19
N105W95	111.8	-8.65	306.14
N106W95	109.2	-8.18	307.03
N107W95	106.4	-7.73	307.99
N120W95	75.24	-6.09	326.67
N121W95	73.6	-5.78	328.59
N122W95	71.7	-5.36	330.79
N123W95	69.9	-5.19	333.15
N124W95	68.4	-5.17	335.52
N125W95	67.35	-4.98	338.00
N126W95	66.02	-5.12	340.64
N127W95	64.8	-4.98	343.38
N128W95	63.69	-4.87	346.17
N129W95	62.87	-4.71	348.86
N130W95	61.86	-4.35	351.86

Table B.2: Continued

Point ID	Distance ft.	Elev. Diff ft.	Relative Decimal Azim.
backsight to	236.28	1.64	328.41
BS-1			
N40W50	130.92	-0.48	331.13
N30W15	113.95	-3.76	321.99
N30W20	98.85	-2.65	318.50
N30W25	84.39	-1.48	313.42
N25W25	76.76	-2.83	323.83
N25W20	92.22	-4.12	327.44
N25W15	108.18	-5.10	329.91
N20W15	104.67	-6.17	338.68
N20W20	88.28	-5.34	337.62
N20W25	72.14	-3.93	336.06
N15W25	71.06	-6.21	349.14
N15W20	87.39	-6.78	348.45
N15W15	103.78	-7.56	347.80
N15W10	119.86	-7.94	347.50
N10W0	153.83	-12.36	353.00
N10W5	137.89	-11.79	353.88
N10W10	121.68	-10.76	355.23
N10W15	105.58	-9.78	356.67
N10W20	89.6	-8.06	358.87
N10W25	73.72	-7.1	1.95
N10W30	58.12	-6.82	6.74
N10W35	43.19	-5.71	14.56

Table B.2: Continued

Point ID	Distance ft.	Elev. Diff ft.	Relative Decimal Azim.
N5W35	52.82	-7.65	29.83
N5W30	66.26	-8.36	19.69
N5W25	80.19	-8.94	13.09
N5W20	94.92	-10.3	8.31
N5W15	110.12	-11.65	5.00
N5W10	125.5	-12.99	2.45
N5W5	141.55	-14.39	0.40
N5W0	157.31	-15.4	358.83
N0W0	162.05	-16.17	4.38
N0W5	146.8	-15.92	6.55
N0W10	131.71	-15.51	9.23
N0W15	117	-13.99	12.49
N0W20	102.62	-11.94	16.67
N0W25	89.25	-11.24	22.35
N0W30	76.91	-10.31	29.85
N0W35	66.34	-9.79	39.80
1 top	176.82	-11.85	349.74
2 top	185.68	-12.16	351.15
3 top	195.88	-12.57	352.35
4 top	204.28	-13.66	354.27
5 bottom	200.74	-16.32	358.08
6 bottom	191.63	-16	356.88
7 bottom	178.86	-16.16	355.44
8 bottom	169.53	-15.36	354.13

Table B.2: Continued

Point ID	Distance ft.	Elev. Diff ft.	Relative Decimal Azim.
1	198.97	-15.97	0.63
2	193.59	-16.15	4.36
3	189.65	-17.18	9.39
4	177.08	-16.81	8.81
5	161.59	-16.6	8.03
6	146.31	-16.24	8.38
7	135.77	-15.72	8.80
8	121.27	-14.83	13.02
9	113.29	-13.71	15.52
10	105.55	-12.42	18.91
11	98.31	-12.22	23.82
12	40.68	-12.25	29.58
13	83.15	-11.6	34.83
14	67.93	-10.07	42.17

Appendix C

GPR PROFILE COLLECTION AND DATA PROCESSING INFORMATION

C.1 GPR Grid/Profile Construction

C.1.1 University of New England (Site 5.06)

Four batch 3D files are included in super 3D Radan file UNE_S3D_080917. Each batch 3D file was unique with respect to grid dimensions and the x- and y-direction origin locations. Refer to D.1 for a map of all UNE survey profile locations.

The batch file UNE_MAINGRID_080917 had an x- and y- direction origin in the lower left corner of the grid which was 14 x 8 meters. This grid contains profiles 5-18, and 26-32.

Radan batch file UNE_SMGRID1 has an x-direction origin in the lower left corner and y-direction origin in the upper left corner. Grid dimensions are 5 x 4 meters, and the batch file contains profiles 33-42.

File UNE_SMGRID2 contains an area of relatively short profiles where surrounding dense vegetation resulted in limited collection. The x- and y-direction origin was assigned to the lower left corner. Profiles 43-51 are contained within the batch 3D file.

Exploratory profiles 52 and 53 were collected to gain further detail in an area adjacent to the proposed excavation. Profile 52 (reversed from the collected direction shown in Figure D.1) was combined with profile 53 in 3D batch file UNE_NEWEXT. The x- and y-direction origin for the grid file is in the lower left corner and the grid dimensions are 7 x 7 meters.

Constructing the super 3D file required attention to detail with respect to the origin of each batch 3D file. The ideal origin for Radan is the lower left corner, and this is particularly critical to remember with 3D grid assembly. Origins used for UNE_NEWEXT, UNE_MAINGRID_080917, UNE_SMGRID1, and UNE_SMGRID2 were (6,-0.6), (0,6), (14,8), and (14,12) respectively. The super 3D file is labeled UNE_S3D_080917.

Each file within the UNE supergrid was processed with the same parameters. A time zero correction was applied as well as an FIR high and low pass filter of 350 and 550 MHz. A dielectric constant of 24.97 was by hyperbolae matching. GPR profiles were not topographically corrected as the area was relatively flat, and software limitations prevented topographic correction of the entire supergrid.

C.1.2 Long Island North (Site 15.95)

The 500 MHz 1 meter orthogonal grid survey at the Long Island North site took place on 7/16/2017. See Figure D.2 for the 500 MHz GPR survey map and Figure D.3 for a map of the survey overlain on Dick Doyle's excavations. A 20 m x 10 m grid and a 10 x 10 m grid were collected adjacent to one another. Each grid survey strategy involved a 1 m perpendicular profile spacing. Exploratory profiles 60-63 were collected in an area with a potential seep, but the irregular layout prevented their incorporation within the Radan super 3D grid. Locations of profiles 60 to 63 are approximate with the exception of the start location of profile 60 and the end location of profile 63 (Figures D.3 and D.2).

Two batch 3D files were constructed within Radan. Filenames LIN_grid1 and LIN_grid2 correspond with the 10 m x 20 m grid and the 10 m by 10 m grids respectively. Grids were set-up so that the x-direction corresponded with D. Doyle's baseline. The origin of each grid is the southeast corner. Partial profiles within LIN_grid2 were the result of obstructions on the northern side of the surveyed area.

The two 3D batch files were combined within the super 3D file LINSUPER3D. Origin points used for the two files LIN_grid1 and LIN_grid2 were (0,0) and (20,0) respectively.

C.1.3 Damariscotta Oyster Farm (Site 26.15)

The overall survey carried out on August 16, 2016 at the Damariscotta Oyster Farm site is depicted in Figure 4.8. Grass and thick milkweed stalks (diameter: 3mm) up to 2 m tall covered the site, excluding 2 m wide mowed swaths for walking paths. The geometry of the long profiles is directly related to walking path location. The vegetation limited detailed 500 MHz GPR survey at site 26.15, but the data collected cover every area possible for the GPR to navigate at the time of collection.

A map of the detailed 0.5 m 500 MHz GPR survey grid at site 26.15 is shown in Figure D.4. Data were collected on 8/16/2016 with a crew of Alice Kelley, Arthur Spiess, and Jacque Miller. A 3D batch file was sufficient for the DAM site as there was only one grid, and the final Radan file is titled

DAM_3DBATCH_T1_TZ_FIRLP550HP350_MIG_RG_LAYERDENSE.

Profiles included within the grid were collected from south to north and east to west. Extensive detailed GPR survey was not possible, but a 10 X 10 meter area was cleared by hand. Though the area was cleared extremely well, milkweed stalks often prevented necessary ground coupling with the antennae.

Exploratory long profiles were collected on the mowed walking paths. An intuitive visual representation of the long profiles collected at site 26.15 involved reversing select profiles and appending them to form a single file within Radan. Reversing the profile applied to the east-west lines only. The origin of each east west profile became the west corner. The origin on the profiles running south to north is the southernmost point.

Long profile 1 runs parallel to the tidal creek. This transect began at the point of site 26.15 and runs to the north. The profile is made up of profiles DAM_1, DAM_2, DAM_3, DAM_4, and DAM_5 appended in that order. The completed profile is represented by transect F to G in Figure 4.8.

GPR profiles included in long profile 2 (DAM_6, DAM_7, DAM_8, and DAM_9) were collected from east to west, starting at the tip of the point. These files were individually flipped and saved as copies DAM_reversed prior to the construction of long profile 2. The reversed lines allowed long profile 2 to run from west to east. This appended profile intersects a testpit (TP A) dug in 1996 by Art Spiess. The northeast corner of TP A is approximately 4.6 m from the end of DAM_6. The completed profile is represented by transect D to F in Figure 4.8.

Long profile 3 runs south to north and includes profiles DAM_10, DAM_11, DAM_12, and DAM_13. Each profile was collected south to north, and did not require flipping in Radan. The long profile begins where DAM_10 begins. The completed profile is represented by transect F to G in Figure 4.8. The completed profile is represented by transect D to E in Figure 4.8.

Long profile 4 is similar to long profile 2 in that it is constructed of reversed files and is shown starting in the west and running east. Long profile 4 contains DAM_15, DAM_16, DAM_17, and DAM_18. Lines were collected from east to west, but were flipped in Radan and saved with the extension "_reversed". The completed profile is represented by transect A to C in Figure 4.8, which runs from the west to east.

Long profile 5 contains runs south to north and includes DAM_19, DAM_20, DAM_21, and DAM_22. Each profile was collected south to north, and did not require flipping in Radan. The long profile begins where DAM_19 begins. The completed profile is represented by transect A to B in Figure 4.8.

C.1.4 Olson (Site 17.13)

The Olson Site required a number of batch 3D files as the site was one of the largest within the study. The GPR maps found in Appendix C provided a means of displaying the profile numbers included within each 3D batch file as well as their assigned coordinates within the super 3D grid. Profile numbers are highlighted in each map, and the notes on each indicate the batch 3D file to which they belong.

The eastern portion of the detailed 500 MHz GPR survey around the archaeological trench is represented by Figure D.6. Collection of the grid occurred on 8/10/2016. Profiles included in the 3D batch file G10lite are highlighted in yellow. Within the blue highlighted region are profiles included within G11lite. Profiles on the southern portion of grid are irregular because the bluff edge determined the length. The trench origin is (N0E0), it extends 2 m to the east (N0E2) and 18 m to the north. See E for ground-truth in the area in the form of trench profiles and photos (Figure E.10 through FigureE.37).

Files included in batch file G8lite are highlighted in green within Figure D.7. The grid represents the western portion of the detailed 500 MHz GPR survey in the area with robust ground-truth information. Grid collection took place on 8/10/2016. See E for ground-truth in the area in the form of trench profiles and photos (Figure E.10 through FigureE.37).

Highlighted in green in Figure D.8 are files included in 3D batch file G12. Notes taken during GPR profile collection indicate that profile 62 was shifted slightly off a straight transect at the end to avoid a stake in the path of survey. Additionally, a metal horse tether stake is likely present in the GPR record approximately 1.5 m from the start of profile 63. The GPR grid was collected on 8/11/2016.

Within the red highlighted area in Figure D.9 are GPR profiles included in batch 3D file G9. The GPR grid was collected on 8/11/2016, except profile 41,

which was collected on 8/10/16. A boulder was in the path of profile 91, and a rock in profile 99. Light rain was falling during the collection of this grid.

Yellow highlighted areas in Figure D.10 outline profiles included in G15. The grid is bordered by a fence on the east side. All but two profiles within the grid were collected on 8/11/2016. A note was written in the field about a potential area of disturbance in the GRR record, approximately two meters from the end of profile 111.

Figure D.11 contains profiles included in batch 3D files G13 (blue highlight) and G14 (red highlight). Profiles at the southern end of the grid are irregular because the bluff edge controlled the length. Profiles within the range 62-199 were collected on 8/11/2016.

Highlighted in green within Figure D.12 are profiles included in 3D batch file G18. All GPR data within the grid were collected on 8/11/2016. Nothing of note occurred during the 500 MHz GPR survey of the area.

Figure D.13 includes batch file G16 (highlighted in green) and G17 (highlighted in yellow). The layout of the surveyed area appears as a partial grid because bushes on the east side obstructed intended transects. Profiles highlighted in green (G16) extended to the bluff edge. Unlabeled lines without arrows were placed within the figure for consistency. The grid represents the last of the data collected on 8/11/2016.

Figure D.14 contains profiles collected on 8/12/2016. Four grids: G1 (yellow), G5 (purple), G4 (green), and G6 (red) illustrate the grouping of profiles into respective 3D batch files. The figure also shows a partial view of the super 3D grid layout with coordinates labeling the vertical and horizontal axes. The profiles within the figure that are not highlighted exist within other grids or are replaced by other profiles. For example, profile 200 was replaced by profile 94 in G9 (Figure

D.9). Profile 252 is included in G7 (Figure D.15), and profile 253 is found in G2 (Figure D.16).

Figure D.15 includes all 500 MHz GPR profiles included in 3D batch file G7. The southern portion of the grid is irregular as it was the bluff edge. Field notes indicate an error occurred during the collection of profile 209. Also, file 215 was collected as a continuous profile. Data included within the grid were collected on 8/12/2016.

Figure D.16 contains 3D batch files G2 and G3 which are designated by blue and green respectively. The southern portion of the grid, included in G3, extended to the bluff edge. Field notes indicate that profile 245 was hung-up on the grid rope at the start. Files within G2 and G3 were collected on 8/12/2016.

Each file within the Olson supergrid was processed with the same parameters. A time zero correction was applied as well as an FIR high and low pass filter of 350 and 550 MHz. A dielectric constant of 61.42 was applied during the migration to force depth agreement between archaeological profiles and interpreted GPR profiles. GPR profiles were topographically corrected for comparison figures, but software limitations prevented topographic correction of the entire supergrid.

C.1.5 Fernald Point (Site 43.24)

The Fernald Point 500 MHz GPR survey took place from 6/21/2017 to 6/23/2017. An overview map for the 5 m 500 MHz GPR survey is depicted in Figure D.17. Figure D.18 shows the 500 MHz GPR survey overlain on D. Sanger's Excavations from 1977. The area was RTK surveyed by Karen Anderson of Acadia National Park prior to the start of GPR work. Karen's survey allowed precise grid corner location data capture at 10 m intervals over the 60 m x 60 m survey area (Figure B.2). Grid locations are last three letters/numbers of the title for each point

in Figure B.2. An example of the grid label format is seen in the detailed grid maps for the survey (Figures D.19 and D.20).

The main survey at the Fernald Point site followed a 5 m perpendicular grid set-up (Figure D.17). Detailed GPR work involved the collection of a 1 meter perpendicular grid as well as a 0.25 m parallel, unidirectional grid over the same 10 m x 10 m area (Figures D.19 and D.20). Nine batch 3D files were individually constructed as 20 m x 20 m grids with x- and y-direction origins in the lower left corner.

Batch 3D files FRN_GRID10 and FRN_GRID11 required unique construction as they contain profiles 95 through 110 that extended to the bluff edge. Radan file FRN_GRID10 contains the eastern group of profiles, and has an x- and y-direction origin in the lower left corner. The x-direction extent was determined by the longest profile, and the y-direction extent was determined by the total number of regularly-spaced profiles. The 3D batch file FRN_GRID11 contains the southern portion of profiles shortened due to the site geometry. The origin of FRN_GRID11 was (0,-8) because the longest line running in the y-direction determined the height. The length of the file was determined by the number of regularly-spaced profiles in the y-direction.

A total of 11 batch 3D files comprise the super 3D grid created for the Fernald Point site. The super 3D grid file FRNSUPER3D contains 3D batch files labeled FRN_GRID1 through FRN_GRID11. Detailed survey grids FRN0_25M (0.25 m parallel grid) and FRN0_5M (1 m perpendicular grid) were not included within the super 3D grid file as there were two surveys collected over the same area.

C.1.6 Tranquility Farm (Site 44.12a)

The most efficient method to compiling the Tranquility Farm profiles required appending files within Radan. Two separate grids with a 5 m profile spacing, and

one 10 x 10 m grid collected with a 0.5 m spacing represent the GPR survey at site 44.12a. The Radan file TRQ_G1TEST1 (Figure D.22) represents the eastern portion of the site, and it follows the established archaeological grid from previous excavation. Radan file TRQ_G2TEST2 (Figure D.24) includes the western portion of the survey, but the grid is offset from the established archaeological grid on the eastern portion of the site. The angle of offset prevented the meshing together of the 3D batch files within a super 3D grid in Radan. In addition to two 5 m resolution grids, a grid represented by Radan file TRQ_DETAILED_HM1 (Figure D.23) was collected with a 0.5 m spacing in the eastern portion of the site. The finer resolution provided detail in an area with dense stratigraphic data.

The "Assemble 3D Batch" option in Radan was used as a first step in compiling each grid file for the Tranquility Farm survey. Additionally, a super 3D file was utilized to place the detailed 0.5 m grid in the proper location within TRQ_G1TEST1. Radan forces an origin in the x- and y-direction from the lower left corner in a super 3D file. Dimensions of the super grid file TRQ_G1_HM1_S3DTEST2 were 75 m in the x-direction and 60 m in the y-direction. The origin of file TRQ_DETAILED_HM1 was (15, 20). Assigning the origin point for the file was simple because the dimensions of the batch 3D file TRQ_DETAILED_HM1 were 10 x 10 m.

Radan file TRQ_G1TEST1 has an x- and y-direction origin in the upper left corner. Appended profiles included within the grid are TRQ_ 105_106, 103_104, 99to102, 95to98, 88to91, 92to93, 1to6, and 57to61. Additionally, the batch 3D file contains profiles 76 and 107.

Radan file TRQ_DETAILED_HM1 has an x- and y-direction origin in the upper right corner. This grid was collected at 0.5 m resolution because known excavations were located nearby, and the grid area was moderately undisturbed. A majority of the profiles are not 10 m long because the grid bordered a steep face

that is likely related to a trench dug by W.K. Moorehead. See Figure D.23 for a map of profile locations.

Batch 3D file TRQ_G2TEST2 has an x- and y-direction origin in the upper left corner. This batch 3D file contains appended profiles TRQ_ 140_141, 136to139, 132to135, 128to131, 108to111, 112to114, 115to118, and 122to123. See Figure D.24 for a map of profile locations.

Appended files included in any version of TRQ_G1_HM1_S3DTEST2 were assigned names by Radan with "Profile" and the numeric position in the file order. The name associated with the raw GPR file is typically placed at the end of the Radan project filename. Table C.1 below contains the profile names assigned by Radan (excluding the long filename that results after processing), and the GPR files associated with each.

Each file within the respective Tranquility Farm grids were processed with the same parameters. A time zero correction was applied as well as an FIR high and low pass filter of 350 and 550 MHz. A dielectric constant of 64.41 was applied at a depth of 13.48 nanoseconds (within midden material) during the migration to force depth agreement between archaeological profiles and interpreted GPR profiles. Limitations within the processing software (Radan Beta7) prevented topographic correction of the entire supergrid.

Table C.1: Tranquility Farm (Site 44.12a) 500 MHz 5 meter GPR survey Radan profile names.

Radan Filename	Associated Profiles
Profile 2	105, 106
Profile 3	103, 104
Profile 4	99-102
Profile 5	95-98
Profile 6	88-91
Profile 7	92, 93
Profile 8	1-6
Profile 9	84-87
Profile 11	81-83
Profile 12	77-79
Profile 14	57-61
Profile 15	62-66
Profile 16	67-69
Profile 17	70, 71
Profile 18	72-73
Profile 19	74, 75
Profile 20	7-12

C.2 Profile Location Data

Profile location information is provided for 3D batch files associated with complex GPR profile arrangements. Location information data were critical during the construction of 3D batch files. Along with the maps found in Appendix D, the information listed in the tables below will allow the user to create 3D batch files from individual GPR profiles.

Table C.2: Tranquility Farm (Site 44.12a) 500 MHz 5 meter GPR survey profile location data table 1. Data are associated with 3D batch file TRQ_G1TEST1 X-direction files.

Profile	X Start	X End	Y Start	Y End
107	25	35.14	60	60
APP105_106	25	45.09	55	55
APP103_104	25	45.40	50	50
APP99to102	20	55.47	45	45
APP95to98	15	55.65	40	40
APP88to91	0	41.22	35	35
APP92_93	45	65.24	35	35
APP1to6	0	64.19	30	30
APP84to87	25	65.45	25	25
80	25	35.19	20	20
APP81to83	45	75.40	20	20
APP77to79	30	59.22	15	15

Table C.3: Tranquility Farm (Site 44.12a) 500 MHz 5 meter GPR survey profile location data table 2. Data are associated with 3D batch file TRQ_G1TEST1 Y-direction files.

Profile	X Start	X End	Y Start	Y End
76	0	0	38	29.76
APP57to61	35	35	60	11.35
APP62to66	25	25	60	15.76
APP67_68_69	20	20	45	21.92
APP70_71	15	15	40	24.87
APP72_73	10	10	40	24.46
APP74_75	5	5	40	26.67
APP7to12	30	30	60	6.27

Table C.4: Tranquility Farm (Site 44.12a) 500 MHz 5 meter GPR survey profile location data table 3. Data are associated with 3D batch file TRQ_G2TEST2 X-direction files.

Profile	X Start	X End	Y Start	Y End
144	15	25.21	40	40
143	15	25.04	35	35
142	15	25.09	30	30
APP140_141	15	30.01	25	25
APP136to139	5	40.17	20	20
APP132to135	5	40.27	15	15
APP128to131	5	39.71	10	10

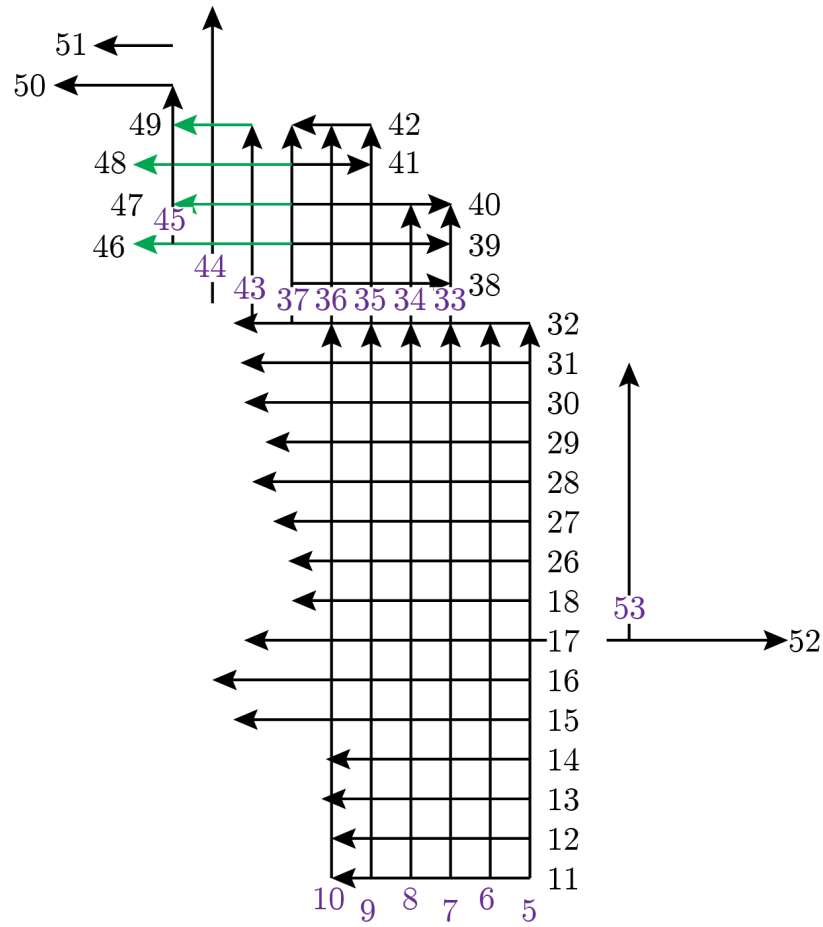
Table C.5: Tranquility Farm (Site 44.12a) 500 MHz 5 meter GPR survey profile location data table 4. Data are associated with 3D batch file TRQ_G2TEST2 Y-direction files.

Profile	X Start	X End	Y Start	Y End
127	5	5	20	9.85
126	10	10	20	10.26
APP108to111	15	15	40	7.44
APP112to114	20	20	40	11.03
APP115to118	25	25	50	11.45
120	30	30	20	10
121	35	35	20	10.05
APP122_123	40	40	20	6.41

Appendix D

GPR PROFILE LOCATION MAPS

D.1 University of New England (Site 5.06) 500 MHz GPR Map



Site: UNE
 Collected: 5/30/2017
 Crew: Jacque Miller,
 Alice Kelley, Arthur
 Anderson


Grid N

 5 meters

Figure D.1: University of New England (UNE Site 5.06) 1 meter 500 MHz GPR survey map.

D.2 Long Island North (Site 15.95) 500 MHz GPR Maps

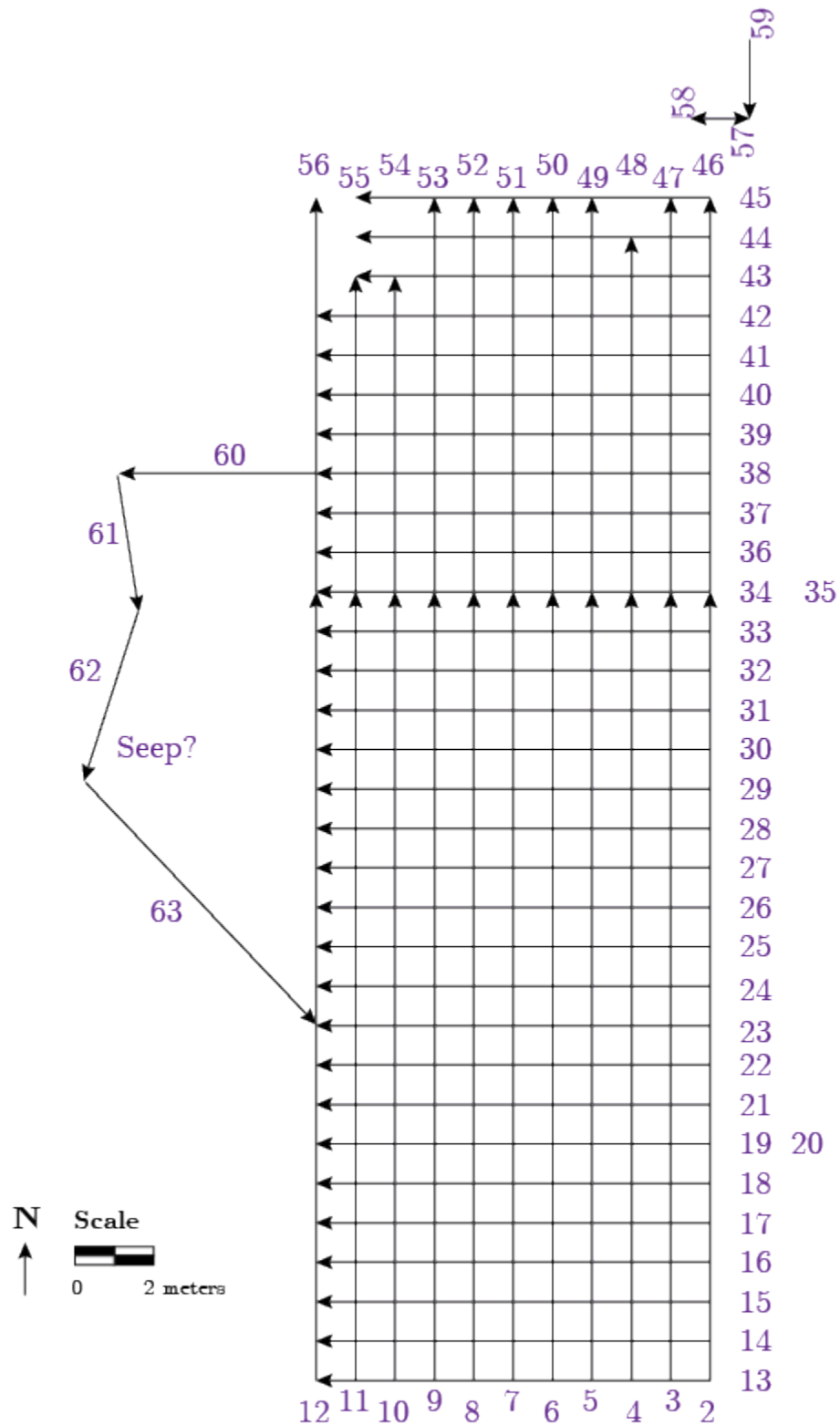


Figure D.2: Long Island North (Site 15.95) 1 meter 500 MHz GPR survey map. Note that profile 60-63 are not drawn to scale, and the transect locations are approximate. The start of profile 60 and the end of profile 63 are certain, and represented on the map.

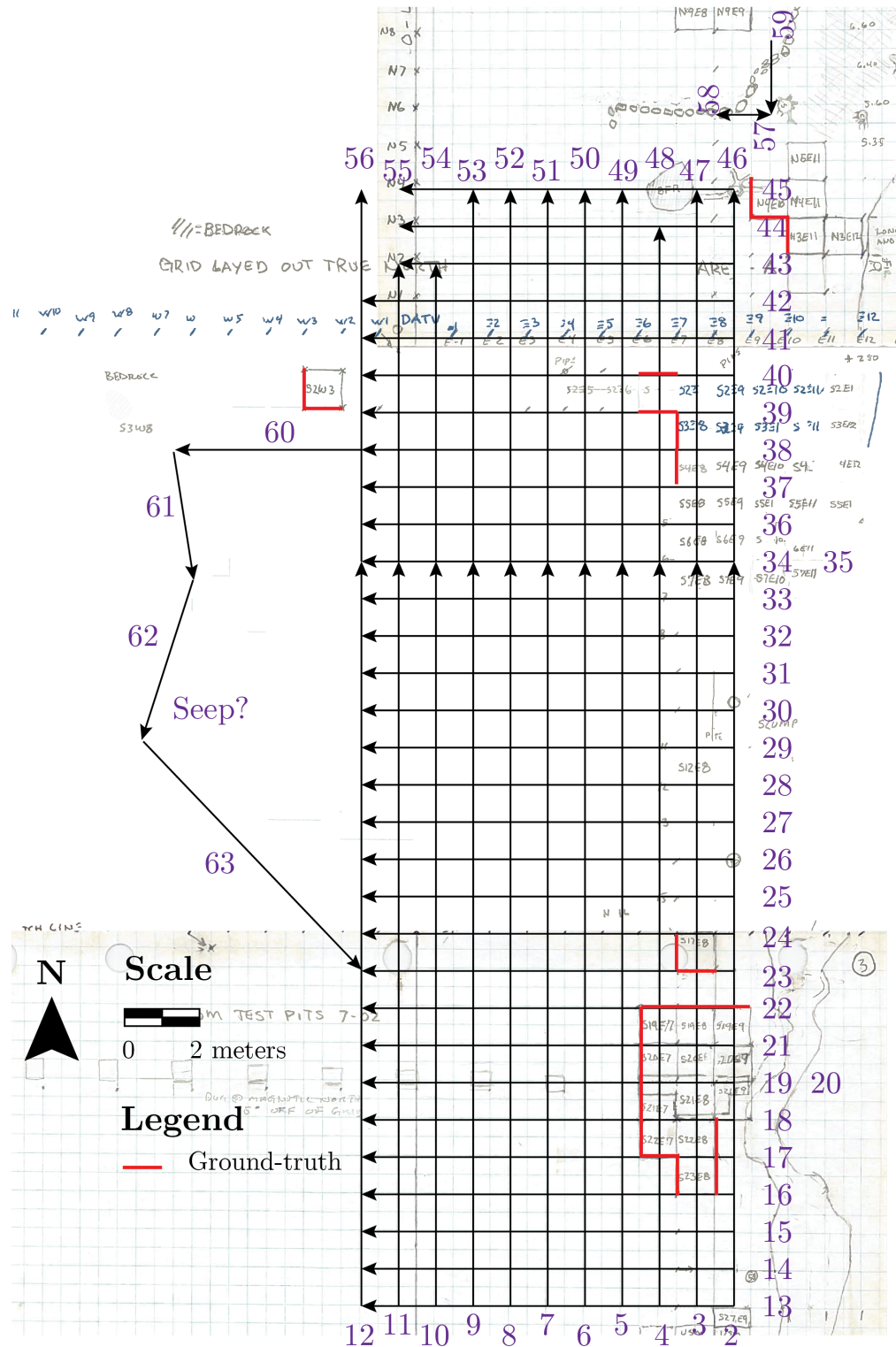


Figure D.3: Long Island North (Site 15.95) 1 meter 500 MHz GPR survey map overlain on Dick Doyle's archaeological excavation map. Basemap courtesy of and drawn by D. Doyle. Note that profile 60-63 are not drawn to scale, and the transect locations are approximate. The start of profile 60 and the end of profile 63 are certain, and represented on the map.

D.3 Damariscotta Oyster Farm (Site 26.15) 500 MHz GPR Maps

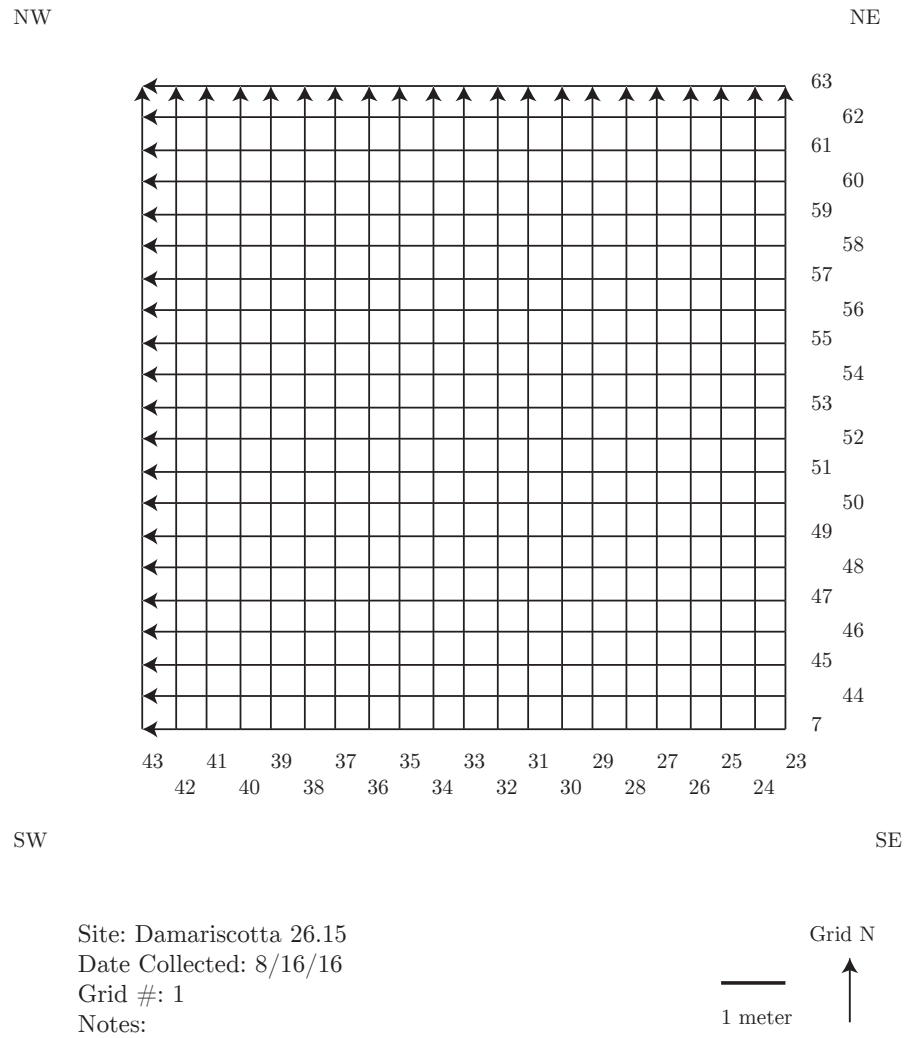


Figure D.4: Damariscotta (Site 26.15) 0.5 meter 500 MHz GPR detailed grid map.

D.4 Olson (Site 17.13) 500 MHz GPR maps

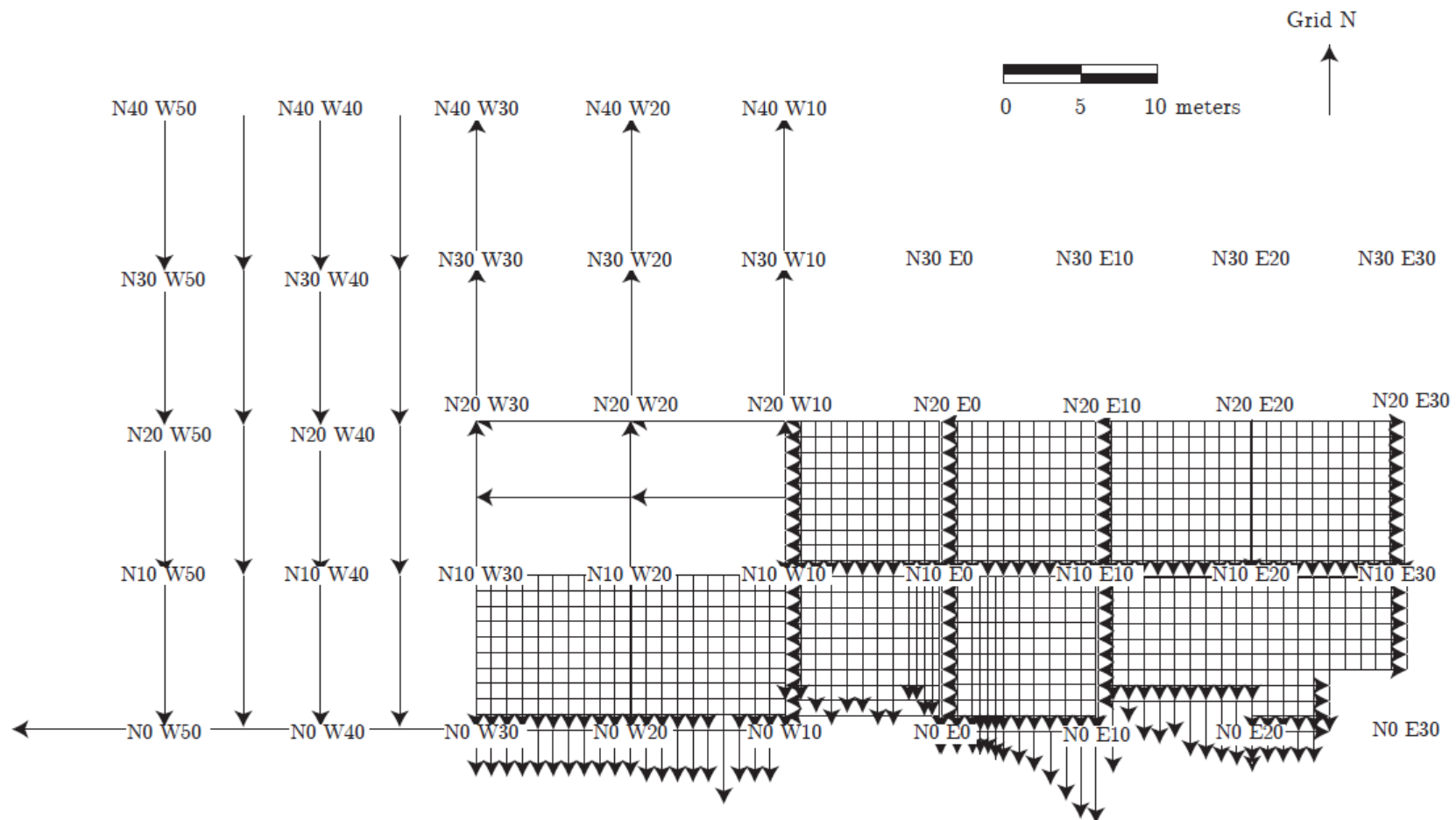


Figure D.5: Olson (Site 17.13) 500 MHz GPR survey overview map with grid corners.

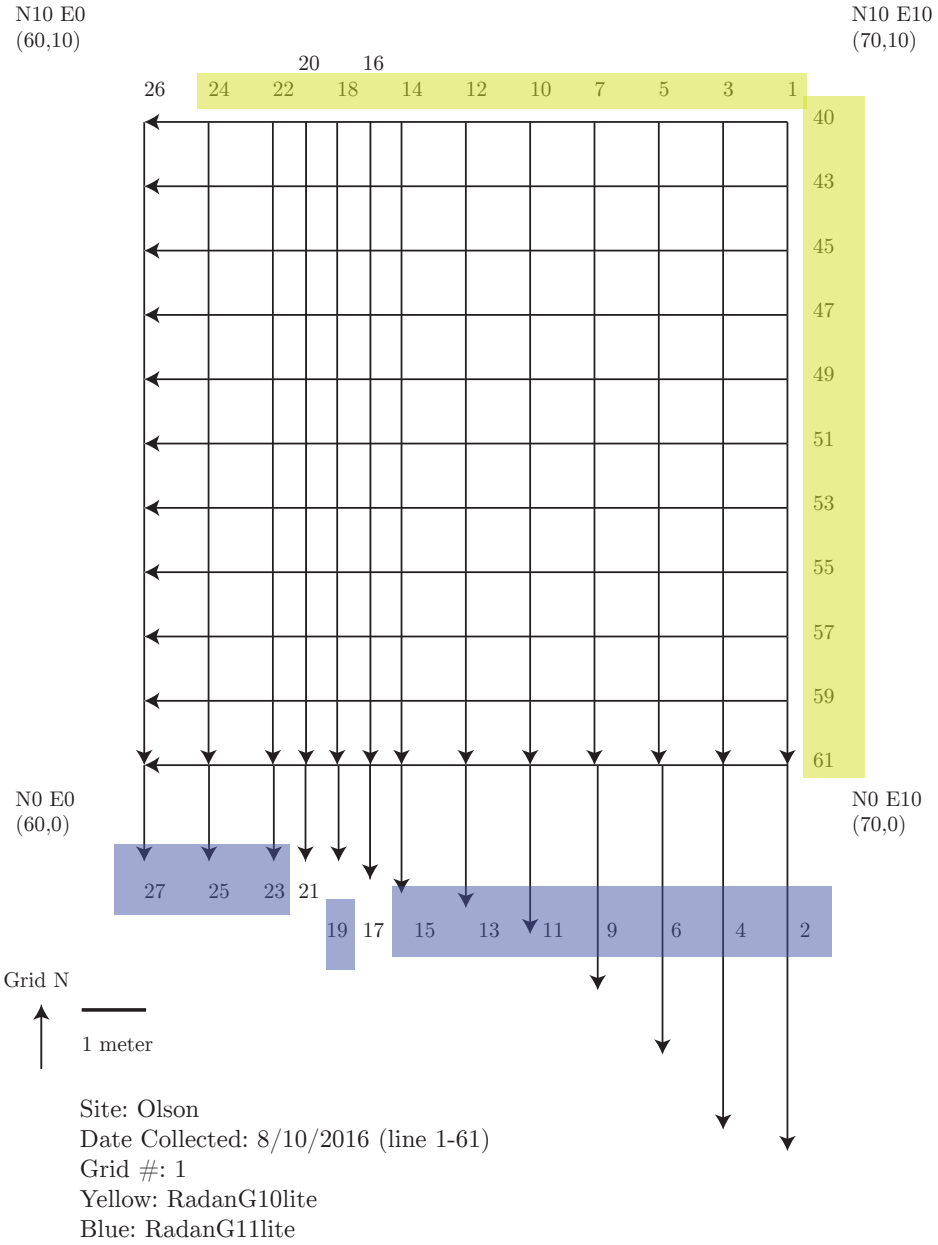


Figure D.6: Olson (Site 17.13) 1 and 0.5 meter 500 MHz GPR grid map 1.

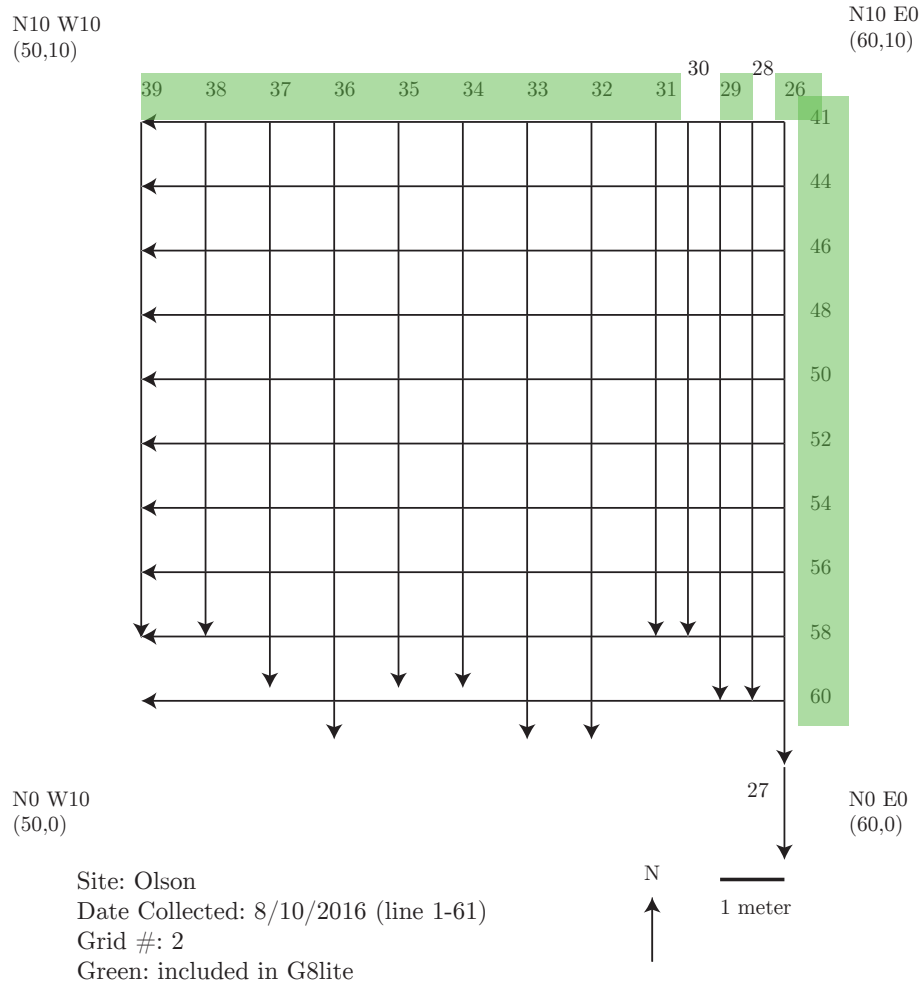


Figure D.7: Olson (Site 17.13) 1 meter 500 MHz GPR grid map 2.

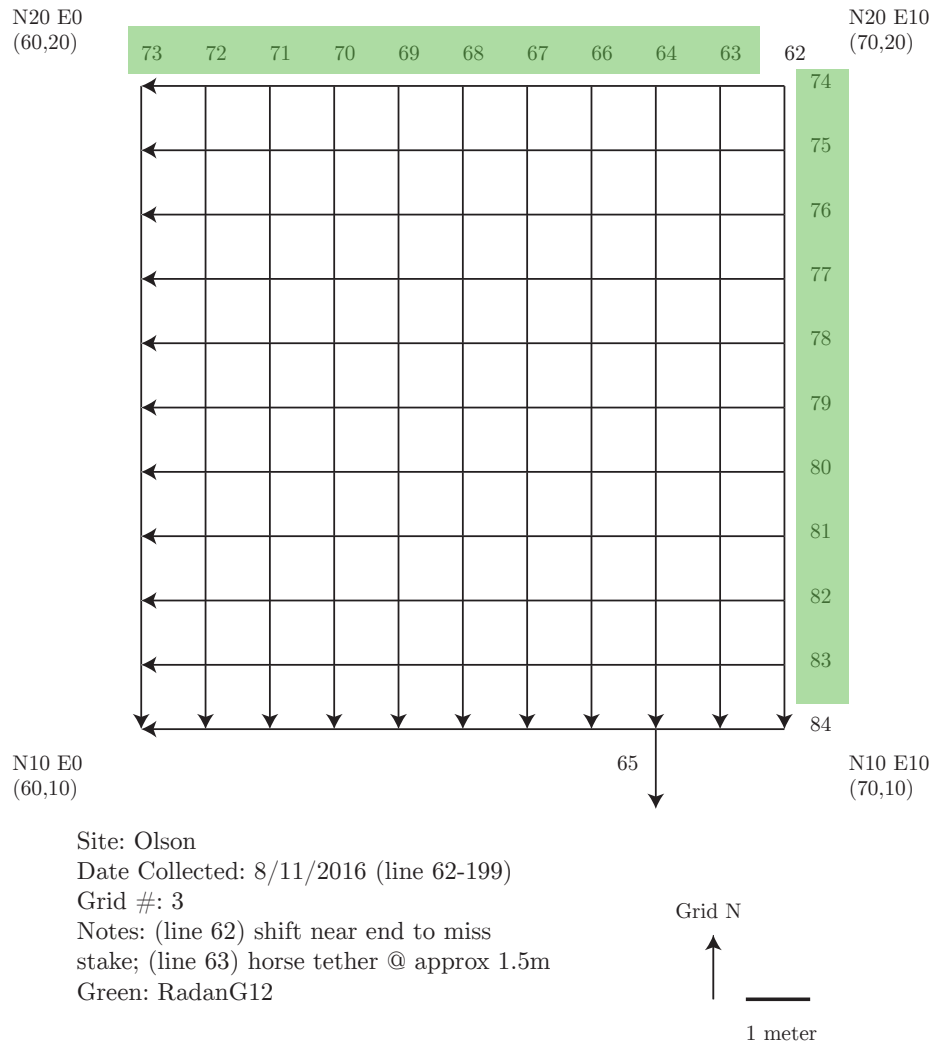


Figure D.8: Olson (Site 17.13) 1 meter 500 MHz GPR grid map 3.

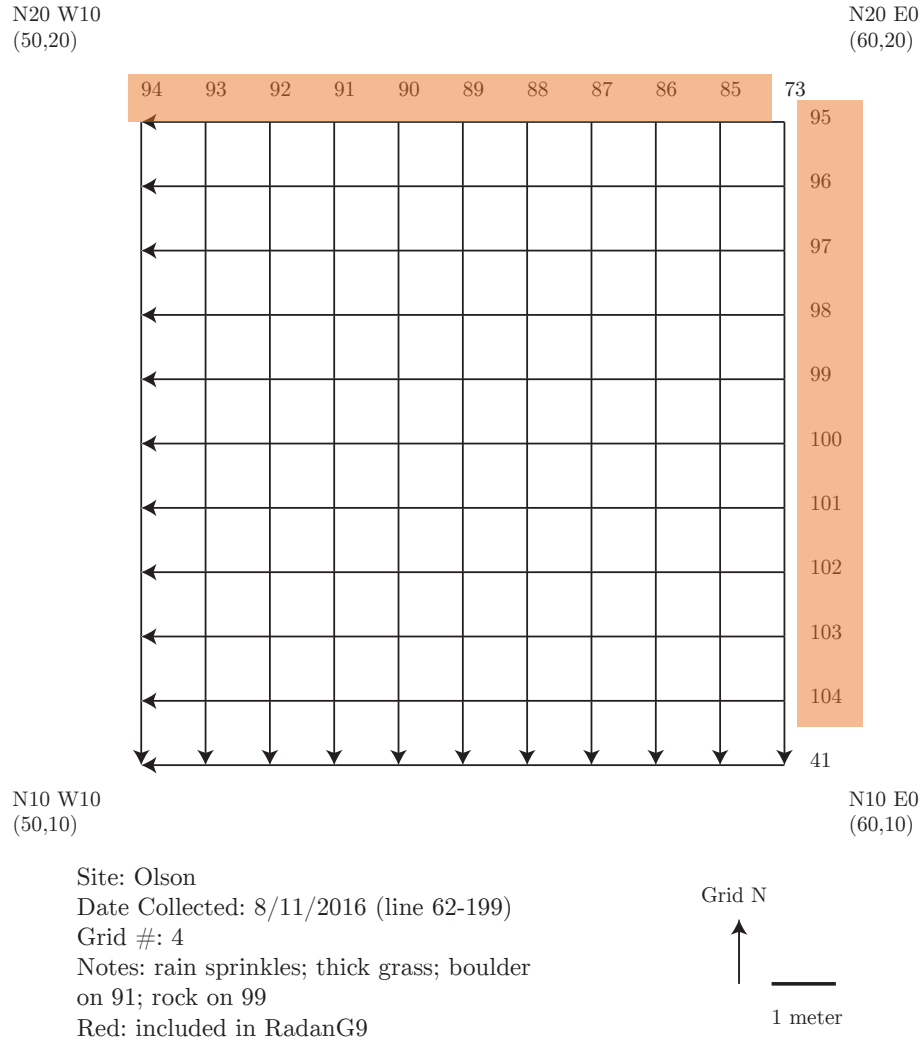
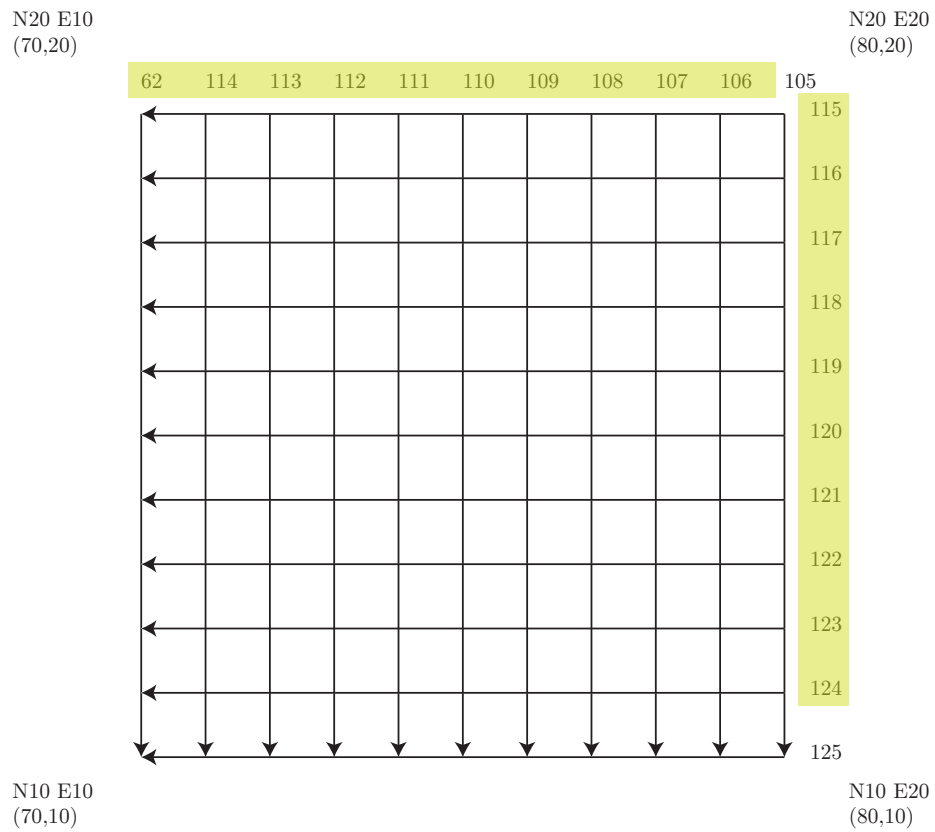


Figure D.9: Olson (Site 17.13) 1 meter 500 MHz GPR grid map 4.



Site: Olson
 Date Collected: 8/11/2016 (line 62-199)
 Grid #: 5
 Notes: (line 111) interesting @ 2m from
 end-- looters pit?; fence on east side
 Yellow: RadanG15

Grid N

 1 meter

Figure D.10: Olson (Site 17.13) 1 meter 500 MHz GPR grid map 5.

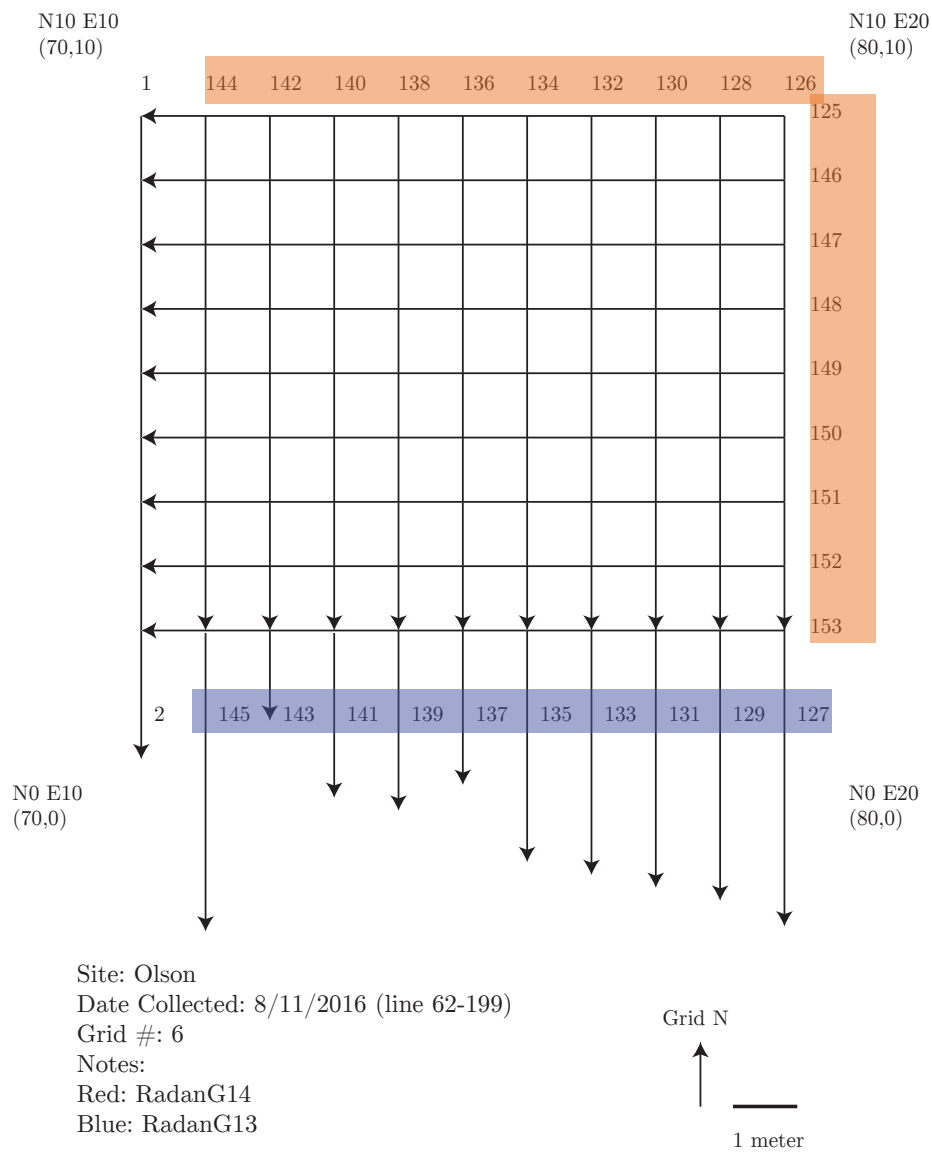


Figure D.11: Olson (Site 17.13) 1 meter 500 MHz GPR grid map 6.

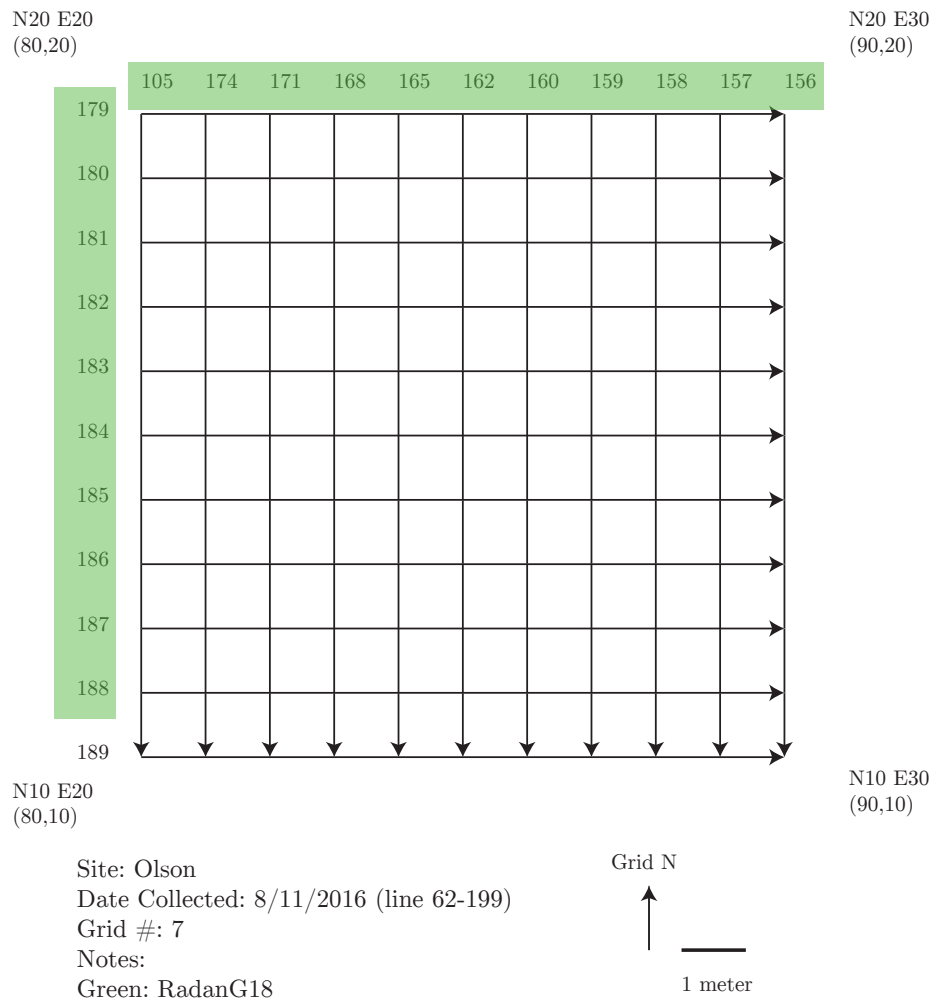


Figure D.12: Olson (Site 17.13) 1 meter 500 MHz GPR grid map 7.

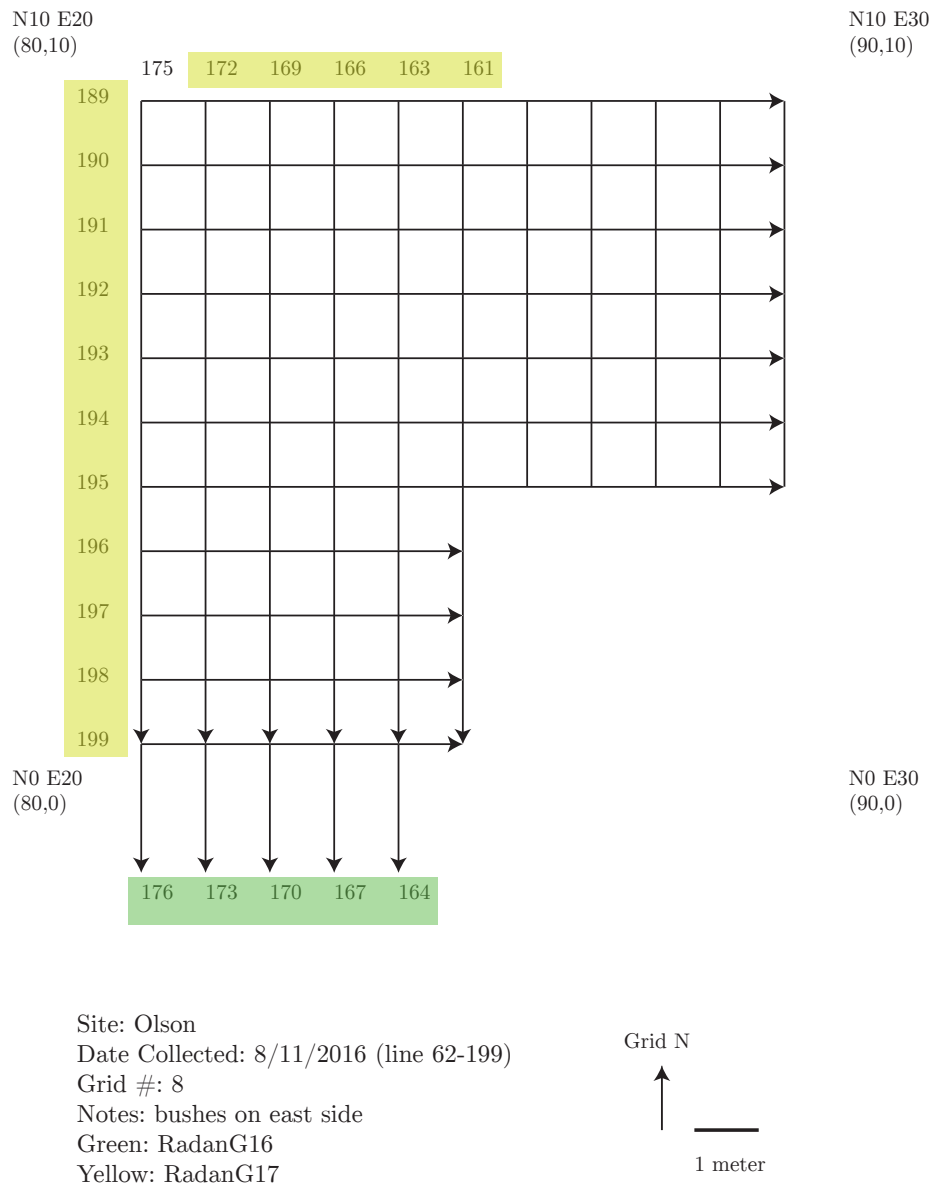
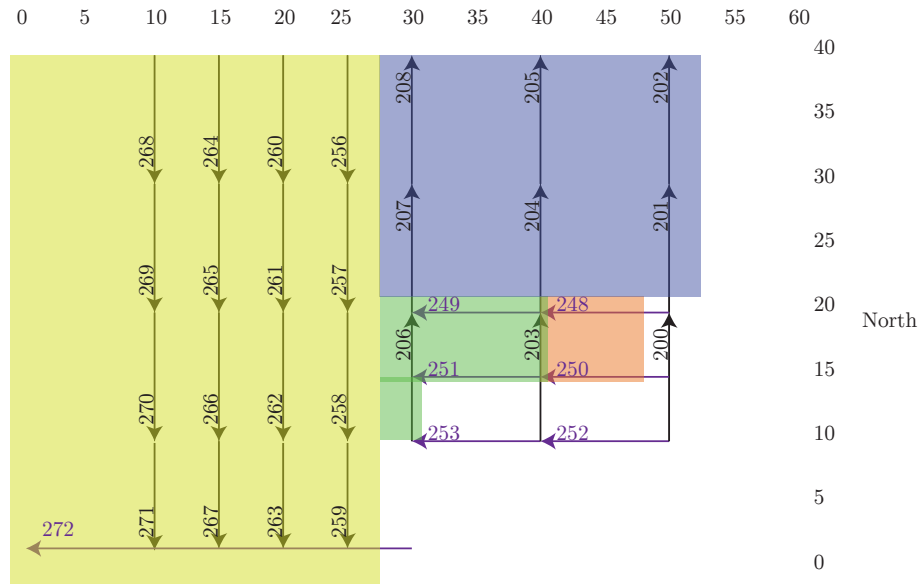


Figure D.13: Olson (Site 17.13) 1 meter 500 MHz GPR grid map 8.



Site: Olson
 Date Collected: 8/12/16 (line 200-272)
 Grid: 9, 12, 13
 Notes: (line 207) 11.8m long
 Yellow: RadanG1
 Purple: RadanG5
 Green: RadanG4
 Red: RadanG6

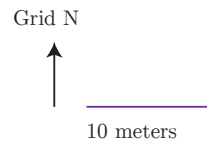


Figure D.14: Olson (Site 17.13) 5 and 10 meter 500 MHz GPR grid maps 9, 12, and 13.

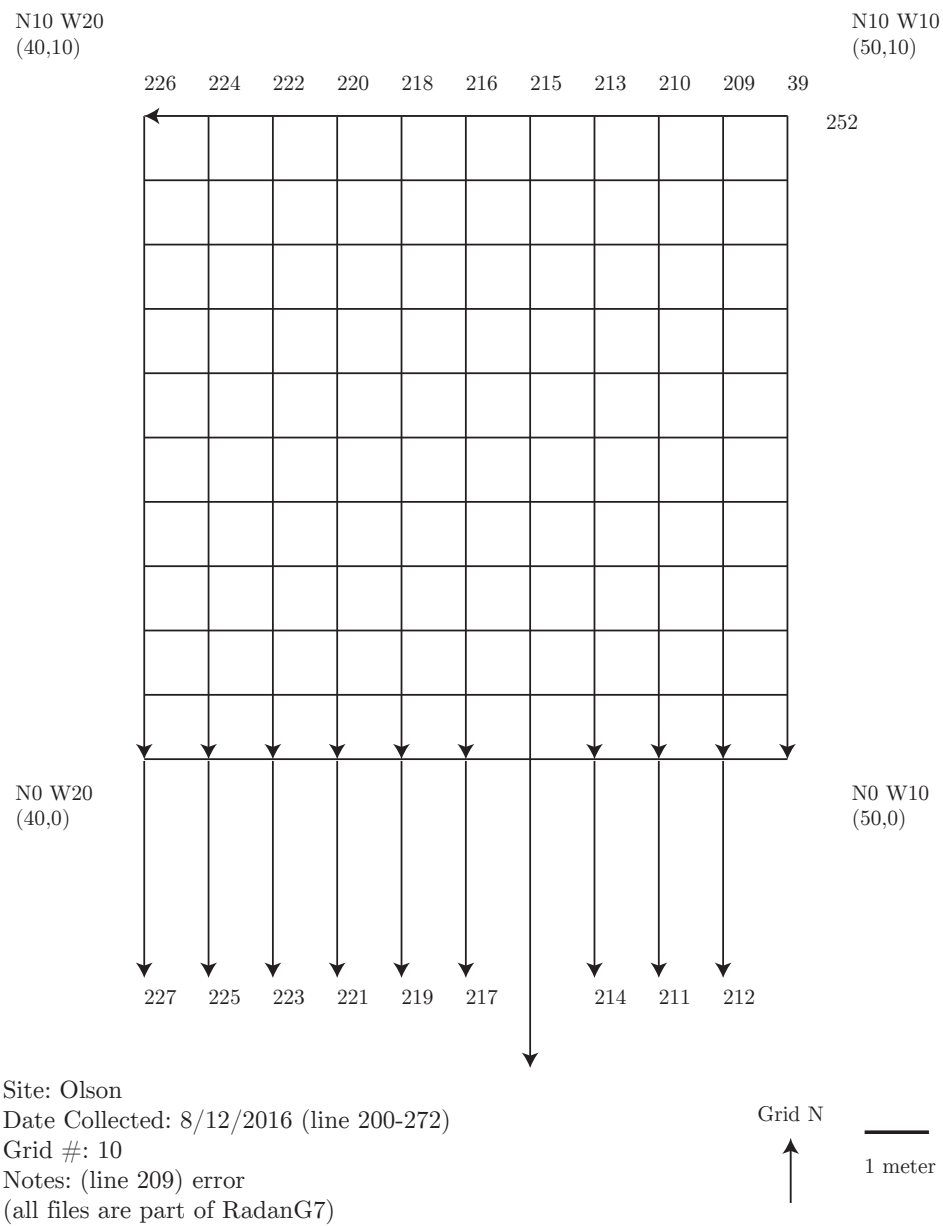
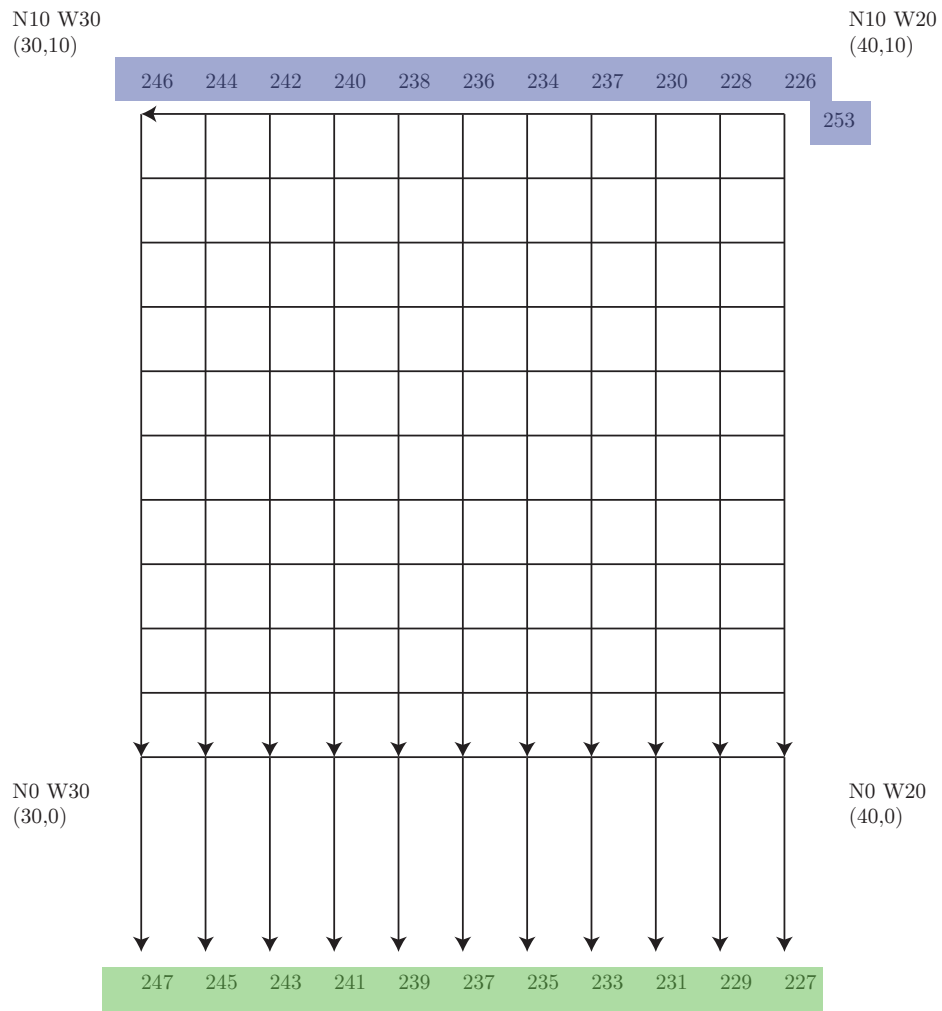


Figure D.15: Olson (Site 17.13) 1 meter 500 MHz GPR grid map 10.



Site: Olson
 Date Collected: 8/12/2016 (line 200-272)
 Grid #: 11
 Notes: (line 245) hung up @ start
 Blue: RadanG2
 Green: RadanG3

Grid N
 ↑
 1 meter

Figure D.16: Olson (Site 17.13) 1 meter 500 MHz GPR grid map 11.

[illegible]

Crew: A. Kelley, J. Miller, K. Bird,
E. Blackwood, K. Pontbriand

16=22	47=48
21=53	52=62
26=28	42=72
11=38	84=85
57=37	61=90

206

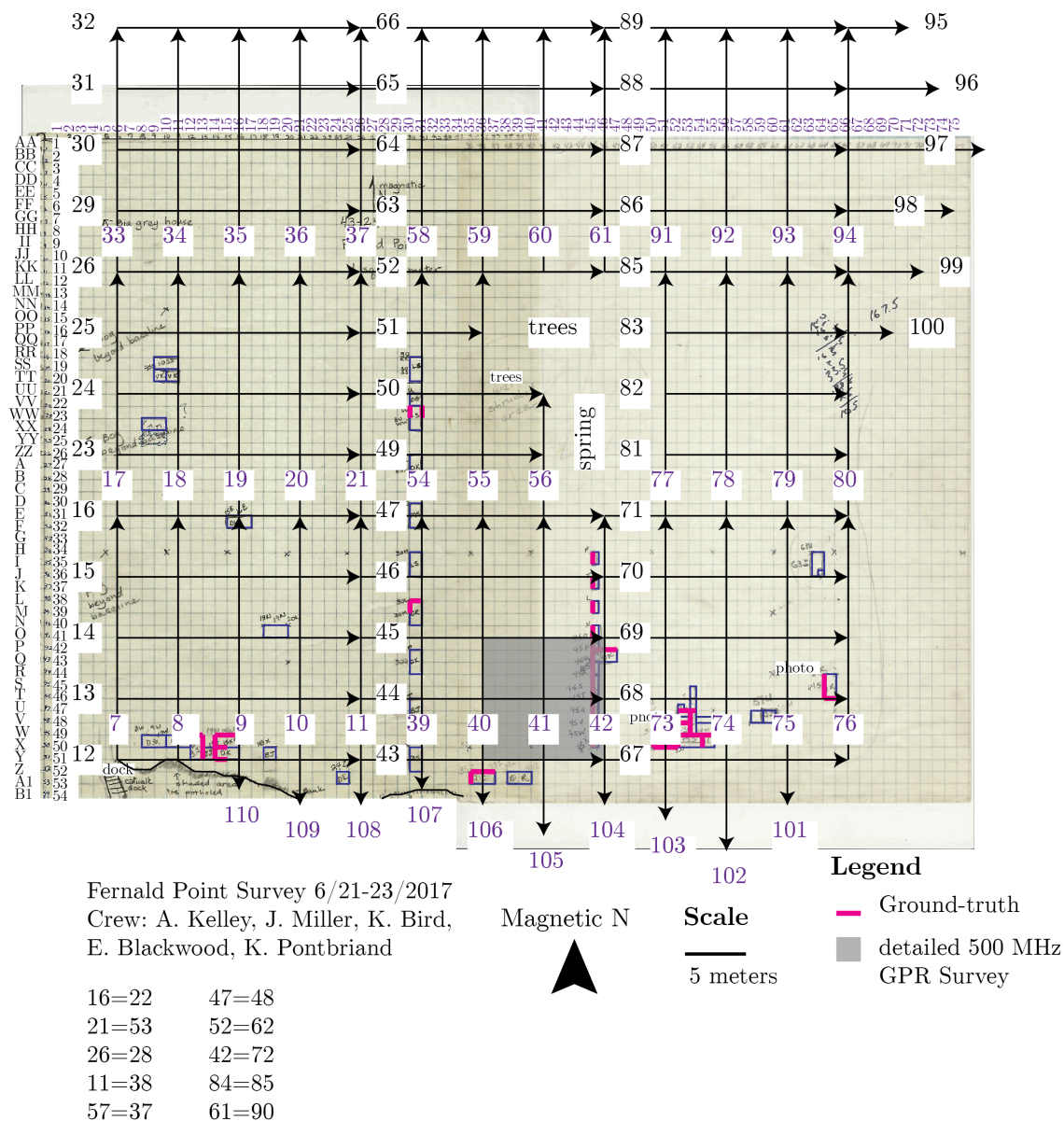


Figure D.18: Fernald Point (Site 43.24) 5 meter 500 MHz GPR grid map overlain on D. Sanger's excavation map. Archaeological map courtesy of the National Park Service, Acadia National Park. Purple boxes represent test pits, and pink lines denote available ground truth data (also courtesy of the National Park Service, Acadia National Park). The grey shaded box represents the area of detailed 500 MHz GPR survey.

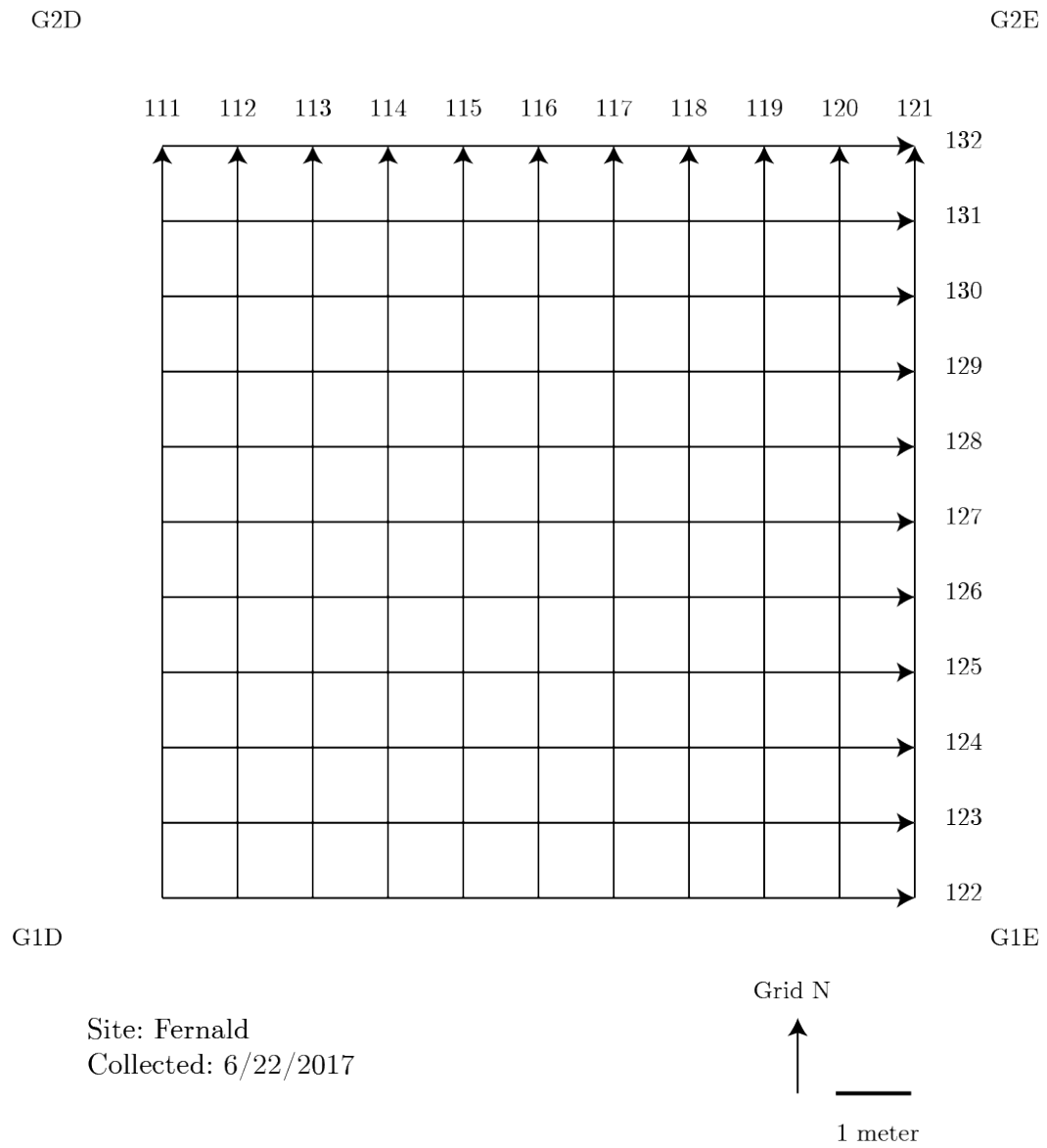


Figure D.19: Fernald Point (Site 43.24) 1 meter 500 MHz GPR grid map.

G2D

G2E

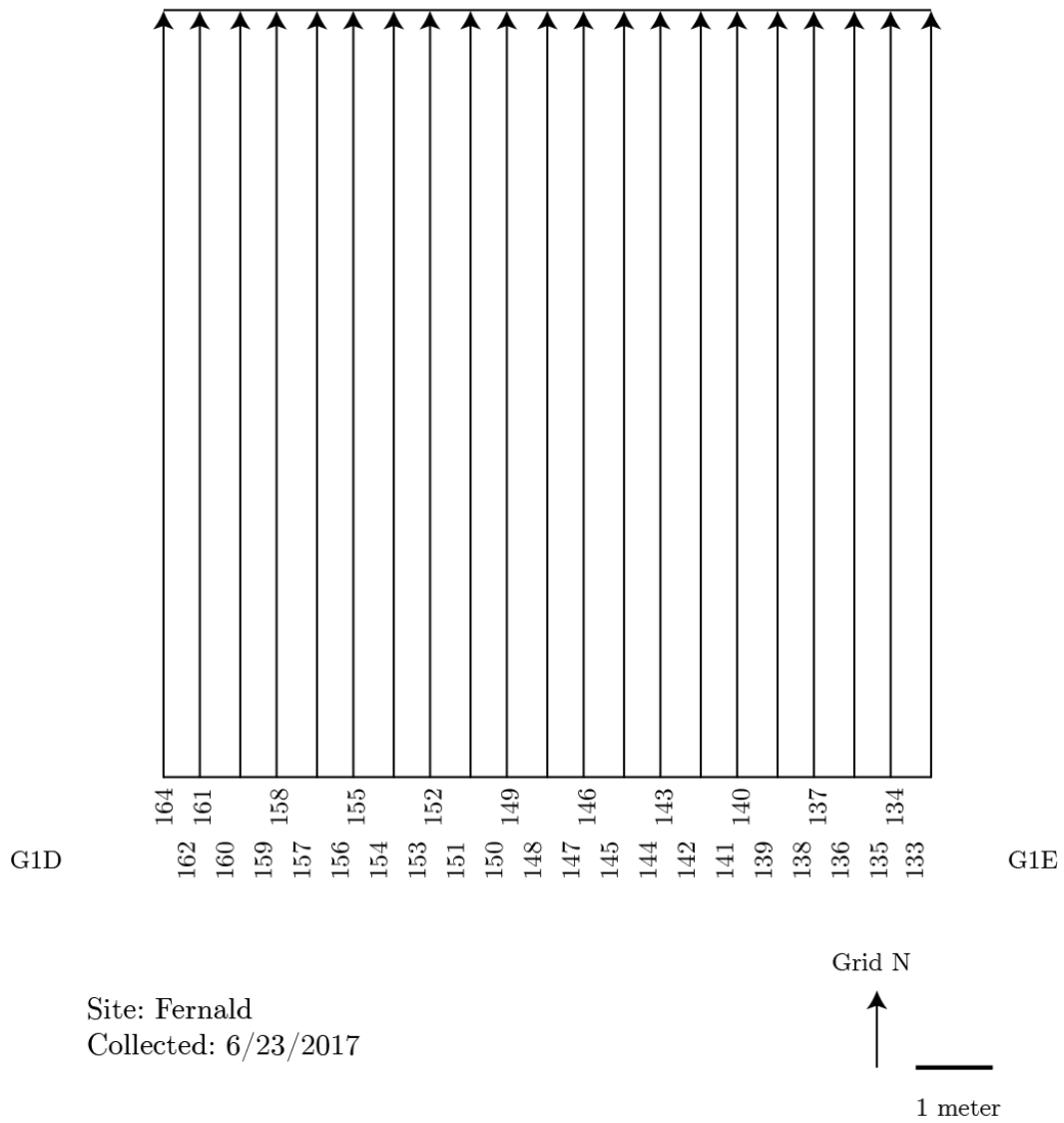


Figure D.20: Fernald Point (Site 43.24) 0.25 meter 500 MHz GPR grid map.

D.6 Tranquility Farm (Site 44.12a) 500 MHz GPR Maps

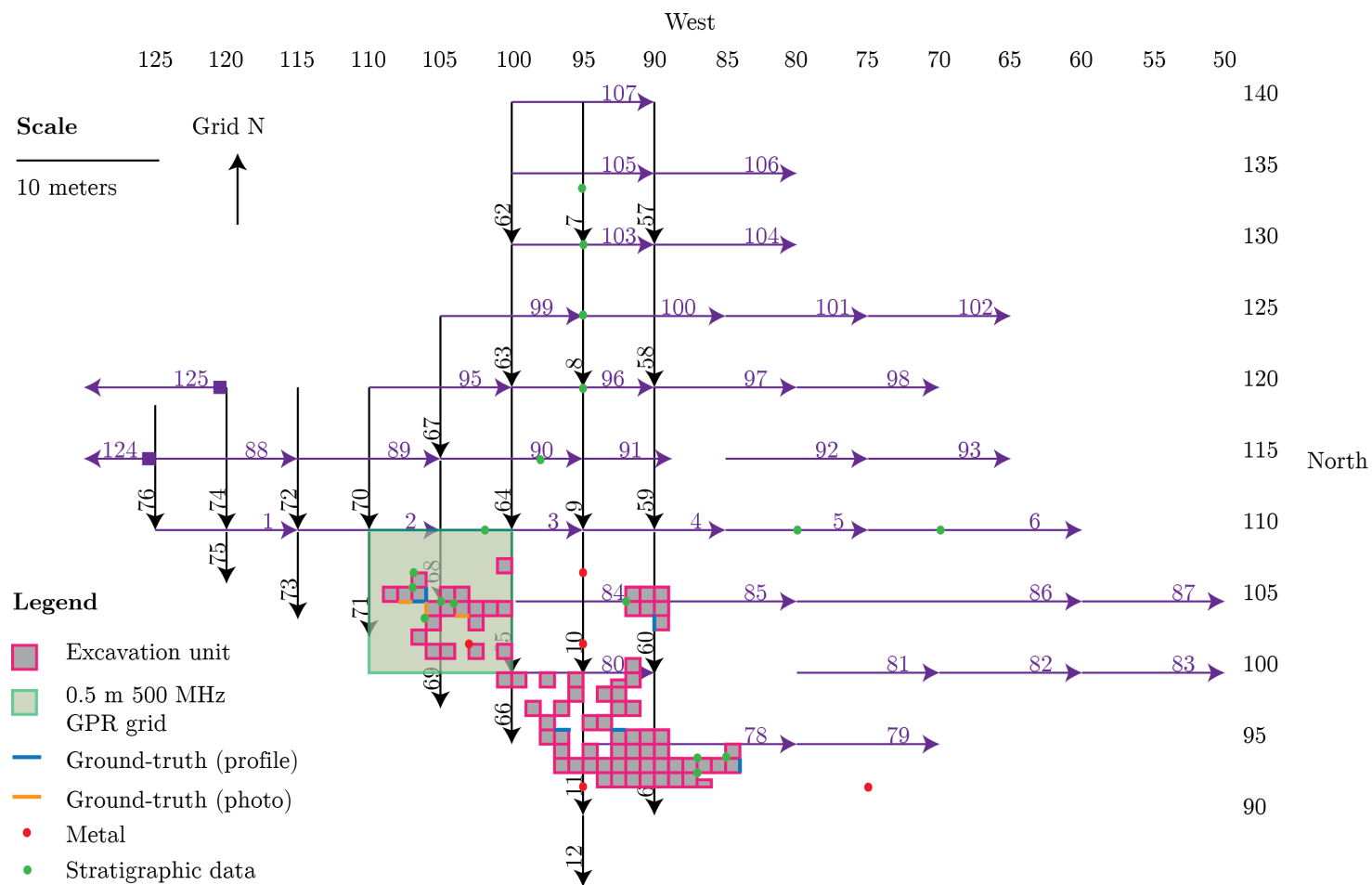
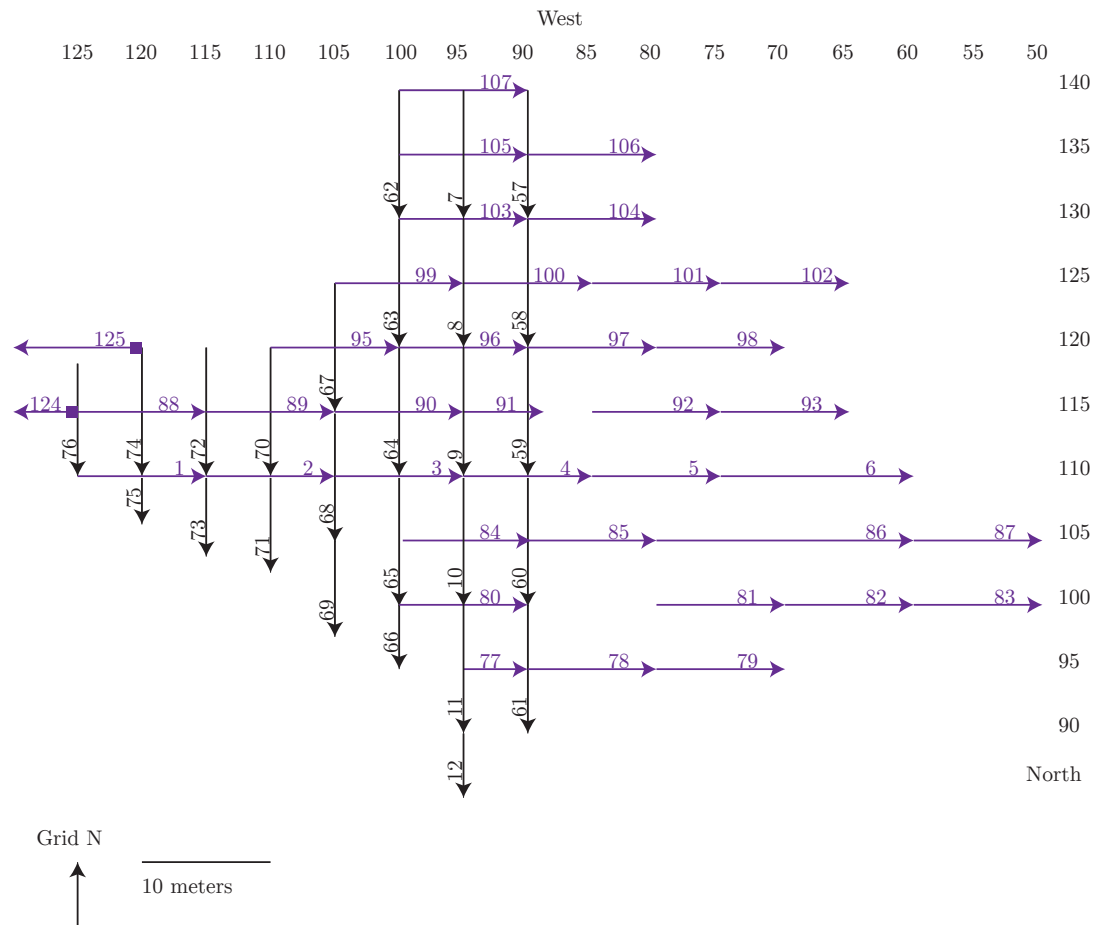


Figure D.21: Tranquility Farm (Site 44.12a) 5 meter 500 MHz GPR grid map 1 with excavation units and 0.5 meter 500 MHz GPR grid location delineated. Note that archaeological profiles are named for the location of the upper left corner of the unit.

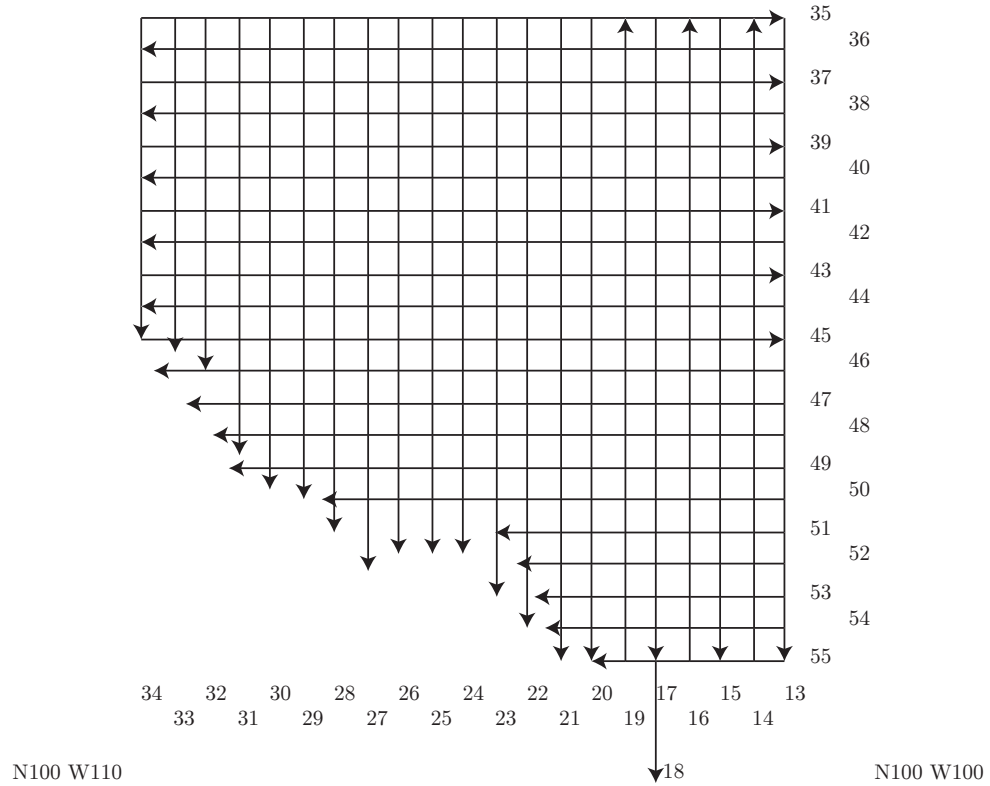


Site: Tranquility Farm
 Date Collected: 8/22/2016
 Grid: 1
 Notes: Rain!; (line 58) road bright 4-5m; (line 76) starts at 118 N;
 (line 91) W95 to W88; (line 124) W125 to N0W0 across disturbed
 area on G2; (line 125) to N10W5 on G2

Figure D.22: Tranquility Farm (Site 44.12a) 5 meter 500 MHz GPR grid map 1.

N110 W110

N110 W100



Site: Tranquility Farm
 Date Collected: 8/19/16
 Grid #: HM1
 Notes:

Figure D.23: Tranquility Farm (Site 44.12a) 0.5 meter 500 MHz GPR grid map.

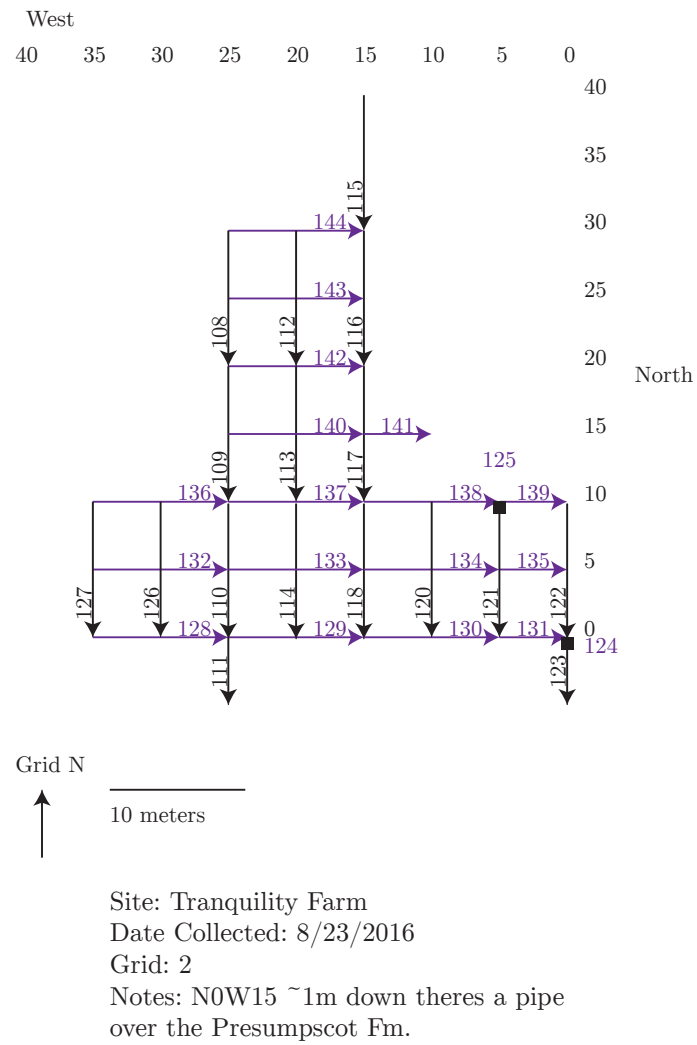


Figure D.24: Tranquility Farm (Site 44.12a) 5 meter 500 MHz GPR grid map 2.

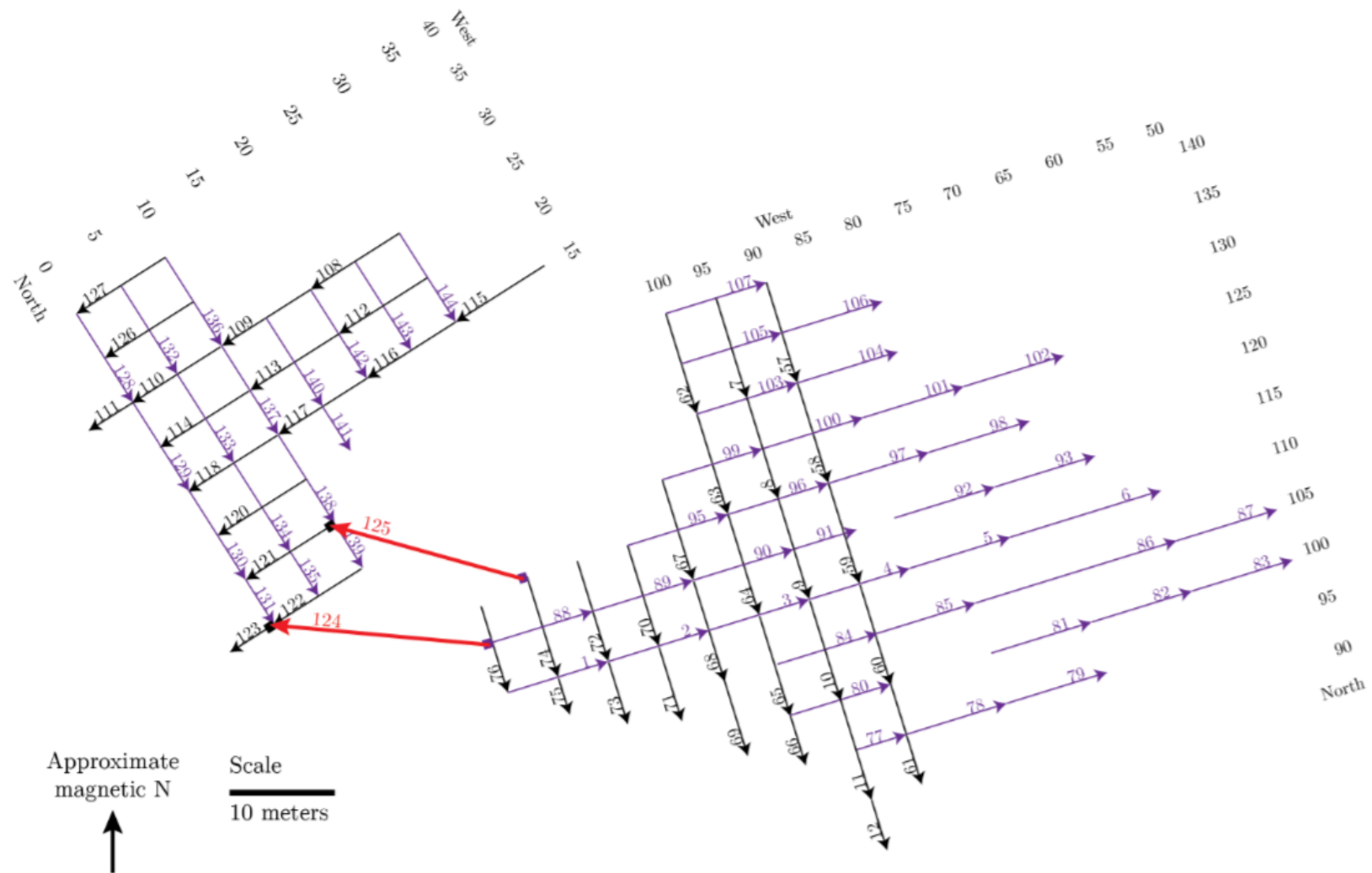


Figure D.25: Tranquility Farm (Site 44.12a) 500 MHz combined 5 meter GPR grid map.

Appendix E
ARCHAEOLOGICAL WALL PROFILES

E.1 Long Island North (Site 15.95) Archaeological Profiles

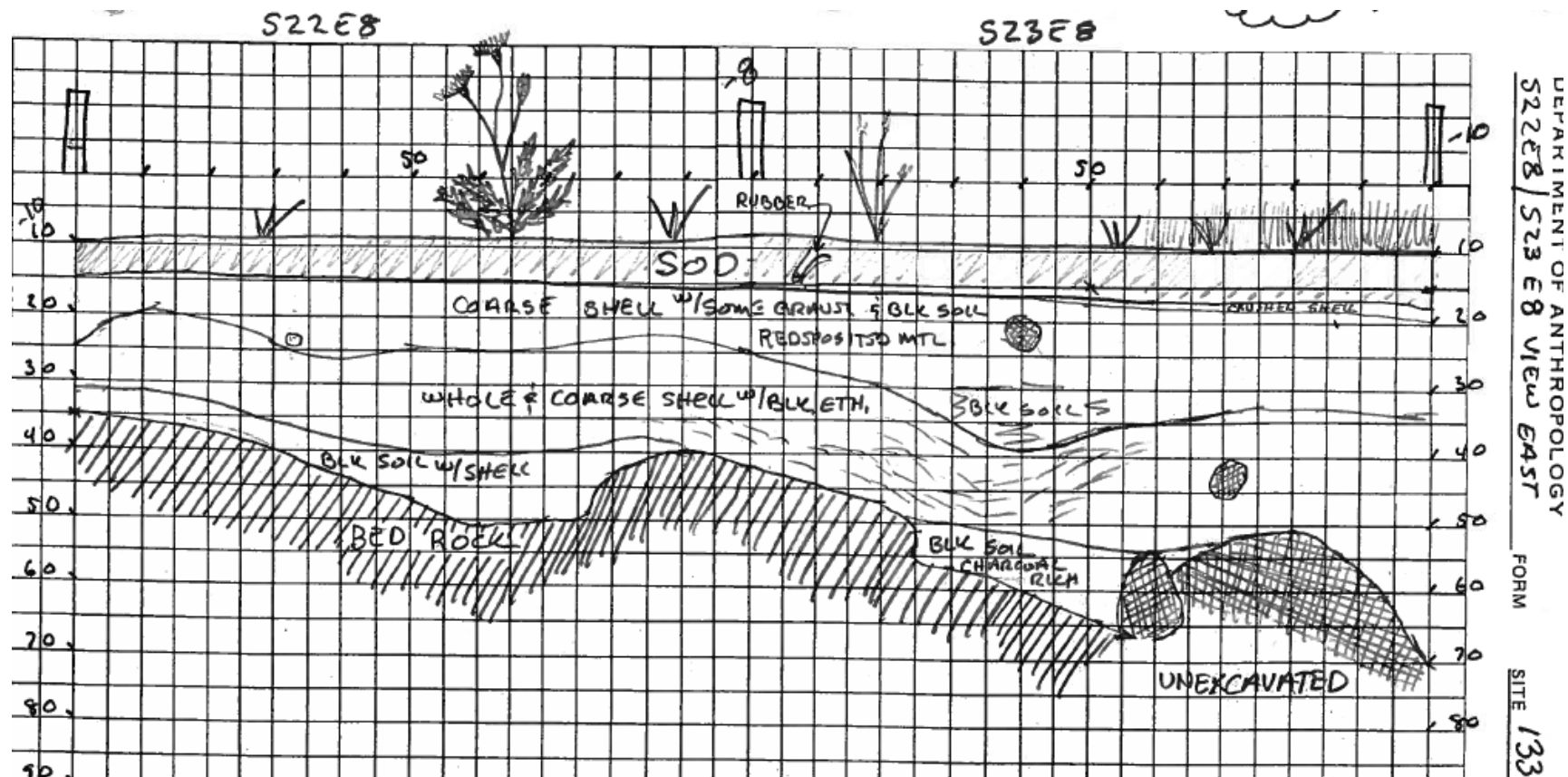


Figure E.1: Long Island North (Site 15.95) S23E8 and S22E8 east wall. Profile courtesy of Doyle (2017).

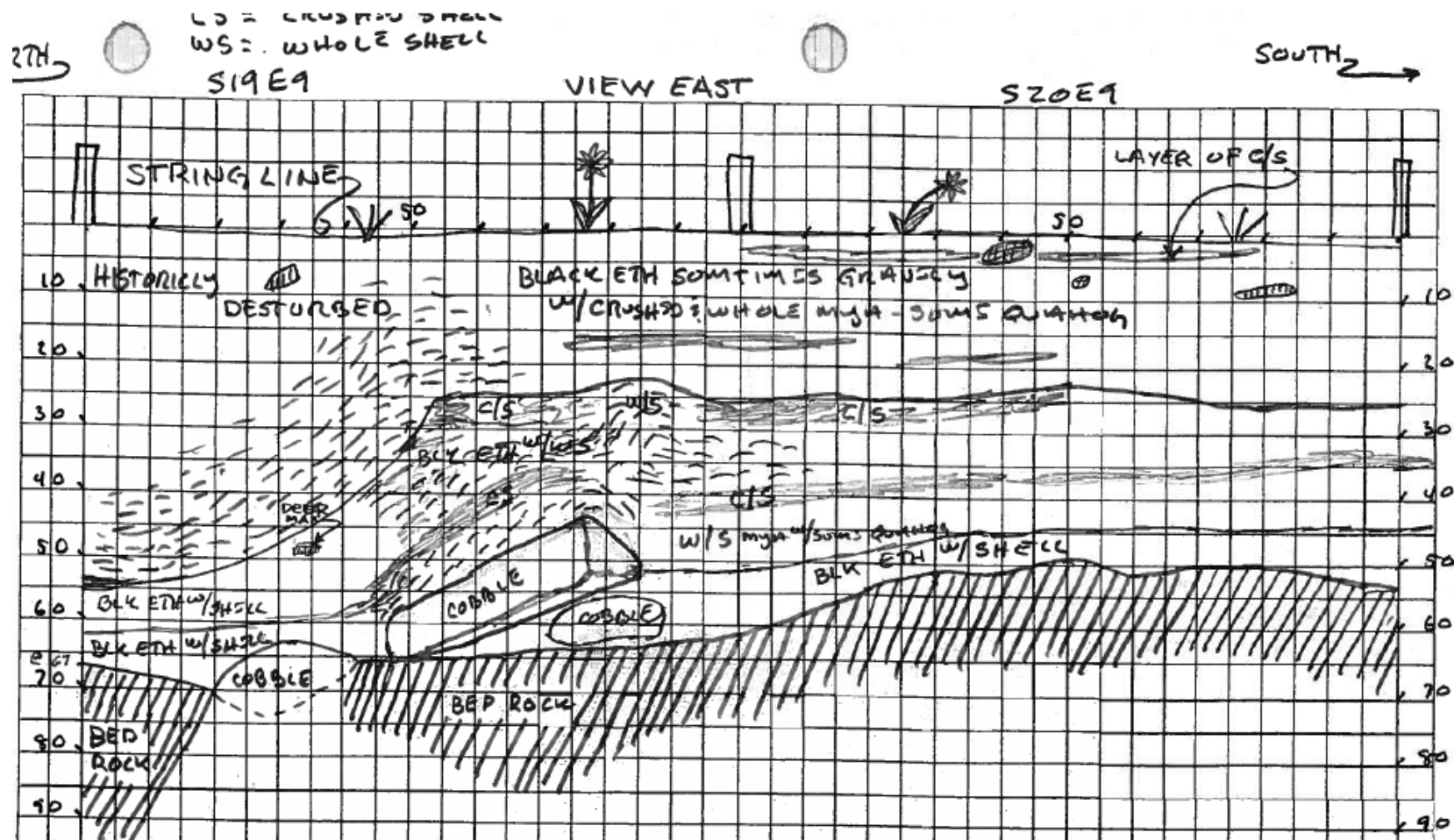


Figure E.2: Long Island North (Site 15.95) S19E9 and S20E9 east wall. Profile courtesy of Doyle (2017).

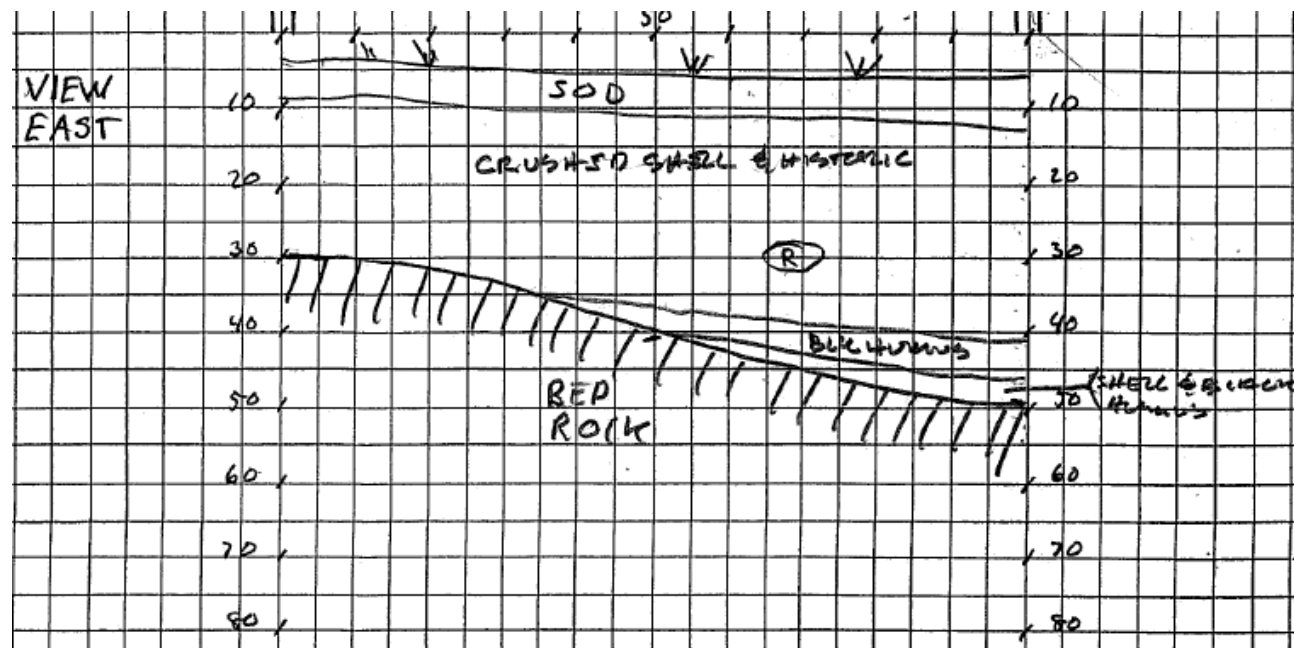


Figure E.3: Long Island North (Site 15.95) S17E8 east wall. Profile courtesy of Doyle (2017).

E.2 Damariscotta Oyster Farm Site (Site 26.15) Archaeological Profiles

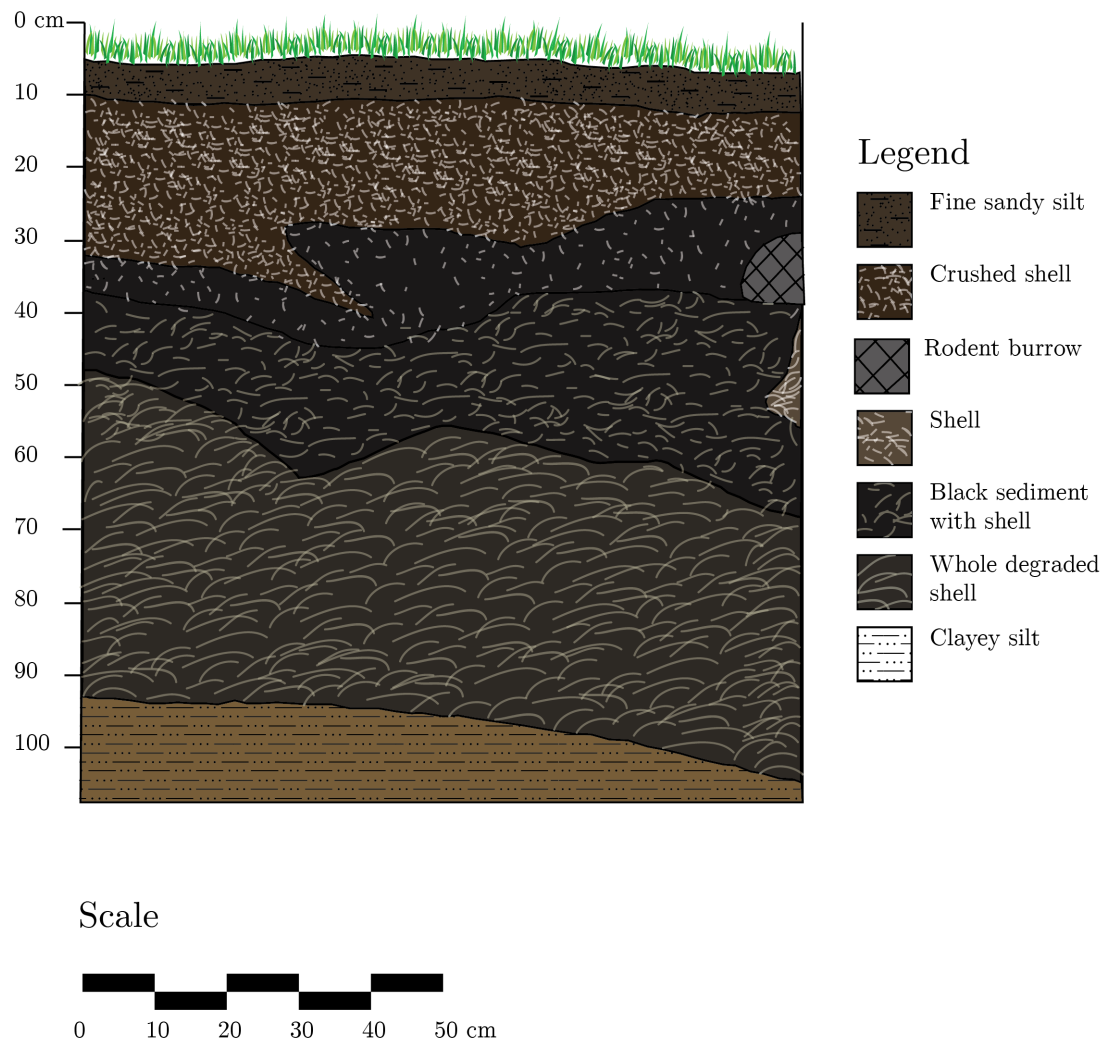


Figure E.4: Redrafted Oyster Farm (Site 26.15) north wall profile. Original profile courtesy of Spiess (2017a).

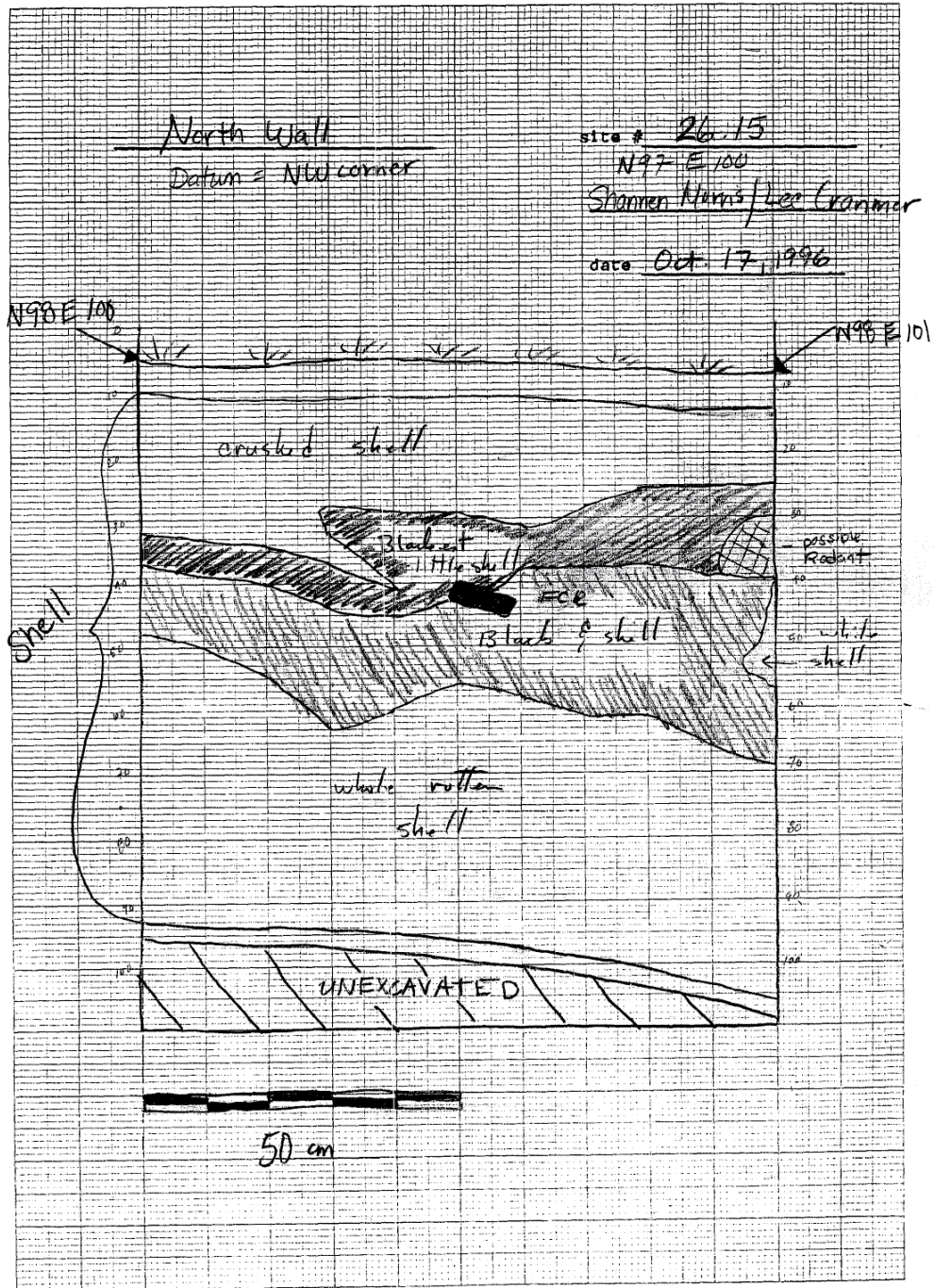


Figure E.5: Oyster Farm (Site 26.15) original north wall profile. Profile courtesy of Spiess (2017a).

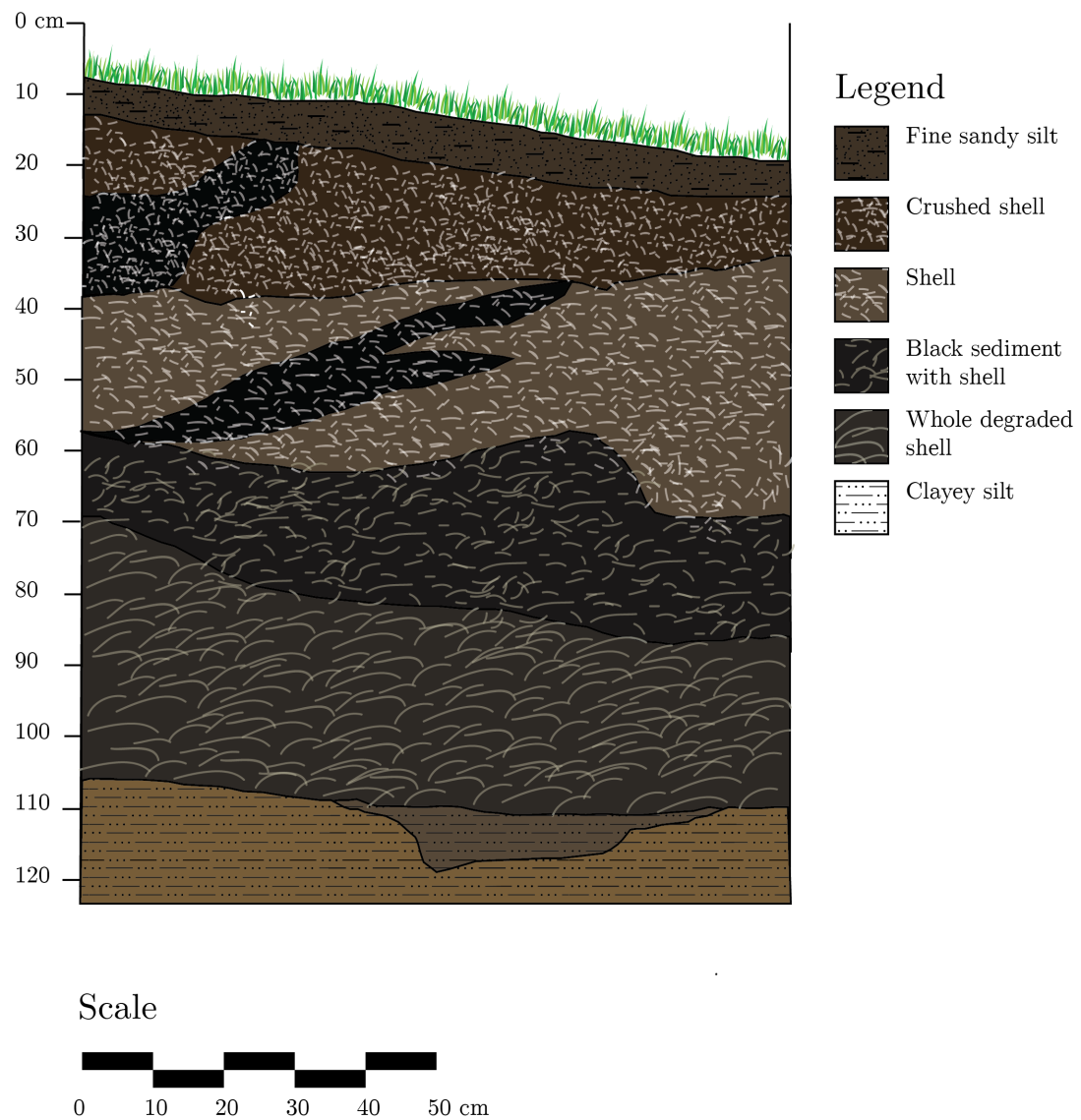


Figure E.6: Redrafted Oyster Farm (Site 26.15) east wall profile. Original profile courtesy of Spiess (2017a).

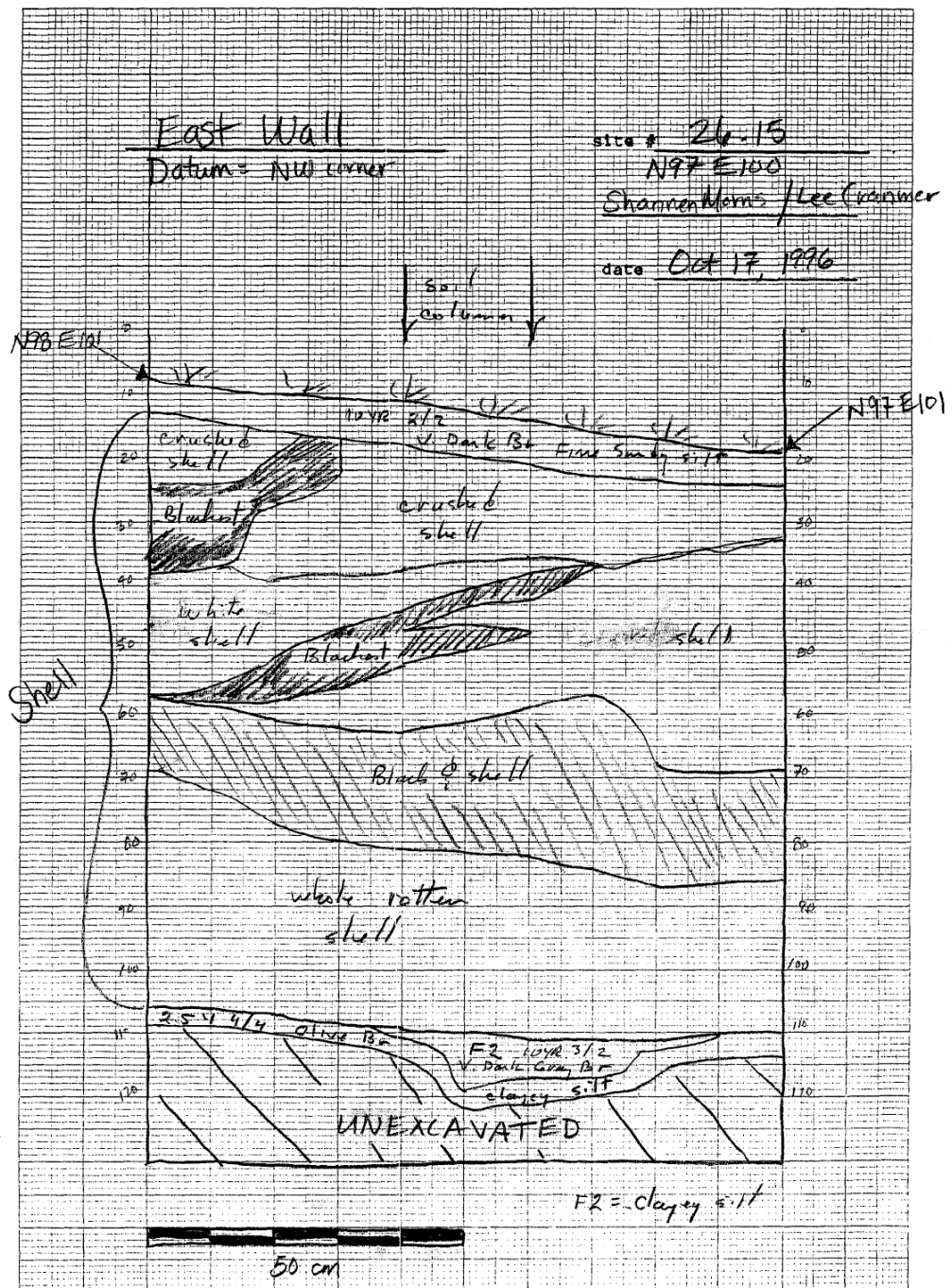


Figure E.7: Oyster Farm (Site 26.15) original east wall profile. Profile courtesy of Spiess (2017a).

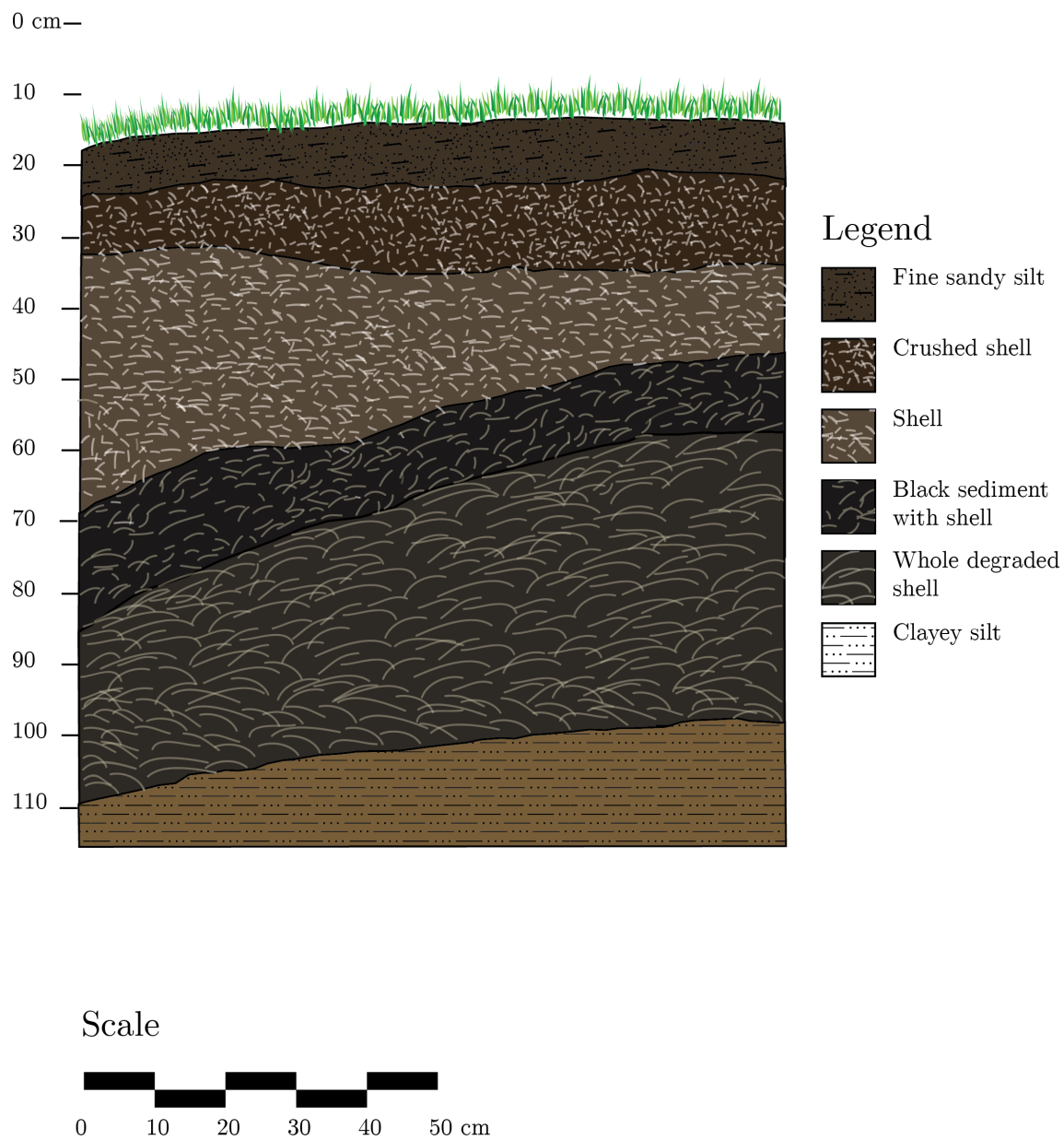


Figure E.8: Redrafted Oyster Farm (Site 26.15) south wall profile. Original profile courtesy of Spiess (2017a).

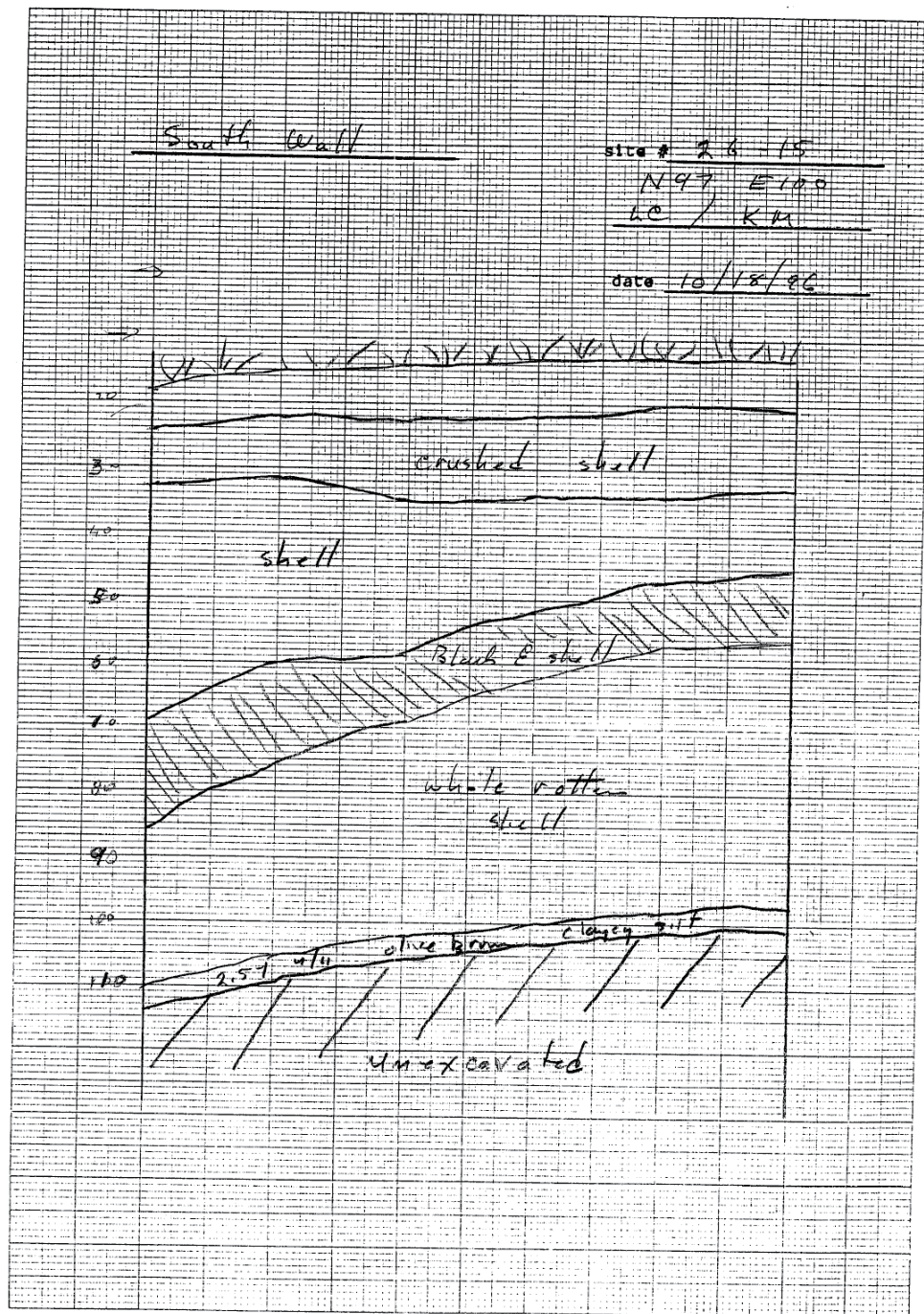


Figure E.9: Oyster Farm (Site 26.15) original south wall profile. Profile courtesy of Spiess (2017a).

E.3 Olson (Site 17.13) Archaeological Wall Profiles and Photos

Olson Site East Wall (1)

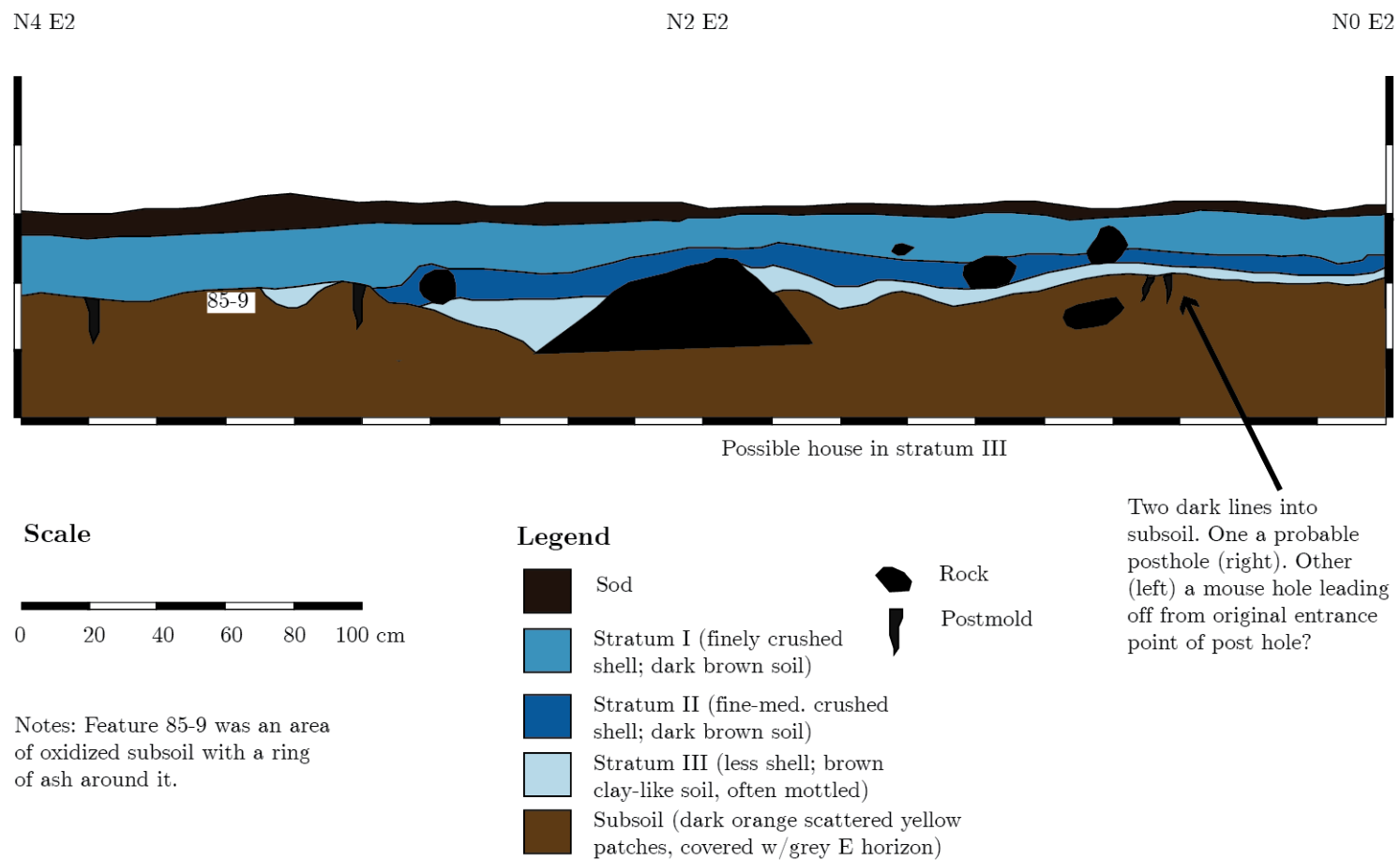


Figure E.10: Redrafted Olson (Site 17.13) east (1) wall profile. Original profile courtesy of Spiess (2017a).

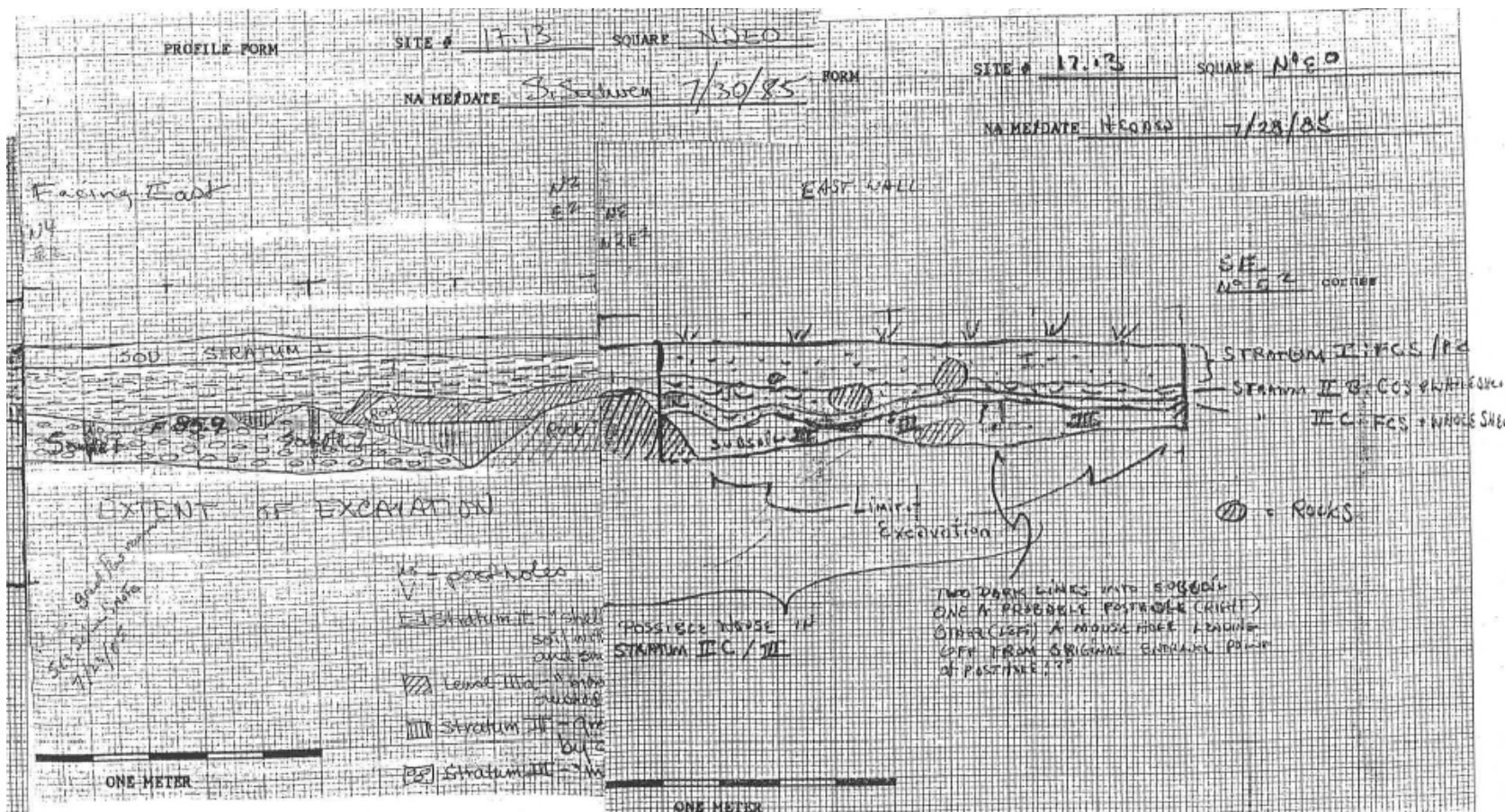


Figure E.11: Olson (Site 17.13) original east (1) wall profile. Profile courtesy of Spiess (2017a).



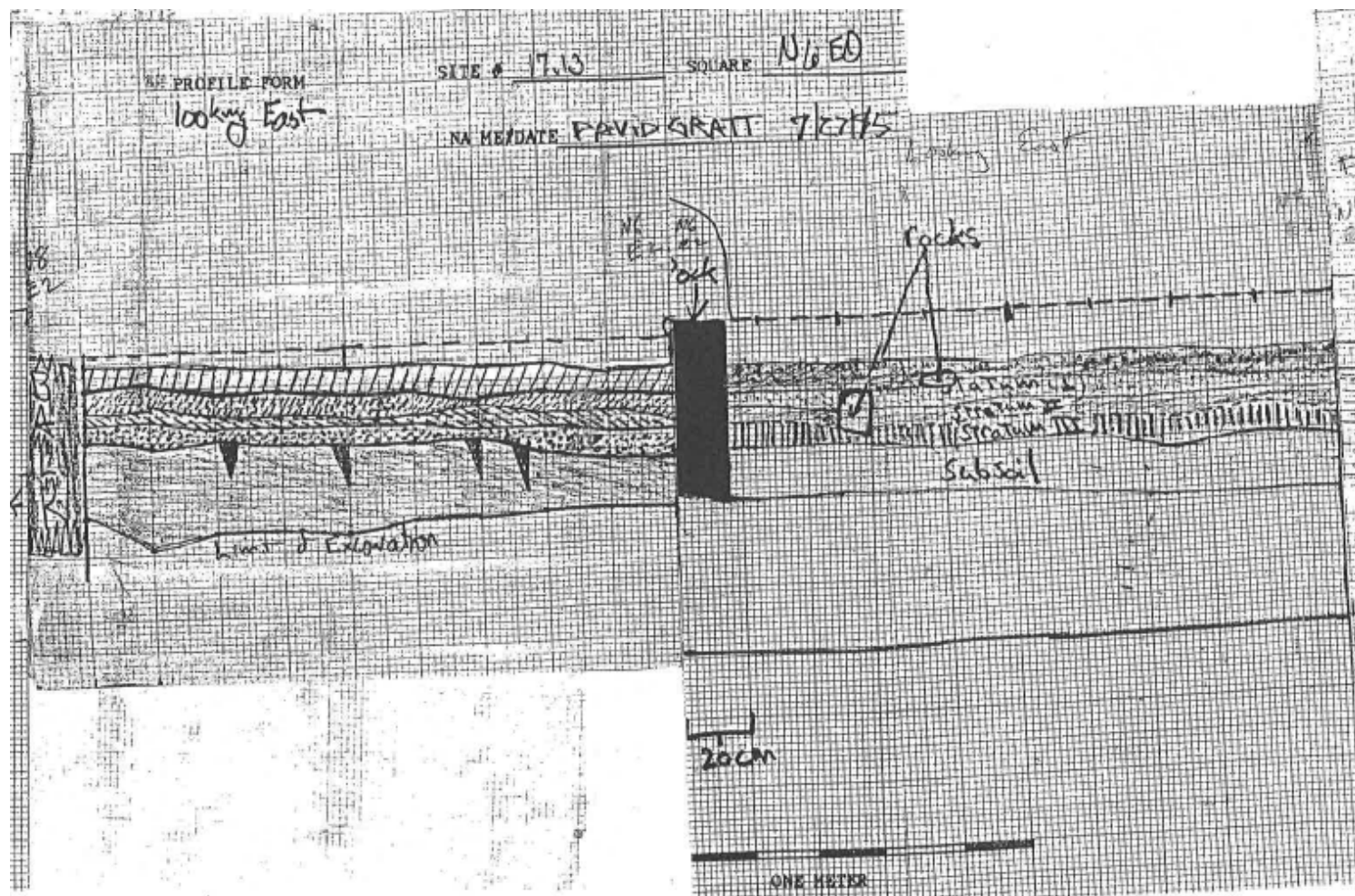


Figure E.13: Olson (Site 17.13) original east (2) wall profile. Profile courtesy of Spiess (2017a).

Olson Site East Wall (3)

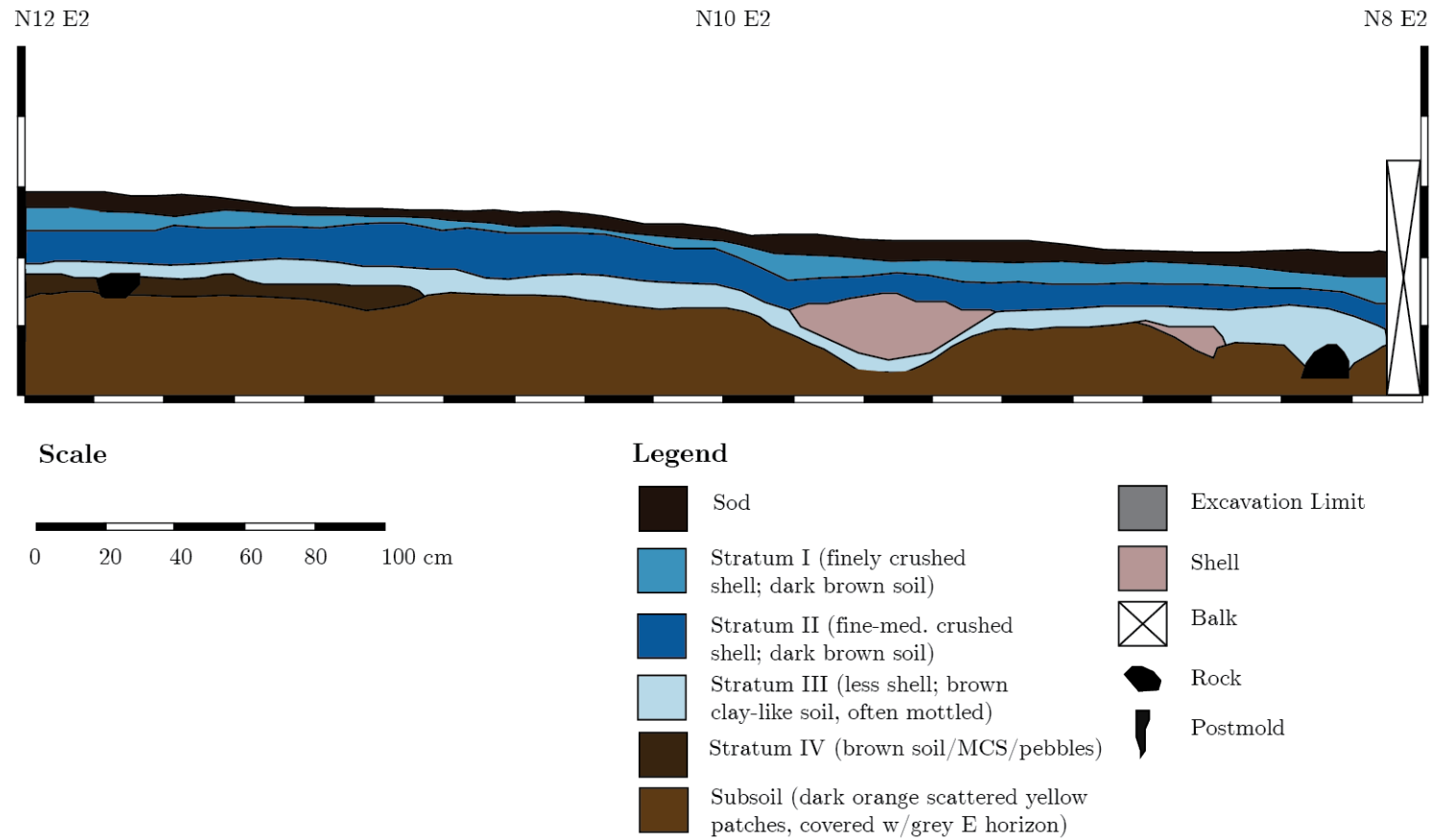


Figure E.14: Redrafted Olson (Site 17.13) east (3) wall profile. Original profile courtesy of Spiess (2017a).

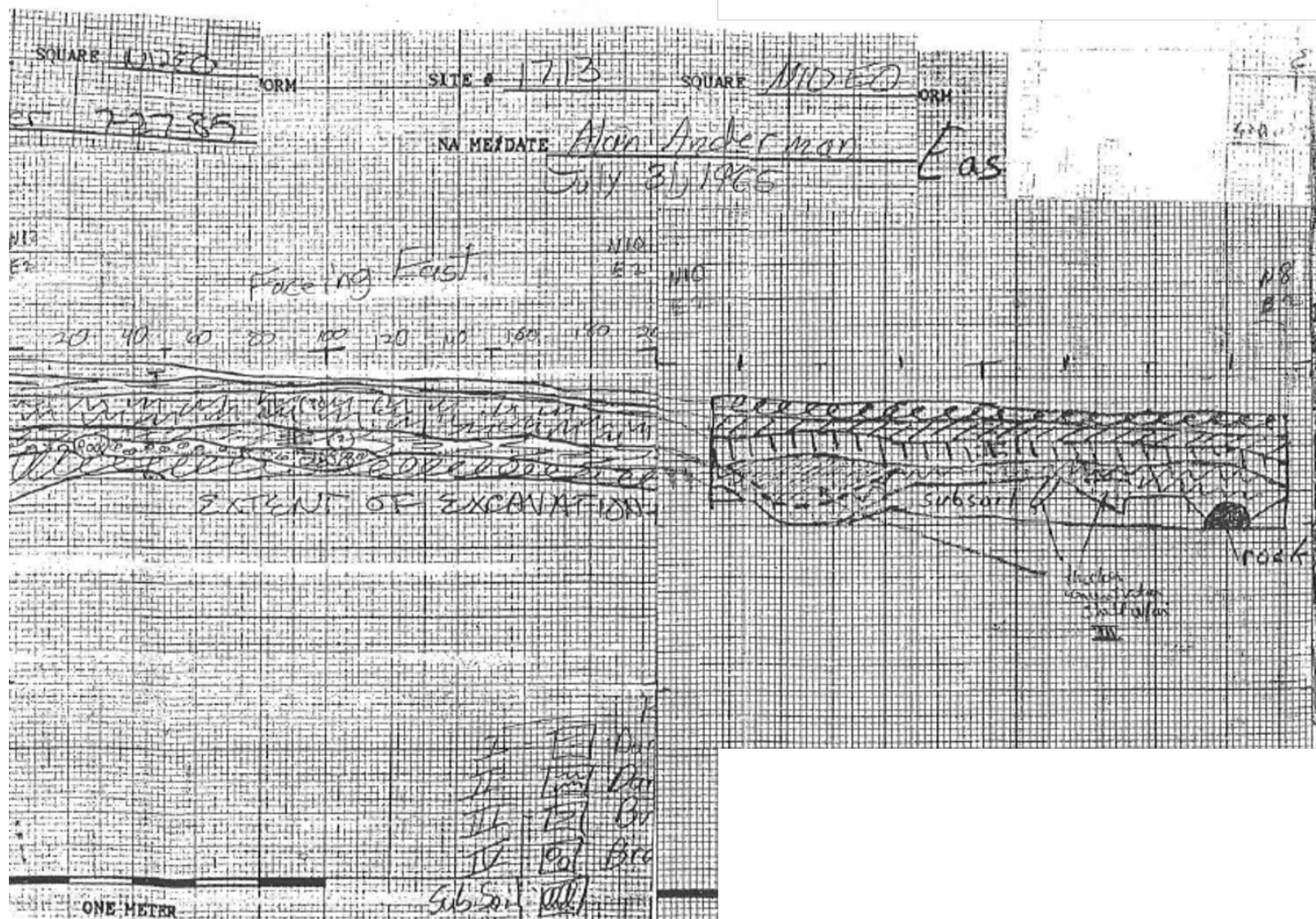


Figure E.15: Olson (Site 17.13) original east (3) wall profile. Profile courtesy of Spiess (2017a).

Olson Site East Wall (4)

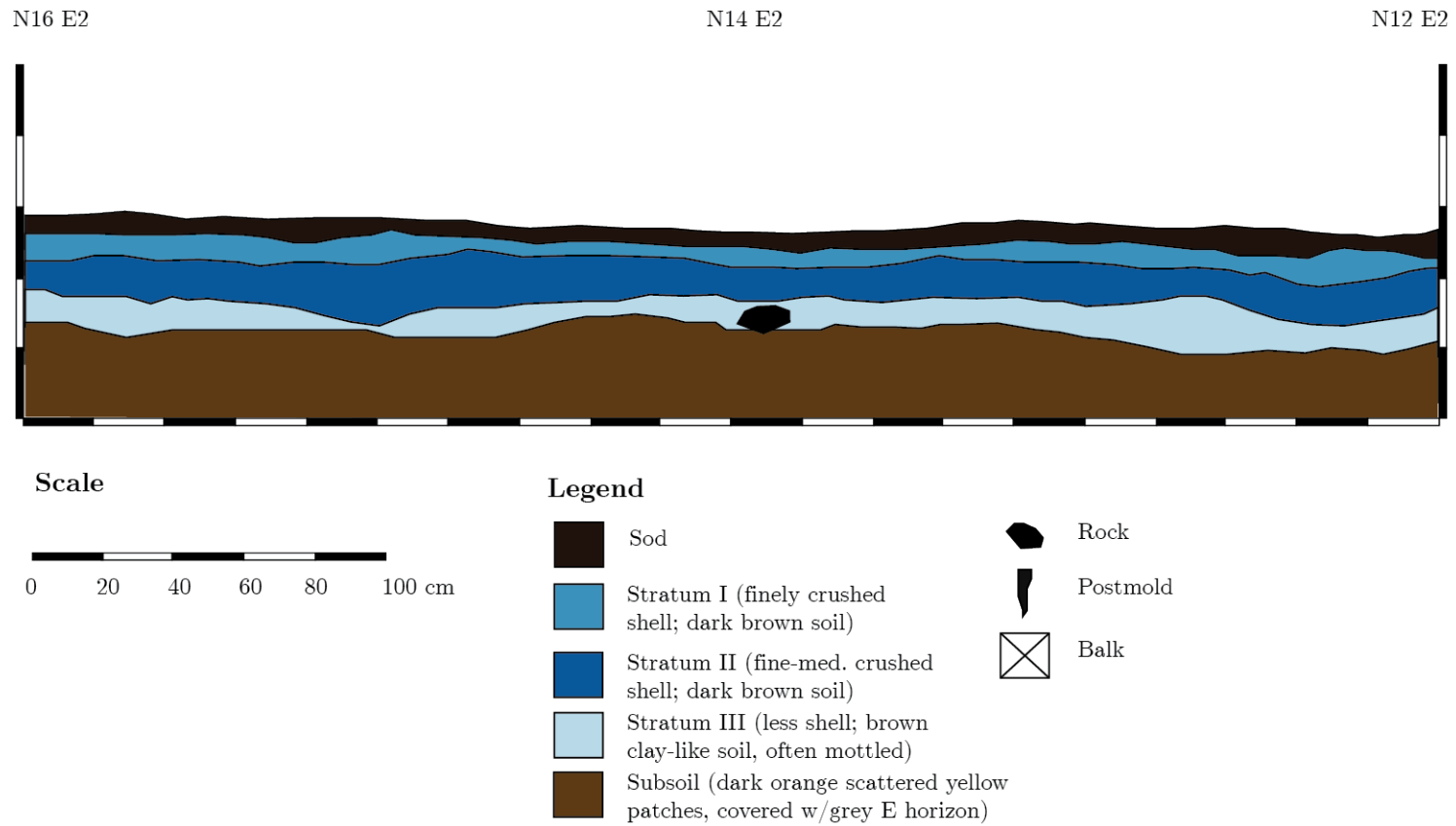


Figure E.16: Redrafted Olson (Site 17.13) wall profile. Original profile courtesy of Spiess (2017a).

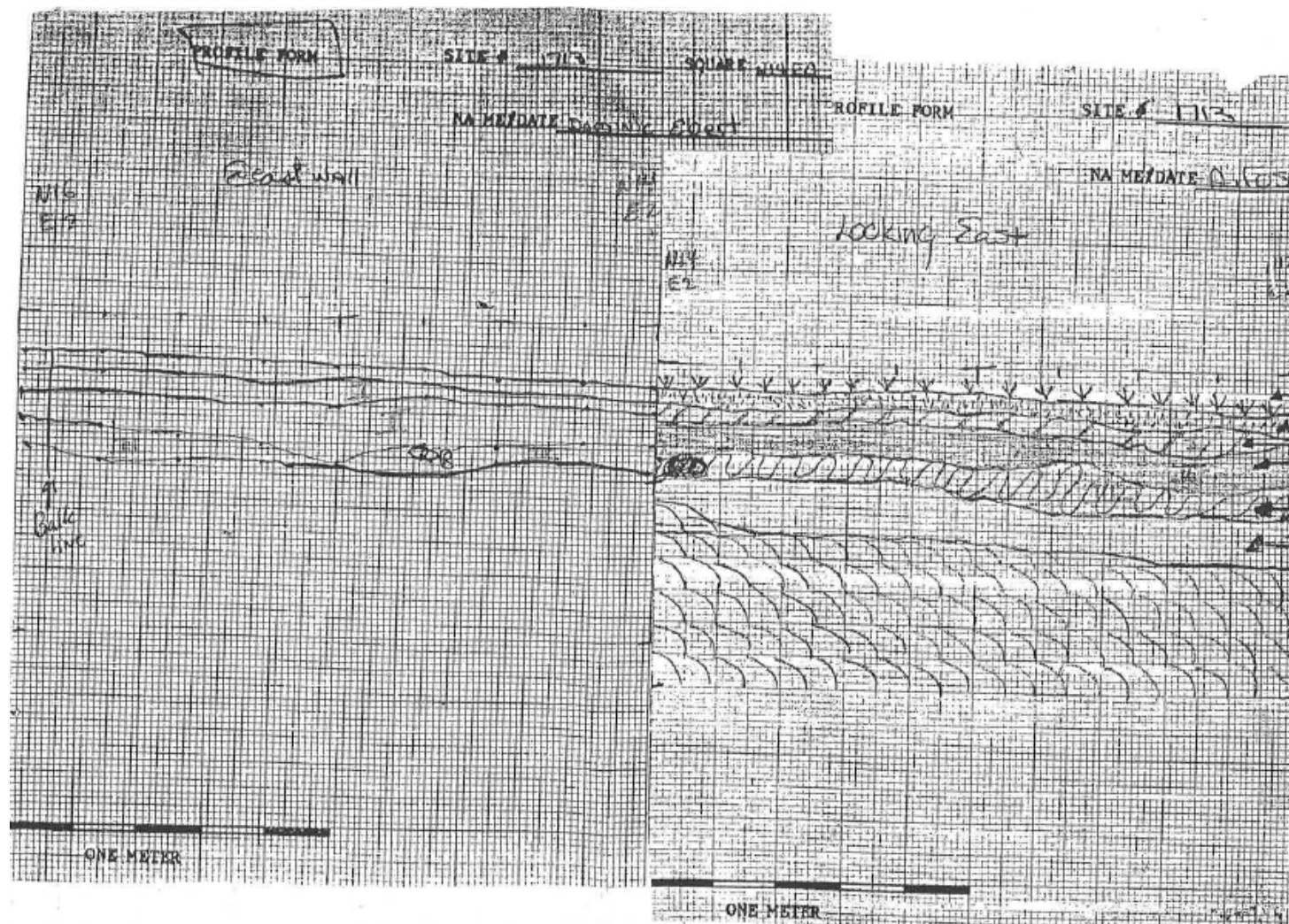
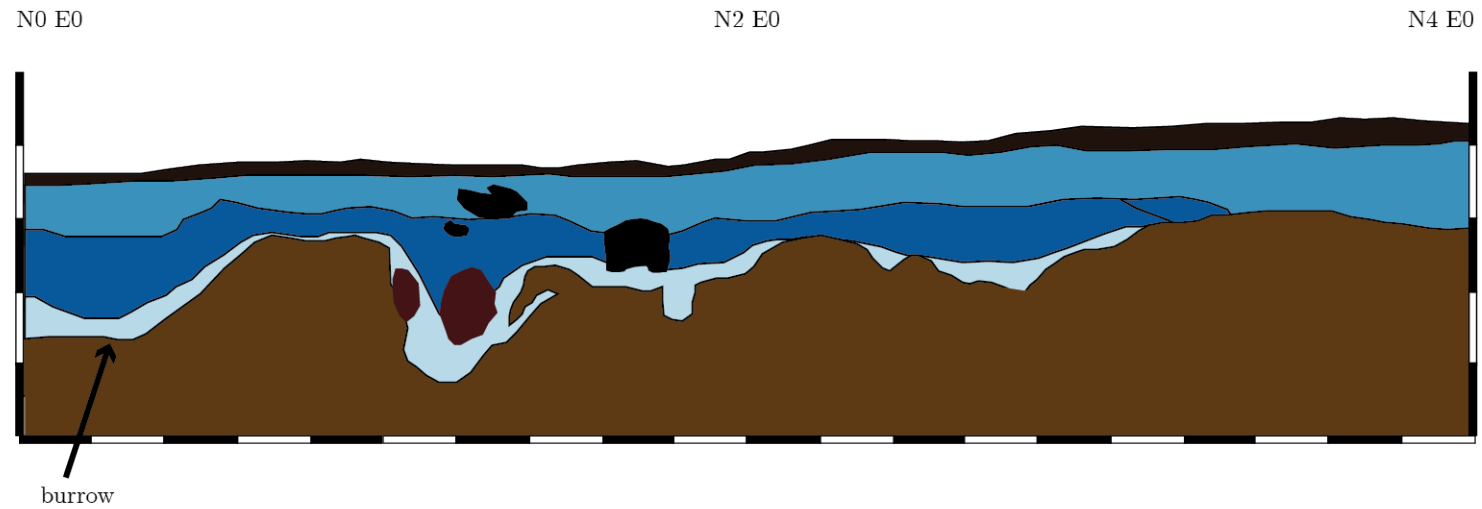


Figure E.17: Olson (Site 17.13) original east (4) wall profile. Profile courtesy of Spiess (2017a).

Olson Site West Wall (1)



Scale



Legend

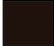








	Sod		Rock
	Stratum I (finely crushed shell; dark brown soil)		Fire-reddened rock
	Stratum II (fine-med. crushed shell; dark brown soil)		Postmold
	Stratum III (less shell; brown clay-like soil, often mottled)		Balk
	Subsoil (dark orange scattered yellow patches, covered w/grey E horizon)		

Figure E.18: Redrafted Olson (Site 17.13) west (1) wall profile. Original profile courtesy of Spiess (2017a).

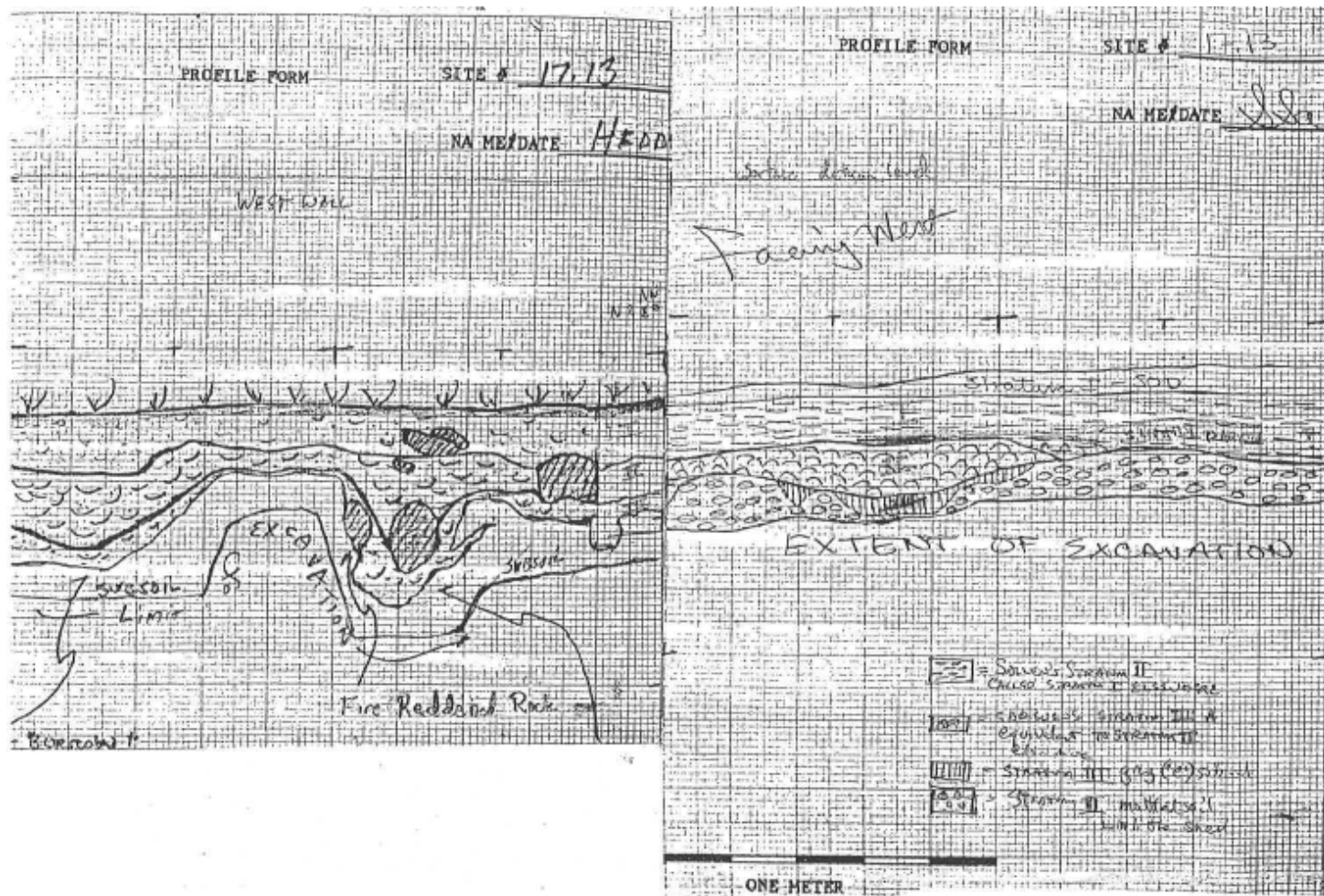


Figure E.19: Olson (Site 17.13) original west (1) wall profile. Profile courtesy of Spiess (2017a).



Figure E.20: Olson (Site 17.13) west wall profile photo N0E0 to N2E0. Photo courtesy of Spiess (2017a).



Figure E.21: Olson (Site 17.13) west wall profile photo N2E0 to N4E0. Photo courtesy of Spiess (2017a).

239



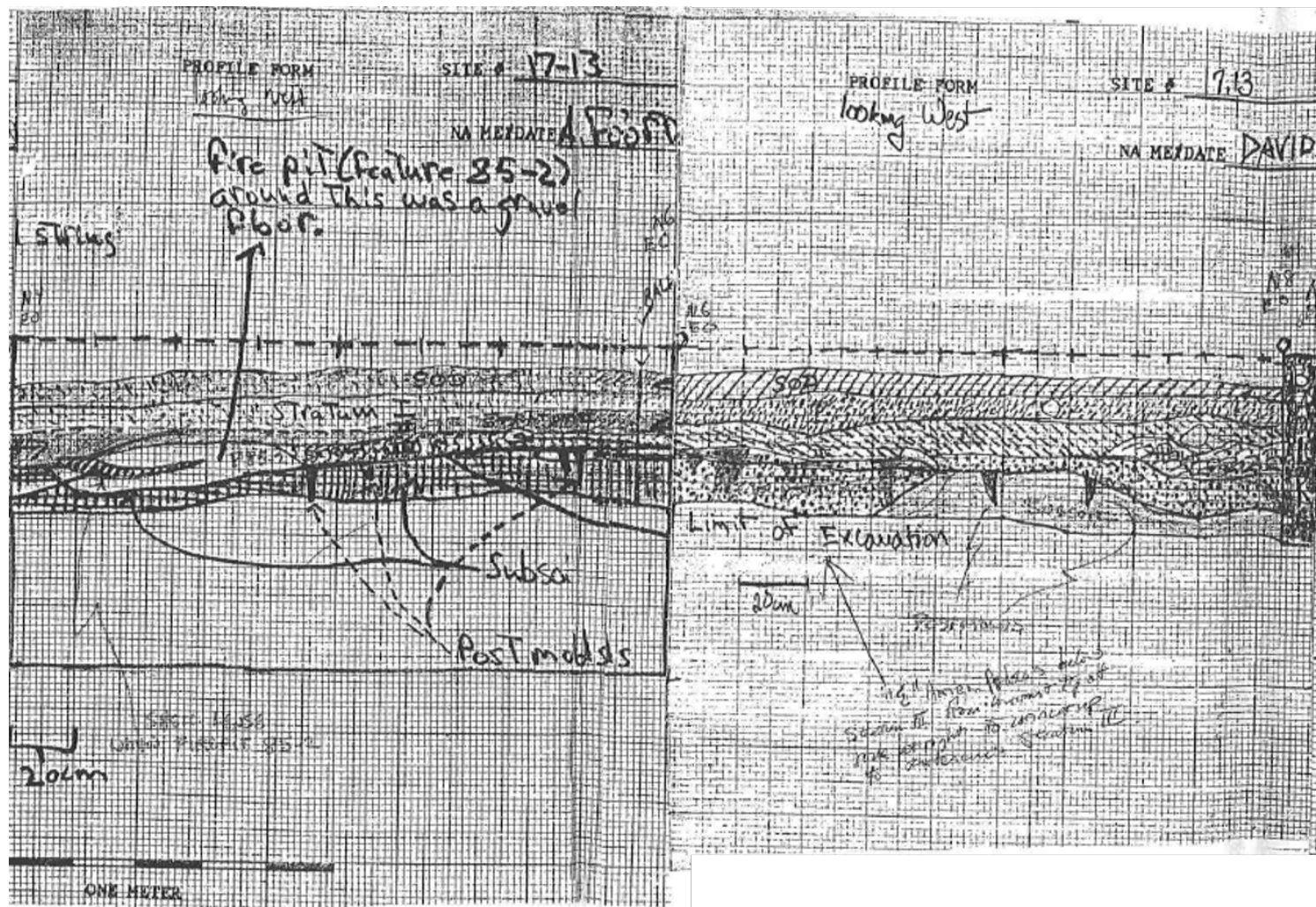


Figure E.23: Olson (Site 17.13) original west (2) wall profile. Profile courtesy of Spiess (2017a).



Figure E.24: Olson (Site 17.13) west wall profile photo N4E0 to N6E0. Photo courtesy of Spiess (2017a).



Figure E.25: Olson (Site 17.13) west wall profile photo N6E0 to N8E0. Photo courtesy of Spiess (2017a).

Olson Site West Wall (3)

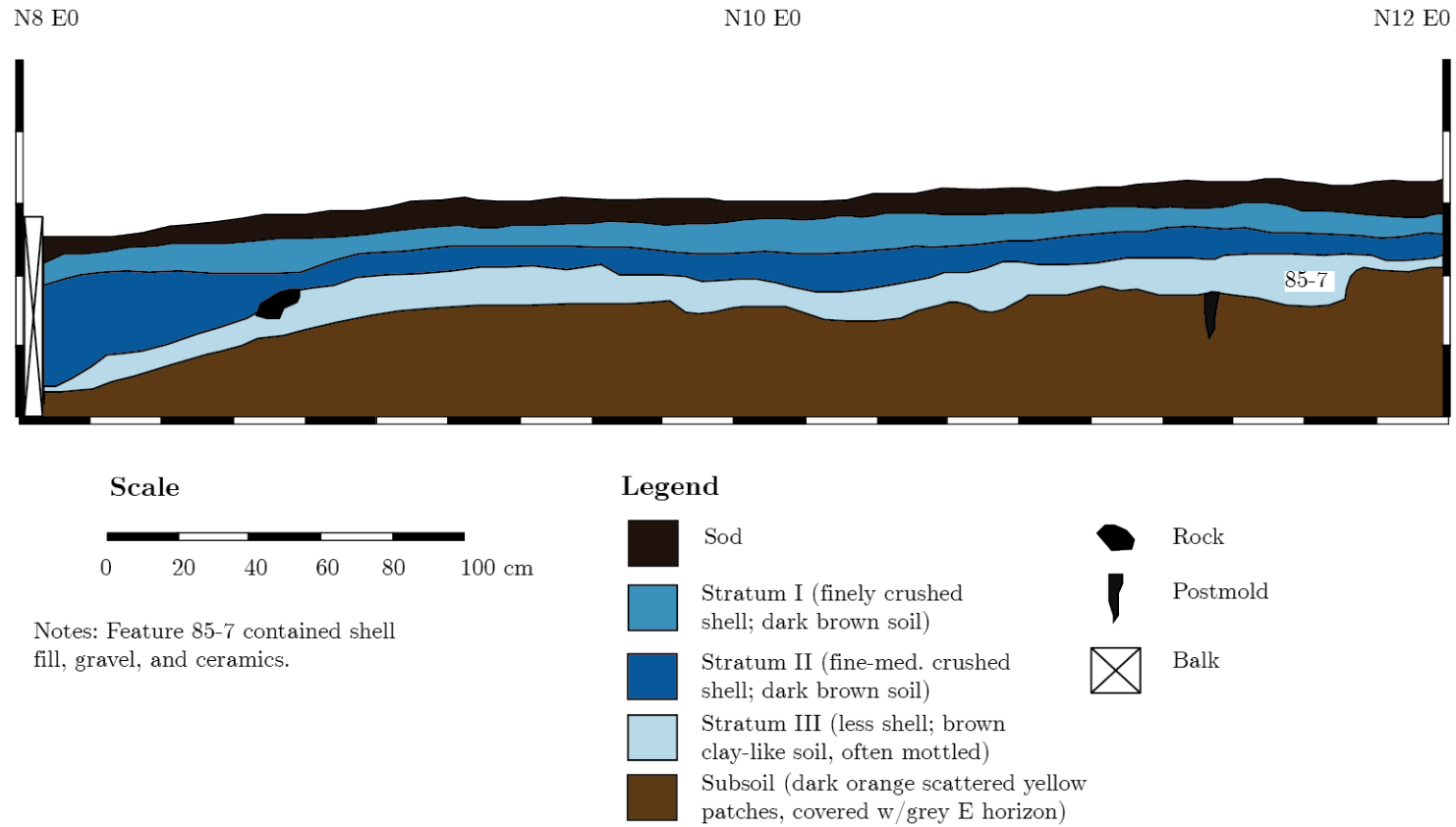


Figure E.26: Redrafted Olson (Site 17.13) west (3) wall profile. Original profile courtesy of Spiess (2017a).

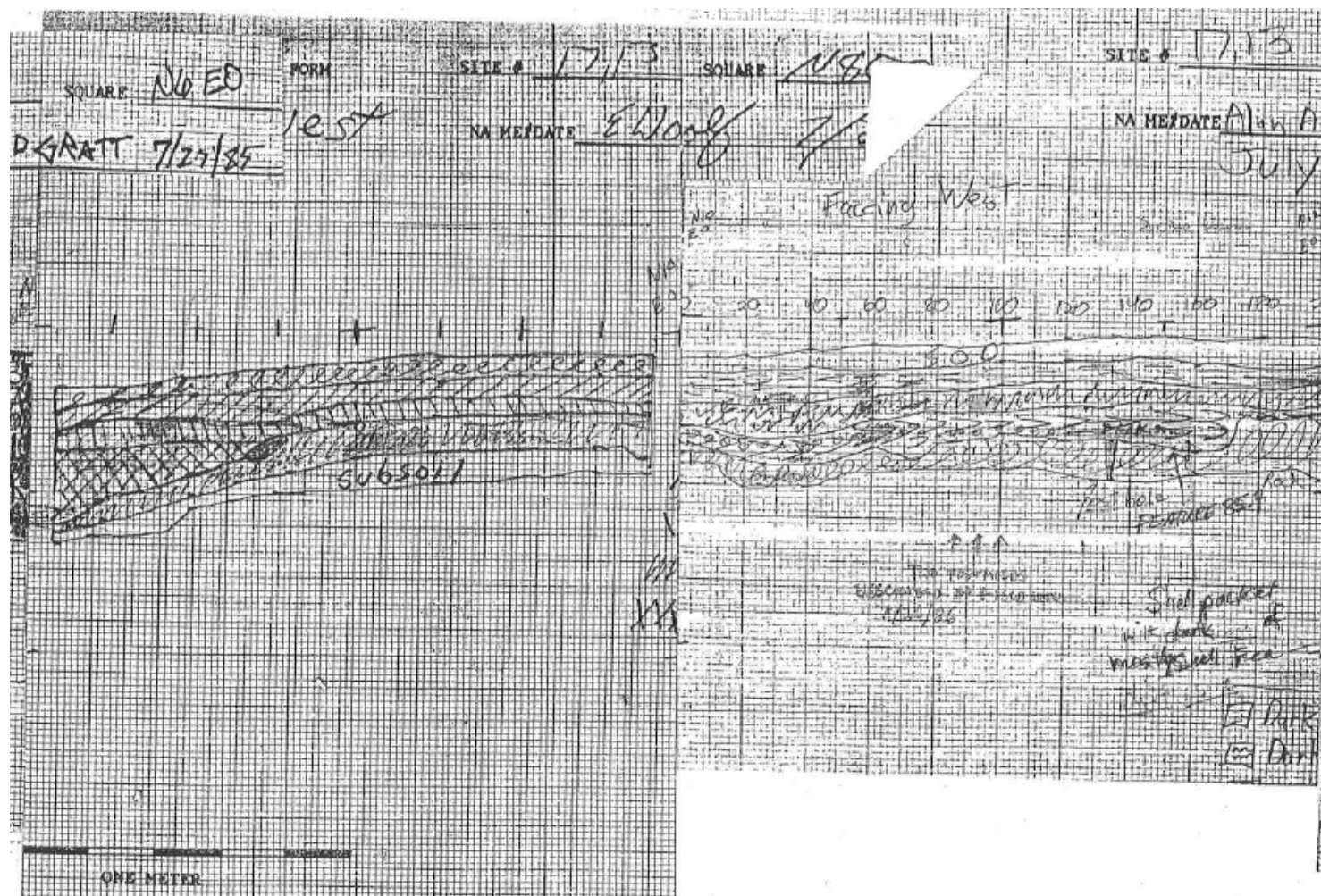


Figure E.27: Olson (Site 17.13) original west (3) wall profile. Profile courtesy of Spiess (2017a).

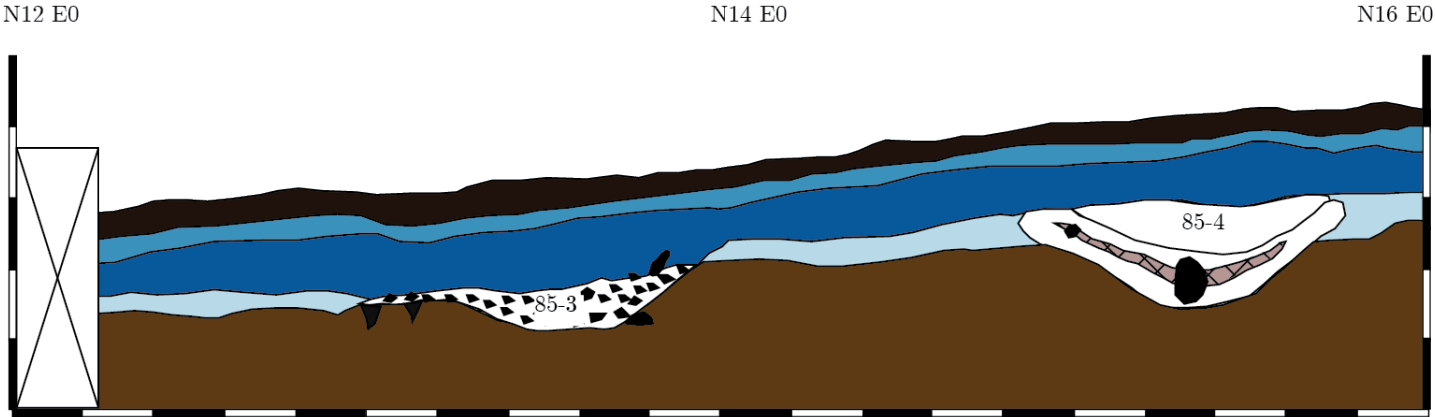


Figure E.28: Olson (Site 17.13) west wall profile photo N8E0 to N10E0. Photo courtesy of Spiess (2017a).



Figure E.29: Olson (Site 17.13) west wall profile N10E0 to N12E0. Photo courtesy of Spiess (2017a).

Olson Site West Wall (4)



Scale



Notes: Feature 85-3 contained dark soil, charcoal, ceramics, large rocks and FCR. This feature was interpreted as a house wall because of a line of postmolds.
Feature 85-4 contained charcoal, brownish orange soil, and produced rocks from a great depth.

Legend

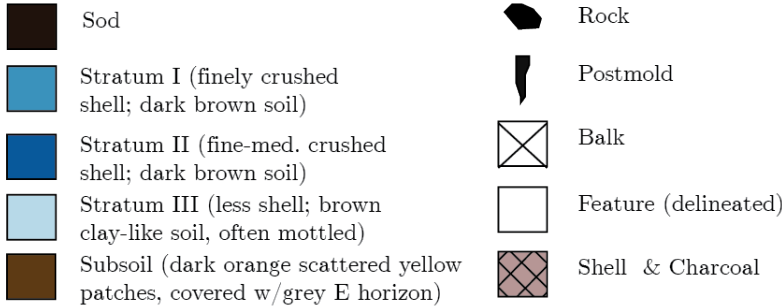


Figure E.30: Redrafted Olson (Site 17.13) west (4) wall profile. Original profile courtesy of Spiess (2017a).

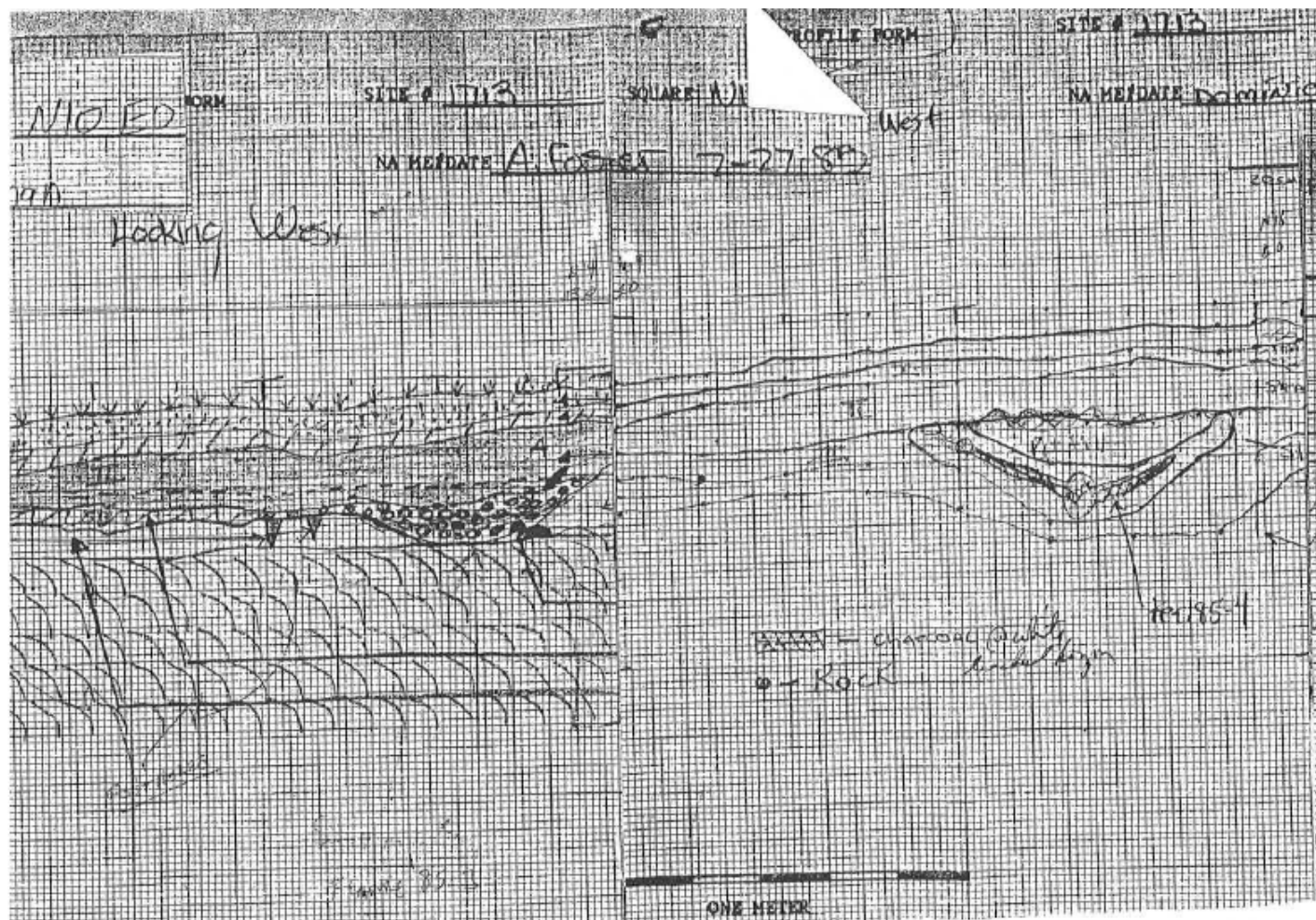


Figure E.31: Olson (Site 17.13) original west (4) wall profile. Profile courtesy of Spiess (2017a).



Figure E.32: Olson (Site 17.13) west wall profile photo N12E0 to N14E0. Photo courtesy of Spiess (2017a).



Figure E.33: Olson (Site 17.13) west wall profile photo N14E0 to N16E0. Photo courtesy of Spiess (2017a).



Figure E.34: Olson (Site 17.13) west wall profile photo N14E0 to N16E0. Photo courtesy of Spiess (2017a).

Olson Site West Wall (5)

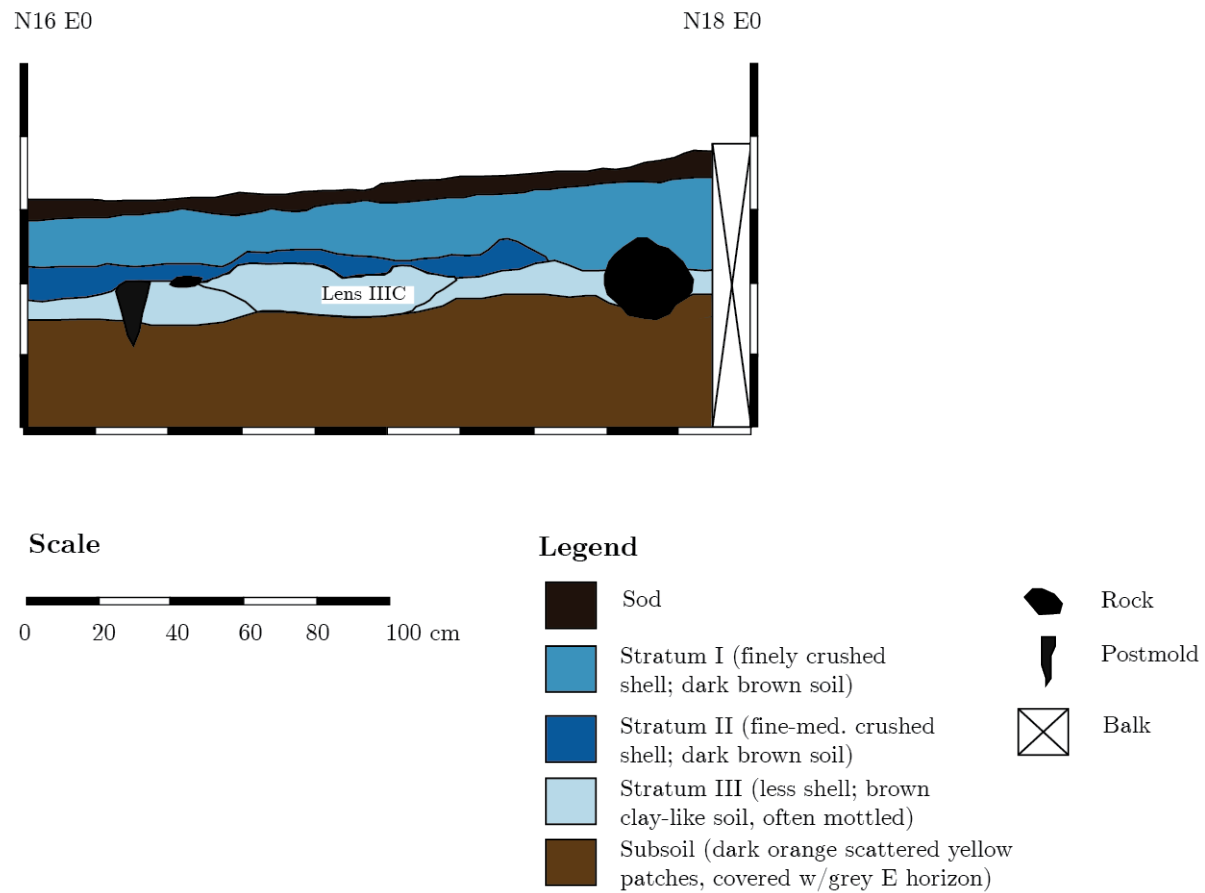


Figure E.35: Redrafted Olson (Site 17.13) west (5) wall profile. Original profile courtesy of Spiess (2017a).

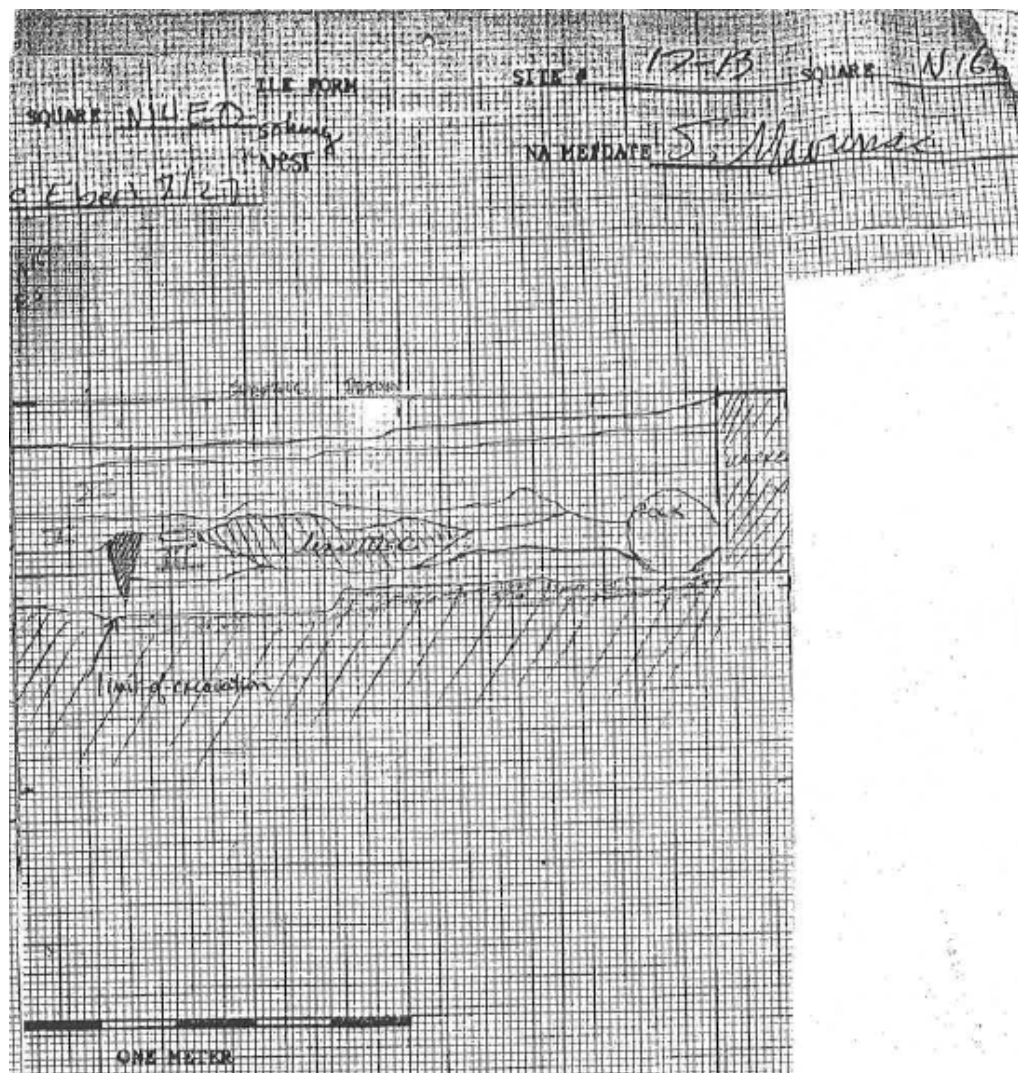


Figure E.36: Olson (Site 17.13) original west (5) wall profile. Profile courtesy of Spiess (2017a).



Figure E.37: Olson (Site 17.13) west wall profile photo N16E0 to N18E0. Photo courtesy of Spiess (2017a).

E.4 Fernald Point (Site 43.24) Archaeological Profiles and Photos



Figure E.38: Fernald Point (Site 43.24) 1977 photo (1) of excavation area 50W-55W. Photo courtesy of Sanger (2008)).



Figure E.39: Fernald Point (Site 43.24) 1977 photo (2) of excavation area 50W-55W. Photo courtesy of Sanger (2008))



Figure E.40: Fernald Point (Site 43.24) photo of surficial geologic materials underlying the shell midden. This photo shows the glacial till underlying the shell midden (courtesy of Sanger (2008)).

E.5 Tranquility Farm (Site 44.12a) Archaeological Profiles and Photos

Table E.1: Tranquility Farm (Site 44.12a) archaeological wall profiles. Note that archaeological profiles are named for the location of the upper left corner of the unit.

Date	Location	Wall
9/15/95	N96W97	North
9/15/95	N96W93	North
8/9/12	N94W85	East
8/2012	N104W90	West
8/9/13	N106W107	East
8/8/13	N106W107	South

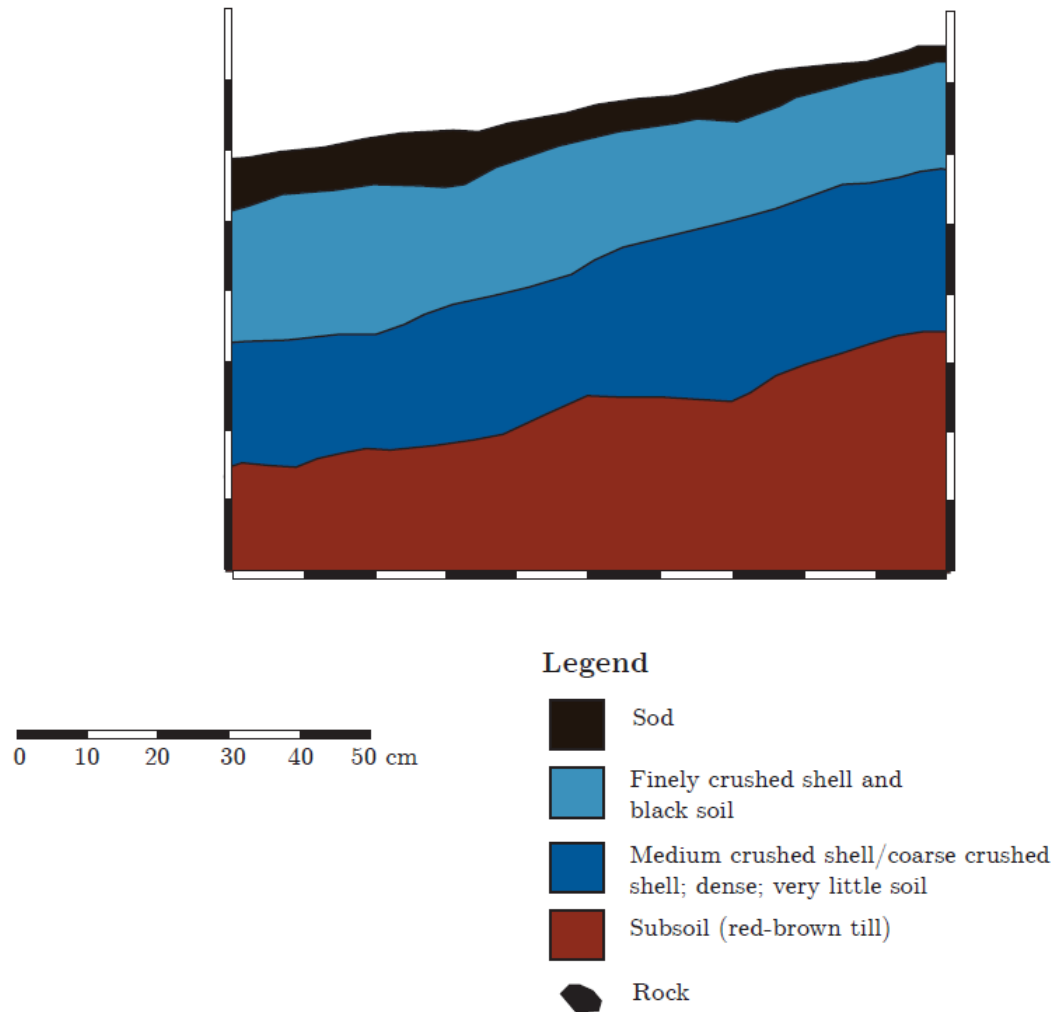


Figure E.41: Redrafted Tranquility Farm (Site 44.12a) N96W97 north wall profile. Original profile courtesy of Spiess (2017a).

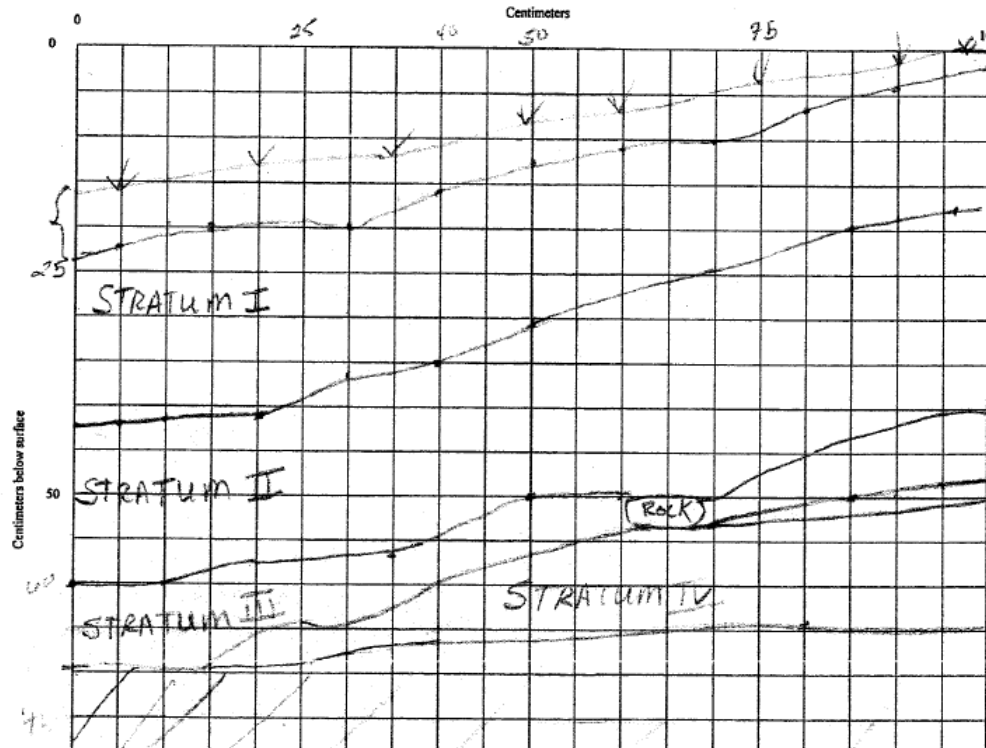
9/15/95

Robert Abbe Museum Field School
Archaeological Testing
Test Unit Wall Profile

N 96 W 97

Tranquility Farm - Site 44.12A
Test Unit(s) N 96 W 97
Face: ~~N~~ E S W

North Wall -
Notes:



I. fingered shell -
Dark loamy soil

II. Large shell most
complete clam
very little soil

II a. very shallow lens
of hoamy Dark Soil
lens - not even a
cm deep

III. Albic lens -
disappearing into
new wall

IV Red Brown B_s
2 Pebbles

Figure E.42: Tranquility Farm (Site 44.12a) original N96W97 north wall profile. Original profile courtesy of Spiess (2017a).

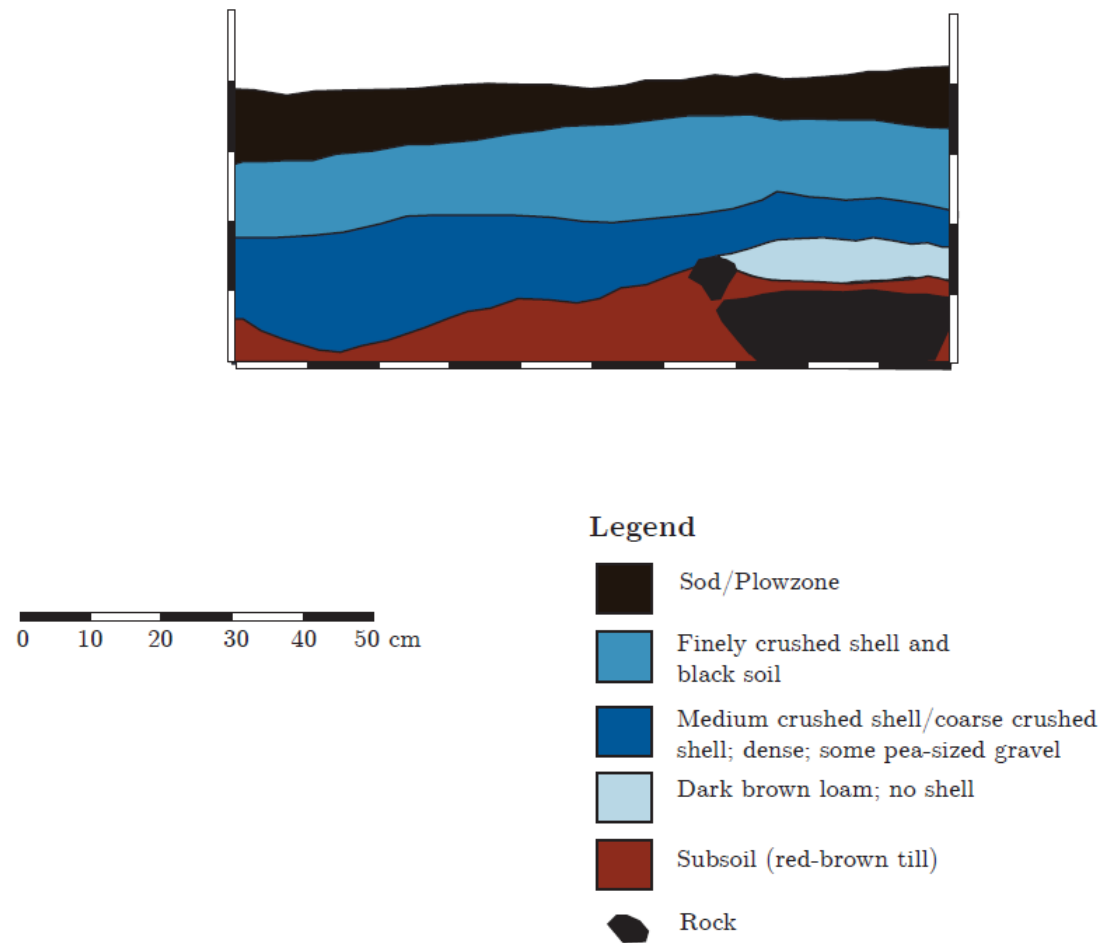
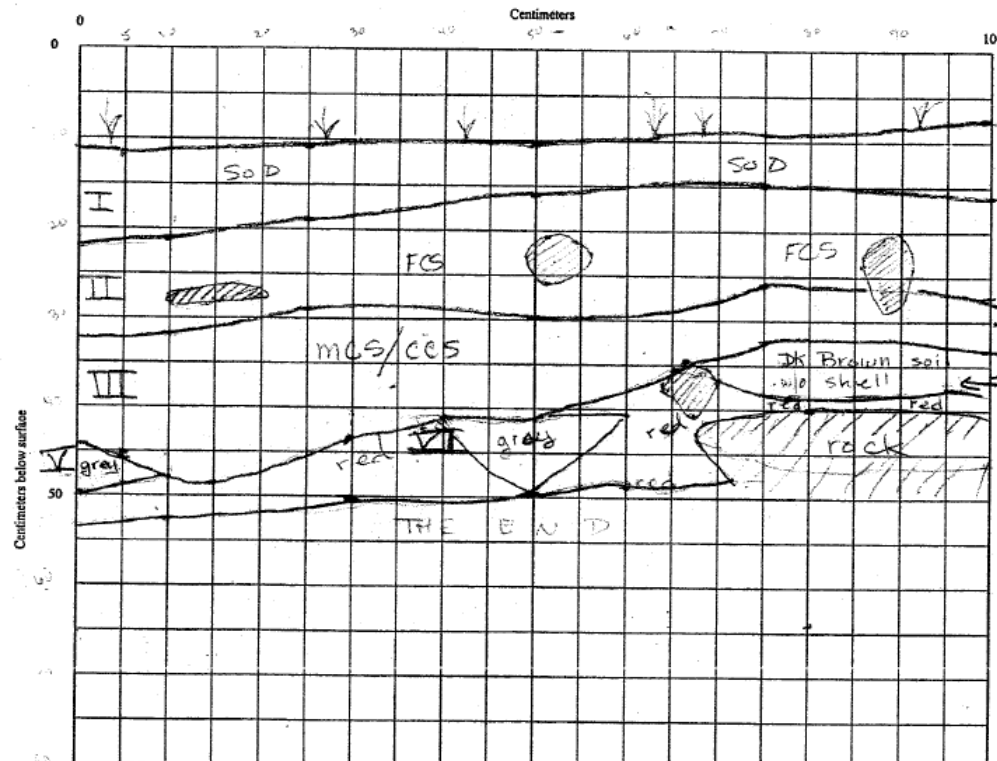


Figure E.43: Redrafted Tranquility Farm (Site 44.12a) N96W93 north wall profile. Original profile courtesy of Spiess (2017a).

Robert Abbe Museum Field School
Archaeological Testing
Test Unit Wall Profile

Tranquility Farm - Site 44.12A
Test Unit(s) N 96 W 93
Face: N ☒ E ☐ S ☐ W ☐



Notes:

- I Sod - fine brown loam
- II FCS High Dens. Dk brown loam silty fine
- III MCS/CCS - Fine dk brown loam little bits of pea gravel. High density shell
- IV DK brown loam no shell - fine texture (A horizon)
- V grey albic loam (E horizon)
- VI red fine loam (B horizon)

Figure E.44: Tranquility Farm (Site 44.12a) original N96W93 north wall profile. Profile courtesy of Spiess (2017a).

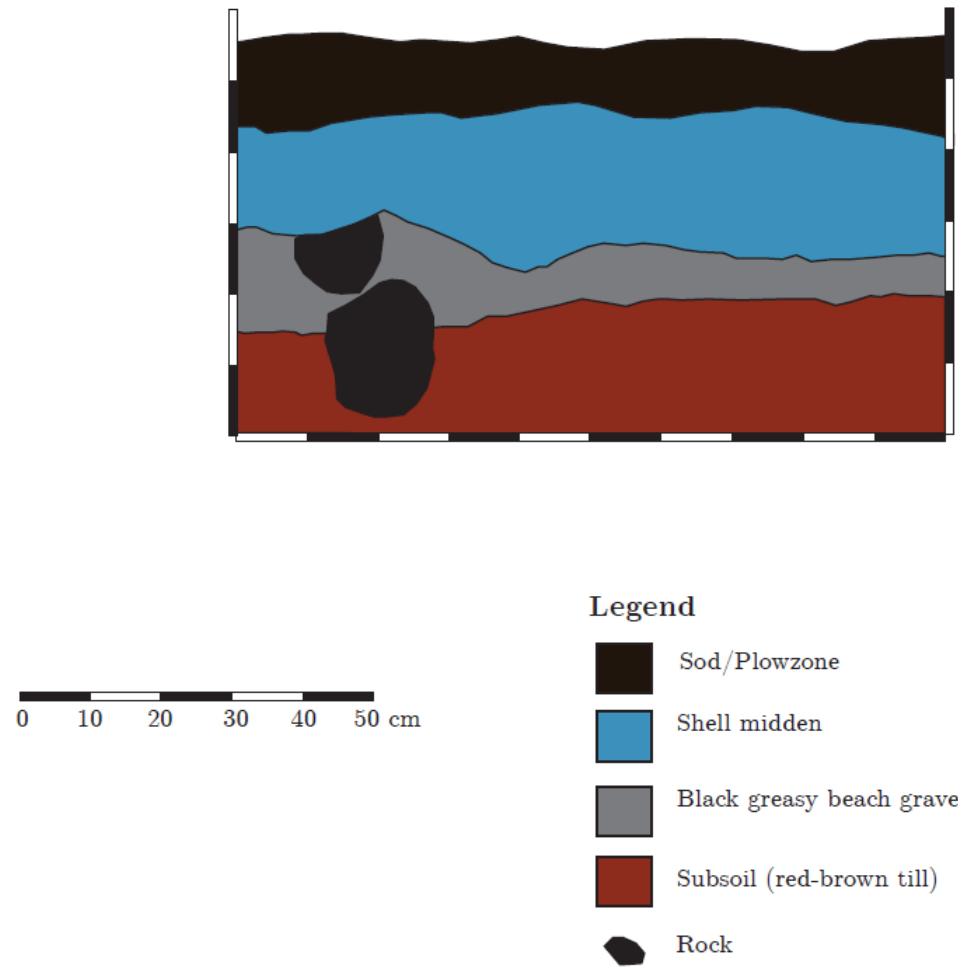


Figure E.45: Redrafted Tranquility Farm (Site 44.12a) N94W85 east wall profile. Original profile courtesy of Spiess (2017a).

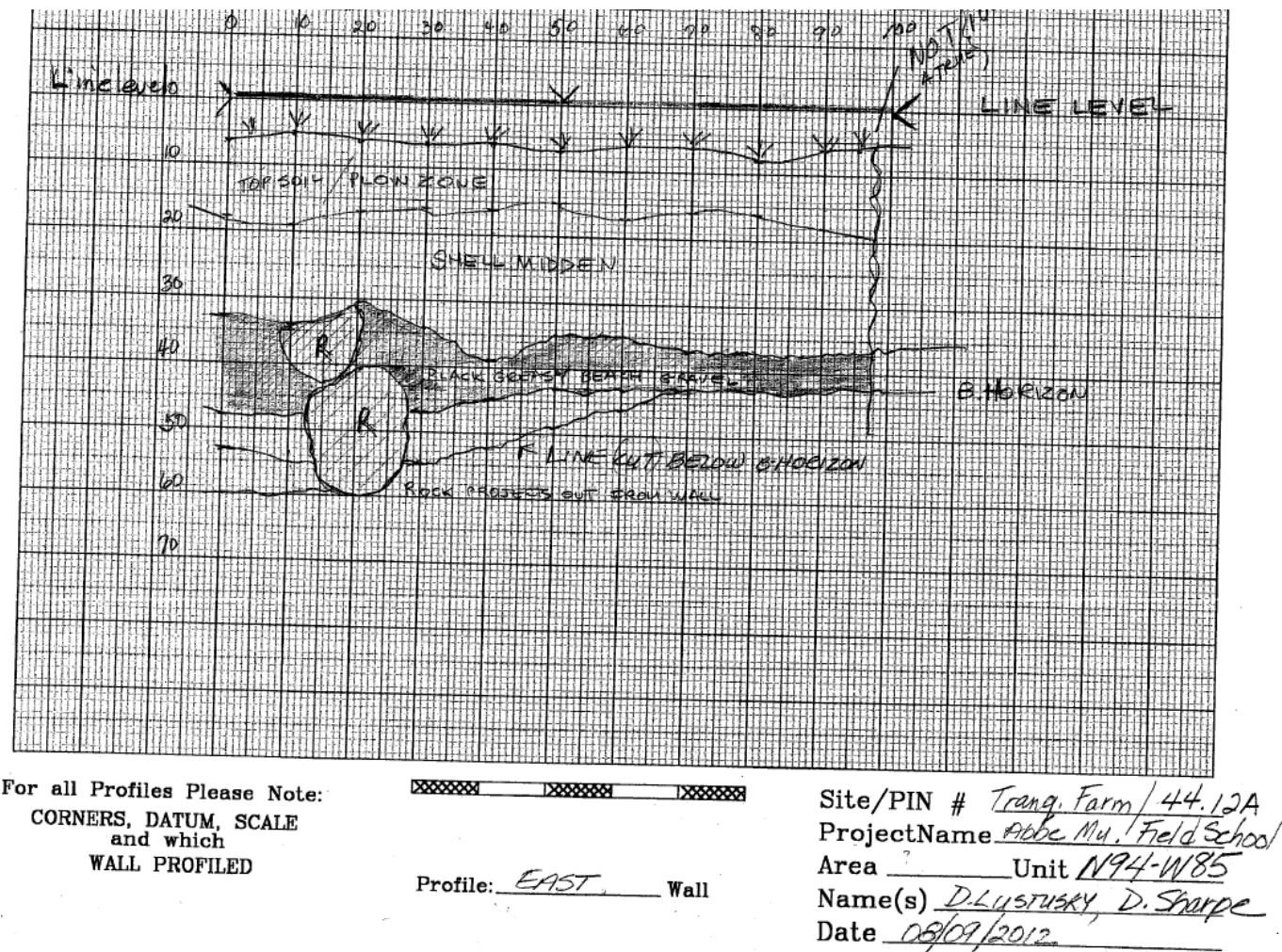


Figure E.46: Tranquility Farm (Site 44.12a) original N94W85 east wall profile. Profile courtesy of Spiess (2017a).

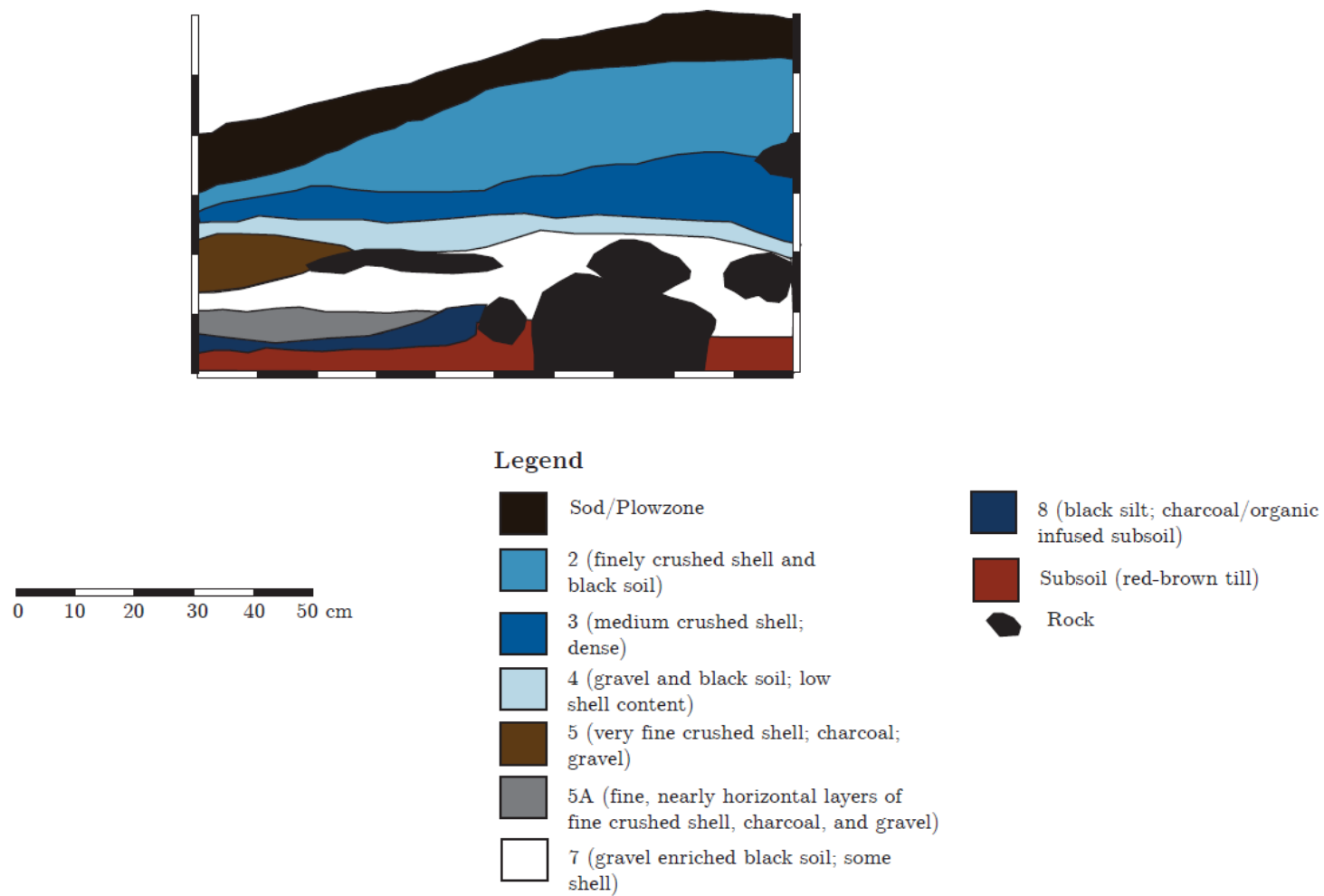


Figure E.47: Redrafted Tranquility Farm (Site 44.12a) N104W90 west wall profile. Original profile courtesy of Spiess (2017a).

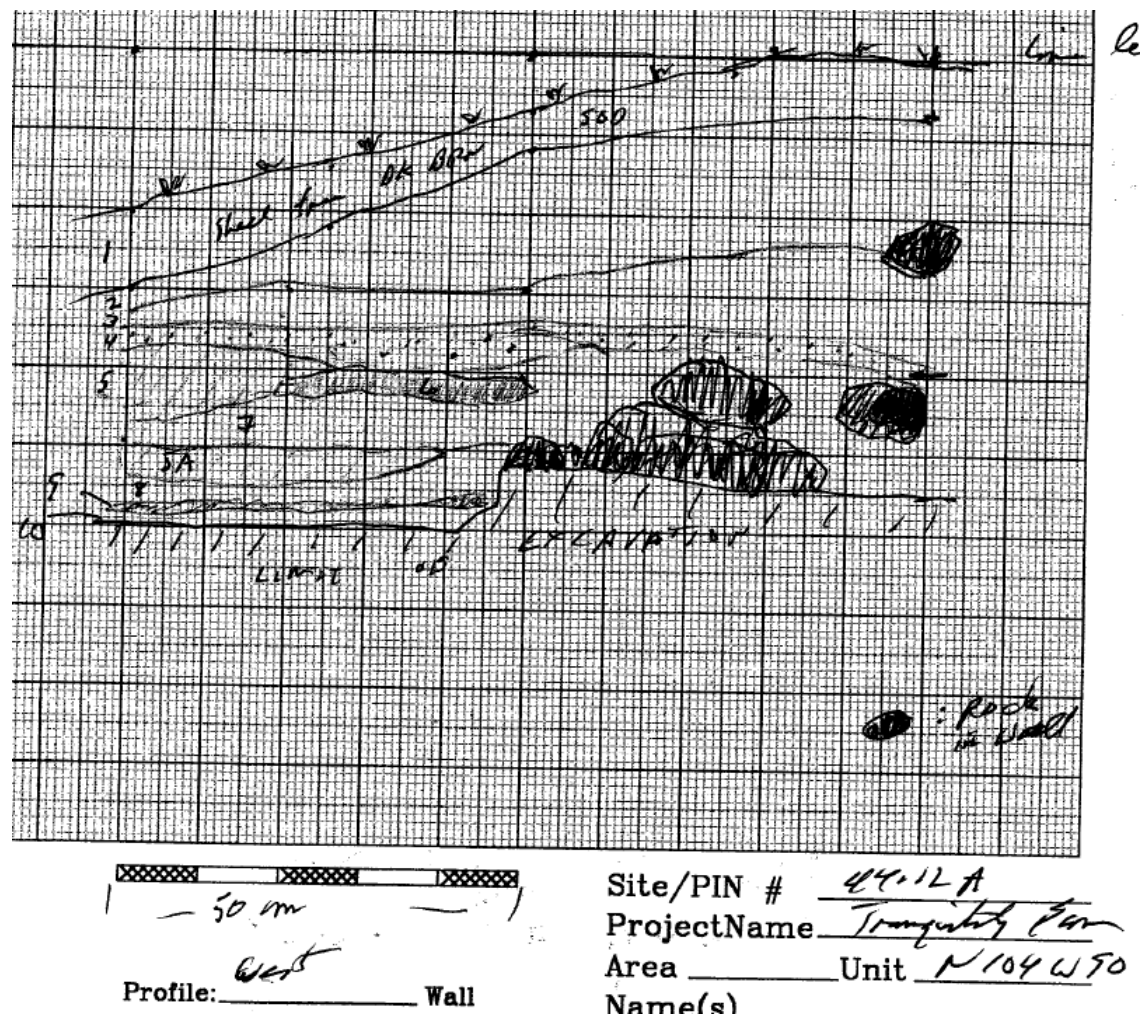


Figure E.48: Tranquility Farm (Site 44.12a) original N104W90 west wall profile. Profile courtesy of Spiess (2017a).

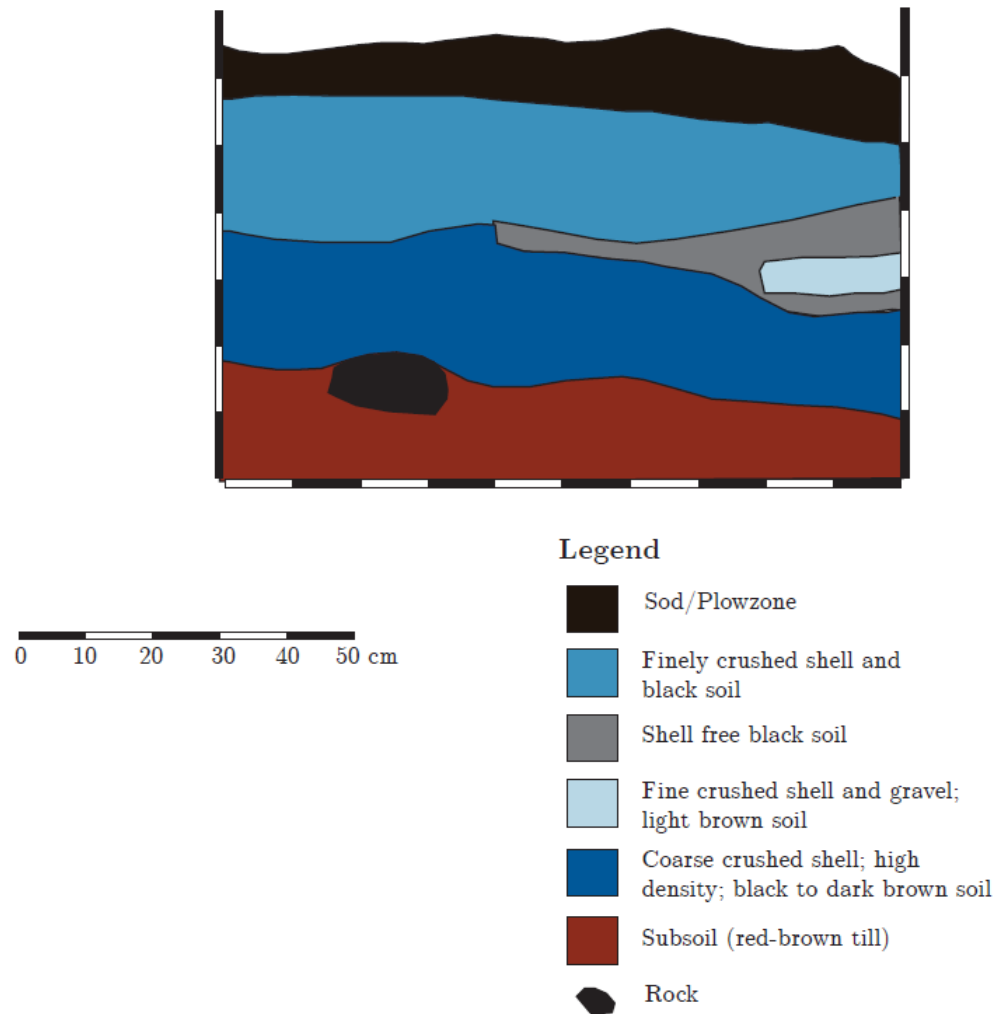


Figure E.49: Redrafted Tranquility Farm (Site 44.12a) N106W107 east wall profile. Original profile courtesy of Spiess (2017a).

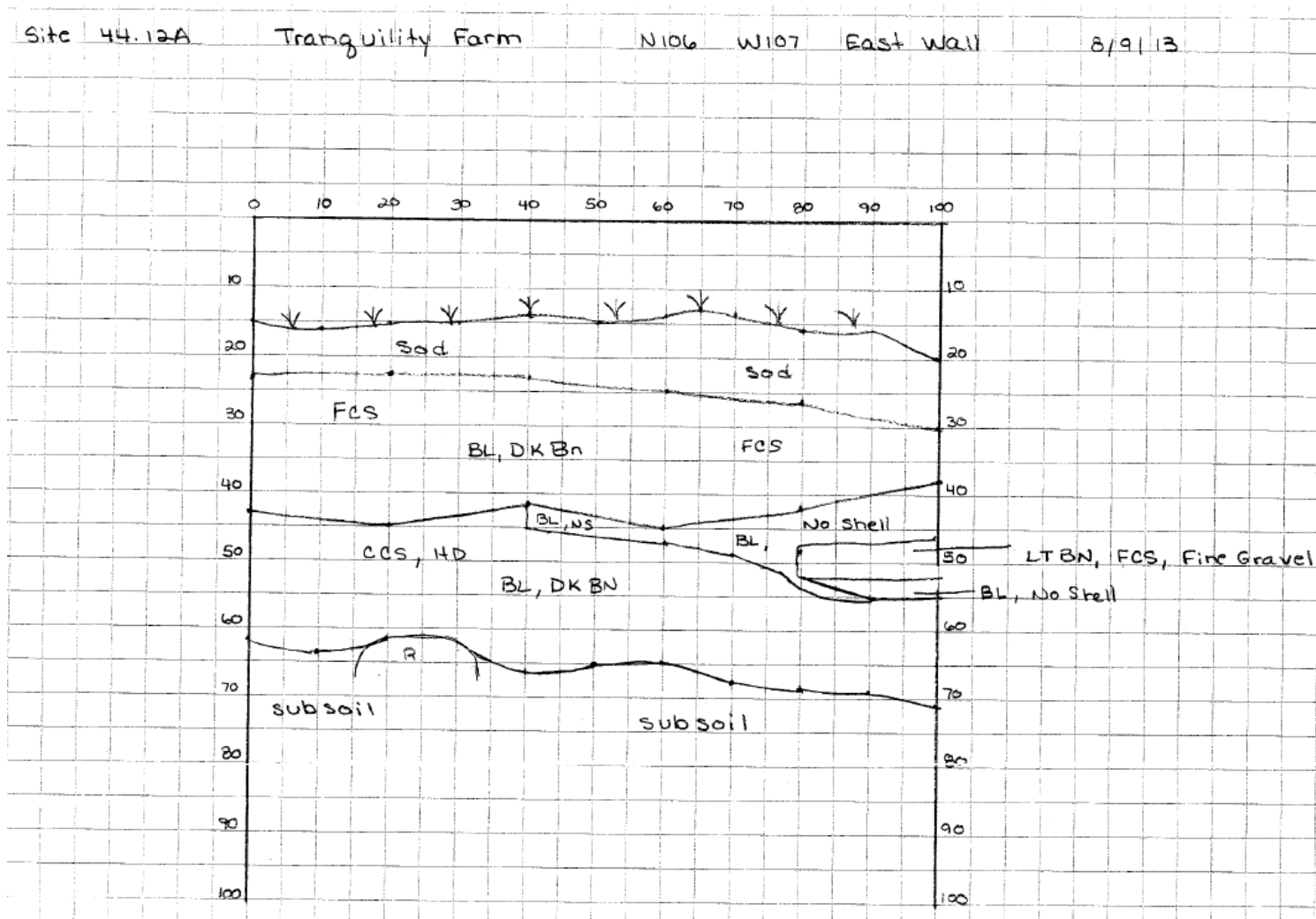


Figure E.50: Tranquility Farm (Site 44.12a) original N106W107 east wall profile. Profile courtesy of Spiess (2017a).

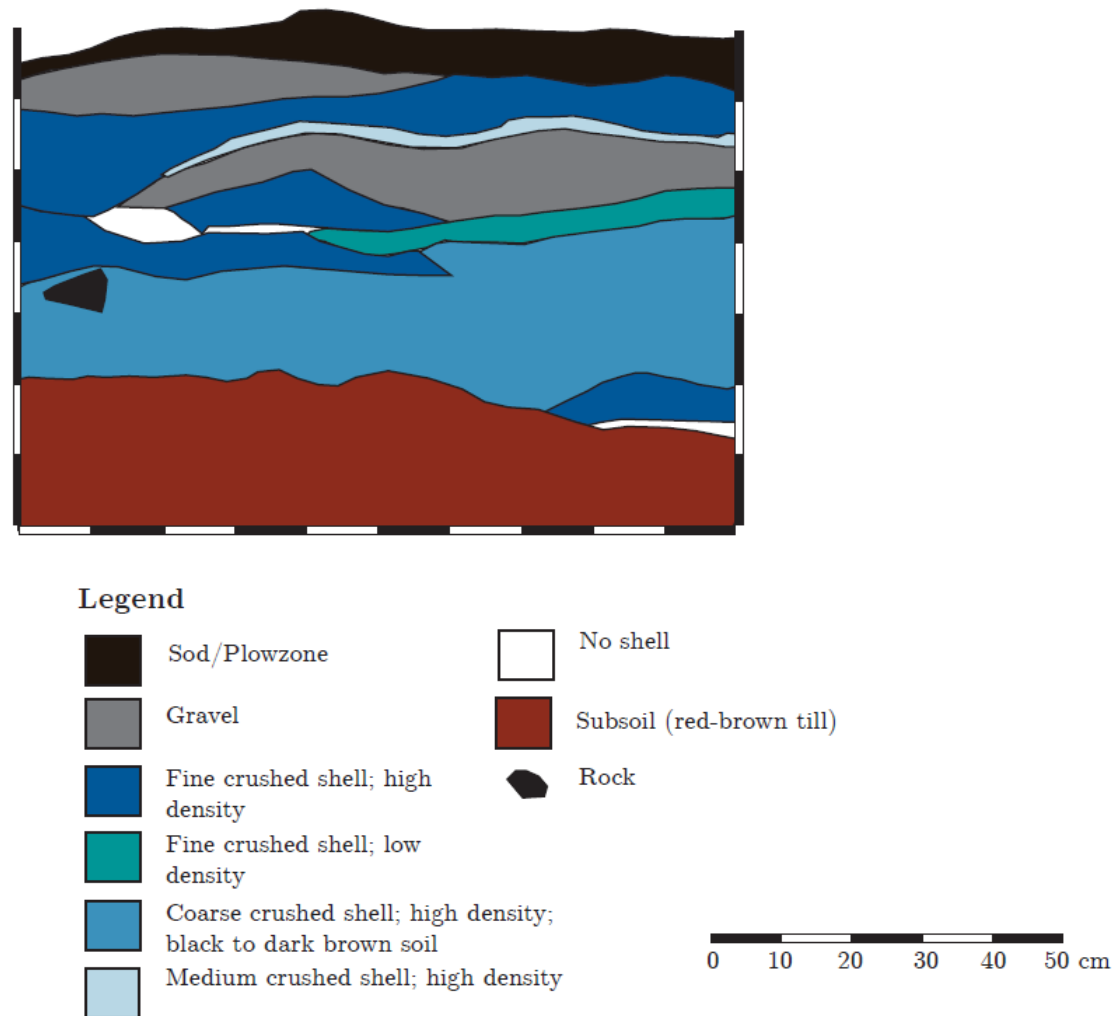


Figure E.51: Redrafted Tranquility Farm (Site 44.12a) N106W107 south wall profile. Original profile courtesy of Spiess (2017a).

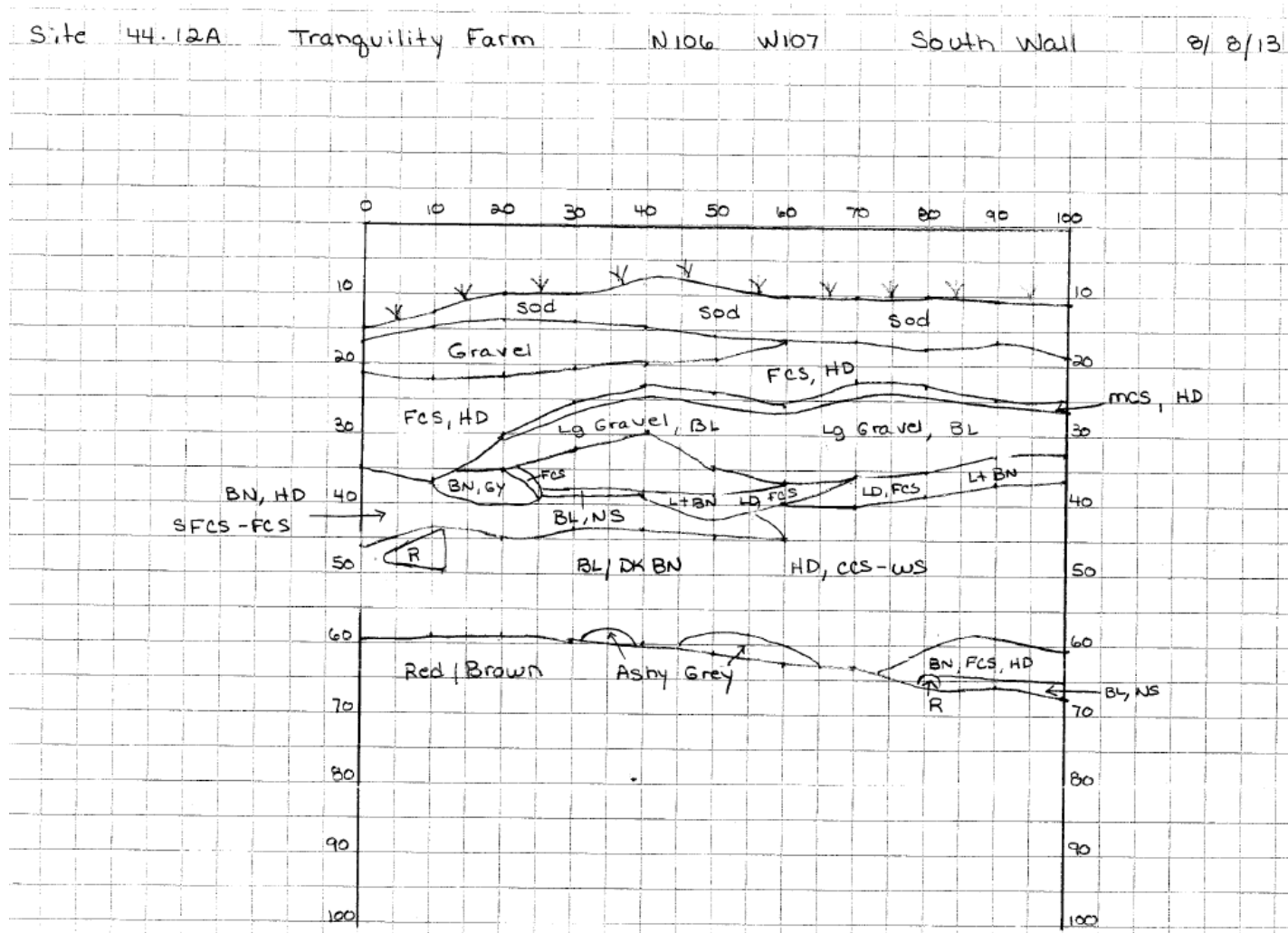


Figure E.52: Tranquility Farm (Site 44.12a) original N106W107 south wall profile. Original profile courtesy of Spiess (2017a).



Figure E.53: Tranquility Farm (Site 44.12a) N105W104 south wall photo. Photo courtesy of Spiess (2017a).



Figure E.54: Tranquility Farm (Site 44.12a) N105W104 east wall photo. Photo courtesy of Spiess (2017a).



Figure E.55: Tranquility Farm (Site 44.12a) N105W104 photo view looking northeast. Photo courtesy of Spiess (2017a).



Figure E.56: Tranquility Farm (Site 44.12a) N105W104 west wall photo. Photo courtesy of Spiess (2017a).



Figure E.57: Tranquility Farm (Site 44.12a) N105W106 north wall. Photo courtesy of Spiess (2017a).



Figure E.58: Tranquility Farm (Site 44.12a) N105W106 west wall photo. Photo courtesy of Spiess (2017a).



Figure E.59: Tranquility Farm (Site 44.12a) N105W106 south wall photo. Photo courtesy of Spiess (2017a).



Figure E.60: Tranquility Farm (Site 44.12a) N105W106 east wall photo. Photo courtesy of Spiess (2017a).



Figure E.61: Tranquility Farm (Site 44.12a) N106W104 west wall photo. Photo courtesy of Spiess (2017a).



Figure E.62: Tranquility Farm (Site 44.12a) N106W107 north wall photo. Photo courtesy of Spiess (2017a).



Figure E.63: Tranquility Farm (Site 44.12a) N106W107 and N105W106 photo view southeast. Photo courtesy of Spiess (2017a).



Figure E.64: Tranquility Farm (Site 44.12a) N106W108 south wall photo. Photo courtesy of Spiess (2017a).

Appendix F

GROUND-TRUTH LOCATION INFORMATION

F.1 University of New England (Site 5.06) Ground-truth Location Information

Table F.1: University of New England (Site 5.06) archaeological profile locations with respect to GPR profiles.

Map ID	GPR Profile ID	Location on GPR Transect	Grid Location
1	32	last 1 m	494E499N
2	27	-1-0 m	500E494N
3	52rev	0.5-2.5 m	504E491N

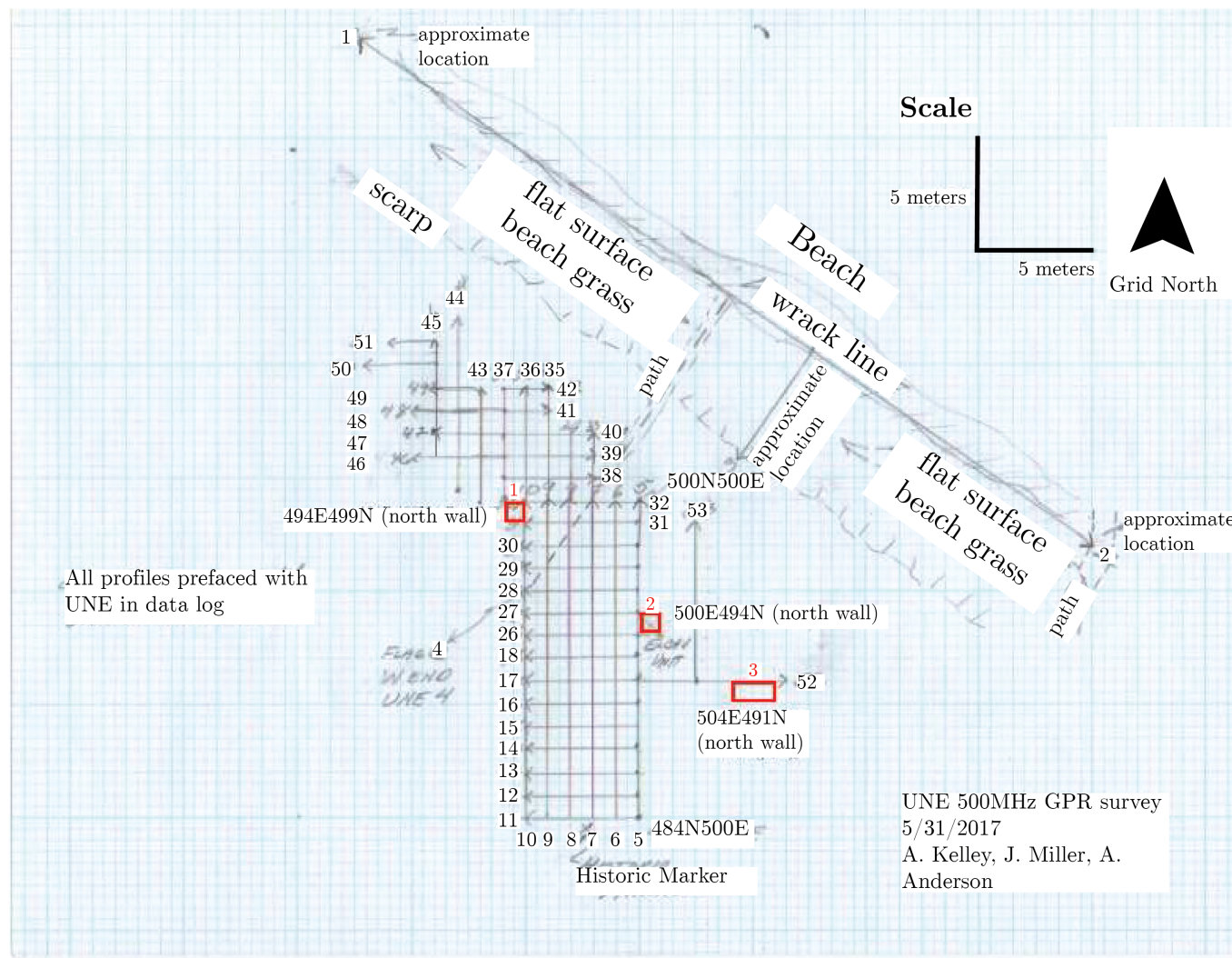


Figure F.1: Map of ground-truth locations and 500 MHz GPR survey at the University of New England site (Site 5.06). Archaeological wall profiles with associated photos are labeled numerically, and the test units are outlined in red.

F.2 Long Island North (Site 15.95) Ground-truth Location Information

Table F.2: Long Island North (Site 15.95) archaeological profile locations with respect to GPR profiles.

Map ID	Location	Wall	GPR Profile Number	Distance From GPR Transect	Profile Location on GPR Transect
1	S23E8	East	2	0.5 m west	3-4 m
2	S23E8	West	4	0.5 m east	3-4 m
1	S22E8	East	2	0.5 m west	4-5 m
4	S22E7	West	5	0.5 m east	4-5 m
3	S22E7	South	17	on profile	1.5-2.5 m
4	S21E7	West	5	0.5 m east	5-6 m
4	S20E7	West	5	0.5 m east	6-7 m
4	S19E7	West	5	0.5 m east	7-8 m
5	S19E7	North	22	on profile	1.5-2.5 m
5	S19E8	North	22	on profile	0.5-1.5 m
5	S19E9	North	22	on profile	-0.5-1.5
7	S17E8	West	4	0.5 m east	9-10 m
6	S17E8	South	23	on profile	0.5-1.5
8	S4E8	West	48	0.5 m east	2-3 m
8	S3E8	West	48	0.5 m east	3-4 m
10	S2E7	North	40	on profile	1.5-2.5 m
9	S2E7	South	39	on profile	1.5-2.5 m
12	S2W3	West	56	off profiles 1.5 m west	4-5 m
11	S2W3	South	39	off profiles but on transect	10.5-11.5
13	N3E11	West	46	off profile 1.5 m to east	8-9 m
15	N4E10	West	46	0.5 m east	9-10 m
14	N4E10	South	44	close on transect	-1.5-(-0.5)

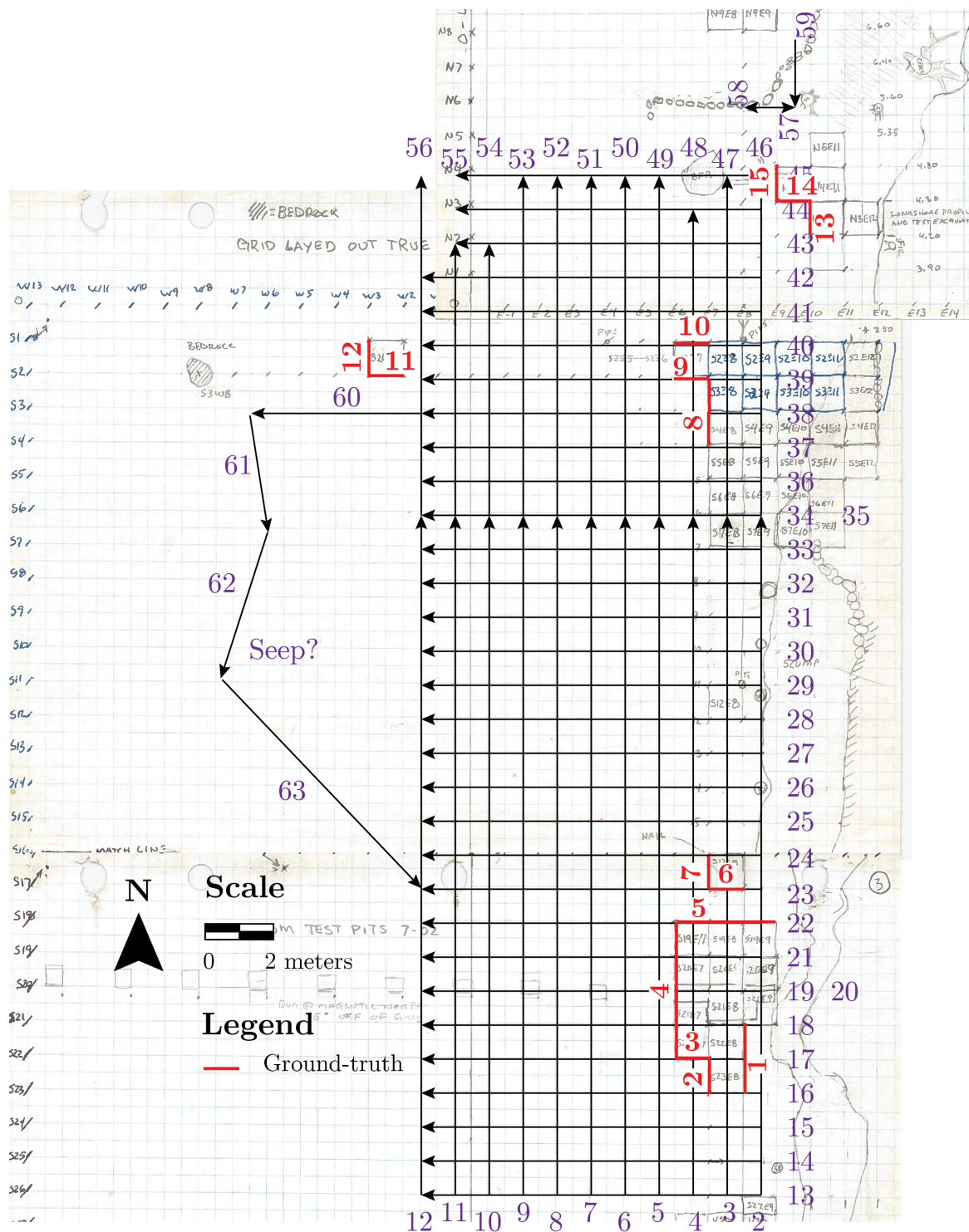


Figure F.2: Long Island North (Site 15.95) ground-truth location map under 500 MHz GPR map (1). Basemap courtesy of Doyle (2017)). Note that profile 60-63 are not drawn to scale, and the transect locations are approximate. The start of profile 60 and the end of profile 63 are certain, and represented on the map.

F.3 Damariscotta Oyster Farm (Site 26.15) Ground-truth Location Information

Table F.3: Damariscotta Oyster Farm (Site 26.15) archaeological profile location with respect to GPR profiles

Location	Wall	GPR Profile ID	Distance from GPR Transect	Location on GPR Transect
tip of point	north	6	on profile	4.6-5.6 m
tip of point	north	Long_L2 (D to F)	on profile	30.4-31.4 m

F.4 Olson (Site 17.13) Ground-truth Location Information

Table F.4: Olson (Site 17.13) locations of stratigraphic note data with respect to GPR profiles.

Map ID	GPR Profile ID	Location on GPR Transect	Grid Location
1	109	8 m	N12E16
2	134	2 m	N8E16
3	134	6 m	N4E16
4	164	0 m	N0E24
5	272	6 m	N0W36
6	272	18 m	N0W48
7	near 259	6 m	N4W36
8	near 259	4 m	N6W36
9	near 259	2 m	N8W36
*10	242	10 m	N0W28
*11	242	6 m	N4W28
12	242	2 m	N8W28
13	210	0 m	N10W12

Table F.5: Olson (Site 17.13) archaeological profile locations with respect to GPR profiles.

Map ID	Location	Wall	GPR Profile	Distance from GPR Transect	Location on GPR Transect
A	N4E2 to N0E2	east	22	on profile	4-0 m
B	N8E2 to N4E2	east	22	on profile	8-4 m
C	N12E2 to N8E2	east	71/22	on profile	2-0 m / 8-10 m
D	N16E2 to N12E2	east	71	on profile	4-2 m
E	N0E0 to N4E0	west	26reversed	on profile	0-4 m
F	N4E0 to N8E0	west	26reversed	on profile	4-8 m
G	N8E0 to N12E0	west	26reversed /73flipped	on profile	8-10 m / 0-2 m
H	N12E0 to N16E0	west	73flipped	on profile	2-6 m
I	N16E0 to N18E0	west	73flipped	on profile	6-8 m

Table F.6: Olson (Site 17.13) archaeological profile photo locations with respect to GPR profiles.

Map ID	Location	Wall	GPR Profile	Distance from GPR Transect	Location on GPR Transect
a	N0E0 to N2E0	west	26reversed	on profile	0-2 m
b	N2E0 to N4E0	west	26reversed	on profile	2-4 m
c	N4E0 to N6E0	west	26reversed	on profile	4-6 m
d	N6E0 to N8E0	west	26reversed	on profile	6-8 m
e	N8E0 to N10E0	west	26reversed	on profile	8-10 m
f	N10E0 to N12E0	west	73flipped	on profile	0-2 m
g	N12E0 to N14E0	west	73flipped	on profile	2-4 m
h	N14E0 to N16E0	west	73flipped	on profile	4-6 m
i	N16E0 to N18E0	west	73flipped	on profile	6-8 m

Olson Site GPR Grid

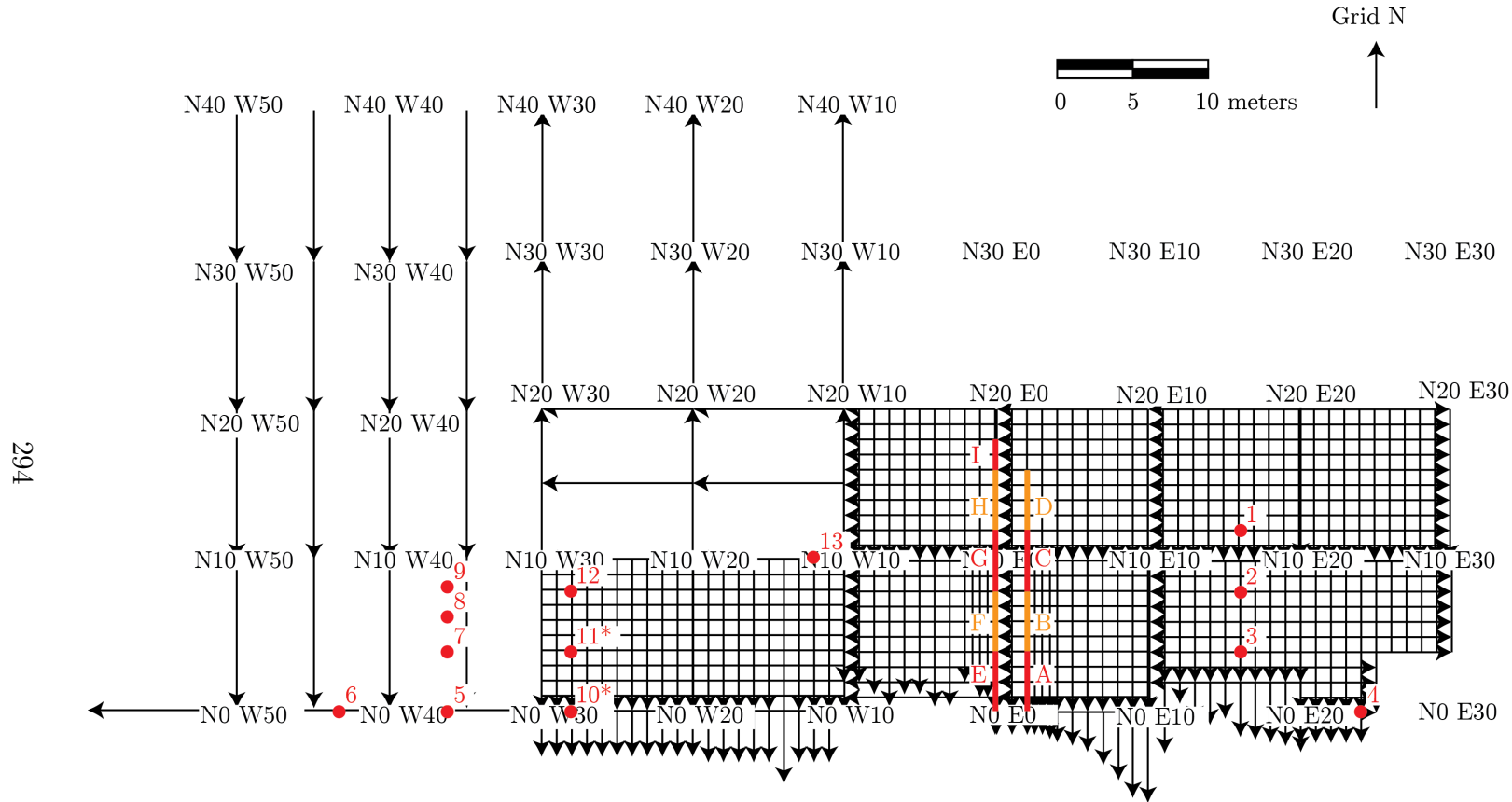


Figure F.4: Map of ground-truth locations overlain on the 500 MHz GPR survey at the Olson site (Site 17.13). Red dots with numeric labels represent locations of ground-truth information from stratigraphic notes, and two trench walls are shown by the lines labeled A-I.

F.5 Fernald Point (Site 43.24) Ground-truth Location Information

Table F.7: Fernald Point (Site 43.24) archaeological profile locations with respect to GPR profiles.

Map ID	Location	Wall	GPR Profile Number	Distance from GPR Transect	Profile Location on GPR Transect
A	8W (column 1)	south	12	1 m north	2-4 m
B	64S (column 2)	west	75	3 m east	5-7 m
B	64S (column 2)	west	76	2 m west	5-7 m
C	9SS (column 3)	west	17	3 m west	11-13 m
C	9SS (column 3)	west	18	2 m east	11-13 m
D	45O (column 4)	west	42	1 m east	9-10 m
D	45O (column 4)	west	120	on profile	9-10 m
D	45O (column 4)	west	119	1 m west	9-10 m

Table F.8: Fernald Point (Site 43.24) archaeological profile locations with respect to GPR profiles.

Map ID	Location	Wall	GPR Profile	Distance from GPR Transect	Location on GPR Transect
1	12W to 13W	north	12	2 m north	6-7 m
1	12W to 13W	north	13	3 m south	6-7 m
2	13Y to 12Y	south	12	on profile	6-7 m
3	13W to 13Y	east	8	2 m east	0-2 m
3	13W to 13Y	east	9	3 m west	0-2 m
4	14W to 16W	north	12	2 m north	8-10 m
4	14W to 16W	north	13	3 m south	8-10 m

Table F.8: Continued

Map ID	Location	Wall	GPR Profile	Distance from GPR Transect	Location on GPR Transect
5	14Y to 14W	west	8	2 m west	0-2 m
5	14Y to 14W	west	9	3 m east	0-2 m
6	15Y to 14Y	south	12	on profile	8-9 m
7	30L to 31L	north	45	3 m north	4-5 m
7	30L to 31L	north	46	2 m south	4-5 m
8	30M to 30L	west	11	4 m east	12-13 m
8	30M to 30L	west	39	1 m west	12-13 m
9	35Z to 37Z	north	12	1 m south	9-11 m
10	35Z	west	106	1 m west	1-2 m
11	45I to 45H	west	41	4 m east	16-17 m
11	45I to 45H	west	42	1 m west	16-17 m
12	45K to 45J	west	41	4 m east	14-15 m
12	45K to 45J	west	42	1 m west	14-15 m
13	45M to 45L	west	41	4 m east	12-13 m
13	45M to 45L	west	42	1 m south	12-13 m
14	45P to 47P	north	45	1 m south	19-20 m
14	45P to 47P	north	69	1 m south	0-1 m
15	45P	east	42	1 m east	8-9 m
15	45P	east	73	4 m west	8-9 m
16	45R to 45P	west	41	4 m east	7-9 m
16	45R to 45P	west	42	1 m west	7-9 m
17	45T to 45R	west	41	4 m east	5-7 m
17	45T to 45R	west	42	1 m west	5-7 m

Table F.8: Continued

Map ID	Location	Wall	GPR Profile	Distance from GPR Transect	Location on GPR Transect
18	45V to 45T	west	41	4 m east	3-5 m
18	45V to 45T	west	42	1 m west	3-5 m
19	45X to 45V	west	41	4 m east	1-3 m
19	45X to 45V	west	42	1 m west	1-3 m
20	50W to 52W	north	67	2 m north	4-6 m
20	50W to 52W	north	68	3 m south	4-6 m
21	50X to 50W	west	42	4 m east	1-2 m
21	50X to 50W	west	73	1 m west	1-2 m
22	52U to 53U	north	67	4 m north	6-7 m
22	52U to 53U	north	68	1 m south	6-7 m
23	52V to 53V	north	67	3 m north	6-7 m
23	52V to 53V	north	68	2 m south	6-7 m
24	52W to 52V	west	73	1 m east	2-3 m
24	52W to 52V	west	74	4 m west	2-3 m
25	52W to 52X	east	73	1 m east	1-2 m
25	52W to 52X	east	74	4 m west	1-2 m
26	52W to 54W	north	67	2 m north	6-8 m
26	52W to 54W	north	68	3 m south	6-8 m
27	52X to 50X	south	67	1 m north	4-6 m
27	52X to 50X	south	68	4 m south	4-6 m
28	53U to 53W	east	73	2 m east	2-4 m
28	53U to 53W	east	74	3 m west	2-4 m
29	54W to 55W	north	67	2 m north	8-9 m

Table F.8: Continued

Map ID	Location	Wall	GPR Profile	Distance from GPR Transect	Location on GPR Transect
29	54W to 55W	north	68	3 m south	8-9 m
30	54X to 54W	west	73	3 m east	1-2 m
30	54X to 54W	west	74	2 m west	1-2 m
31	55U to 53V	south	67	3.5m north	3-4 m
31	55U to 53V	south	68	1.5m south	3-4 m
32	64R to 64S	east	75	4 m east	6-7 m
32	64R to 64S	east	76	1 m west	6-7 m
33	64T to 64R	west	75	3 m east	5-7 m
33	64T to 64R	west	76	2 m west	5-7 m
34	65T to 64T	south	68	on profile	18-19 m
35	31WW to 31OO	east	54	on profile	8-9 m
36	31UU to 31WW	east	54	on profile	9-10 m
37	30WW to 30VV	west	54	1 m west	8-9 m
37	30WW to 30VV	west	21	4 m east	8-9 m
38	45N to 45P	west	41	4 m east	9-11 m
38	45N to 45P	west	42	1 m west	9-11 m

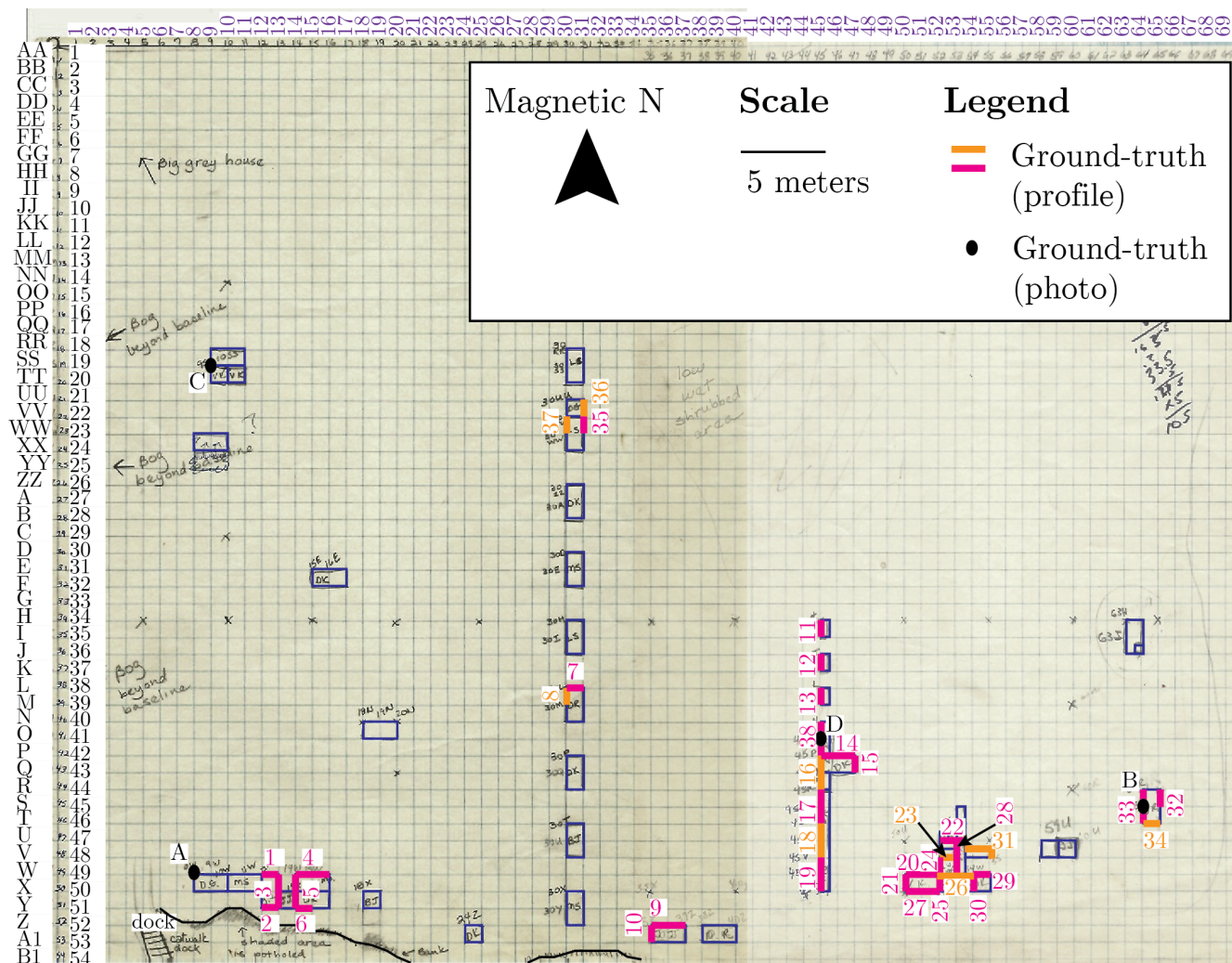


Figure F.5: Fernald Point (Site 43.24) ground-truth location map.

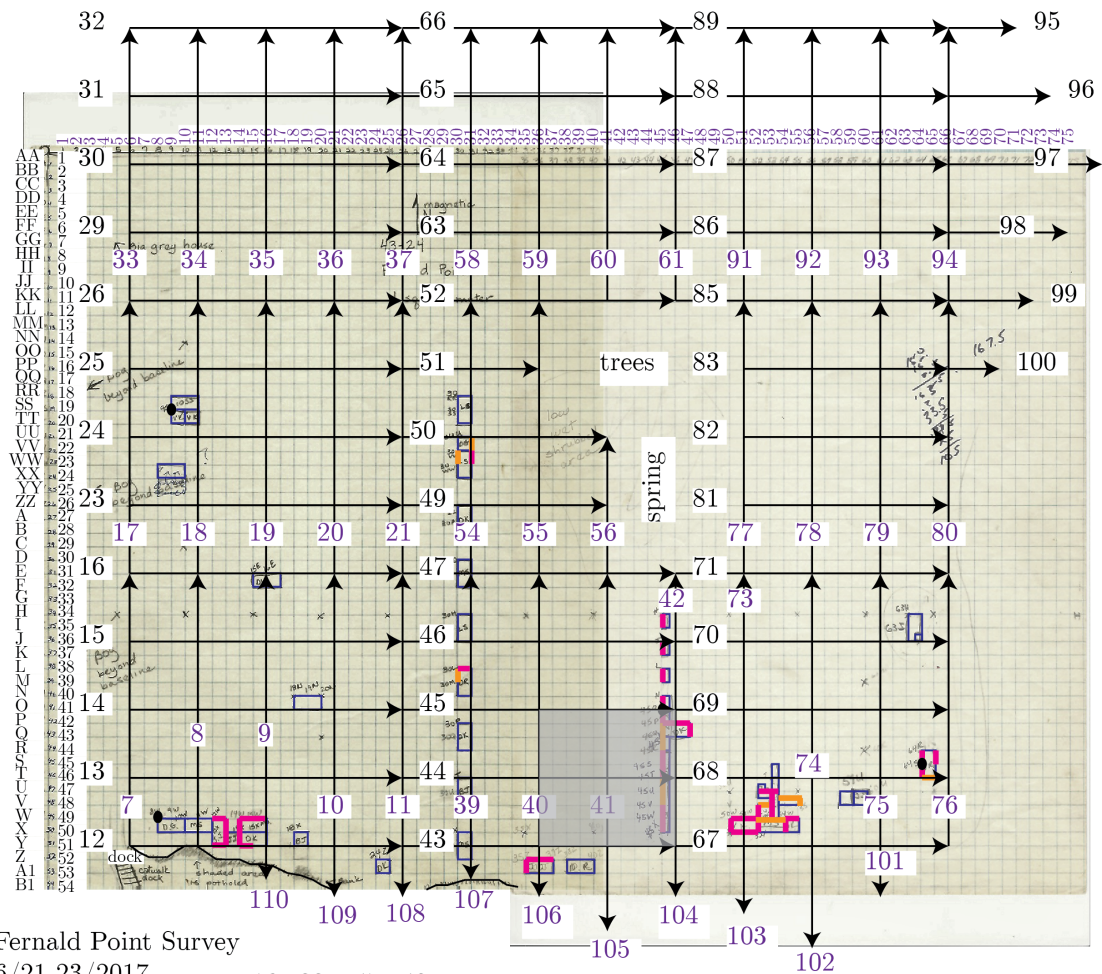


Figure F.6: Unlabeled Fernald Point (Site 43.24) ground-truth location map with the 500 MHz GPR survey transects overlain.

F.6 Tranquility Farm (Site 44.12a) Ground-truth Location Information

Table F.9: Tranquility Farm (Site 44.12a) archaeological profile locations with respect to GPR profiles. Note that archaeological profiles are named for the location of the upper left corner of the unit.

Location	Wall	GPR Profile Number	Distance From GPR Transect	Profile Location on GPR Transect
N96W97	north	80	4 m south	3-4 m
N96W93	north	77 (disturbed)	1 m north	2-3 m
N96W93	north	orth option: 61	2 m west	at 4 m
N94W85	east	61	6 m east	9-10 m
N94W85	east	orth option: 78	1 m south	at 6 m
N104W90	west	60	on profile	6-7 m
N106W107	east	68	1 m west	9-10 m
N106W107	east	24	1 m west	4-5 m
N106W107	east	25	0.5 m west	4-5 m
N106W107	east	26	on profile	4-5 m
N106W107	east	27	0.5 m east	4-5 m
N106W107	south	44 (disturbed)	0.5m south	6-7 m
N106W107	south	45	on profile	3-4 m
N106W107	south	46	0.5 m north	6-7 m
N106W107	south	47	1 m north	6-7 m

Table F.10: Tranquility Farm (Site 44.12a) archaeological wall profile photo locations with respect to GPR profiles. Note that archaeological profiles are named for the location of the upper left corner of the unit.

Location	Wall	GPR Profile Number	Distance From GPR Transect	Profile Location on GPR Transect
N105W104	south	47	on profile	4 m
N105W104	east	20 (disturbed)	on profile	5-6 m
N105W104	west	22 (disturbed)	on profile	5-6 m
N105W106	north	45 (disturbed)	on profile	5-6 m
N105W106	west	26	on profile	5-6 m
N105W106	south	47 (disturbed)	on profile	5-6 m
N105W106	east	69 (disturbed)	on profile	0-1 m
N106W104	west	22 (disturbed)	on profile	4-5 m
N106W107	north	43 (disturbed)	on profile	6-7 m
N106W108	south	45	on profile	7-8 m

Table F.11: Tranquility Farm (Site 44.12a) location of metal placed during archaeological excavation with respect to GPR profiles.

Map ID	Location	Object	GPR Profile Number	Location on GPR Transect
M1	N92W95	rebar	Profile20	48 m
M2	N92W75	14" rebar	none	n/a
M3	N102W95	14" rebar	Profile20	38 m
M4	N107W95	14" rebar	Profile20	33 m
M5	N102W103	spike nail 8"	51	3 m

Table F.12: Tranquility Farm (Site 44.12a) stratigraphic information locations with respect to GPR profiles.

Map ID	Grid Location	GPR Profile Number	Distance From GPR Transect	Profile Location on GPR Transect	Midden Notes
a	N94W85	Profile12	1 m south	10 m	base of shell: 24 cm
b	N106W107	43	on profile	7 m	dense gravel layer: 25 cm
c	N105W92	Profile9	on profile	8 m	base of shell: 45 cm (0-30 cm FCS)
d	N93W87	Profile12	2 m south	8 m	black/orange subsoil: 30 cm
e	N105W104	45/22	on profile	4m/5m	3-4 postmolds 8 cm diameter; interpreted as housefloor
f	N94W87	Profile12	1 m south	8 m	base of shell: 34 cm
g	N105W105	45/24	on profile	5 m	40 cm MCS
h	N104W106	47/26	on profile	6 m	30 cm subsoil

Table F.12: Continued

Map ID	Grid Location	GPR Profile Number	Distance From GPR Transect	Profile Location on GPR Transect	Midden Notes
i	N107W107	41/28	on profile	7m/3m	45 cm subsoil
j	N110W102	Profile8 35/17	on profile	23 m 2m/0m	>30 cm MCS, beach gravel, black soil
k	N115W98	Profile6	on profile	27 m	>30 cm MCS, black soil
l	N120W95	Profile5	on profile	15 m	>30 cm MCS, beach gravel, dark brown soil; potential house floor
m	N125W95	Profile4	on profile	10 m	>25 cm MCS, gravel; S edge of field road
n	N130W95	Profile3	on profile	5 m	>25 cm black sandy soil
o	N134W95	Profile2	1 m south	5 m	no site
p	N110W80	Profile8	on profile	45 m	>30 cm MCS and beach gravel in black soil

Table F.12: Continued

Map	Grid	GPR	Distance	Profile	Midden Notes
ID	Location	Profile Number	From GPR Transect	Location on GPR Transect	
q	N110W70	Profile8	on profile	55 m	20 cm FCS

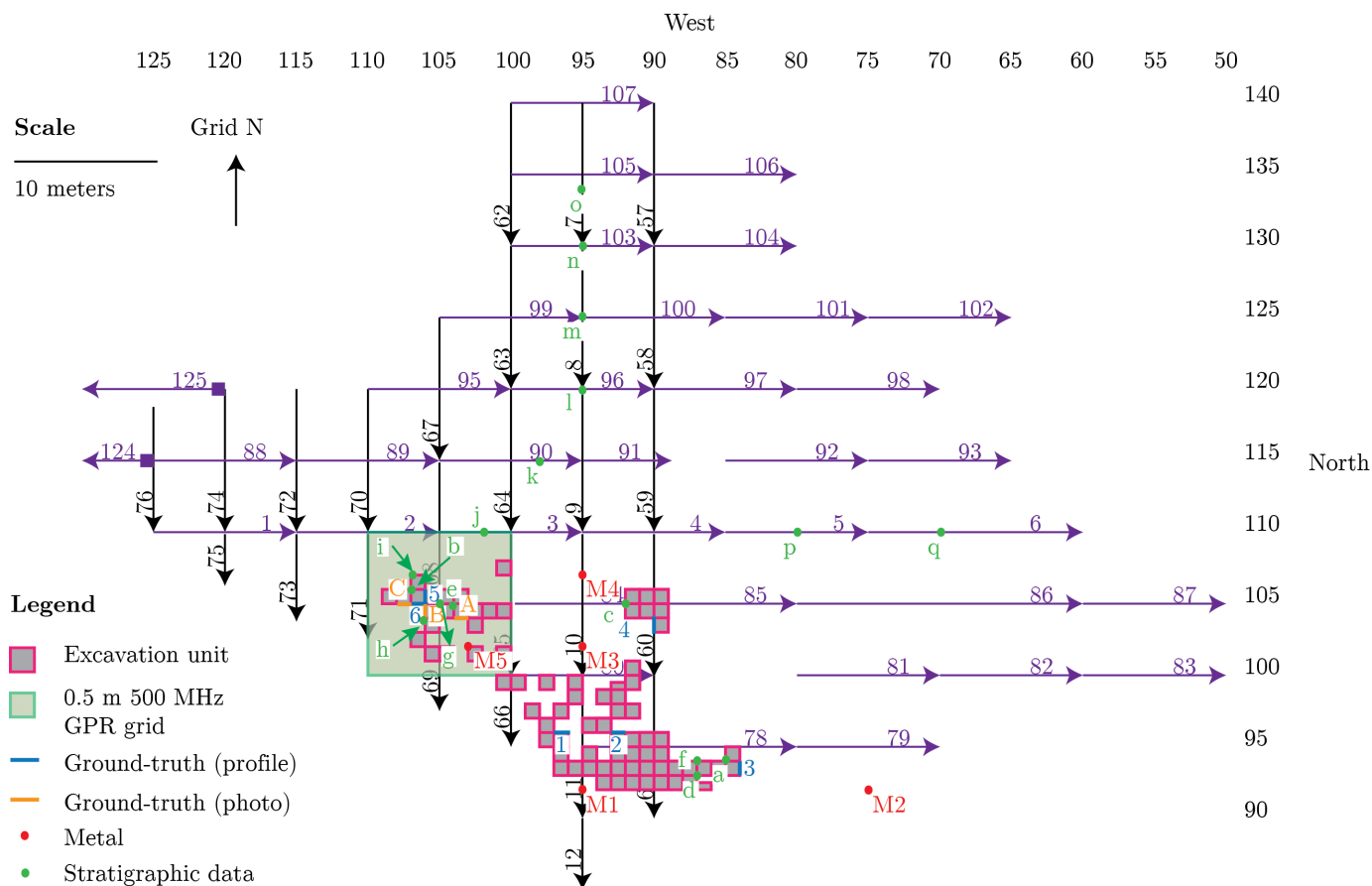


Figure F.7: Labeled map of ground-truth locations at Tranquility Farm (Site 44.12a) with 500 MHz GPR survey transects overlain. Metal placed during archaeological work is represented by red dots labeled with M#. Photos are labeled with letters and represented by an orange line. Archaeological profiles are labeled numerically and delineated with a blue line.

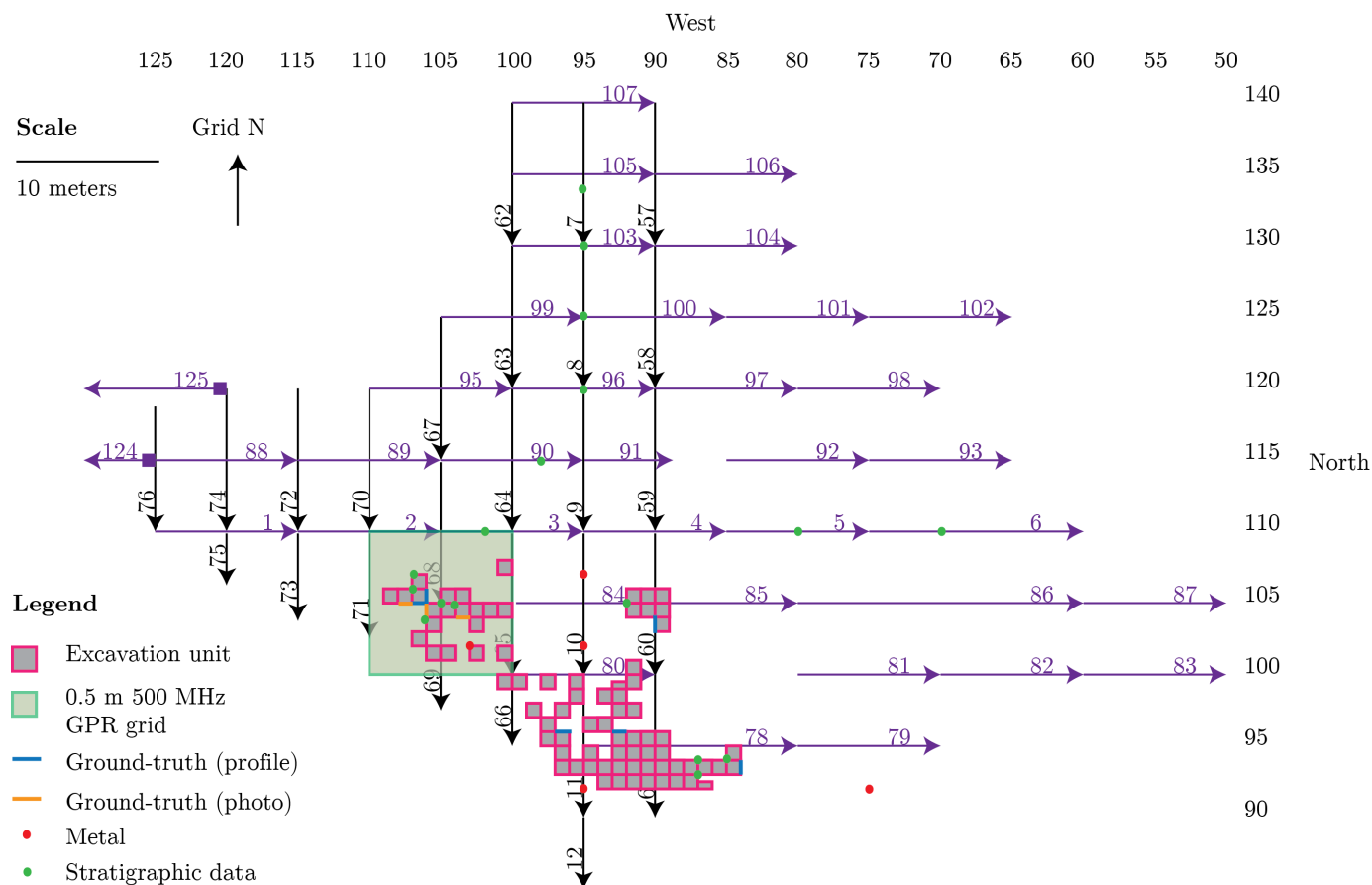


Figure F.8: Unlabeled ground-truth locations at Tranquility Farm (Site 44.12a) with 500 MHz GPR survey transects overlain. Metal placed during archaeological work is represented by red dots labeled with M#. Photos are labeled with letters and represented by an orange line. Archaeological profiles are labeled numerically and delineated with a blue line.

Appendix G
STRATIGRAPHIC INFORMATION FROM EXCAVATION FIELD
NOTES

G.1 Olson Site (17.13) Archaeological Testing Data

The following information was obtained from an unpublished archaeological testing report. Locations follow from the (0,0) baseline, consistent through the GPR survey maps. The original archaeological grid was reestablished at the Olson site during the summer 2016 GPR survey and mirrors the original archaeological grid (Figures B.1 and D.5).

G.1.1 1985 Test Pit Descriptions

G.1.1.1 Amy Foster and Arthur Spiess 7/20/1985

N4E16

0-20 cm heavy FCS, black soil, plow zone

20-35 cm MCS, charcoal, some black soil, mussel, fire cracked rock

N8E16

0-5 cm shell-free sod

upper 30 cm fine and MCS

N12E16

0-10 cm light brown shell-free sod

10-27 cm lightly concentrated FCS

S8E24

0-10 cm sterile dark brown

10-39 cm FCS, thickly packed shell without stratigraphy

39 cm clay till

S16E32

0-10 cm sterile dark brown, sandy loam, medium density, MCS

10-35 cm high density, FCS

35 cm subsoil

S12E32

34 cm orange till subsoil

S20E40

2 m from bank edge

37 cm subsoil

medium density, FCS mixed with dark brown loam

N0E24

0-10 cm lightly concentrated, FCS

S4E24

possible house floor at base

0-7 cm sterile black loam

7-27 cm densely packed, FCS

27-34 cm black loam, occasional shell and charcoal

34 cm E horizon over orange clay till

S20E32

in disturbed area

0-50 cm brown sandy loam fill over black clay loam, medium shell

shell heap thickness is 18 cm

S20E48

0-10 cm light brown sandy loam fill

10-39 cm black loam mixed with fine to MCS

39 cm subsoil

S20E56

bank edge at S24

light brown sandy loam fill, fine to MCS

thick dark brown soil

47 cm sandy orange subsoil

S16E56

32 cm light brown sandy loam fill; dark brown loam with FCS

49 cm subsoil

S20E64

0-20 cm brown sandy loam mixed with very few fragments of FCS

20 cm subsoil

G.1.1.2 David Gratt 7/13/85

N10W12

0-12 cm dark brown, shell-free

12-21 cm dark brown loam with concentrated FCS

21 cm orange silty, pebbly, coarse sand

N14W12

0-16 cm dark brown without shell

16-32 cm dark brown loam with light scatter of FCS

N0W48

0-14 cm very dark brown loam

14-22 cm dark brown loam with light, FCS

22 cm sterile yellow subsoil

N0W36

in dug over area

0-22 cm fine crushed shell with occasional fire cracked rock

22-29 cm black soil and CCS

29 cm subsoil

N6W36

22 cm subsoil

N8W36

brown loam, no shell

N4W36

0-12 cm dark brown loam

12-29 cm FCS with dark brown loam

29 cm yellow clay till subsoil

N0W28

heavily dug down to subsoil

46 cm of concentrated FCS and black loam over E horizon and orange B horizon

N4W28

heavily dug-over

47 cm of FCS mixed with black loam from surface

N8W28

0-12 cm dark black loam without shell

12-30 cm concentrated, FCS with dark brown loam

30 cm orange subsoil

N12W28

0-19 cm brown loam

19-29 cm brown loam mixed with light scattering of FCS

29 cm yellow till subsoil

G.2 Tranquility Farm (Site 44.12a) Stratigraphic Information

The following data were obtained from field notes taken during excavations (2012, 2014) and limited testing (2016) at the Tranquility Farm site. Data were

provided by Dr. Arthur Spiess. Information extracted from the reports relates to objects that would appear in the GPR profiles (i.e. metal), and shell midden thickness.

G.2.1 2012 Field Season Notes

G.2.1.1 Metal Notes Courtesy of A. Spiess

N92W95

Site datum is rebar at grid point N92W95

N92W75

Rebar 14" long

N102W95

Rebar 14" long

N107W95

Rebar 14" long

N102W103

Spike nail 8" long

G.2.1.2 Stratigraphic Notes

N94W85

Shell disappears at 24 cm in NW quad

N106W107

Dense gravel layer at 25 cm

N94W85

Base of shell midden at 25-30 cm

N105W92

Gravel layer in adjacent squares

Bottom of shell at 45 cm

N93W87

Black/orange subsoil mixture at 30 cm

N105W92

0-30 cm in FCS

50 cm gravel floor and little shell

N105W104

3-4 postmolds (8 cm in diameter) interpreted as a house floor

N94W87

0-9 cm Plow zone

9-29 cm moderate amount of FCS

29-34 cm black soil with very light shell

34-40 cm silty, gravelly, rocky till

G.2.2 2014 Field Notes

G.2.2.1 Stratigraphic Notes Courtesy of A. Spiess

N105W105

40 cm in MCS

N104W106

30 cm subsoil

N107W107

0-10 cm sod

10-24 cm FCS with occasional rock

24-40 cm CCS

40-43 cm black layer with gravel

43-45 cm E soil horizon

G.2.3 2016 Field Notes

G.2.3.1 Stratigraphic Notes Courtesy of A. Spiess

Evaluation of GPR data in the field revealed a larger shell midden than previously expected. Ground-truth data were collected by A. Spiess in areas where archaeological testing had not occurred. Spiess dug 25 cm square, shovel test pits to 30 cm depth. The contents of each test pit were put back in place.

N110W102

0-18 cm FCS and plow zone

>30 cm MCS and beach gravel in black soil

N115W98

plow zone

>30 cm MCS and black soil

N120W95

>30 cm MCS and beach gravel with dark brown soil

potential house floor?

N125W95

plow zone and FCR

>25 cm MCS and gravel

on south edge of field road

N130W95

>25 cm black sandy soil

N134W95

light brown silty cobbly till

sterile soil, no site

boundary between N130 and N134

N110W80

>30 cm MCS and beach gravel in black soil

N110W70

20 cm FCS

very light FCS in dark brown sandy soil with beach gravel

FCR

Appendix H

ADDITIONAL GPR AND ARCHAEOLOGICAL PROFILE COMPARISONS

H.1 Olson (Site 17.13)

H.1.1 Archaeological and GPR Profile Comparisons

An archaeological trench excavated during 1985 provided ground-truth for GPR and archaeological data comparison. Eighteen meters of GPR interpretation of the west wall of the trench are displayed in Figures H.1, H.2, H.3, H.4, and H.5.

Interpretations of the eastern wall can be found in Chapter 4.7. Each figure contains one unmigrated profile and two of the same migrated profiles, the only difference in the latter being one has interpretation overlain. The scale of the unmigrated profile differs from the two migrated profiles as a result of the migration.

Figure H.1 shows N0E0 to N4E0. Circled in yellow is a rock that corresponds to the fire-reddened stone in the archaeological profile. The red arrow at approximately 6.5 m is pointing to a strong reflector discussed in the next profile. Shell thickness in the GPR profile ranges from 25-40 cm, and 20-60 cm in the archaeological profile. The undulating surface of the glacial material depicted in the archaeological profile was not resolved by the 500 MHz antenna.

The trench wall from N4E0 to N8E0 is depicted in Figure H.2. Postmolds are delineated in the archaeological profile, and the surface that they were placed in is directly correlated with the strong reflector (red arrows in Figure H.2). The compacted surface appears to be basin-shaped and is approximately 2.3 m in length. The red arrow at 5 m also points to the location of the base of the rightmost portion of the delineated feature. The GPR data suggest the feature is dug into the compacted surface as shown in the archaeological profile. The thickness of the shell

layer ranges from 25-40 cm in the GPR profile, and 20-42 cm in the archaeological profile.

Figure H.3 shows the trench section N8E0 to N12E0. The thickness of the shell layer ranged from 40-50 cm, but was anywhere from 20-40 cm in the archaeological profile. The feature delineated in the archaeological profile was not identified in the GPR profile.

The trench wall from N12E0 to N16E0 is depicted in Figure H.4. The rightmost feature in the archaeological profile is shown at the end of the red arrow in the GPR profile (Figure H.4). GPR data suggest the feature is dug into the glacial material, this is confirmed by the archaeological profile drawing. The leftmost feature was not identified in the GPR profile. Shell layer thickness ranged from 20-45 cm in the GPR profile, and 20-44 cm in the archaeological profile.

Figure H.5 illustrates the trench wall from N16E0 to N18E0. The 20 cm diameter rock shown in the archaeological profile is underneath the word "rock." The shell lens noted in the drawn profile was not delineated in the GPR profile. Shell thickness in the GPR profile ranged from 15-25 cm, and 15-30 cm in the archaeological profile.

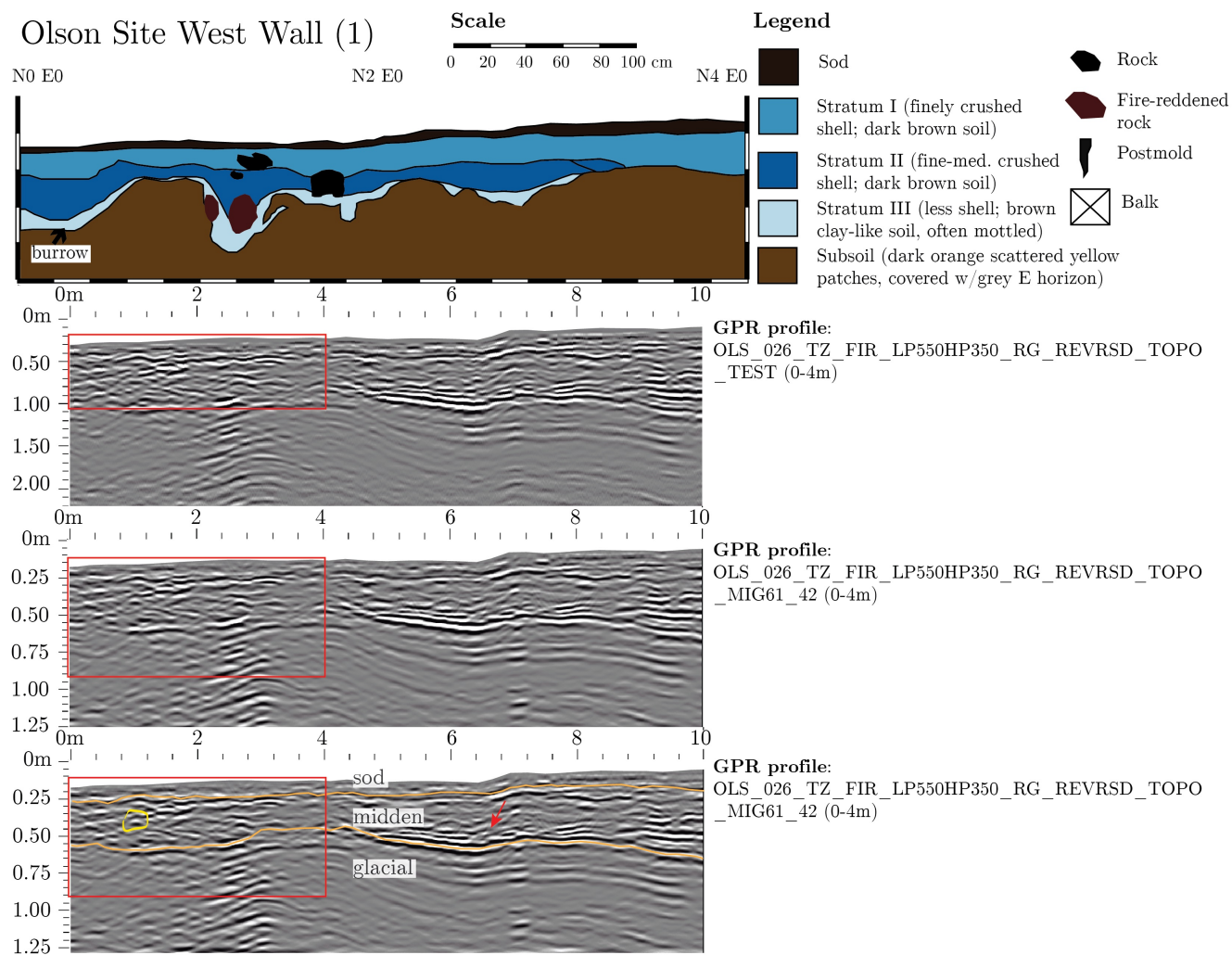


Figure H.1: Olson (Site 17.13) west (1) GPR and archaeological profile comparison.

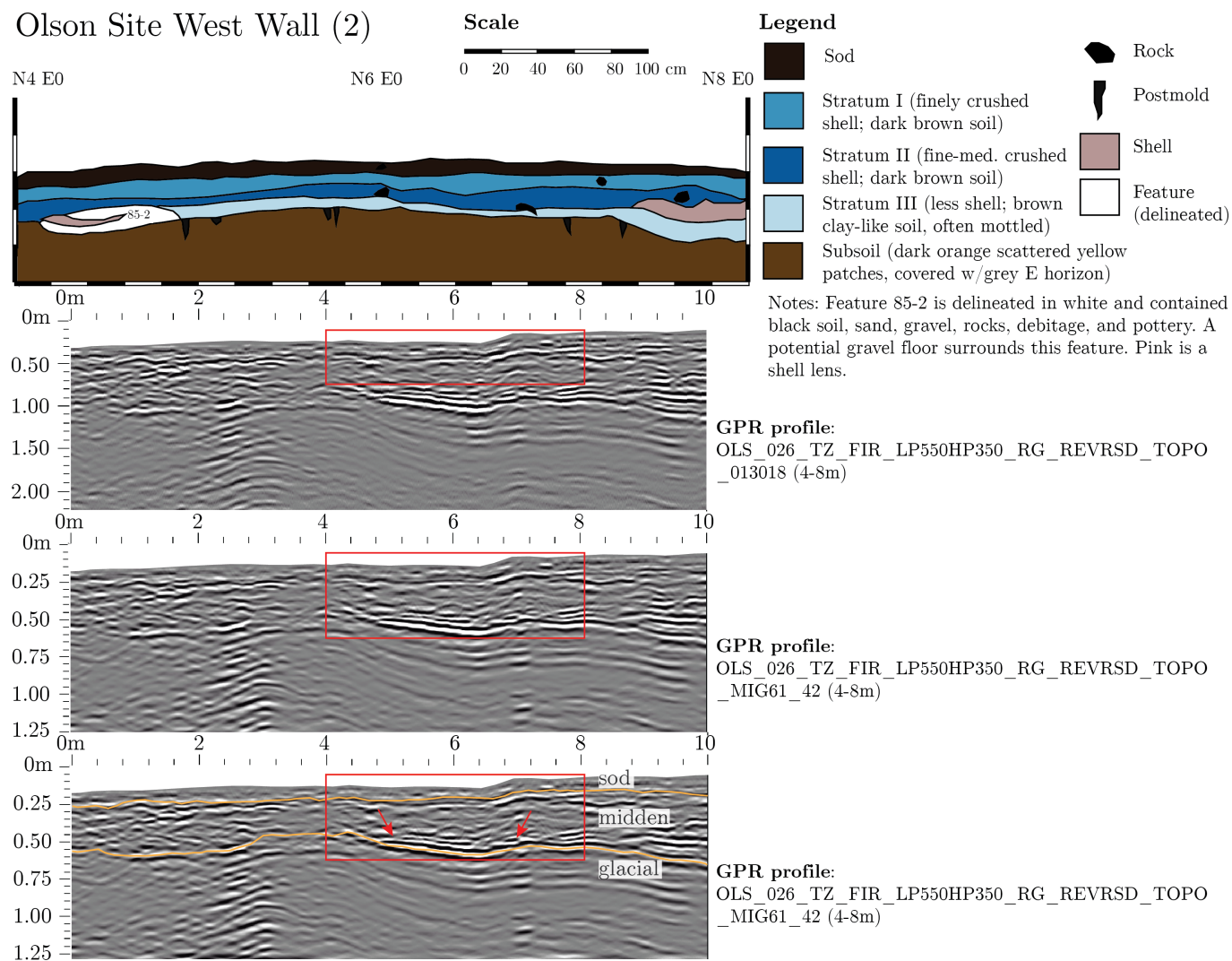


Figure H.2: Olson (Site 17.13) west (2) GPR and archaeological profile comparison.

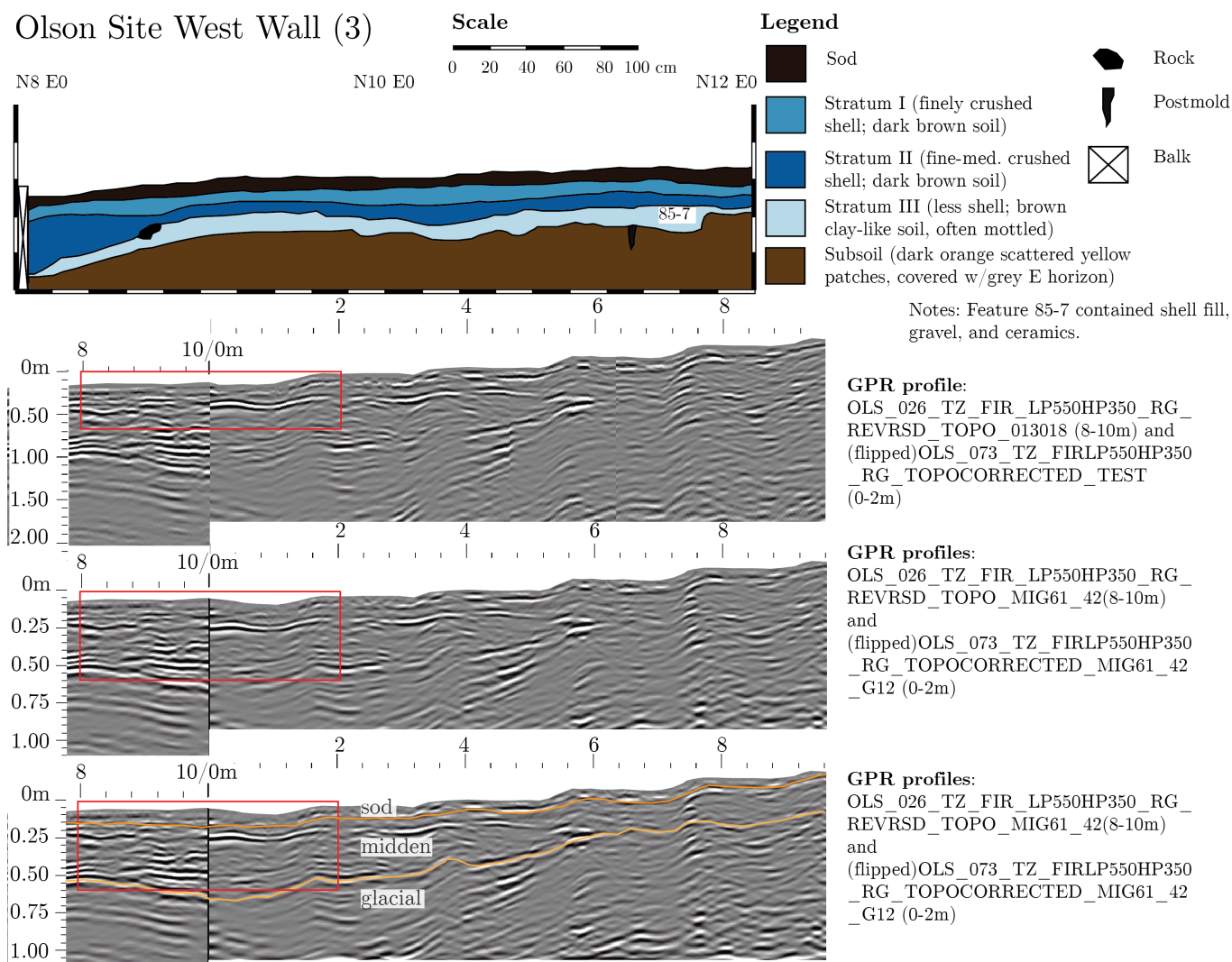


Figure H.3: Olson (Site 17.13) west (3) GPR and archaeological profile comparison.

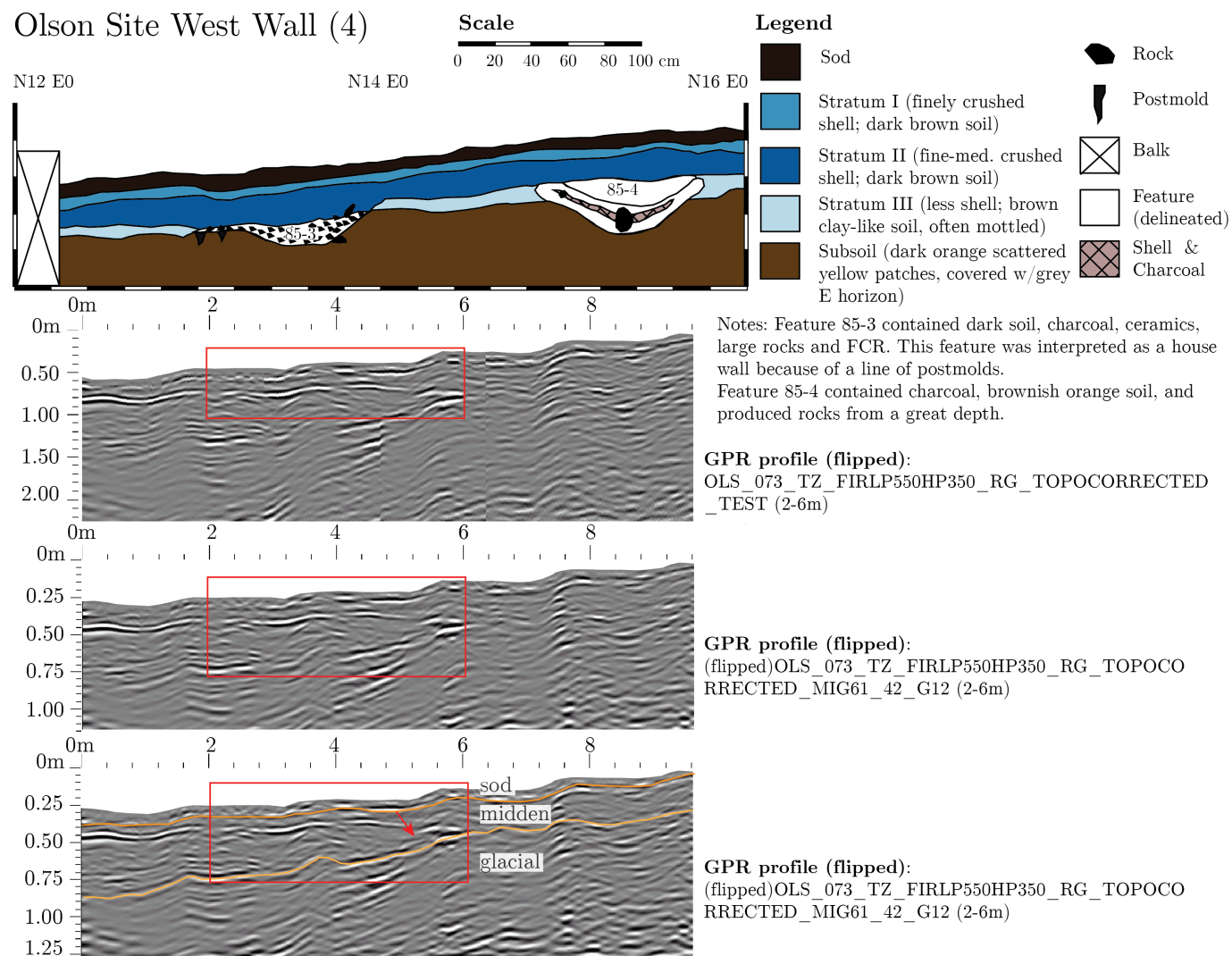


Figure H.4: Olson (Site 17.13) west (4) GPR and archaeological profile comparison.

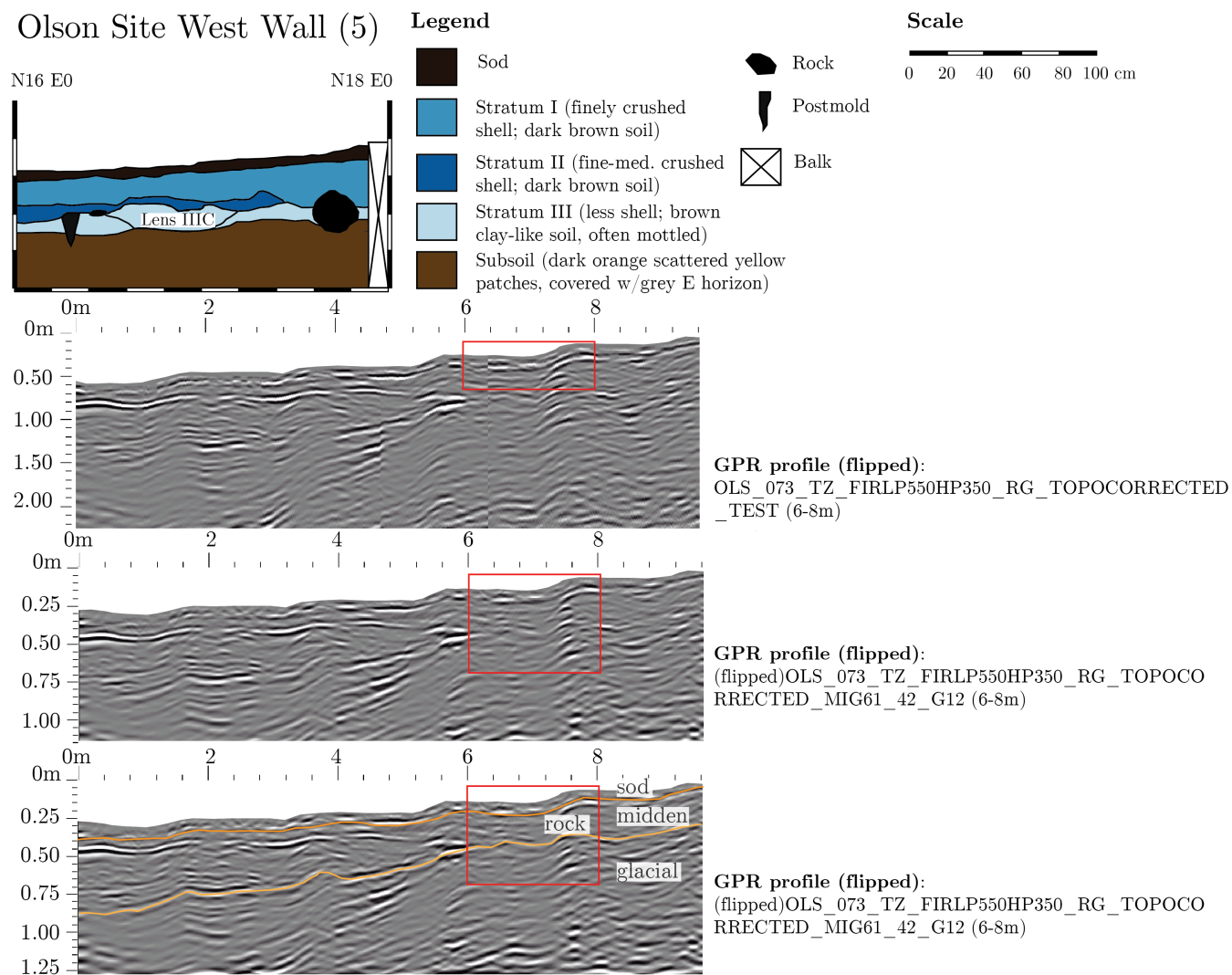


Figure H.5: Olson (Site 17.13) west (5) GPR and archaeological profile comparison.

H.1.2 GPR Depth Correction

This subsection highlights instances where the original interpretation of the overall site thickness differed significantly from the observed archaeological profile. The midden base was traced prior to receiving extensive ground-truth information, and these shifts in the interpretation are suggested so the GPR data more closely follow the archaeological information.

Map ID points 2 and 3 in Table H.1 are shown in Figure H.6 as two areas where ground-truth indicated the original pick required adjustment. The original reflector is delineated by yellow dots, and was chosen because it was consistent across the profile, and the signal above was interpreted as shell midden. The new position of the midden base is represented by a stronger reflector, that is more discontinuous than the original due to signal absorption in the upper portions of the profile. The adjusted picks (red arrows at 2 m and 6 m) bring the base of the midden to 30 cm and 32 cm. These new depths agree well with the archaeologist's observed base of midden at 30 cm and 35 cm.

Figure H.7 represents the GPR profile for map point 4 in Table H.1. Ground-truth indicated that the midden depth was approximately 10 cm, but the original GPR pick (yellow dots) is at 45 cm at the start of the profile. The red arrow at 25 cm is pointing to the suggested reflector for the base of the midden. The new reflector interpretation follows a stronger reflector that becomes difficult to trace at approximately 7.5 m.

Map point 6 in Table H.1 is at the red arrow on Figure H.8. A closer look at the GPR profile with the ground-truth information revealed that the original pick did not follow the same reflector outlined at the start, which resulted in an exaggerated depth of 40 cm. Energy was likely absorbed in the lower portion of the profile, and resulted in a washing out of the upper reflector from 15 m to 17.5 m. The new

position of the shell midden base (red arrow) is at a depth of 21 cm, and in close agreement with the base of midden depth of 22 cm, identified in ground-truth data.

Map points 7, 8, and 9 in Table H.1 are located at 6 m, 4 m, and 2 m, approximately 1 m to the west of the profile shown in Figure H.9. The interpreted midden bottom in locations 7 and 8 agrees well with the observed midden thickness. Brown loam without shell was observed at location 9, but the interpreted midden base is shown by the yellow dots at 20 cm in Figure H.9. The overestimated midden depth was due, in part, to the absence of a strong reflector from 0 m to 2 m, and the lack of a strong midden signal like that seen from 4-10+ m in Figure H.9.

Table H.1: Olson (Site 17.13) site midden thickness comparison: stratigraphic data and GPR interpretations. An asterisk next to the map ID indicates an area which A. Spiess noted as disturbed.

Map ID	GPR Profile ID	Location on GPR Transect	Map Location	GPR Pick Depth (cm)	Actual Depth to Subsoil (cm)
1	109	8m	N12E16	28	27
2	134	2m	N8E16	39	30
3	134	6m	N4E16	44	35
4	164	0m	N0E24	45	10
5*	272	6m	N0W36	30	29
6	272	18m	N0W48	40	22
7	near 259	6m	N4W36	32	29
8	near 259	4m	N6W36	20	22
9	near 259	2m	N8W36	20	no shell
10*	242	10m	N0W28	34	46
11*	242	6m	N4W28	36	47
12	242	2m	N8W28	30	30
13	210	0m	N10W12	33	21

GPR profile:

OLS_SUPER1_TZ_FIRLP550HP350_MIG1_RG2_PICKS_042517_DIELTEST_MIG61_42_PICKS
OLS_134

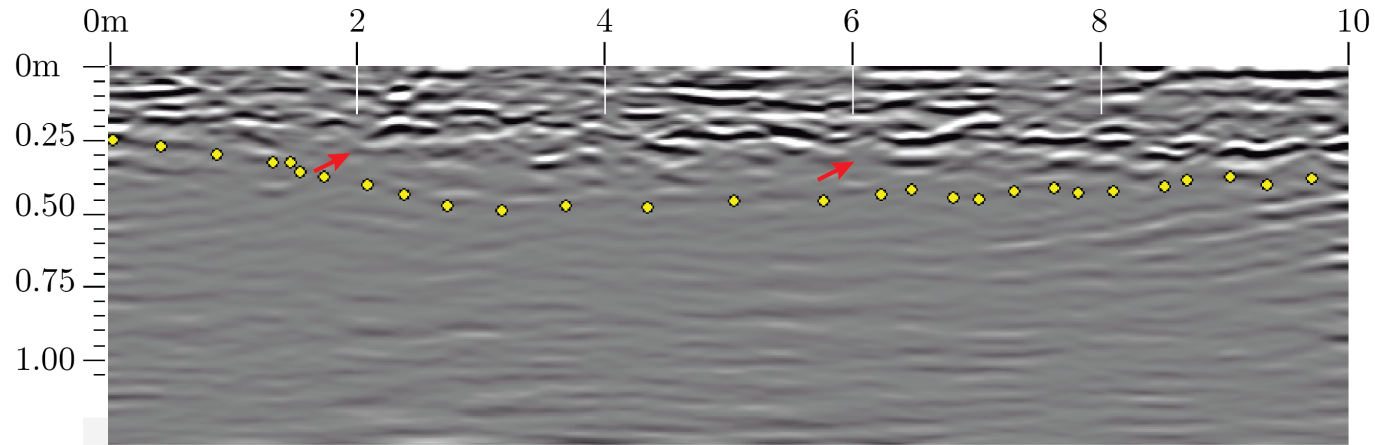


Figure H.6: Olson (Site 17.13) N8E16 and N4E16 original base of midden pick on GPR profile. The original pick of the midden base is shown by yellow points along the reflector. Red arrows indicate the new, suggested location for map point 2 and 3, at 2 m and 6 m along profile 134.

GPR profile:

OLS_SUPER1_TZ_FIRLP550HP350_MIG1_RG2_PICKS_042517_DIELTEST_MIG61_42_PICKS
OLS_164

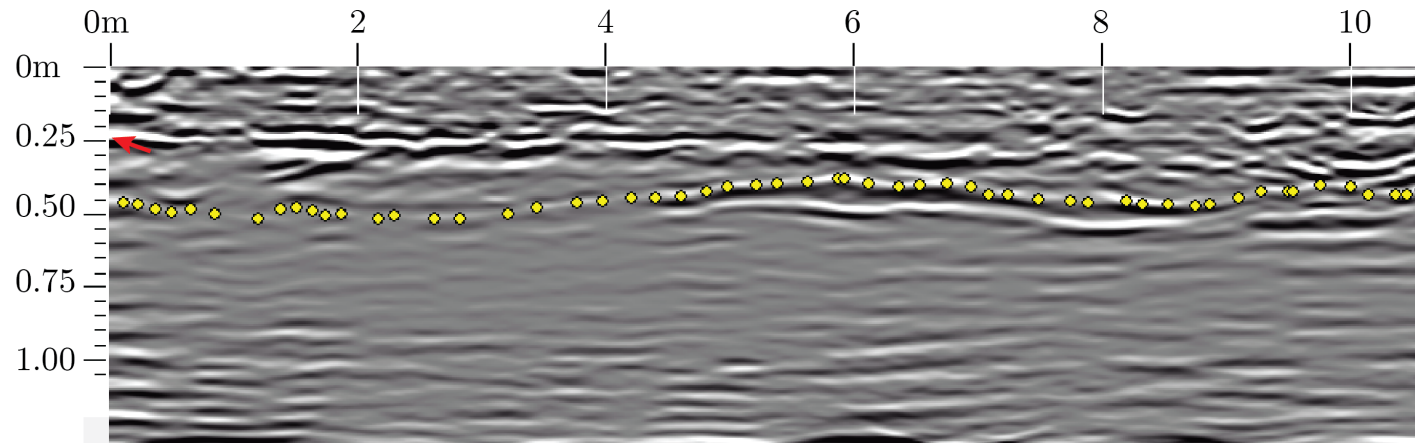


Figure H.7: Olson (Site 17.13) N0E24 original base of midden pick on GPR profile. The original pick of the midden base is shown by yellow points along the reflector. The red arrow indicates the new, suggested location for map point 4, at 0 m on profile 164.

GPR profile: (OLS_272)

OLS_SUPER1_TZ_FIRLP550HP350_MIG1_RG2_PICKS_042517_DIELTEST_MIG61_42_PICKS

OLS_SUPER1_TZ_FIRLP550HP350_MIG1_RG2_PICKS_042517_DIELTEST P_1

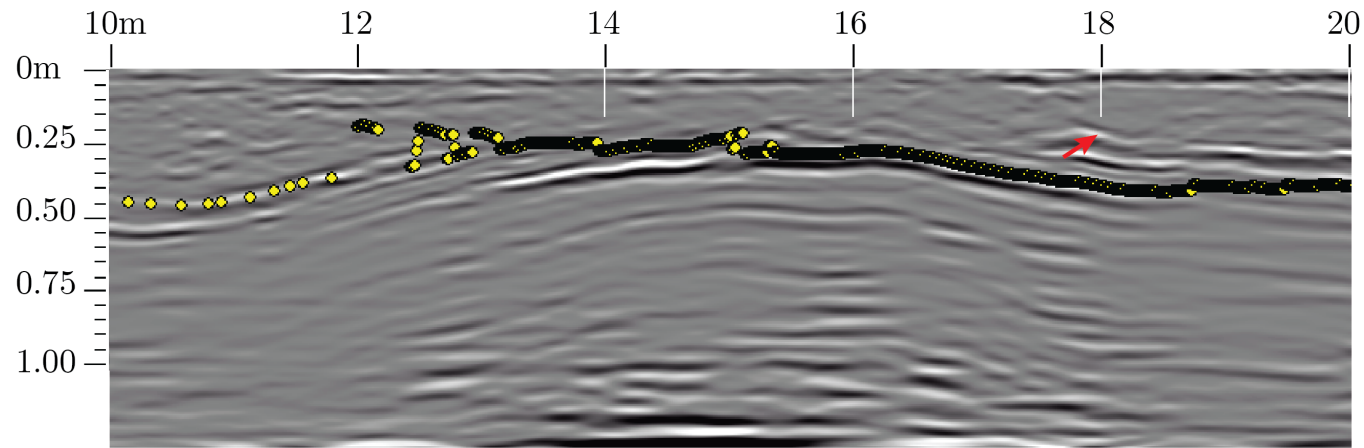


Figure H.8: Olson (Site 17.13) N0W48 original base of midden pick on GPR profile. The original pick of the midden base is shown by yellow points along the reflector. The red arrow indicates the new, suggested location for map point 6, at 18 m on profile 272.

GPR profile:

OLS_SUPER1_TZ_FIRLP550HP350_MIG1_RG2_PICKS_042517_DIELTEST_MIG61_42_PICKS

OLS_259

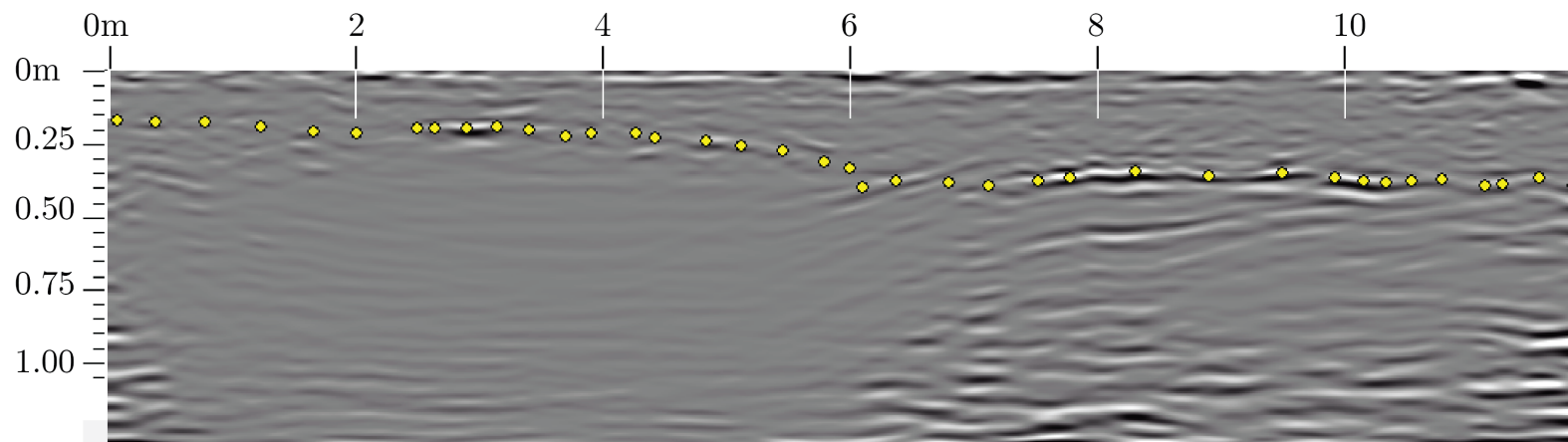


Figure H.9: Olson (Site 17.13) original base of midden pick on GPR profile for map points 7-9. The original pick of the midden base is shown by yellow points along the reflector.

Appendix I

ISOPACH MAPS

I.1 Isopach Map Construction

Isopach maps were ideal for the visual display of shell midden thickness and extent. An isopach map was made after the creation of a super 3D grid, processing of the files within the grid, and comparison of the GPR profiles with ground-truth information from archaeological excavation. Isopach grid construction requires tracing the bottom of the shell midden in each file within the super 3D grid. Appendix A contains a brief guide to Radan steps taken over the course of the project, and Section A.5 outlines steps to trace and export layer picks. The layer file created in Radan provides the data required for the construction of an isopach map in the desired program (ArcGIS for this project).

I.2 A Guide to Isopach Map Construction in ArcGIS

To illustrate the extent and thickness of the shell midden via an isopach map, a .csv file was created following the steps described in Appendix A Section A.5. Import the .csv into ArcGIS. Right-click the imported file within the file tree and select "Display XY Data". A window will appear that prompts the user for x, y, and z fields. The labels for each of these column will appear in the drop-down menus associated with each field. Select the elevation as the z field. Click OK. A warning window will likely appear that states "table doesn't have Object-ID field," select OK.

The next step is converting newly displayed points, labeled "Events", to a more permanent file format within ArcGIS. Right-click the file labeled "Events" and select "export data". A window will pop-up with an option to assign a coordinate

system. Under "Use same coordinate system as:" select "the data frame". Within the same pop-up box, label the file and check that it is assigned to the correct geodatabase. Select OK. A window will appear asking "Do you want to add the exported data to the map as a layer?". Select yes.

Assigning an interpolation technique within ArcGIS will produce the isopach map. The isopachs that appear in this work were made using the natural neighbor interpolation technique. Use the search bar to find your method of interpolation or navigate to "3D Analyst Tools" in the toolbox. Under "3D Analyst Tools", select "Raster Interpolation", and a variety of interpolation techniques appear. Once a technique is selected, a window will appear asking for "input point features". A drop-down box should list the layer file that contains the xyz data. Select the desired file. Check that the next box contains the proper z value field. The last box contains the output cell size, which will determine the smoothness of the isopach. Select OK.

I.3 Isopach Map Files

I.3.1 Long Island North (Site 15.95)

Condensed xyz data from picking the bottom of the shell midden at site 15.95 is contained within file LINSUPER3D_TZ_HP350LP550_RGTEST_INTEGRATE_DIEL51_55_PICKS022518. The original .csv file can be exported from the Radan file with the same descriptive title. The filename of the final version of the isopach maps contain Natural_ followed by the filename of the respective Radan and .csv files. The cell size of the isopach map is 0.5 meters by 0.5 meters. The map resides in ArcMap file LIN_isopach022718.

I.3.2 Damariscotta Oyster Farm (Site 26.15)

The .csv file DAM_3DBATCH_T1_TZ_FIRLP550HP350_MIG_RG_LAYERDENSE_MOD was used for the creation of the detailed isopach map, and it contains condensed xyz data for midden thickness and extent. The raw pick data can be exported from Radan file DAM_3DBATCH_T1_TZ_FIRLP550HP350_MIG_RG_LAYERDENSE_MOD. The detailed grid has a cell size of 0.4 m by 0.4 m, and is found in ArcMap file L2S_DAM_BWdetailed.

The overall site isopach map was created using the interpretations from the GPR profiles that followed the mowed transects. Following the process described in Appendix A.4.2, an ArcMap file was created, lines were drawn that represented the GPR transects, and points were extracted to each transect. The UTM coordinates associated with each point, in each attribute table, for each individual GPR transect, were copied to create a single .csv file. File DAM_siteisopach.csv was then added to ArcGIS file DAM_siteisopach_BW. A field was added to the attribute table in ArcGIS, and the shell midden thickness was entered every 5 m. The .csv file does not contain midden thickness information, but the file (DAM_siteisopachdata_complete), used to create the isopach map, was exported to the Damariscotta geodatabase. The natural neighbor option was selected to make the isopach map, and the cell size is 0.25 m by 0.25 m. The ArcGIS file DAM_siteisopach is a color version of DAM_siteisopach_BW.

I.3.3 Olson (Site 17.13)

Condensed xyz data from picking the bottom of the shell midden at site 17.13 is contained within file OLS_SUPER_TZ_FIRLP550HP350_MIG1_RG2_PICKS_042517_DIELTEST_MIG61_42_ACYUAL.csv. This file, exported after picking the midden bottom, was assigned the same descriptive title associated with the specific Radan file. Processing steps taken within Radan are apparent in the .csv

file. The filename of the final version of the isopach map is Natural_MIG61, and it is located in ArcGIS file Olson_112117_blackandwhite. The cell size of the isopach map is 0.21 m by 0.21 m.

I.3.4 Tranquility Farm (Site 44.12a)

Condensed xyz data from picking the bottom of the shell midden at site 44.12a is contained within file TRQ_G1_HM1_S3DTEST2_TZ_FIR_LP550HP350_RG_MIG64_41_PICKS_021418 and TRQ_G2TEST2_TZ_FIR_LP550HP350_RG_MIG64_41_PICKS_021518. The original .csv file can be exported from the Radan file with the same descriptive title. The filename of the final version of the isopach maps contain Natural_ followed by the filename of the respective Radan and .csv files. ArcGIS project TRQ_isopach021618aa contains contains both maps, and an additional version of the western isopach map that contains the same color scale for midden thickness as the eastern grid. The cell size for all grids created for Tranquility Farm is 0.2 m by 0.2 m.

I.4 Isopach Maps

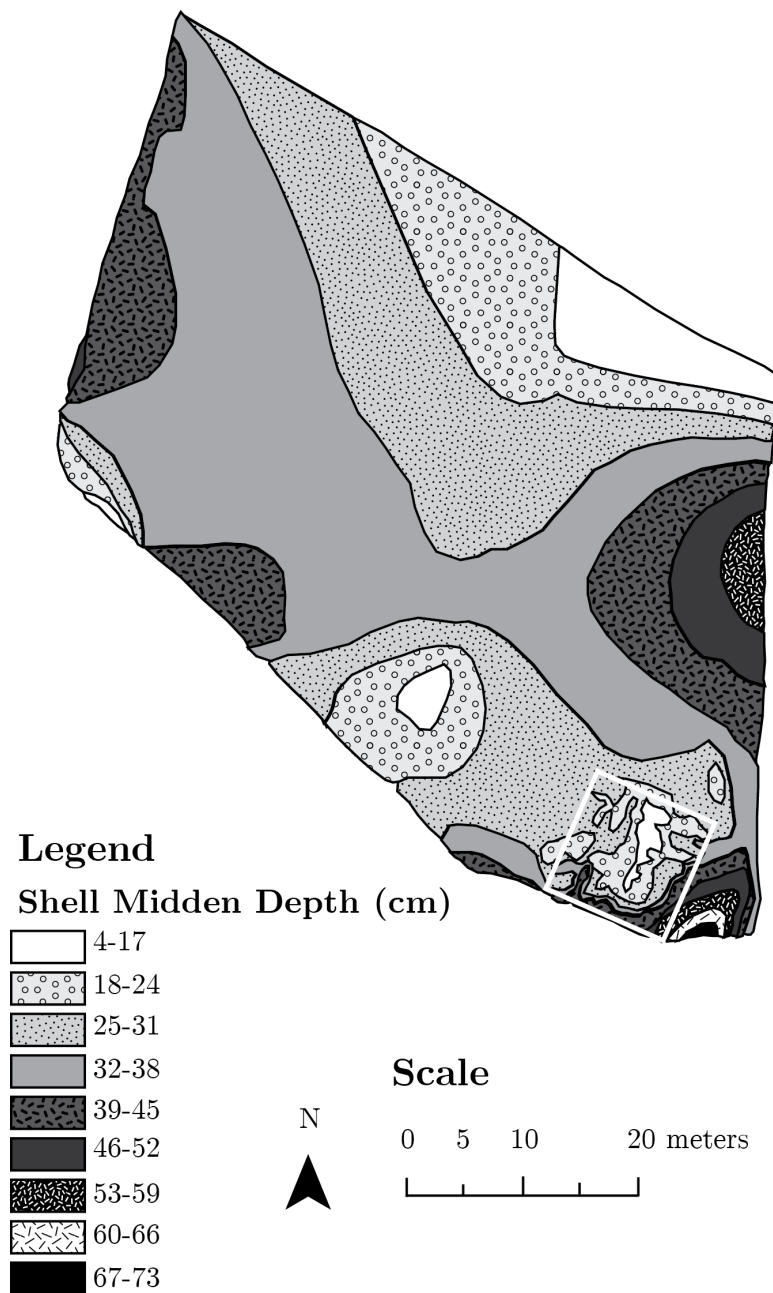


Figure I.1: Damariscotta (Site 26.15) isopach map.

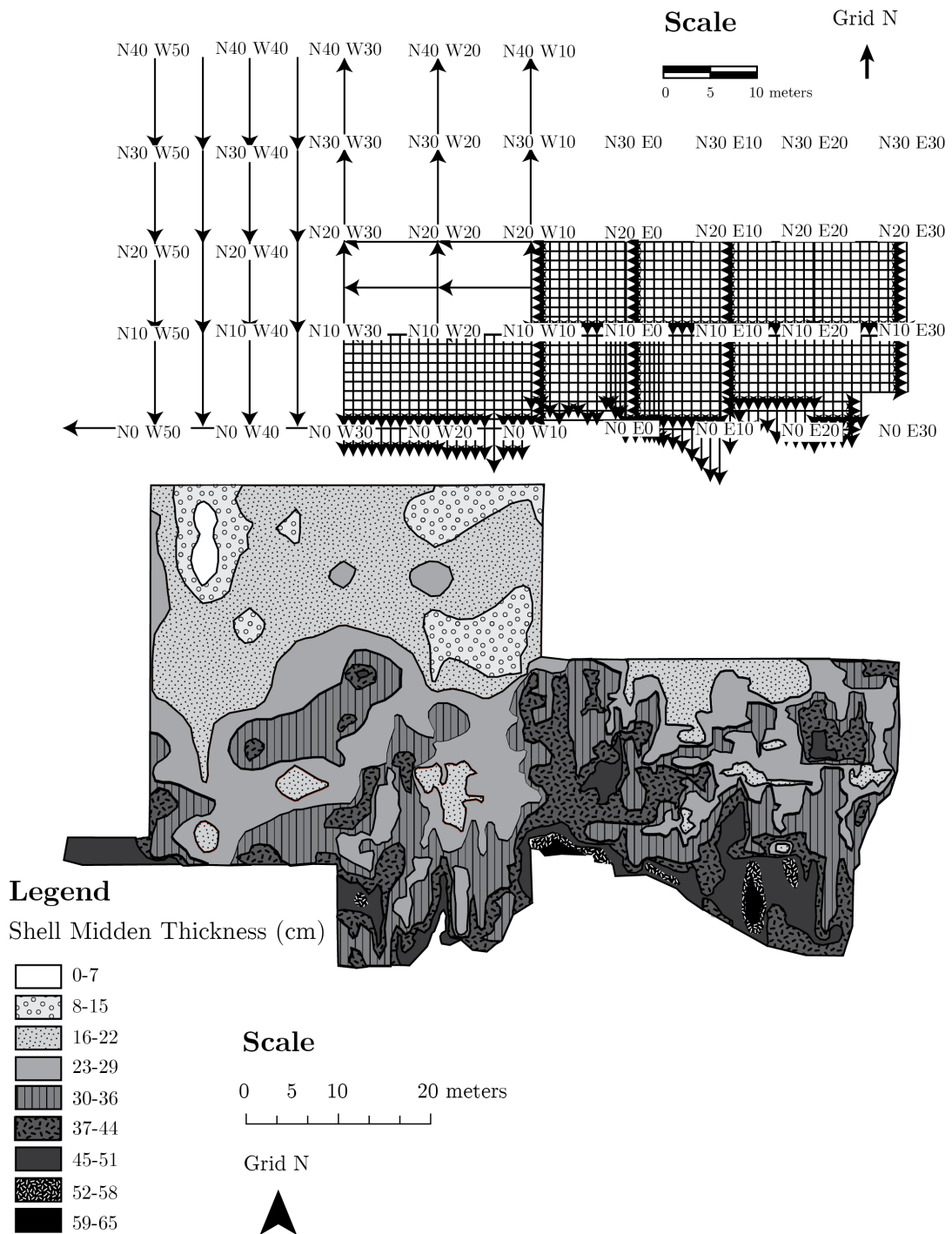


Figure I.2: Olson (Site 17.13) isopach map.

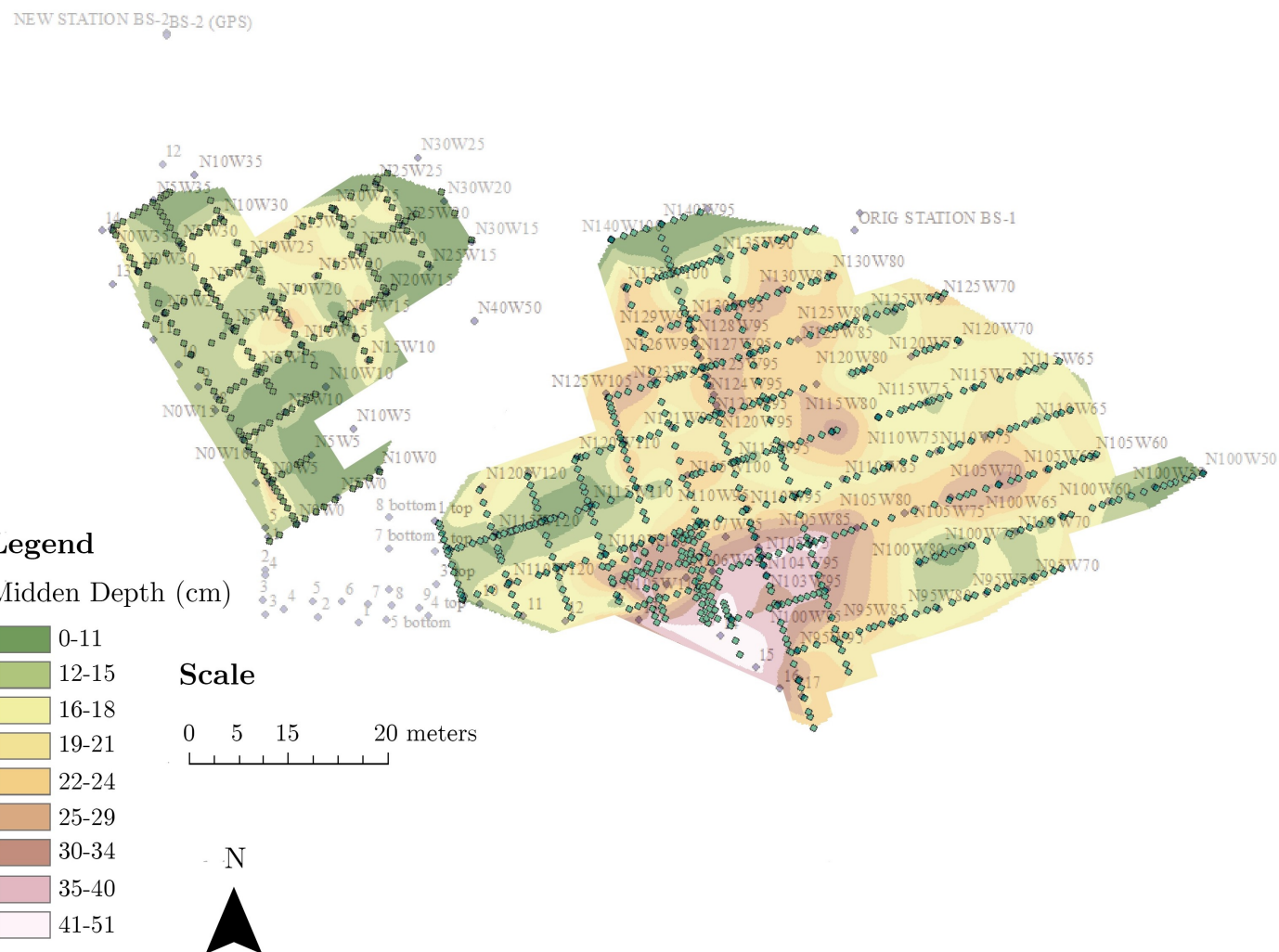


Figure I.3: Tranquility Farm (Site 44.12a) isopach map with grids and total station survey points overlain.

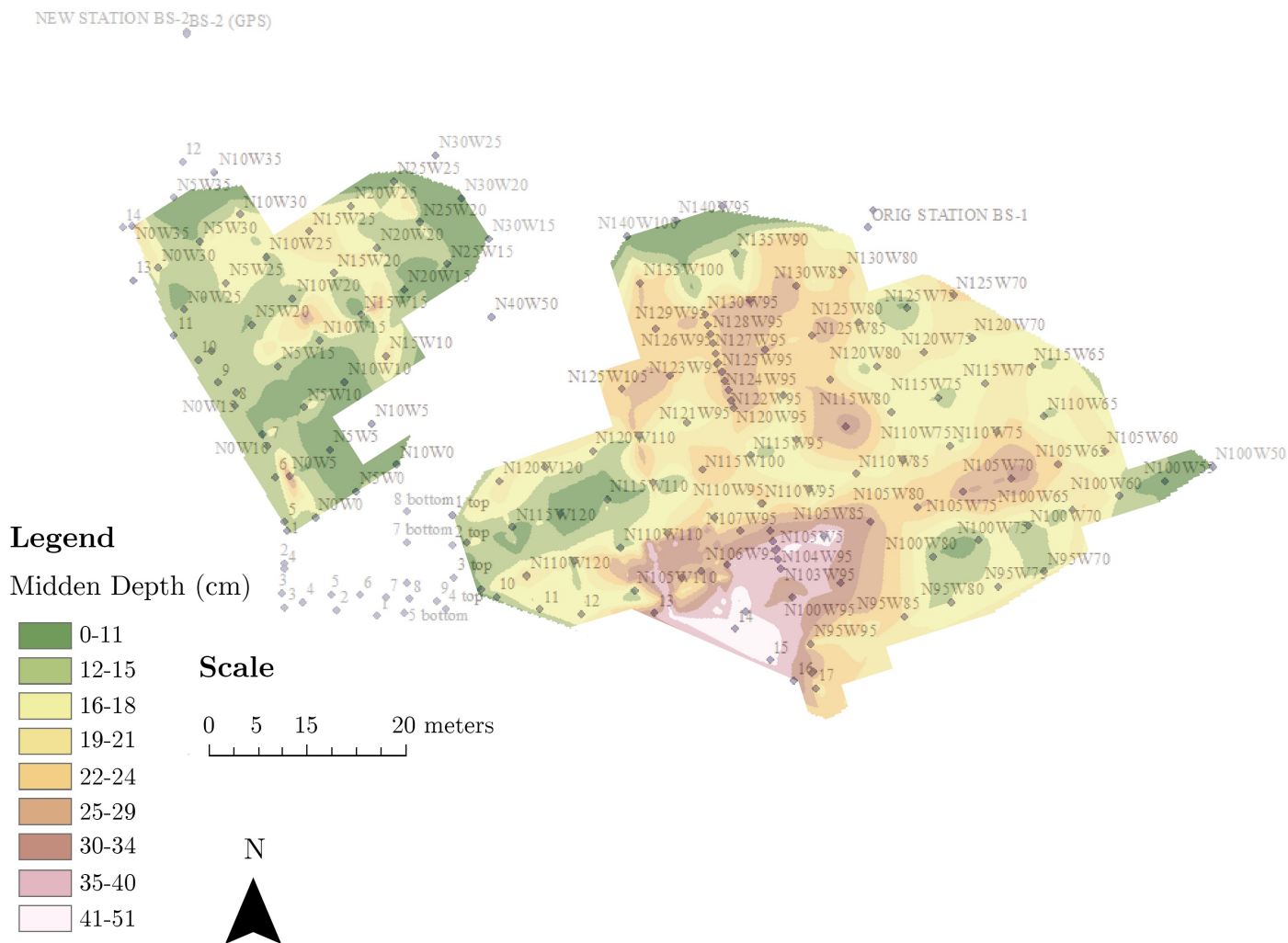


Figure I.4: Tranquility Farm (Site 44.12a) isopach map with total station survey points overlain.

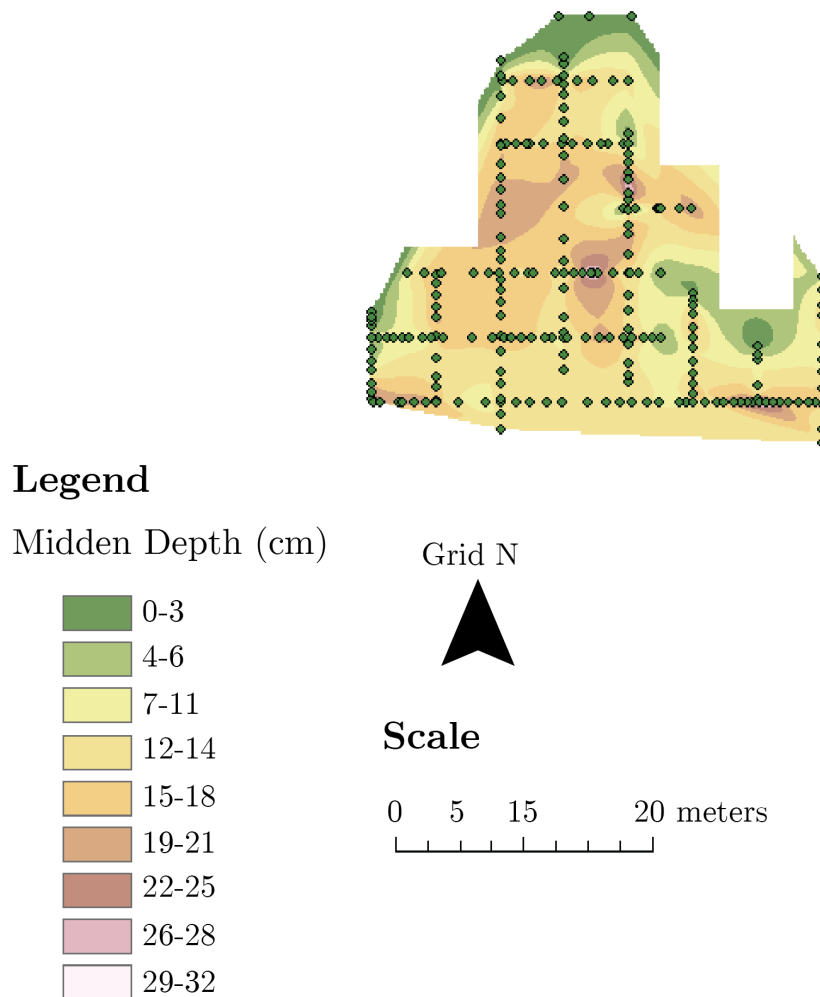
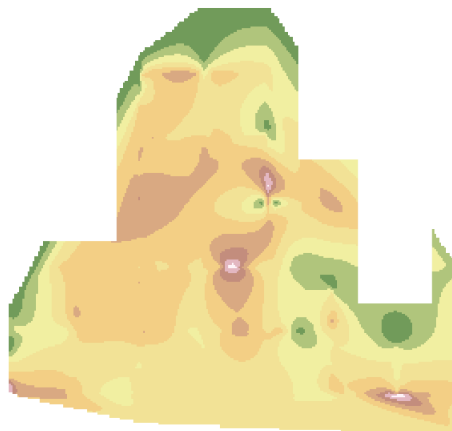
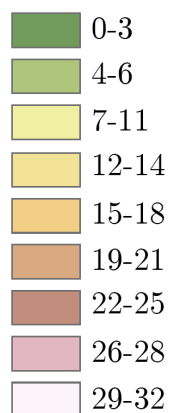


Figure I.5: Tranquility Farm (Site 44.12a) isopach map (1) of the western portion of the 500 MHz GPR survey with transects overlain. Note that the scale range denoted by the color scheme differs from the isopach included in the figure of the whole site.



Legend

Midden Depth (cm)



Grid N



Scale



Figure I.6: Tranquility Farm (Site 44.12a) isopach map (1) of the western portion of the 500 MHz GPR survey. Note that the scale range denoted by the color scheme differs from the isopach included in the figure of the whole site.

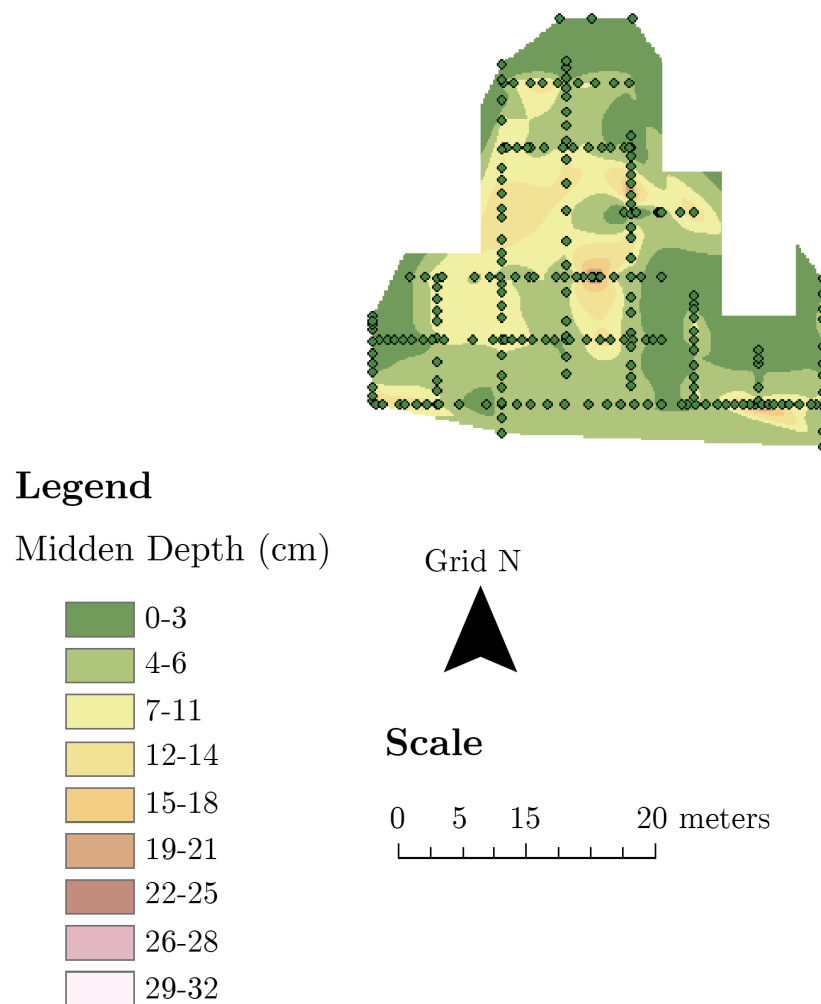


Figure I.7: Tranquility Farm (Site 44.12a) isopach map (2) of the western portion of the 500 MHz GPR survey with transects overlain. Survey transects are represented by the green dots.

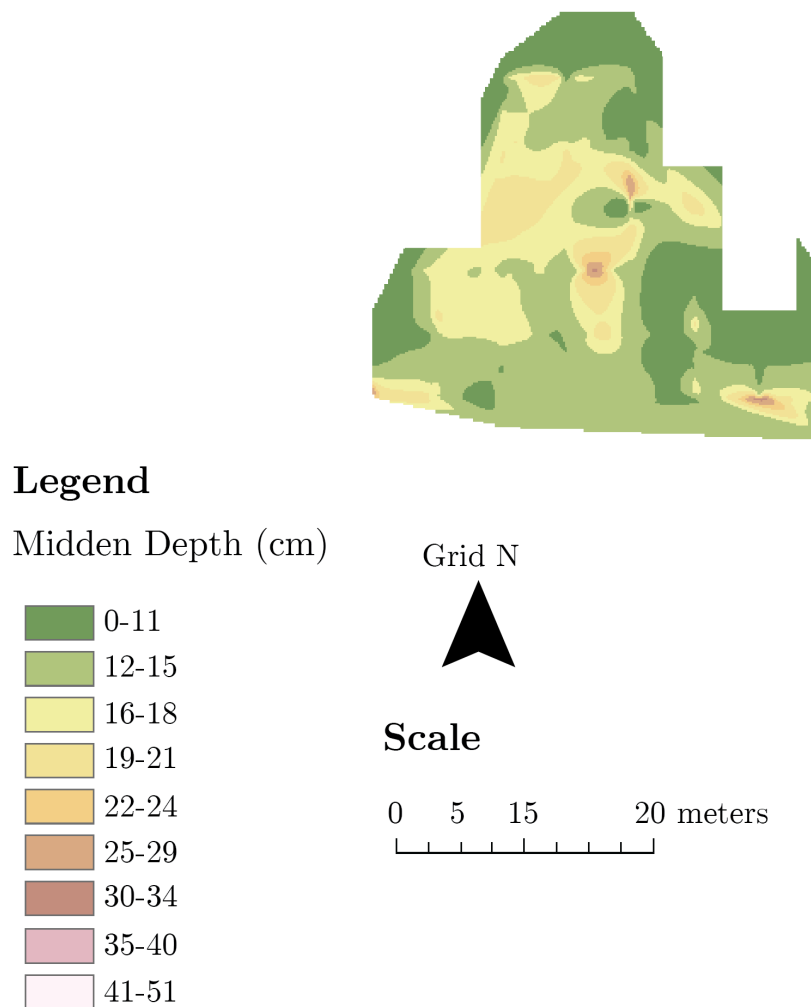


Figure I.8: Tranquility Farm (Site 44.12a) isopach map (2) of the western portion of the 500 MHz GPR survey.

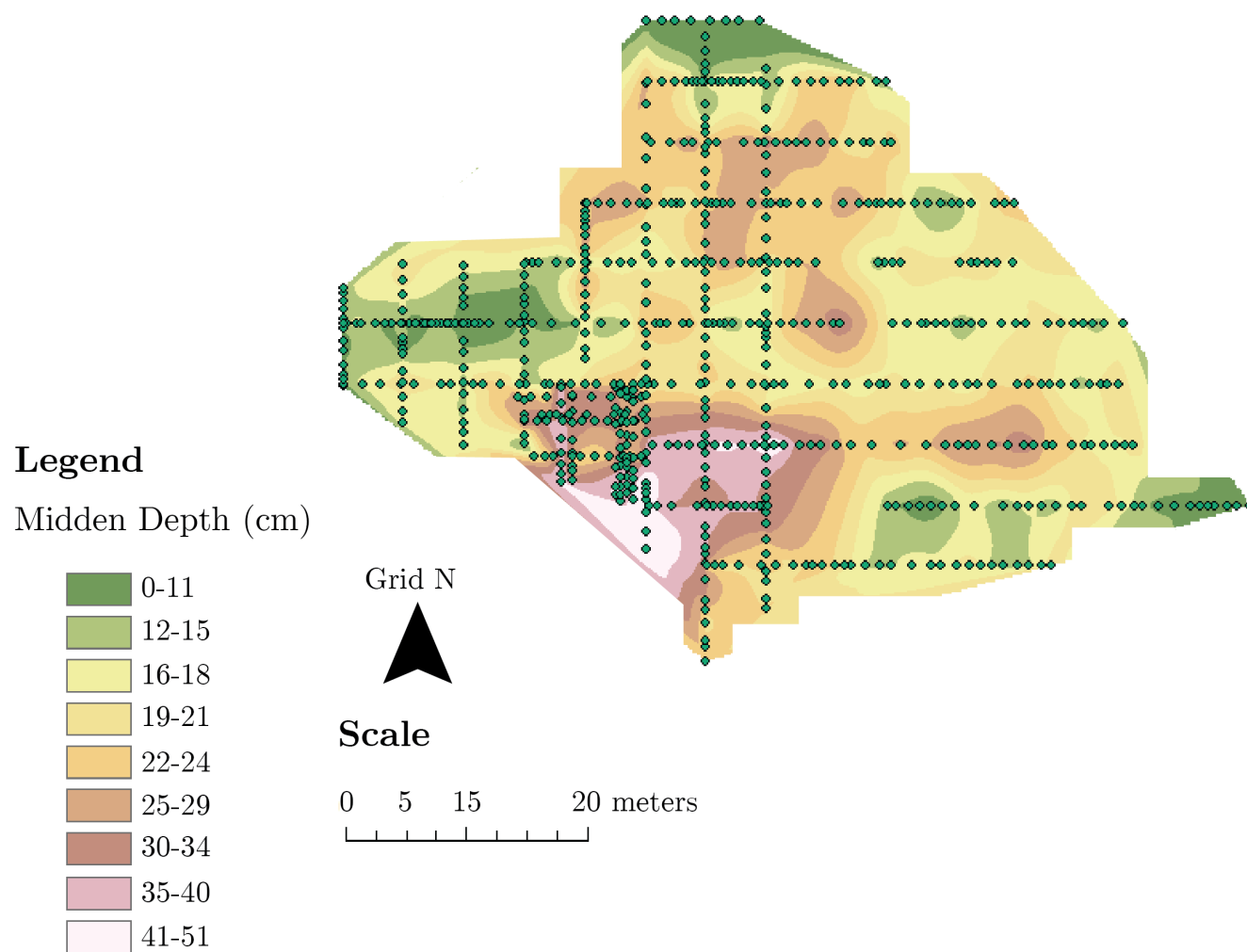


Figure I.9: Tranquility Farm (Site 44.12a) isopach map of the eastern portion of the 500 MHz GPR survey with transects overlain. Survey transects are represented by green dots.

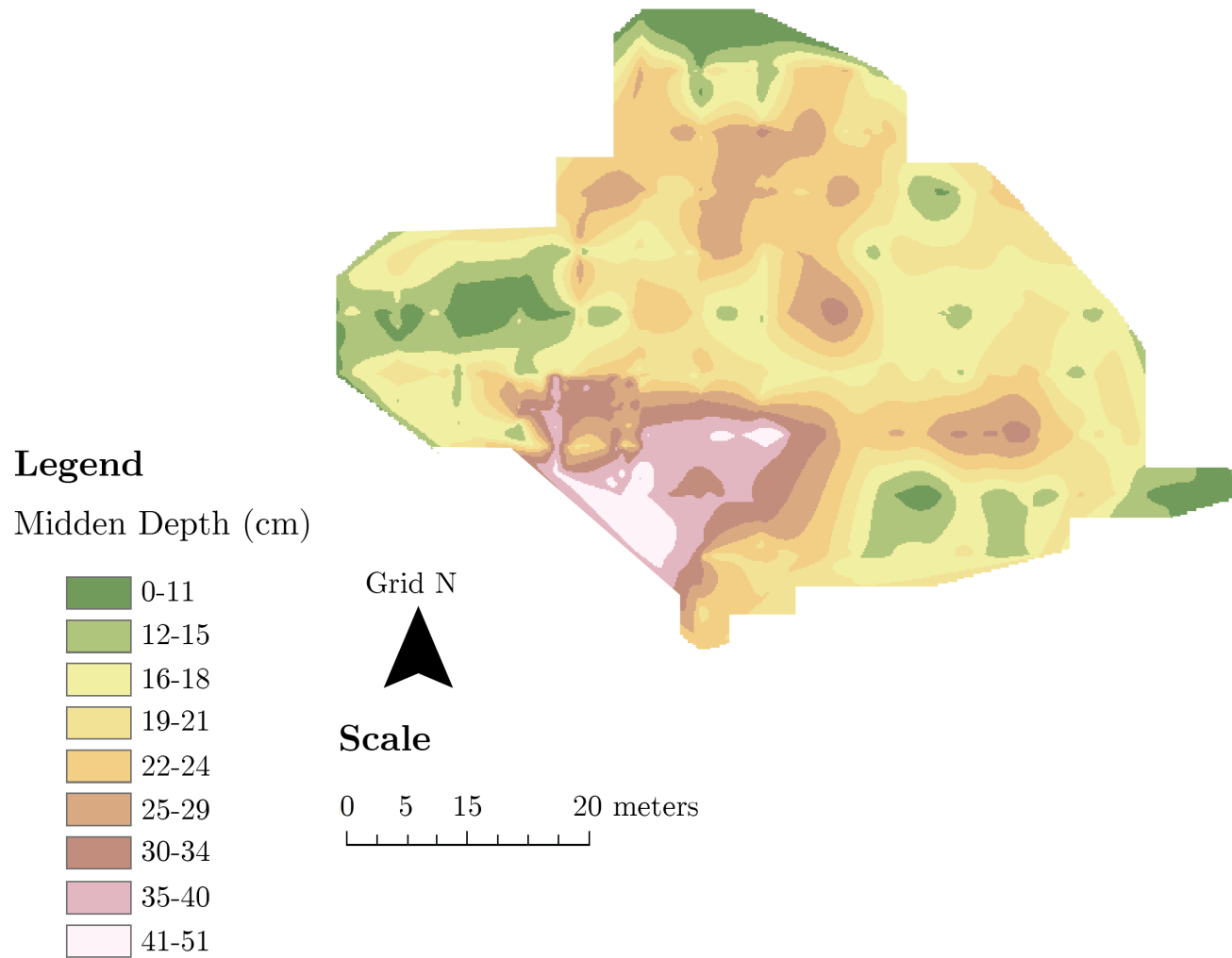


Figure I.10: Tranquility Farm (Site 44.12a) isopach map of the eastern portion of the 500 MHz GPR survey.

BIOGRAPHY OF THE AUTHOR

Jacquelynn F. Miller was born in Pratt, Kansas on July 17, 1993. After moving several times within the state, to Colorado and Missouri, and finally back to Kansas, she graduated valedictorian from Oxford High School in December, 2010. Upon graduation she moved to Durango, Colorado where she enrolled at Fort Lewis College. She transferred to the University of Kansas in the fall of 2011, and earned a Bachelor's of Science in Geology with a minor in Geography in May 2015. Upon graduation, she began working as a contractor to the U.S. Environmental Protection Agency in the Ground Water and Ecosystems Restoration Division (GWERD) of the National Risk Management Research Laboratory (NRMRL). In June, 2016, she moved to Maine to begin work as a graduate research assistant on the Lost to the Sea Project and began graduate study at the University of Maine. Jacquelynn is a candidate for the Master of Science degree in Earth and Climate Sciences from the University of Maine in May 2018.